BioMed Research International

Experimental Heart Failure Models and Their Pathophysiological Characterization

Guest Editors: Peter Moritz Becher, Bodh I. Jugdutt, John Baugh, and Bastian Schmack

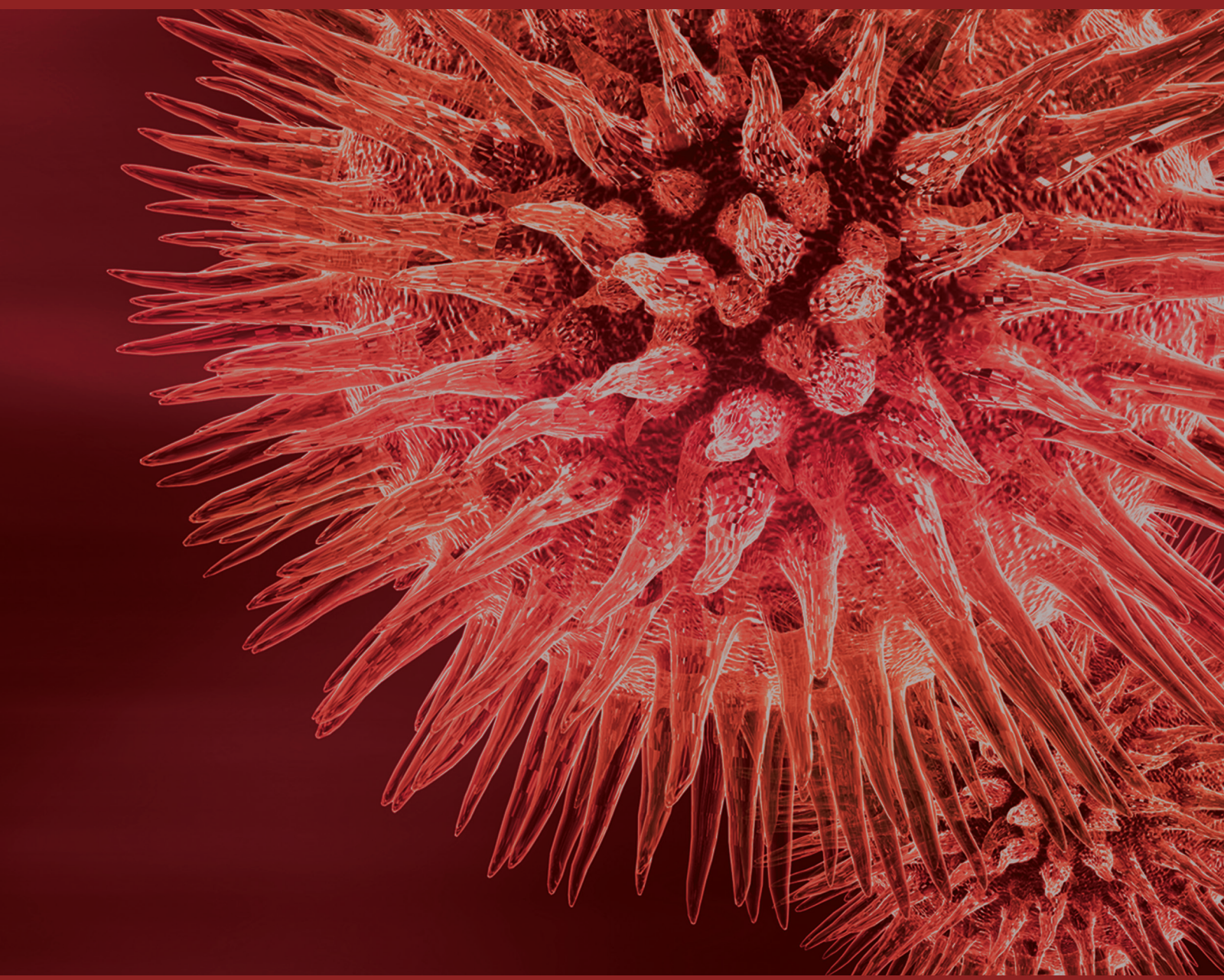

Experimental Heart Failure Models and Their Pathophysiological Characterization

BioMed Research International

Experimental Heart Failure Models and Their Pathophysiological Characterization

Guest Editors: Peter Moritz Becher, Bodh I. Jugdutt, John Baugh, and Bastian Schmack

Contents

Hindawi Publishing Corporation
BioMed Research International
Volume 2016, Article ID 2538263, 3 pages
http://dx.doi.org/10.1155/2016/2538263

Editorial

Experimental Heart Failure Models and Their Pathophysiological Characterization

Peter Moritz Becher,[1] Bodh I. Jugdutt,[2] John Baugh,[3] and Bastian Schmack[4]

[1]*Department of General and Interventional Cardiology, University Heart Center Eppendorf, 20246 Hamburg, Germany*
[2]*Division of Cardiology, Department of Medicine, Mazankowski Alberta Heart Institute, University of Alberta and Hospitals, 8440-112 Street, Edmonton, AB, Canada T6G 2B7*
[3]*Conway Institute of Biomolecular and Biomedical Research, School of Medicine and Medical Science, University College Dublin, Belfield, Dublin 4, Ireland*
[4]*Department of Cardiac Surgery, Heart and Marfan Center, University of Heidelberg, 69120 Heidelberg, Germany*

Correspondence should be addressed to Peter Moritz Becher; m.becher@uke.de

Received 17 December 2015; Accepted 17 December 2015

Heart failure (HF) is a leading cause of morbidity and mortality in the Western world. Despite implementation of current recommended therapies for the treatment of the HF syndrome [1, 2], prevalence, mortality, and costs associated with HF are rising. Expansion of our aging population with high prevalence of such comorbidities as coronary artery disease, myocardial infarction, hypertension, diabetes, and obesity that predispose patients to this complex syndrome is expected to increase HF prevalence even further in the future. Current treatment options and strategies [1, 2] predominantly slow the progression of the HF syndrome. There is a need to develop novel preventative and reparative therapy options. However, development of these novel HF therapies requires testing of the putative therapeutic strategies in appropriate HF animal models [3]. The primary goal of experimental animal HF models is to simplify an indeed complex syndrome into manageable research questions in reproducible settings. The ultimate goal is to elucidate pathophysiological mechanisms and identify key pathways that can be targeted for developing therapies that can be tested in appropriate translational animal models before evaluation in clinical trials for prevention and improving outcome of HF in humans. While there are multiple causes of HF, the dominant ones are valvular heart disease, dilated cardiomyopathies, hypertensive heart disease, and restrictive cardiomyopathies.

The two major clinical phenotypes are HF with reduced ejection fraction (HFrEF) and HF with preserved ejection fraction (HFpEF) [4]. Right-sided HF and pulmonary hypertension also play important roles in the HF phenotype. Various small and large animal models have been used to induce HF [3], including volume and pressure overload, rapid pacing, myocardial infarction with or without coronary reperfusion, coronary embolization, cardiotoxic drugs, or genetic variations (in small animals).

The number of HF patients is increasing owing to the deficiency of therapeutic approaches to treat this population of patients. A discourse between clinicians and scientists seems to be essential to develop novel experimental animal models of HF that accurately imitate the complex clinical syndrome of HF.

During the past decades, the use of experimental animal models to examine complex cardiovascular pathophysiology has been confirmed to be irreplaceable in this field [5]. As a result of basic and translational experiments in small animal models, our understanding of the pathophysiology of HF and its treatment has advanced significantly.

In addition, the ability to manipulate the mouse genome has simplified a particularly important approach to detect novel therapeutic targets, offering a significant approach to explore the mechanisms underlying development and progression of the HF syndrome [5].

Moreover, the adaptation of present experimental animal models will be required to entirely translate scientific findings into new drugs and therapeutic approaches. Future animal models of HF will hopefully give mechanistic insights that could lead to novel options of therapies.

Experimental animal models of HF, as opposed to isolated organ and/or cell preparations, do empower examination of the physiological effects of cardiac functioning, which are of excessive significance in the HF phenotype [3].

Moreover, manipulation of the mouse and rat genomes has allowed significant mechanistic insights into different HF phenotypes in humans.

Although mice are relatively economical and suitable, substantial differences exist between mouse and human heart physiology and especially during development and/or progression of HF [5]. For instance, mouse hearts are very small and do beat very fast (400–600 beats per minute) [6] compared with human hearts (60–90 beats per minute). These dissimilarities lead to important alterations in calcium handling and ion currents between the two species.

Mutations in the giant sarcomeric protein titin (Ttn) are a major cause for inherited forms of dilated cardiomyopathy (DCM). In this issue, Q. Zhou et al. investigated a pattern of DCM that can be induced by TAC-mediated pressure overload in a Ttn-truncated mouse model. This model expands the resource of cardiac disease models, adding a valuable tool to understand cardiac pathophysiological remodeling processes and to develop therapeutic approaches to combat HF.

J. Talavera et al. examined an improved protocol in the rabbit model of anthracycline-induced cardiomyopathy. Current protocols of anthracycline-induced cardiomyopathy in rabbits had disadvantages for long-term studies such as high premature mortality and toxicities (e.g., nephrotoxicity). With the aim of obtaining a more appropriate protocol for this kind of research, the researchers developed a shortened protocol of anthracycline-induced cardiomyopathy using daunorubicin of 4 mg/kg/week over a period of six weeks resulting in high incidence of overt dilated cardiomyopathy with more stable signs of congestive HF, associated with reduced systemic compromise and very low premature mortality. This refined model in rabbits can be very useful for long-term studies aimed at evaluation of the functional effects of novel therapies for HF in anthracycline-induced cardiomyopathy.

E. Roussel et al. performed a gene expression profile of the model of chronic volume overload in rats with severe aortic valve regurgitation (AR) over a period of 9 months. The investigators focused on the study of genes associated with myocardial energetics in that model. Their results displayed that the myocardium with chronic volume overload sustained significant metabolic stress and developed important energetics adaptations. Clinicians currently follow those patients without any intervention for a good number of years, simply waiting for the left ventricle to become too dilated, for the occurrence of symptoms, or until systolic function begins to fall. The findings of E. Roussel et al. in this issue suggest that those hearts develop severe metabolic abnormalities even when systolic function appears to be preserved and that intervention then can limit the dilation and metabolic abnormalities. Focusing on myocardial metabolism by various interventions such as targeted drugs, specific diets, or exercise may help this metabolically stressed myocardium to improve its energy production and may prolong the pre-HF state significantly. However, E. Roussel et al. have observed that treatment with fenofibrate, a PPARα-agonist, normalized both fatty acid and glucose uptakes while reducing left ventricular dilation caused by AR.

Right ventricular (RV) dysfunction due to chronic pressure overload is a common feature of congenital heart diseases. Here, M. Hirata et al. propose an improved pulmonary artery (PA) banding procedure using a half-closed clip (PAC) instead of partial ligation in the rat model of RV dysfunction secondary to chronic pressure overload.

T.-H. Chen et al. used the conditional HSP60 transgenic mouse model to demonstrate neonatal death and HF with transgenic HSP60 expression, likely due to atrial septal defects, increased apoptosis, and myocyte degeneration and other cardiac developmental defects. Since this mitochondrial heat shock protein is essential for maintaining life, they suggest that the model can be useful for addressing other important biological questions about HSP60.

There exists a solid body of evidence that the carotid body (CB) chemoreflex is relevant during the progression of chronic HF. Here, D. C. Andrade et al. reviewed the relevance of CB chemoreflex during the progression of HF. The authors emphasize that several HF experimental models also display a heightened CB chemoreflex drive which correlates positively with the severity of the disease. Moreover, recent exciting studies indicate that ablation of the CB chemoreceptors not only improves autonomic function and reduces disordered breathing patterns in experimental CHF, but also improves survival.

These findings raise the question of whether the CB chemoreflex should be tested in all types of HF (i.e., HFrEF and HFpEF). To sum up, future studies should discuss the role of the CB in the progression of autonomic imbalance and disordered breathing patterns in nonsystolic chronic HF (HFpEF).

We hope that this special issue will help readers become familiarized with recent progress regarding experimental heart failure models and their pathophysiological mechanisms.

Acknowledgments

We want to give special thanks to all the authors who shared their excellent work to be included in our special issue and the reviewers whose input was critical for the selection of the best work. Finally, we want to acknowledge the Editorial Board of Biomed Research International for giving us this opportunity to publish this special issue on Experimental Heart Failure Models and Their Pathophysiological Characterization.

Peter Moritz Becher
Bodh I. Jugdutt
John Baugh
Bastian Schmack

References

[1] J. J. McMurray, S. Adamopoulos, S. D. Anker et al., "Esc guidelines for the diagnosis and treatment of acute and chronic heart failure 2012: the task force for the diagnosis and treatment of acute and chronic heart failure 2012 of the european society of cardiology. Developed in collaboration with the heart failure association (hfa) of the esc," *European Journal of Heart Failure*, vol. 14, no. 8, pp. 803–869, 2012.

[2] C. W. Yancy, M. Jessup, B. Bozkurt et al., "2013 ACCF/AHA guideline for the management of heart failure: executive summary: a report of the American college of cardiology foundation/American Heart Association task force on practice guidelines," *Circulation*, vol. 128, no. 16, pp. 1810–1852, 2013.

[3] S. R. Houser, K. B. Margulies, A. M. Murphy et al., "Animal models of heart failure: a scientific statement from the American Heart Association," *Circulation Research*, vol. 111, no. 1, pp. 131–150, 2012.

[4] P. M. Becher, D. Lindner, N. Fluschnik, S. Blankenberg, and D. Westermann, "Diagnosing heart failure with preserved ejection fraction," *Expert Opinion on Medical Diagnostics*, vol. 7, no. 5, pp. 463–474, 2013.

[5] R. Breckenridge, "Heart failure and mouse models," *Disease Models & Mechanisms*, vol. 3, pp. 138–143, 2010.

[6] P. M. Becher, D. Lindner, K. Miteva et al., "Role of heart rate reduction in the prevention of experimental heart failure: comparison between if-channel blockade and beta-receptor blockade," *Hypertension*, vol. 59, no. 5, pp. 949–957, 2012.

Hindawi Publishing Corporation
BioMed Research International
Volume 2015, Article ID 465342, 13 pages
http://dx.doi.org/10.1155/2015/465342

Research Article

An Upgrade on the Rabbit Model of Anthracycline-Induced Cardiomyopathy: Shorter Protocol, Reduced Mortality, and Higher Incidence of Overt Dilated Cardiomyopathy

Jesús Talavera,[1] Alejandro Giraldo,[2] María Josefa Fernández-Del-Palacio,[1] Obdulio García-Nicolás,[3,4] Juan Seva,[3] Gavin Brooks,[2] and Jose M. Moraleda[5]

[1] *Departamento de Medicina y Cirugía Animal, Facultad de Veterinaria, Universidad de Murcia, Campus de Excelencia Internacional Regional "Campus Mare Nostrum", 30100 Murcia, Spain*
[2] *School of Biological Sciences, Institute for Cardiovascular and Metabolic Research, University of Reading, Reading RG6 6AS, UK*
[3] *Departamento de Anatomía y Anatomía Comparada, Facultad de Veterinaria, Universidad de Murcia, Campus de Excelencia Internacional Regional "Campus Mare Nostrum", 30100 Murcia, Spain*
[4] *Institute of Virology and Immunology (IVI), Sensemattstrasse 293, 3147 Mittelhäusern, Switzerland*
[5] *Unidad de Trasplante Hematopoyético y Terapia Celular, Departamento de Hematología, Hospital Universitario Virgen de la Arrixaca, IMIB, Universidad de Murcia, 30120 Murcia, Spain*

Correspondence should be addressed to Jesús Talavera; talavera@um.es and Alejandro Giraldo; a.giraldoramirez@reading.ac.uk

Received 21 August 2015; Revised 24 November 2015; Accepted 26 November 2015

Academic Editor: Peter M. Becher

Current protocols of anthracycline-induced cardiomyopathy in rabbits present with high premature mortality and nephrotoxicity, thus rendering them unsuitable for studies requiring long-term functional evaluation of myocardial function (e.g., stem cell therapy). We compared two previously described protocols to an in-house developed protocol in three groups: Group DOX2 received doxorubicin 2 mg/kg/week (8 weeks); Group DAU3 received daunorubicin 3 mg/kg/week (10 weeks); and Group DAU4 received daunorubicin 4 mg/kg/week (6 weeks). A cohort of rabbits received saline (control). Results of blood tests, cardiac troponin I, echocardiography, and histopathology were analysed. Whilst DOX2 and DAU3 rabbits showed high premature mortality (50% and 33%, resp.), DAU4 rabbits showed 7.6% premature mortality. None of DOX2 rabbits developed overt dilated cardiomyopathy; 66% of DAU3 rabbits developed overt dilated cardiomyopathy and quickly progressed to severe congestive heart failure. Interestingly, 92% of DAU4 rabbits showed overt dilated cardiomyopathy and 67% developed congestive heart failure exhibiting stable disease. DOX2 and DAU3 rabbits showed alterations of renal function, with DAU3 also exhibiting hepatic function compromise. Thus, a shortened protocol of anthracycline-induced cardiomyopathy as in DAU4 group results in high incidence of overt dilated cardiomyopathy, which insidiously progressed to congestive heart failure, associated to reduced systemic compromise and very low premature mortality.

1. Introduction

Anthracyclines (AC) such as doxorubicin and daunorubicin are regarded as one of the most effective chemotherapeutic groups ever developed for the treatment of malignancies, with a broad spectrum of action encompassing solid and haematologic tumours [1, 2]. Unfortunately, AC-induced cardiomyopathy (AICM) is a frequent toxic consequence of AC. It is estimated that in the USA alone there are at least 10 million cancer survivors, with a similar number in Europe [3, 4]. Thus, the recent success of chemotherapy in clinical oncology means that the population affected by AICM will likely increase substantially in the future.

Several animal models and protocols for the induction of AICM in rodents (e.g., mice and rats) and lagomorphs (e.g., rabbits) have been published over the past decades. Of note, rabbit models of cardiac disease appear to have several advantages over animal models of other species. For example,

whilst being medium size animals, rabbits maintain a cellular electrophysiology and Ca^{+2} transport system, much like in the human or larger animals (e.g., dogs and pigs), which is not the case for mice and rats [5]. One of the first long-term animal models of AICM was established in rabbits by administering daunorubicin and demonstrating myocardial damage and fibrosis [6]. Subsequent studies in rabbits characterized the cumulative and delayed nature of myocardial lesions secondary to administration of doxorubicin 2 mg/kg weekly at different time points [7]. Most studies using rabbit models of AICM have focused on the evaluation of potential cardioprotective agents aimed at preventing AICM development [8–13]. However, with the current trend of increased life expectancy of cancer patients and their associated risk of long-term cardiovascular sequelae, the preclinical assessment of novel therapies (e.g., stem cell therapy) to treat this condition requires the refinement of current animal models to maximise their potential.

One of the main disadvantages of current protocols of induction of AICM in rabbits is the high mortality rate during the induction period (30–70%) [10, 14–16]. This not only increases the number of animals required but also limits their utility in the evaluation of the beneficial effects of novel therapies for AICM. Another disadvantage is that even though cardiac toxicity is readily reproducible with some protocols using daunorubicin or doxorubicin concomitant systemic toxicity (e.g., nephrotoxicity) occurs with these protocols of induction [10, 17–20]. This systemic toxicity is often responsible for the premature death of the animals even before they can develop clinically evident signs of overt dilated cardiomyopathy (DCM) and congestive heart failure (CHF). The availability of an experimental model that provides animals in a stable clinical stage of heart failure would offer a valuable tool to researchers interested in evaluating the benefits of therapies that require long-term follow-up of the animals.

Our goal has been to study the benefits of stem cell therapy in AICM, but in the process we have come across the pitfalls of current protocols of induction, thus motivating us to develop our own in-house protocol. Since cardiac toxicity is directly related to the cumulative dose administered to the subject of study [21] and rabbits are very sensitive to myocardial damage by AC [7], we hypothesised that increasing the weekly dose of daunorubicin and reducing the length of the protocol of induction could result in a rabbit model of AICM potentially exhibiting reduced nonspecific toxicities and lower mortality. Of the several experimental protocols trialled, here we report the incidence of overt DCM, CHF, premature mortality, and associated systemic toxicities when using an in-house developed shortened protocol (daunorubicin 4 mg/kg per week for up to 6 weeks) compared to other protocols reported in the literature which are frequently used for the evaluation of cardioprotective agents.

2. Materials and Methods

2.1. Animals. The experiments in the present study were performed in accordance with Directive 2010/63/EU of the European Commission and were approved by the Ethical Research Committee of the University of Murcia, Spain. A total of 37 New Zealand Rabbits (2 months old, 1.5–2.0 kg weight with 1 : 1 ratio of males/females) were randomly allocated into one of the following three groups: 6 rabbits were injected I.V. 0.9% saline weekly for up to 10 weeks and constituted the age matched controls (control group); 12 rabbits constituted DOX2 group receiving doxorubicin (Tedec-Meiji Farma, Madrid, Spain) 2 mg/kg in weekly intravenous injections for 8 weeks; 6 rabbits constituted the DAU3 group which was injected with daunorubicin (Daunoblastina, Pfizer, Madrid, Spain) 3 mg/kg in weekly for 10 weeks; and 13 rabbits constituted the DAU4 group (daunorubicin 4 mg/kg per week for 6 weeks). Due to inherent differences in the induction times for each protocol, three time points were defined for the comparisons of biochemical, haematological, and echocardiographic analyses between study groups: the first time point is the baseline time point, just before starting the first administration of anthracycline in treated groups or saline in control group; the second time point is the intermediate time point, two weeks before the end of the protocol; thus intermediate time points were at 8 weeks for control group, 6 weeks for DOX2 group, 8 weeks for DAU3 group, and 4 weeks for DAU4 group; and the third time point is the final time point, the last measurement taken upon completion of the protocol.

2.2. Mortality. The premature death of the animals during the period of induction of cardiomyopathy (i.e., death before completing the corresponding experimental induction protocol of weekly AC injections) was classified as follows: (1) deaths due to systemic toxicity (i.e., directly related to the administration of AC) which manifested as diarrhoea, weight loss, and emaciation and included animals that died or required euthanasia for this cause, (2) deaths secondary to CHF (see below), which were confirmed either by echocardiogram and/or by autopsy, (3) other causes such as respiratory failure during anaesthesia or animals that required euthanasia (e.g., spontaneous spinal fracture). Kaplan-Meier survival analysis was performed throughout the induction period and up to two weeks after completion of the respective induction protocol for each group.

2.3. Incidence of Overt DCM and CHF. For the analysis of incidence of overt DCM and development of CHF in the different groups of study, these were defined as follows. Overt DCM is defined as unequivocal echocardiographic signs of cardiac remodelling and/or functional impairment objectively assessed by the presence of several of the following findings: eccentric hypertrophy of cardiac chambers, loss of the oval shape of the left ventricle, ventricular wall thinning, increased left atrial-to-aortic root ratio > 1.5 (2D-mode, short axis view), fractional shortening (FS) < 20%, left ventricular ejection fraction (LVEF) < 40%, and presence of atrioventricular valve regurgitation (assessed by colour and/or spectral Doppler) (Figures 1(c) and 1(d)). On the other hand, CHF was defined as echocardiographic and/or postmortem evidence of pleural, pericardial, and peritoneal effusions and/or pulmonary oedema in conjunction with echocardiographic

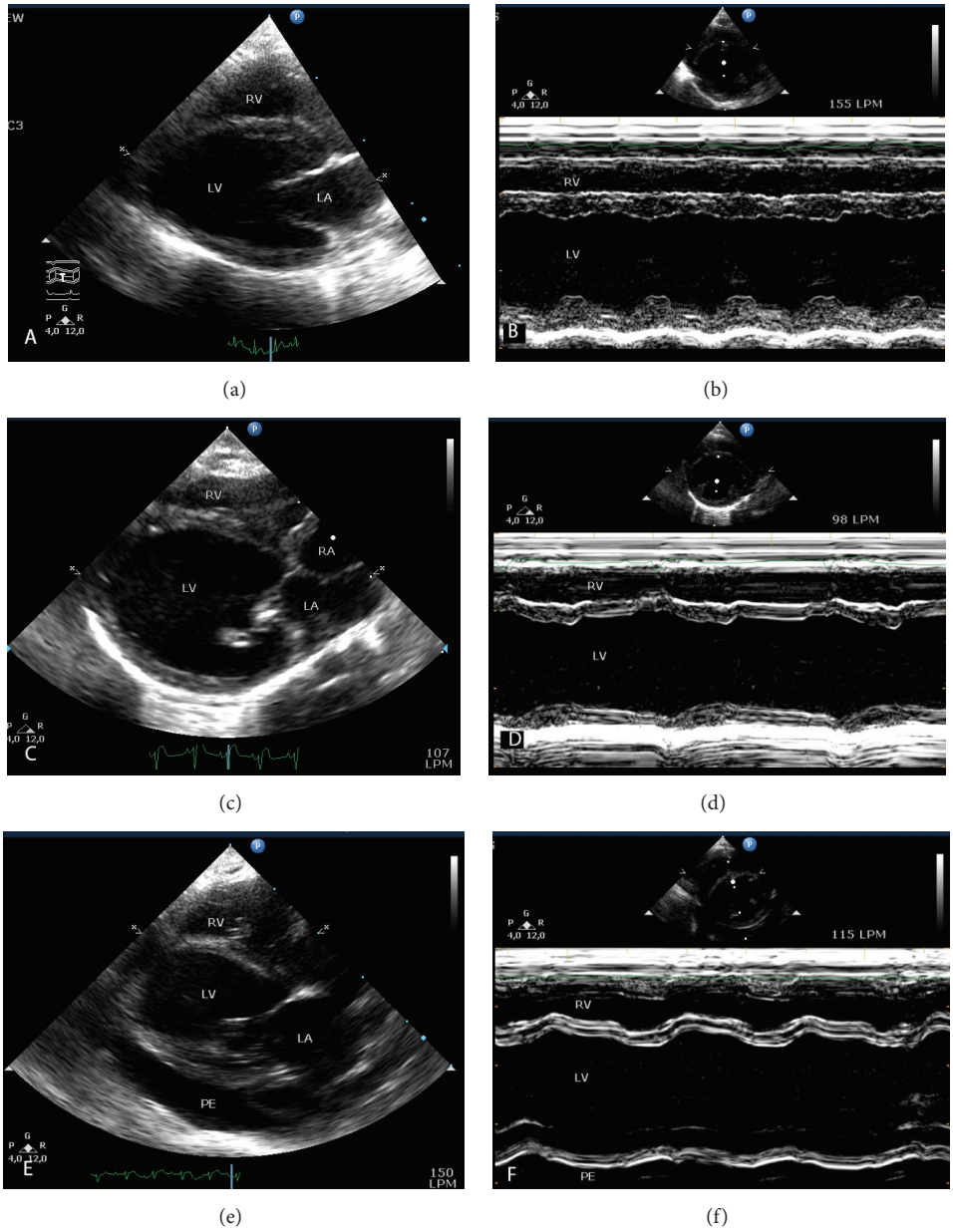

(a) (b)

(c) (d)

(e) (f)

Figure 1: Echocardiograms in 2D and M-mode during induction of AICM. Echocardiograms in 2D parasternal long axis view (a, c, e) and M-mode of the left ventricle (LV) at the level of the papillary muscles (b, d, f). (a-b) Baseline, normal rabbit. (c-d) Rabbit with overt DCM. (e-f) Rabbit with CHF showing 4-chamber dilatation, pericardial effusion (PE), and severely reduced LV contractility. RV, right ventricle; LA, left atrium; RA, right atrium.

signs of overt DCM and/or severe cardiomegaly confirmed by postmortem study (Figures 1(e) and 1(f)).

2.4. Administration of Drugs and Blood Sampling. Animals were immobilised in acrylic restrainers to reduce stress and facilitate the administration of drugs. AC were diluted according to the weight of the animal in 8 mL of 0.9% sterile saline for I.V. injections in AC treated groups, whilst in control group 8 mL of 0.9% sterile saline without AC were injected at each time point. After hair clipping of the ear and careful asepsis, a 24 G catheter was advanced into one of the marginal auricular veins and fixed with micropore to the skin. A winged needle (21 G) with prolongator was then inserted into the catheter and AC were administered at a rate of 0.5 mL/min. Blood samples from jugular vein were collected before first dose of AC and then every 2 weeks until the final administration at 8 weeks (DOX2 group), 10 weeks (DAU3 group), or 6 weeks (DAU4 group).

2.5. Biochemical and Haematological Study. Haematological parameters in plasma samples were analysed using the Advia 120 Hematology System (Siemens, Erlangen, Germany).

Biochemical parameters were evaluated in plasma using the analyser AU2700 (Olympus Corporation, Tokyo, Japan).

2.6. Echocardiographic Study. A transthoracic echocardiographic examination using a HD7 XE System, equipped with a 4–12 MHz transducer (Philips, Andover, Massachusetts, USA) under light anaesthesia (ketamine (Imalgene, Merial, Villeurbanne, France) 10 mg/kg, combined with dexmedetomidine (Domtor, Esteve, Madrid, Spain) 200 μg/kg), was performed longitudinally at baseline and every two weeks until the end of the study. The procedure was performed by or under direct supervision of a European board-certified veterinary cardiologist (MJFP), in a blinded fashion, according to the recommendations of the Echocardiography Committee of the American College of Veterinary Internal Medicine and the American Society of Echocardiography [22, 23]. Simultaneous 1-lead electrocardiographic tracings were recorded during the study. Total circumferential shortening area (CSA) was obtained using the following formula: CSA = CSAd − CSAs/CSAd × 100. Fractional shortening (FS (%)) was calculated according to the following formula: FS = (LVDd − LVDs)/(LVDd × 100). Left ventricular systolic and diastolic volumes (LVVd and LVVs) were calculated using the Teichholz formula $(7 \times (\text{LVD})^3)/(2.4 + \text{LVD})$ and LVEF (%) was calculated according to the following formula: LVEF = (LVVd − LVVs)/(LVVd × 100).

2.7. Cardiac Troponin I Evaluation. Cardiac troponin I (cTnI) levels were determined in plasma samples obtained from the jugular vein using the Immulite Kit (Siemens, Germany) according to the manufacturer's instructions with a detection limit <0.049 ng/mL.

2.8. Histopathological Study. Heart tissue blocks were sectioned to cover 5 different anatomical regions in ascending order: the apex, free wall bellow the papillary muscles, at the level of the papillary muscles, end of papillary muscles and beginning of *chordae tendineae*, and at the atrial level [7]. Tissue was fixed for 24 h in 10% formalin, dehydrated with increasing ethanol concentrations, which was then substituted for xylene, and finally embedded in paraffin using the Leica TP1050 cyclic tissue processor (Leica Biosystems GmbH, Germany) and the Tissue-Tek thermal console (Sakura, USA). Sections of 5 μm were then obtained with a microtome RM2155 (Leica Biosystems GmbH, Germany) and stained with haematoxylin-eosin and Masson's trichrome. Two pathologists blinded to study group performed the histopathological evaluations. Myocardial lesions were assigned a score from 1–4 by lesion grade, and the extension of myocardial lesions was classified 1–4 as previously described [7]. A similar lesion grade scoring (1–4) and classification of extension of lesions (1–4) system was followed for kidney and liver tissue.

2.9. Statistical Analysis. Statistical analysis was performed using SPSS Statistics version 19 for Windows and GraphPad Prism 6. Data are expressed as means ± SEM. One-way ANOVA with Tukey's post hoc test or paired t test/Wilcoxon signed-rank test or two-way ANOVA to assess the global effect of sex and treatment, where appropriate, was performed. Survival curves were plotted using Kaplan-Meier analysis (Log-Rank with Mantel-Cox test). Values of $p \leq 0.05$ were considered statistically significant.

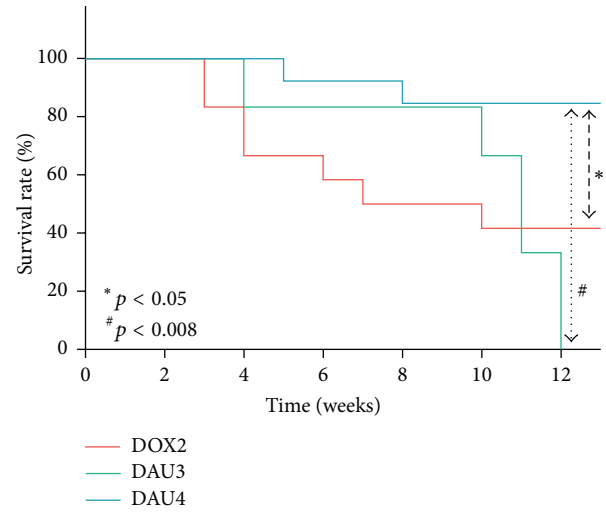

Figure 2: Kaplan-Meier survival curves.

3. Results

3.1. Mortality. Survival analysis curves are shown in Figure 2. In the DOX2 group, 6 out of 12 animals (50%) died prematurely (premature mortality defined as death of the animal during the course of weekly I.V. administrations on each group) during weeks 3–7 of the induction period (up to 8 weeks), all secondary to systemic toxicity. In the DAU3 group, 33.3% died prematurely during the induction period (up to 10 weeks); one of these deaths occurred secondary to systemic toxicity at 4 weeks and the other occurred secondary to CHF at week 9. In the DAU4 group, only one animal required euthanasia at week 5 due to spontaneous spinal fracture resulting in a premature mortality of 7.6% during the induction period (up to 6 weeks). No deaths occurred in the control group. Gender of the animal did not influence mortality in all AC treated groups since this did not differ substantially from that of whole cohort within each group. Thus, of the six deaths in group DOX2 during the induction period, three corresponded to males and three to females. Similarly, one death occurred in males and one in females in the DAU3 group during the induction period, whilst for the DAU4 group the premature death occurred in a male rabbit. Cumulative mortality up to two weeks after completion of the induction period continued to increase in all groups (Figure 2). However, whilst one additional rabbit died in the DOX2 group from 8 to 10 weeks, secondary to systemic toxicity, and 4 more deaths occurred in the DAU3 group from 10 to 12 weeks, 3 of these secondary to CHF, resulting in a cumulative mortality of 58.3% and 100%, respectively, only one more death secondary to CHF occurred in the DAU4

Table 1: Selected biochemical parameters.

Parameter	Basal	Intermediate[§]	Final
Cholesterol (mg/dL)			
Control	41.5 ± 10.3	37.5 ± 10.2	44.7 ± 3.8
DOX2	36.10 ± 11.25	70.46 ± 16.66$^{bc\#¶}$	241.04 ± 59.5$^{bc\#¶}$
DAU3	40.80 ± 4.34	45.66 ± 6.40	79.73 ± 8.20^{bc}
DAU4	35.24 ± 7.71	44.38 ± 4.05	59.08 ± 7.81^{bc}
Triglycerides (mg/dL)			
Control	72.3 ± 22.9	45.3 ± 7.3	55.3 ± 7.1
DOX2	68.23 ± 17.48	184.70 ± 47.74^{b¶}	405.88 ± 38.80^{bc¶}
DAU3	78.09 ± 20.39	150.31 ± 65.32^{b¶}	446.22 ± 102.9^{bc¶}
DAU4	72.50 ± 22.85	85.04 ± 12.35	115.88 ± 15.72^{bc}
Creatinine (mg/dL)			
Control	0.86 ± 0.10	0.77 ± 0.11	0.83 ± 0.10
DOX2	0.93 ± 0.06	1.08 ± 0.08	1.62 ± 0.22^{bc}
DAU3	0.79 ± 0.04	1.06 ± 0.10	2.54 ± 0.50^{bc*¶}
DAU4	0.98 ± 0.10	0.92 ± 0.10	0.87 ± 0.07
BUN (mg/dL)			
Control	37.00 ± 4.95	38.54 ± 6.62	41.79 ± 8.50
DOX2	36.43 ± 3.45	30.50 ± 3.74	39.40 ± 8.69
DAU3	26.61 ± 2.99	30.92 ± 2.47	85.47 ± 12.34^{bc*¶}
DAU4	35.42 ± 4.57	28.35 ± 1.38	29.96 ± 2.50
Total Proteins (g/dL)			
Control	5.39 ± 0.21	5.37 ± 0.22	5.33 ± 0.24
DOX2	5.48 ± 0.17	4.90 ± 0.37	3.92 ± 0.37^{bc¶}
DAU3	5.31 ± 0.17	5.90 ± 0.30	4.42 ± 0.81^{bc}
DAU4	5.55 ± 0.16	5.20 ± 0.12	4.96 ± 0.17
AST (U/L)			
Control	23.02 ± 4.90	18.47 ± 4.10	20.77 ± 4.34
DOX2	27.59 ± 4.71	24.36 ± 6.86	30.42 ± 1.01
DAU3	20.96 ± 2.93	22.72 ± 5.82	270.9 ± 124.0^{bc*¶}
DAU4	35.94 ± 5.73	23.30 ± 3.84	28.31 ± 5.67
ALT (U/L)			
Control	44.67 ± 8.16	39.97 ± 7.89	37.45 ± 7.37
DOX2	53.02 ± 5.34	36.98 ± 7.45	35.46 ± 4.30
DAU3	48.75 ± 6.47	54.56 ± 12.34	226.70 ± 97.2^{bc*¶}
DAU4	58.25 ± 13.44	45.03 ± 5.96	42.19 ± 6.88

[§]Intermediate time point values were from blood samples obtained on week 8 of the study in control group, on week 6 in DOX2 group, on week 8 in DAU3 group, and on week 4 in DAU4 group. BUN, blood urea nitrogen; AST, aspartate aminotransferase; ALT, alanine aminotransferase. Data expressed as mean ± SEM. Statistical significance is at $p < 0.05$; [b]compared to basal value; [c]compared to control; [*]compared to DOX2; [#]compared to DAU3; [¶]compared to DAU4.

group from 6–8 weeks, resulting in a cumulative mortality of 15.3%.

3.2. Incidence of DCM and CHF. None of the animals from the DOX2 group developed overt DCM or CHF, which on the contrary were greatly affected by general toxicity. In the DAU3 group, 4 out of 6 animals (66%) developed overt DCM and CHF, of which two were males and two were females. In the DAU4 group, 12 out of 13 animals presented with overt DCM (92%), whilst CHF was confirmed in 8 animals (61%). In DAU4 group, the incidence of overt DCM and CHF according to sex of the animal revealed that 6 out of 7 males and 6 out of 6 females presented with overt DCM, whilst HF was present in 4 out of 7 males and 4 out of 6 females.

3.3. Biochemical Study. Selected biochemical parameters are shown in Table 1. No differences were observed between the different groups at baseline. Triglycerides and cholesterol plus triglycerides were significantly increased at the intermediate time point in the DOX2 and DAU3 groups, respectively, compared to basal values and control group, whilst in the DAU4 group no significant differences were observed. Also, there were slight increases in other biochemical parameters such as creatinine for DOX2 and DAU3 groups at the intermediate time point; however, these remained within the normal range for the species [24]. Groups DOX2 and DAU3 developed marked changes in several biochemical parameters at the final time point of the study. Thus, rabbits in the DOX2 and DAU3 groups exhibited a significant increase in creatinine

and marked combined hyperlipidaemia associated with a concomitant reduction of total proteins. In addition, the DAU3 group also showed significant increases in blood urea nitrogen (BUN), aspartate aminotransferases (AST), and alanine aminotransferases (ALT). Apart from mild combined hyperlipidaemia, no significant changes were observed in biochemical parameters in the DAU4 group at the final time point (Table 1). Supplemental Table 1 in Supplementary Material available online at http://dx.doi.org/10.1155/2015/465342 shows the subanalysis of selected biochemical parameters in male and female animals from all groups at final time point. Consistent with the general analysis, both male and female rabbits in the DOX2 and DAU3 groups had comparable increases in creatinine values, marked combined hyperlipidaemia, and reduction of total proteins in blood relative to control group, suggesting that none of these alterations had an underlying causality associated with sex of the animal. However, even though these changes were marked enough compared to control group, they were only significant in DOX2 group, provided the low n of animals in DAU3 group at this time point (type II error). Similarly, and in line with the findings of the general analysis, DAU3 group also presented marked alterations in BUN, AST, and ALT values in both males and females, although low n at this time point in DAU3 group leads to type II error (Supplemental Table 1). Male and female rabbits from the DAU4 group only exhibited mild hyperlipidaemia.

3.4. Haematological Study. In all AC treated groups, a significant reduction in red blood cells (RBC), haemoglobin, and haematocrit and increased red cell distribution width (RDW) were observed at the intermediate time point relative to basal time point and control group. However, whilst in groups DOX2 and DAU4 these parameters returned to normal levels at the end of the induction period, these remained abnormal or even worsened in the DAU3 group at the end of the induction period (Table 2). Consistent with increased haematological toxicity with the DAU3 protocol, white blood cell (WBC) count also was significantly affected at the intermediate time point compared to baseline values and those of control group, although these values returned to nearly normal at the end of the induction period (Table 2).

3.5. Echocardiographic Study. All groups of the study had comparable LVEF, FS, and total CSA at basal time point (Figures 3(a)–3(c)). A repeated measures test within the control group demonstrated no significant differences on these parameters of ventricular function at the different time points of the study. In the DOX2 group, a decrease in LVEF and FS was observed at the intermediate time point (6 weeks) and final time point (8 weeks), but this was only statistically significant for LVEF at the intermediate time point (Figures 3(a) and 3(b)). Whilst at the intermediate time point LVEF, FS, and total CSA remained unchanged in DAU3 and DAU4 groups compared to basal time point and control group, all these parameters of ventricular function were markedly and significantly reduced in rabbits from these groups at the final time point (Figures 3(a)–3(c)). These changes were also significantly different in DAU4 group when compared to DOX2 at this time point (Figures 3(a)–3(c)). Subanalysis of ventricular function in all groups at the final time point indicated that AC-induced myocardial damage affected males and females in DAU3 and DAU4 groups to a similar extent. Thus, marked alterations in LVEF, FS, and total CSA in males and females were observed at final time point (Supplemental Figures 1(A)–1(C)). However, whilst these changes were significant in DAU4 group, low n at final time point in DAU3 group resulted in type II error. On the contrary, ventricular function remained equally unaffected in males and females from DOX2 group (Supplemental Figures 1(A)–1(C)).

3.6. Cardiac Troponin I Evaluation. At the basal time point, no differences in cTnI levels were observed among all groups. Significant elevations were observed at intermediate time points in all AC treated groups relative to basal time point and control group (Figure 3(d)). The levels of cTnI further increased at the final time point in all groups, although the most marked increase was observed in the DAU4 group to the extent of being statistically significant at this time point compared to values for the DOX2 group (Figure 3(d)). The cTnI levels in males and females were also analysed at final time point in all groups (Supplemental Figure 1(D)). In line with the findings for the general population, marked elevations of cTnI were observed in both males and females from all groups, whilst males and females from DAU4 group exhibited the highest levels of cTnI elevation relative to control (Supplemental Figure 1(D)).

3.7. Histopathological Examination. Figure 4 shows representative photomicrographs of grades 1 and 4, within the spectrum of AC induced lesions in the myocardium, kidney, and liver, according to the grading scale used to determine the score of lesions per organ [7]. The myocardial lesions from all groups showed similar scores in grading scale as shown in Table 3. Thus, the myocardium of most animals presented predominantly with moderate myocytolysis associated with atrophy and degeneration of myofibrils and replacement fibrosis (Figures 4(b) and 4(c)). However, the extent of myocardial lesions was different for all groups. Whilst DOX2 group animals presented mostly circumscribed lesions in isolated myofibrils, myocardial lesions in animals from the DAU3 group affected focal groups of myofibrils at 1 level, and animals of the DAU4 group exhibited lesions involving more extensive (diffuse) groups of myofibrils at 2 or more levels (Table 3). Nonpurulent myocarditis associated with the presence of mononuclear cell infiltration was also a frequent observation in animals from all groups. Kidney and liver lesions from all groups showed similar scores, as well as similar extension of lesions (see Table 4).

4. Discussion

An animal model of AICM suitable to test novel therapies aimed at ameliorating this condition not only should reproduce the cardiomyopathic effect of AC in scheduled intravenous injections, thus simulating clinical scenarios [25], but also should have low mortality at the end of

Table 2: Haematological parameters.

Parameter	Basal	Intermediate[§]	Final
RBC ($10^6/\mu$L)			
Control	5.95 ± 0.24	5.93 ± 0.12	6.12 ± 0.20
DOX2	6.06 ± 0.20	4.76 ± 0.26[bc]	5.44 ± 0.74
DAU3	6.29 ± 0.27	4.87 ± 0.19[bc]	3.83 ± 0.87[bc*¶]
DAU4	6.33 ± 0.25	4.84 ± 0.20[bc]	5.23 ± 0.23
Haematocrit (%)			
Control	36.93 ± 1.76	36.88 ± 0.61	39.53 ± 0.90
DOX2	37.11 ± 1.75	28.42 ± 1.54[bc]	33.29 ± 2.67
DAU3	36.47 ± 1.10	29.56 ± 0.65	25.40 ± 3.56[bc*¶]
DAU4	39.36 ± 0.98	29.16 ± 1.32[b]	33.94 ± 2.46
Hemoglobin (g/dL)			
Control	12.52 ± 0.47	11.75 ± 0.23	12.82 ± 0.30
DOX2	12.21 ± 0.63	9.14 ± 0.32[b]	10.40 ± 1.23
DAU3	12.18 ± 0.24	8.68 ± 0.24[b]	6.83 ± 1.08[bc*¶]
DAU4	13.07 ± 0.44	9.19 ± 0.40[b]	9.57 ± 0.59[bc]
MCV (μm^3)			
Control	62.17 ± 2.12	62.35 ± 1.41	62.75 ± 1.78
DOX2	61.18 ± 1.87	59.95 ± 3.18	62.40 ± 3.27
DAU3	58.08 ± 1.52	60.88 ± 1.33	62.33 ± 5.03
DAU4	62.29 ± 1.75	60.28 ± 1.36	64.73 ± 3.15
RDW			
Control	13.37 ± 0.74	13.95 ± 0.72	13.42 ± 1.14
DOX2	13.08 ± 0.38	18.44 ± 1.15[bc]	17.32 ± 1.34[bc]
DAU3	13.48 ± 0.28	20.26 ± 0.83[bc¶]	20.47 ± 1.44[bc*]
DAU4	12.27 ± 0.41	15.98 ± 0.76[bc]	19.78 ± 0.78[bc]
WBC ($10^3/\mu$L)			
Control	5.08 ± 1.22	4.86 ± 0.69	5.05 ± 0.82
DOX2	5.77 ± 0.99	6.52 ± 1.14	5.53 ± 0.76
DAU3	4.42 ± 0.64	2.88 ± 0.46[bc*¶]	7.41 ± 0.62[bc*]
DAU4	5.43 ± 0.63	4.80 ± 0.72[*]	8.59 ± 1.92[bc*]
Differential count (%)			
Neutrophils			
Control	15.55 ± 2.52	17.57 ± 1.91	22.78 ± 5.20
DOX2	18.20 ± 3.66	12.78 ± 2.49	25.70 ± 9.89
DAU3	14.10 ± 2.19	10.18 ± 4.35	11.10 ± 0.95
DAU4	31.16 ± 9.79	6.58 ± 1.60[bc]	27.44 ± 3.03
Lymphocytes			
Control	68.55 ± 5.25	65.48 ± 2.97	63.50 ± 4.68
DOX2	68.38 ± 4.55	70.63 ± 5.21	55.90 ± 10.34
DAU3	73.27 ± 2.67	76.52 ± 5.47	72.20 ± 1.30
DAU4	55.86 ± 8.73	82.56 ± 2.14	57.15 ± 3.47

[§]Intermediate time point values were from samples obtained on week 6 in DOX2 group, on week 8 in DAU3 group, and on week 4 in DAU4 group. RBC, red blood cells; MCV, mean corpuscular volume; RDW, red cell distribution width; WBC, white blood cells. Data expressed as mean ± SEM. Statistical significance is at $p < 0.05$; [b]compared to basal value; [c]compared to control; [*]compared to DOX2; [¶]compared to DAU4.

the induction period, thereby allowing sufficient time to complete experiments to evaluate their efficacy in recovering myocardial function and animal well-being. It also is desirable that nonspecific toxicities, such as nephrotoxicity, which do not occur in humans treated with AC [18], are reduced or absent from the model to avoid the potential confounding effect of comorbidities in the outcome of the experiments. Such an animal model is currently unavailable. The present study presents an experimental protocol for AICM that generates a high percentage of animals with overt DCM and CHF with mild manifestations of systemic toxicity and very low mortality both premature (7.6%) and within

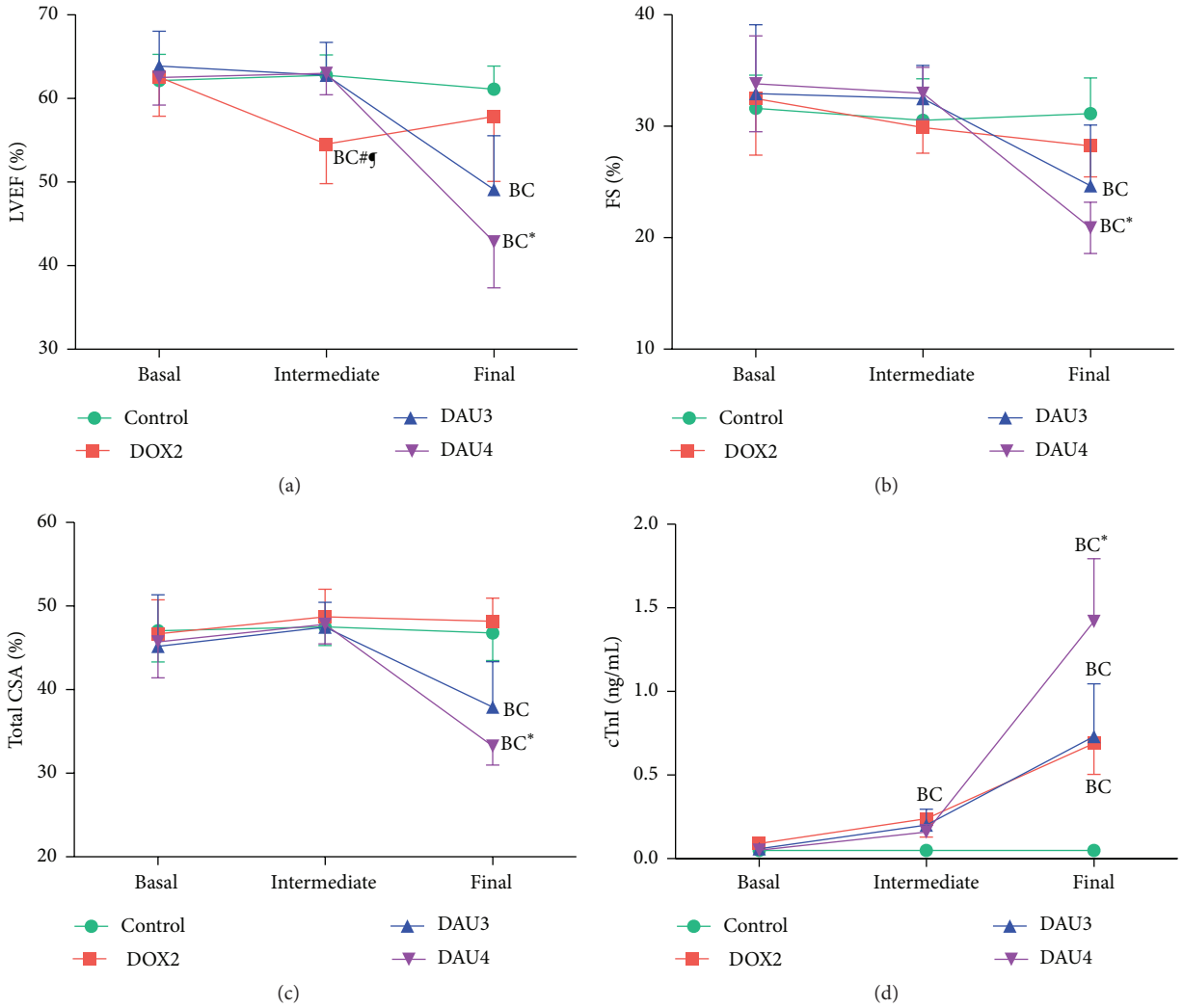

Figure 3: Changes in echocardiographic parameters and cTnI values during induction of AICM. (a) Left ventricular ejection fraction (LVEF). (b) Fractional shortening (FS). (c) Total circumferential shortening area (CSA). (d) Cardiac troponin I (cTnI) levels. Data expressed as mean ± SEM. Statistical significance is at $p < 0.05$; (B), compared to basal; (C), compared to control; (∗), compared to DOX2; (#), compared to DAU3; (¶), compared to DAU4.

Table 3: Scores for grade and extension of histopathological lesions in the heart.

Group	Lesion grade	Lesion extension
DOX2	2.65 ± 0.39	1.65 ± 0.44
DAU3	2.63 ± 0.43	2.68 ± 0.47*
DAU4	2.76 ± 0.32	3.18 ± 0.43*#

Data expressed as mean ± SEM. Statistical significance is at $p < 0.05$; *compared to DOX2; #compared to DAU3.

Table 4: Scores for grade and extension of histopathological lesions in kidney and liver.

Group	Lesion grade	Lesion extension
	Kidney	
DOX2	3.50 ± 0.71	3.50 ± 0.71
DAU3	2.75 ± 0.50	3.50 ± 0.58
DAU4	3.35 ± 0.57	3.17 ± 0.65
	Liver	
DOX2	3.00 ± 0.10	3.00 ± 0.10
DAU3	3.00 ± 0.75	3.00 ± 0.71
DAU4	2.88 ± 0.90	3.04 ± 0.75

Data expressed as mean ± SEM.

two weeks of completing the induction protocol (15.3%). Furthermore, the occurrence of CHF manifests insidiously whilst cardiogenic death did not occur abruptly at the end of the induction period, thus allowing time for functional evaluation of the animal over an extended period of time. These qualities result in an improvement over previously published protocols of AICM in rabbits particularly in the setting of evaluation of novel therapies for AICM (e.g., stem cell therapy). This refined model is in line with the principles of the 3Rs and the guidelines of the National Centre for the Replacement, Refinement and Reduction of Animals in Research. Thus, lower premature mortality translates into

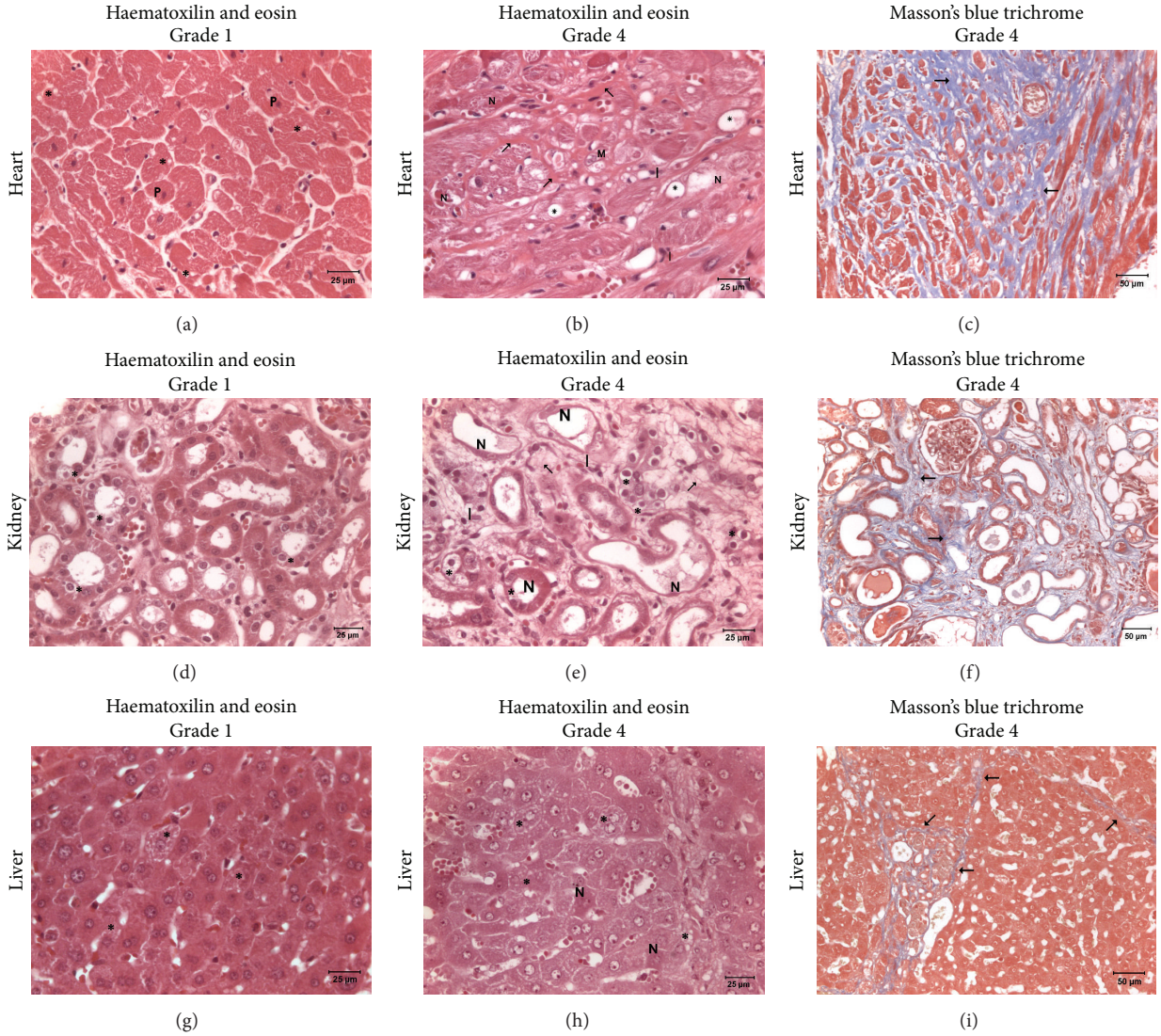

Figure 4: Myocardial, renal, and hepatic lesions induced by anthracyclines. (a–c) Representative photomicrographs of myocardial damage. (a) DOX2 group, grade 1: primary damage of the left ventricular myocardium. Highly intense eosinophilia of the cytoplasm, pyknotic nuclei [P], and diffuse vacuolar degenerations in cardiomyocytes [∗] are present. (b) DAU3 group, grade 4: conspicuous disperse toxic myocardial damage. Extensively vacuolated cardiomyocytes [∗] with intense eosinophilic cytoplasm are present. Necrotic cardiomyocytes [N] phagocytized by macrophages [M] were gradually replaced by proliferated connective tissue (e.g., thick wavy collagen fibers [arrows]). Mononuclear infiltrate [I] is present within the bundles of these fibers. (c) DAU3 group, grade 4: extensive fibrosis [arrows] in areas with myocytolysis and necrosis of cardiomyocytes. (d–f) Representative photomicrographs of renal damage. (d) DOX2 group, grade 1: initial renal tubular necrosis. Lesions of nephrosis with tubular degeneration [∗] are present. (e) DAU3 group, grade 4: focal severe nephropathy. Lesions of nephrosis with tubular degeneration [∗] and extensive necrosis [N] of tubular cells are frequent. Fibrosis [arrow] and mononuclear infiltrate [I] are present in these areas. (f) DAU3 group, grade 4: extensive fibrosis [arrows] in areas of toxic nephropathy with degenerations and tubular necrosis. (g–i) Representative photomicrographs of hepatic damage. (g) DOX2 group, grade 1: initial damage of the liver. Some hepatocytes show diffuse vacuoles inside cytoplasm [∗]. (h) DAU3 group, grade 4: hepatocytes revealed an extensive toxic damage. Necrotic hepatocytes are present [N] and abundant hepatocytes show numerous and extensive vacuoles inside cytoplasm [∗]. (i) DAU3 group, grade 4: diffuse fibrosis [arrows] in areas with necrotic hepatocytes. (a-b), (d-e), and (f-g): haematoxylin and eosin; (c), (f), and (i): Masson's blue trichrome.

lower number of animals required to complete a study (reduction), and reduced nonspecific toxicities translate into reduced unnecessary suffering and improved well-being of the rabbits throughout the study (refinement).

One of the salient findings of our study is that, in contrast to the high attrition rate associated with the protocols of induction used in DOX2 and DAU3 groups (Figure 2), the DAU4 group exhibited very low premature mortality (7.6%) during the induction period (with premature mortality defined as death of the animal during the course of weekly I.V. administrations on each group). DAU4 group also exhibited a significantly higher survival rate within two weeks after

completion of the induction protocol (Figure 2). Mortality associated with the induction of heart failure secondary to AICM in animal models using rabbits is rarely reported. Among the studies that do report mortality using protocols of induction similar to those employed in our DOX2 and DAU3 groups, the premature mortality is consistent with our findings (30–50%) [10, 14, 19]. The significantly lower mortality in DAU4 group compared to that of DAU3 could be in part attributable to the fact that whilst higher weekly doses were administered in DAU4 (3 mg/kg/week in DAU3 compared to 4 mg/kg/week in DAU4), these were administered over a shorter period of time (10 weeks in DAU3 versus 6 weeks in DAU4). This likely minimises the period of AC exposure, thus reducing the overall total cumulative dose at the end of the induction period (30 mg/kg in DAU3 group compared to 24 mg/kg in DAU4). This resulted in comparable myocardial damage between DAU4 group and DAU3 group, whilst it reduced extracardiac toxicity/compromise in DAU4 (see also relevant discussion below). Other protocols experimentally trialled by us (e.g., 6 mg/kg/week for 4-5 weeks) resulted in mortalities above 50%, primarily due to toxicity, and were therefore stopped for ethical reasons and deemed inadequate.

Another important finding of our study is that the induction protocol used in the DAU4 group is less prone to induce nonspecific toxicity such as nephrotoxicity and hepatotoxicity compared to the induction protocols used in the DOX2 and DAU3 groups. Thus, whilst the DAU4 group did not exhibit changes in renal or hepatic function, animals from the DOX2 and DAU3 groups presented changes in renal function suggestive of nephrotic syndrome. Similarly, the DAU3 group showed increased levels of AST and ALT, suggesting compromised liver function in this group. Taking into account these findings, it is likely that the high mortality rate observed in the DOX2 and DAU3 groups is, at least in part, explained by the increased incidence of nonspecific toxic effects also observed in these groups (see also relevant discussion below). The sensitivity to the nephrotoxic effects of AC in rodents, which is not observed in humans [18], has been extensively used as a model of nephrotic syndrome which replicates most of the pathological features of focal and segmental glomerulosclerosis seen in humans [26, 27]. The nephrotoxicity observed in the DOX2 and DAU3 groups is consistent with previous reports [10, 19, 28, 29]. Hepatotoxicity induced by doxorubicin in rabbits has been described previously in one report [20]; however, we did not find alterations in biochemical markers of liver function in the DOX2 group. Interestingly, previous studies that used a protocol of induction as in the DAU3 group in the present study did not report alterations in liver function tests [10, 19]. The reasons for these differences are unknown. Nevertheless, the changes in AST and ALT at the final time point in the DAU3 group suggest marked hepatocellular damage. Whilst this could be a consequence of direct AC-induced hepatotoxicity, other mechanisms could be partially responsible as well (see also relevant discussion below). Given the shorter period of exposure in the DAU4 group and the absence of nonspecific toxicities/compromise such as nephrotoxicity and hepatotoxicity as suggested by elevations in biomarkers of kidney and liver damage, it is reasonable to conclude that these toxicities are in part related to the length of exposure to AC, as opposed to cardiotoxicity, which is directly related to the cumulative dose received, although other potential explanations are also possible (see also relevant discussion below) [21].

In our study, haematological toxicity mostly affected red blood cells and was common to all groups of this study even though for most altered parameters this was transient since this was observed at the intermediate time point and recovered to normal or near normal levels at the final time point in the DOX2 and DAU4 groups, whilst it remained altered in the DAU3 group (Table 2). Haematological toxicity consistent with myelosuppression (i.e., reduced number of RBC, WBC, and platelets) has been reported previously in patients treated with AC [30, 31] and appears to be a common feature of many antineoplastic drugs [32]. We did not observe alterations in platelet count in any of the groups studied and only transient leukopenia in the DAU3 group, which is consistent with previous studies using protocols of induction similar to those used in the DAU3 group [10, 19]. The finding that this is also observed in the DAU4 group suggests that this toxicity is independent of the scheduled dosing of AC. Indeed, given the high activity of AC in haematological malignancies, this toxicity could be related to their therapeutic benefits [1, 2].

Evaluation of left ventricular function by echocardiography is a reliable noninvasive method for diagnosis of AICM, which has good correlation with invasive catheter-based functional analysis in rabbit models of AICM [10]. It is interesting to note that in this study the echocardiographic studies were planned and supervised by European board-certified veterinary cardiologists with extensive clinical experience, which adds value to the results and ensures the rigorousness of the studies. Monitoring of LVEF and FS demonstrated progressive reduction in these parameters only in the DAU3 and DAU4 groups. On the other hand, with the exception of a transient decline in LVEF at the intermediate time point (6 weeks) in animals of the DOX2 group, these parameters remained almost unchanged throughout the induction period, and none of the animals from this group developed overt DCM or CHF. This is in contrast to a previous study by Gava et al. who used an induction protocol as in the DOX2 group in our study, which found a progressive decline in both LVEF and FS from as early as 6 weeks [15]. Similar to our findings, another study, using even higher doses of doxorubicin (doxorubicin 3 mg/kg per week for 10 weeks), also failed to demonstrate significant changes in left ventricular function [19]. The reasons for these discrepancies are unknown at present, however, since our histopathological studies indicate that this group exhibited the lowest score of extension of myocardial damage (see also relevant discussion below); the cause of death in this group was exclusively due to systemic toxicity, and mortality in the study of Gava et al. was 70% (causes and timing of these deaths were not reported) as opposed to 50% in our study [15]; we suggest that this protocol of induction may not be suitable for exploring the potential benefits of novel therapies for HF secondary to AICM.

The incidence of overt DCM for the DAU3 and DAU4 groups was 66% and 92%, respectively, which ultimately translated to an incidence of CHF of 66% (group DAU3) and

61% (group DAU4). Of note, whilst the development of overt DCM and CHF in the DAU3 group was simultaneous in all cases, this was usually full blown severe CHF and very quickly (within a couple of days) resulted in the death of the animal, in contrast to a more insidious presentation in the DAU4 group, in which incidence of overt DCM was very high followed in most cases within days by CHF, which persisted for several weeks before death ensued. Other parameters of myocardial damage were also more exacerbated in DAU4 group. Thus, whilst an elevation of cTnI, a marker of myocardial cellular damage, was observed in all groups, much higher levels were detected in the DAU4 group at the final time point (Figure 3(d)). Of note, none of the differences observed in LVEF, FS, total CSA, or cTnI between DAU3 and DAU4 groups were statistically significant, despite a clear trend (Figure 3). Elevation of cTnI has been documented previously in rabbits treated with an induction protocol as in the DAU3 group in our study [33].

Histopathological examination revealed that whilst animals of all groups have a similar grade of myocardial lesions, these were more conspicuous in the DAU4 group, since the score of extension of lesions observed in this group was significantly higher than that in the other groups (Table 3). The histopathological findings of the heart, kidney, and liver in the DOX2 and DAU3 groups are consistent with previous reports [10, 15, 19]. Of note, despite marked elevations in surrogate biomarkers of renal injury in DOX2 and DAU3 groups and of liver injury in DAU3 group compared to DAU4 group and control group at final time point, the scores of kidney and liver lesions in grade and extension of damage amongst the AC treated groups were similar upon histopathological examination (Table 4). Whilst nephrotoxicity and hepatotoxicity have been described in rabbits treated with AC, these may not completely explain this lack of correlation between blood biomarkers and histopathology findings and it is worth elucubrating about other potential explanations. The rabbits from DOX2 group were greatly affected by general toxicity and exhibited the highest mortality (50%). Rabbits from this cohort were often observed to be asthenic, subsequently developed anorexia, and near the end of the protocol (or end of their life) appeared cachectic, which likely resulted from an increased catabolic state, leading to emaciation, a condition often associated with multisystem organ failure, including kidney damage. These observations could explain, at least in part, the elevated creatinine observed in this group. On the other hand, 66% of rabbits from DAU3 group developed overt DCM which was quickly followed by progression to a severe form of CHF, which resembled acute severe decompensated CHF, with death ensuing within days. Hepatic (retrograde) congestion could in part explain the increased elevations of ALT and AST. Hypoperfusion secondary to poor pump performance and neuroendocrine activation (which is more marked in some forms of CHF such as acute decompensated CHF) and associated peripheral and renal-splanchnic vasoconstriction could contribute to increased renal damage (even though renal damage secondary to CHF (cardiorenal syndrome) is multifactorial) [34] and thus explain to some extent elevated biomarkers of kidney injury (e.g., creatinine and BUN) in the setting of AC treatment in this group.

Some long-term association studies indicate that among childhood cancer survivors treated with AC girls appear to have increased risk of developing long-term AICM [35, 36]. Interestingly, amongst adults, men appear to be more sensitive than women to AICM [37]. Gender differences also appear to play a role in rodent models of AICM and AC nephropathy, with males and ovariectomized females being more affected than females [38–40]. Although evidence is still inconclusive, with recent metaregression analyses and association studies indicating that female sex is not a risk factor for AICM [41, 42], most of the current available evidence points to the conclusion that oestrogen could have a protective role in AICM. We did not find any clear difference attributable to gender in terms of mortality, incidence of overt DCM, or congestive heart failure, as suggested by a similar percentage of males and females from DAU3 and DAU4 groups being affected in the present study. Similarly, at the final time point, we did not find any significant differences in biomarkers of cardiac (i.e., LVEF, FS, total CSA, and cTnI levels), renal (e.g., creatinine and BUN), or hepatic (i.e., AST and ALT) function amongst males and females on each of the AC treated groups (Supplemental Table 1 and Supplemental Figure 1). Thus, in contrast to experimental studies in rodents, taken together, our data do not support a link between gender differences and AC toxic sensitivity in rabbits. Of note, beyond a clear AC mediated toxicity, our study was not powered to assess sex differences to AC sensitivity in the DAU3 group, thus limiting our conclusions in this respect.

Taken together, our results suggest that during the induction of AICM the overall extracardiac physiology of rabbits from DOX2 and DAU3 groups was more severely compromised compared to that of the rabbits from DAU4 group, whilst DAU4 induced comparable myocardial damage to that of DAU3 group (Figure 3). We believe that the refined induction protocol used in the DAU4 group could be better suited for evaluation of novel therapies (e.g., stem cell therapy) aimed at ameliorating the condition, given the high incidence of overt DCM and the insidious and more stable form of CHF that follows, which translates into increased survival at the end of the induction period. As a note added in proof, we have recently reported that, using the protocol of induction as in DAU4 group and successful induction of AICM, stem cell therapy with amniotic membrane-derived mesenchymal stem cells (AM-MSC), administered percutaneously via intramyocardial injection, significantly improved ventricular function at 2 and 4 weeks after transplant and also significantly improved survival compared with control group [43]. We also believe that the protocol used in DAU3 group is still very valuable in evaluation of novel cardioprotective drugs, aimed at preventing development AICM in the preclinical setting and serving as a model for the study of pathophysiological aspects of AICM.

5. Conclusion

Our results indicate that, compared to other protocols of induction of AICM (as in the DOX2 and DAU3 groups), a protocol using daunorubicin 4 mg/kg per week for 6 weeks (as in the DAU4 group) results in a high percentage of

animals with overt DCM (92%) and CHF (61%), with mild manifestations of nonspecific systemic compromise, very low premature mortality (7.6%) during the induction period, and low cumulative mortality within the two weeks after completion of the induction protocol, which translated into a significantly higher survival rate at this stage, whilst development of CHF was more insidious (compared to the DAU3 group, in which abrupt development of CHF was quickly followed by death of the animals). We propose that this refinement of the model of AICM in rabbits, which translates into a more predictable cardiotoxicity, represents a useful tool for the preclinical evaluation of novel therapies (e.g., drugs or stem cell therapy) for the treatment of heart failure secondary to AICM, as well as the study of the molecular mechanisms involved in the development of AICM. This refinement is also in line with the guidelines of the National Centre for the Replacement, Refinement and Reduction of Animals in Research and the 3Rs principles, since the reduced nonspecific toxicity and lower mortality would ultimately translate into improved overall well-being of the animals and reduced amount of animals required for this type of research. However, we believe that the protocol used in DAU3 group is still very valuable in evaluation of novel cardioprotective drugs, aimed at preventing development AICM in the preclinical setting, and for the study of the pathophysiology of AICM.

Abbreviations

AC: Anthracyclines
AICM: Anthracycline-induced cardiomyopathy
CHF: Congestive heart failure
DCM: Dilated cardiomyopathy
LVEF: Left ventricular ejection fraction
FS: Fractional shortening.

Disclosure

The funders had no role in study design, data collection and analysis, decision to publish, or preparation of the paper.

Conflict of Interests

The authors declare that there is no conflict of interests regarding the publication of this paper.

Authors' Contribution

Conception and design of study and this paper were by Jesús Talavera, Alejandro Giraldo, and Jose M. Moraleda. Conducting experiments and participating in data collection were by Jesús Talavera, Alejandro Giraldo, and María Josefa Fernández-Del Palacio. Histopathological study was by Obdulio García-Nicolás and Juan Seva. Data analyses were performed by Jesús Talavera and Alejandro Giraldo. Drafting of the paper was performed by Alejandro Giraldo, Jesús Talavera, and Gavin Brooks. Revision of the paper was performed by all authors. All authors gave final approval to the paper. The first two authors (Jesús Talavera and Alejandro Giraldo) contributed equally to this work.

Acknowledgments

The authors thank Giorgia Santarelli for the excellent research support provided during the collection of data. This study was supported by Fundación Séneca, Agencia de Ciencia y Tecnología, Región de Murcia, Spain (Jesús Talavera) (Grant no. 11935/PI/09), Red de Terapia Celular, ISCIII-Sub. Gral. Redes, VI PN de I+D+I 2008-2011 (Grant no. RD12/0019/0001) (José M. Moraleda), Cofinanciado con Fondos Estructurales de la Unión Europea (FEDER) (José M. Moraleda), and University of Reading, United Kingdom (Alejandro Giraldo and Gavin Brooks) (central funding).

References

[1] G. Minotti, P. Menna, E. Salvatorelli, G. Cairo, and L. Gianni, "Anthracyclines: molecular advances and pharmacologic developments in antitumor activity and cardiotoxicity," *Pharmacological Reviews*, vol. 56, no. 2, pp. 185–229, 2004.

[2] P. K. Singal and N. Iliskovic, "Doxorubicin-induced cardiomyopathy," *The New England Journal of Medicine*, vol. 339, no. 13, pp. 900–905, 1998.

[3] J. R. Carver, C. L. Shapiro, A. Ng et al., "American society of clinical oncology clinical evidence review on the ongoing care of adult cancer survivors: cardiac and pulmonary late effects," *Journal of Clinical Oncology*, vol. 25, no. 25, pp. 3991–4008, 2007.

[4] A. Verdecchia, S. Francisci, H. Brenner et al., "Recent cancer survival in Europe: a 2000-02 period analysis of EUROCARE-4 data," *The Lancet Oncology*, vol. 8, no. 9, pp. 784–796, 2007.

[5] S. M. Pogwizd and D. M. Bers, "Rabbit models of heart disease," *Drug Discovery Today: Disease Models*, vol. 5, no. 3, pp. 185–193, 2008.

[6] R. Maral, G. Bourat, R. Ducrot et al., "Toxicologic study and experimental antitumor activity of rubidomycin," *Pathologie et Biologie*, vol. 15, pp. 903–908, 1967.

[7] R. S. Jaenke, "Delayed and progressive myocardial lesions after adriamycin administration in the rabbit," *Cancer Research*, vol. 36, no. 8, pp. 2958–2966, 1976.

[8] E. H. Herman, V. J. Ferrans, W. Jordan, and B. Ardalan, "Reduction of chronic daunorubicin cardiotoxicity by ICRF-187 in rabbits," *Research Communications in Chemical Pathology and Pharmacology*, vol. 31, no. 1, pp. 85–97, 1981.

[9] E. H. Herman and V. J. Ferrans, "Pretreatment with ICRF-187 provides long-lasting protection against chronic daunorubicin cardiotoxicity in rabbits," *Cancer Chemotherapy and Pharmacology*, vol. 16, no. 2, pp. 102–106, 1986.

[10] T. Šimůnek, I. Klimtová, J. Kaplanová et al., "Rabbit model for in vivo study of anthracycline-induced heart failure and for the evaluation of protective agents," *European Journal of Heart Failure*, vol. 6, no. 4, pp. 377–387, 2004.

[11] O. Popelová, M. Sterba, P. Haková et al., "Dexrazoxane-afforded protection against chronic anthracycline cardiotoxicity in vivo: effective rescue of cardiomyocytes from apoptotic cell death," *British Journal of Cancer*, vol. 101, no. 5, pp. 792–802, 2009.

[12] O. Popelova, M. Sterba, T. Simunek et al., "Deferiprone does not protect against chronic anthracycline cardiotoxicity in vivo," *Journal of Pharmacology and Experimental Therapeutics*, vol. 326, no. 1, pp. 259–269, 2008.

[13] A. Vávrová, O. Popelová, M. Štěrba et al., "In vivo and in vitro assessment of the role of glutathione antioxidant system in anthracycline-induced cardiotoxicity," *Archives of Toxicology*, vol. 85, no. 5, pp. 525–535, 2011.

[14] M. Chen, Z.-C. Fan, X.-J. Liu et al., "Effects of autologous stem cell transplantation on ventricular electrophysiology in doxorubicin-induced heart failure," *Cell Biology International*, vol. 30, no. 7, pp. 576–582, 2006.

[15] F. N. Gava, E. Zacché, E. M. G. Ortiz et al., "Doxorubicin induced dilated cardiomyopathy in a rabbit model: an update," *Research in Veterinary Science*, vol. 94, no. 1, pp. 115–121, 2013.

[16] N. Engberding, S. Spiekermann, A. Schaefer et al., "Allopurinol attenuates left ventricular remodeling and dysfunction after experimental myocardial infarction: a new action for an old drug?" *Circulation*, vol. 110, no. 15, pp. 2175–2179, 2004.

[17] D. Deprez-DeCampeneere, R. Jaenke, and A. Trouet, "Comparative cardiac and renal toxicity of daunorubicin in the rat and rabbit," *Cancer Treatment Reports*, vol. 66, no. 2, pp. 395–397, 1982.

[18] E. H. Herman and V. J. Ferrans, "Preclinical animal models of cardiac protection from anthracycline-induced cardiotoxicity," *Seminars in Oncology*, vol. 25, no. 4, pp. 15–21, 1998.

[19] I. Klimtová, T. Šimůnek, Y. Mazurová, R. Hrdina, V. Geršl, and M. Adamcová, "Comparative study of chronic toxic effects of daunorubicin and doxorubicin in rabbits," *Human & Experimental Toxicology*, vol. 21, no. 12, pp. 649–657, 2002.

[20] J. F. Van Vleet and V. J. Ferrans, "Clinical and pathologic features of chronic adriamycin toxicosis in rabbits," *American Journal of Veterinary Research*, vol. 41, no. 9, pp. 1462–1469, 1980.

[21] S. M. Swain, F. S. Whaley, and M. S. Ewer, "Congestive heart failure in patients treated with doxorubicin," *Cancer*, vol. 97, no. 11, pp. 2869–2879, 2003.

[22] D. J. Sahn, A. DeMaria, J. Kisslo, and A. Weyman, "Recommendations regarding quantitation in M-mode echocardiography: results of a survey of echocardiographic measurements," *Circulation*, vol. 58, no. 6, pp. 1072–1083, 1978.

[23] W. P. Thomas, C. E. Gaber, G. J. Jacobs et al., "Recommendations for standards in transthoracic two-dimensional echocardiography in the dog and cat. Echocardiography Committee of the Specialty of Cardiology, American College of Veterinary Internal Medicine," *Journal of Veterinary Internal Medicine*, vol. 7, no. 4, pp. 247–252, 1993.

[24] K. E. Quesenberry, *Saunders Manual of Small Animal Practice*, W.B. Saunders Company, Philadelphia, Pa, USA, 1994.

[25] L. Gianni, E. H. Herman, S. E. Lipshultz, G. Minotti, N. Sarvazyan, and D. B. Sawyer, "Anthracycline cardiotoxicity: from bench to bedside," *Journal of Clinical Oncology*, vol. 26, no. 22, pp. 3777–3784, 2008.

[26] S. Okuda, Y. Oh, H. Tsuruda, K. Onoyama, S. Fujimi, and M. Fujishima, "Adriamycin-induced nephropathy as a model of chronic progressive glomerular disease," *Kidney International*, vol. 29, no. 2, pp. 502–510, 1986.

[27] H.-F. Liu, L.-Q. Guo, Y.-Y. Huang et al., "Thiazolidinedione attenuate proteinuria and glomerulosclerosis in Adriamycin-induced nephropathy rats via slit diaphragm protection," *Nephrology*, vol. 15, no. 1, pp. 75–83, 2010.

[28] O. A. Badary, A. B. Abdel-Naim, M. H. Abdel-Wahab, and F. M. A. Hamada, "The influence of thymoquinone on doxorubicin-induced hyperlipidemic nephropathy in rats," *Toxicology*, vol. 143, no. 3, pp. 219–226, 2000.

[29] N. R. Bachur, R. C. Hildebrand, and R. S. Jaenke, "Adriamycin and daunorubicin disposition in the rabbit," *Journal of Pharmacology and Experimental Therapeutics*, vol. 191, no. 2, pp. 331–340, 1974.

[30] S. L. Curry, H. B. Muss, J. A. Blessing, and J. Arseneau, "Hematologic monitoring in patients with cancer. A study of the Gynecologic Oncology Group," *American Journal of Clinical Oncology*, vol. 10, no. 2, pp. 163–166, 1987.

[31] G. Falkson, B. Klein, and H. Falkson, "Hematological toxicity: experience with anthracyclines and anthracenes," *Experimental Hematology*, vol. 13, supplement 16, pp. 64–71, 1985.

[32] J. N. Barreto, K. B. McCullough, L. L. Ice, and J. A. Smith, "Antineoplastic agents and the associated myelosuppressive effects: a review," *Journal of Pharmacy Practice*, vol. 27, no. 5, pp. 440–446, 2014.

[33] M. Štěrba, O. Popelová, J. Lenčo et al., "Proteomic insights into chronic anthracycline cardiotoxicity," *Journal of Molecular and Cellular Cardiology*, vol. 50, no. 5, pp. 849–862, 2011.

[34] P. P. Liu, "Cardiorenal syndrome in heart failure: a cardiologist's perspective," *Canadian Journal of Cardiology*, vol. 24, supplement B, pp. 25B–29B, 2008.

[35] S. E. Lipshultz, S. R. Lipsitz, S. M. Mone et al., "Female sex and higher drug dose as risk factors for late cardiotoxic effects of doxorubicin therapy for childhood cancer," *The New England Journal of Medicine*, vol. 332, no. 26, pp. 1738–1743, 1995.

[36] M. Amigoni, C. Giannattasio, D. Fraschini et al., "Low anthracyclines doses-induced cardiotoxicity in acute lymphoblastic leukemia long-term female survivors," *Pediatric Blood & Cancer*, vol. 55, no. 7, pp. 1343–1347, 2010.

[37] O. Hequet, Q. H. Le, I. Moullet et al., "Subclinical late cardiomyopathy after doxorubicin therapy for lymphoma in adults," *Journal of Clinical Oncology*, vol. 22, no. 10, pp. 1864–1871, 2004.

[38] J. Zhang, A. Knapton, S. E. Lipshultz, T. R. Cochran, H. Hiraragi, and E. H. Herman, "Sex-related differences in mast cell activity and doxorubicin toxicity: a study in spontaneously hypertensive rats," *Toxicologic Pathology*, vol. 42, no. 2, pp. 361–375, 2014.

[39] M. M. Freeland, J. Angulo, A. L. Davis et al., "Sex differences in improved efficacy of doxorubicin chemotherapy in Cbr1+/– mice," *Anti-Cancer Drugs*, vol. 23, no. 6, pp. 584–589, 2012.

[40] M. Moulin, J. Piquereau, P. Mateo et al., "Sexual dimorphism of doxorubicin-mediated cardiotoxicity: potential role of energy metabolism remodeling," *Circulation: Heart Failure*, vol. 8, no. 1, pp. 98–108, 2015.

[41] M. Lotrionte, G. Biondi-Zoccai, A. Abbate et al., "Review and meta-analysis of incidence and clinical predictors of anthracycline cardiotoxicity," *The American Journal of Cardiology*, vol. 112, no. 12, pp. 1980–1984, 2013.

[42] J. G. Blanco, C.-L. Sun, W. Landier et al., "Anthracycline-related cardiomyopathy after childhood cancer: role of polymorphisms in carbonyl reductase genes—a report from the Children's Oncology Group," *Journal of Clinical Oncology*, vol. 30, no. 13, pp. 1415–1421, 2012.

[43] A. Giraldo, J. Talavera, M. J. Fernandez-Del-Palacio et al., "Percutaneous intramyocardial injection of amniotic membrane-derived mesenchymal stem cells improves ventricular function and survival in non-ischaemic cardiomyopathy in rabbits," *European Heart Journal*, vol. 36, p. 149, 2015.

Hindawi Publishing Corporation
BioMed Research International
Volume 2015, Article ID 467597, 7 pages
http://dx.doi.org/10.1155/2015/467597

Review Article

Relevance of the Carotid Body Chemoreflex in the Progression of Heart Failure

David C. Andrade,[1] Claudia Lucero,[1] Camilo Toledo,[1] Carlos Madrid,[2] Noah J. Marcus,[3] Harold D. Schultz,[4] and Rodrigo Del Rio[1,5]

[1]*Laboratory of Cardiorespiratory Control, Center of Biomedical Research, Universidad Autónoma de Chile, 8900000 Santiago, Chile*
[2]*Centro de Fisiología Celular e Integrativa, Clínica Alemana-Universidad del Desarrollo, 7500000 Santiago, Chile*
[3]*Department of Physiology and Pharmacology, Des Moines University, Des Moines, IA 50312, USA*
[4]*Department of Cellular & Integrative Physiology, University of Nebraska Medical Center, Omaha, NE 68198, USA*
[5]*Dirección de Investigación, Universidad Científica del Sur, Lima 15067, Peru*

Correspondence should be addressed to Rodrigo Del Rio; rodrigo.delrio@uautonoma.cl

Received 22 July 2015; Accepted 8 October 2015

Academic Editor: Peter M. Becher

Chronic heart failure (CHF) is a global health problem affecting millions of people. Autonomic dysfunction and disordered breathing patterns are commonly observed in patients with CHF, and both are strongly related to poor prognosis and high mortality risk. Tonic activation of carotid body (CB) chemoreceptors contributes to sympathoexcitation and disordered breathing patterns in experimental models of CHF. Recent studies show that ablation of the CB chemoreceptors improves autonomic function and breathing control in CHF and improves survival. These exciting findings indicate that alterations in CB function are critical to the progression of CHF. Therefore, better understanding of the physiology of the CB chemoreflex in CHF could lead to improvements in current treatments and clinical management of patients with CHF characterized by high chemosensitivity. Accordingly, the main focus of this brief review is to summarize current knowledge of CB chemoreflex function in different experimental models of CHF and to comment on their potential translation to treatment of human CHF.

1. Introduction

Chronic heart failure (CHF) is a disease condition characterized by high mortality, frequent hospitalizations, poor quality of life, multiple comorbidities, and complex therapeutic management [1]. Accordingly, CHF is considered a major public health problem throughout the world [2]. In addition, it has been estimated that approximately 20% of the worldwide population will suffer a certain degree of cardiac failure at some point in their lifetime [3].

CHF is characterized by a progressive decrease in cardiac function, which severely impacts blood and oxygen supply to several organs [4–6]. Two pathophysiological hallmarks of CHF are the presence of autonomic imbalance and disordered breathing patterns, both of which are strongly related to the progression of the disease [7–10]. In addition, a heightened carotid body (CB) chemoreflex drive has been shown to play a pivotal role in the development of cardiorespiratory disorders in CHF [11, 12].

Remarkably, it has been shown that CHF patients with an enhanced CB chemoreflex sensitivity have significantly higher mortality rates compared to patients with normal CB chemoreflex sensitivity [12]. In experimental CHF, Del Rio et al. (2013) [13] has shown that elimination of the CB chemoreflex markedly attenuated deterioration of cardiac function and improved survival. Together, these results strongly support a crucial role of the CB chemoreflex in the progression of CHF. The physiological mechanisms related to heightened CB chemoreflex drive in CHF and its deleterious effects are not completely known. Therefore, understanding the contribution of the CB chemoreflex in the pathophysiology of CHF is important to improve current treatments

Table 1: Incidence of autonomic imbalance, breathing disorders and carotid body chemoreflex potentiation in experimental CHF.

	Autonomic imbalance	Breathing disorders	Altered CB chemoreflex	References
MI-CHF	•	•	•	[13]
RP-CHF	•	•	•	[35]
AB-CHF	•	—	—	[39]
G-CHF	•	•	•	[41]
ACS-CHF	•	—	—	[44]

•: described in the literature; —: not described in the literature. MI-CHF: myocardial infarct chronic heart failure; RP-CHF: rapid pacing chronic heart failure; AB-CHF: aortic banding chronic heart failure; G-CHF: genetic chronic heart failure; ACS-CHF: aortocaval shunt chronic heart failure.

and clinical management of CHF patients and to further develop new therapeutic strategies intended to normalize CB chemoreflex function in CHF. Accordingly, the main focus of this review is to summarize current knowledge of CB chemoreflex function in several CHF models and comment on the potential translational significance to human CHF.

2. Carotid Body Chemoreflex and Heart Failure

The CB are the main arterial chemoreceptors involved in cardiovascular and ventilatory adjustments following changes in blood levels of O_2, CO_2, pH, and blood flow [14–17]. The CB is organized in clusters of chemoreceptor cells (type I) in charge of sensing bloodstream stimuli, which are surrounded by sustentacular glial cells (type II). The current model of CB chemotransduction theorizes that a chemoreceptor stimulus elicits depolarization of the glomus cells which in turn triggers an increase in $[Ca^{2+}]_i$ and the release of several neurotransmitters which act on sensory nerve endings projecting centrally from the petrosal ganglion [18]. Chemosensory nerve fibers from the CB project to the nucleus tractus solitarius (NTS), which integrates the CB afferent input [19–21]. Central CB chemoreflex integration takes place in the NTS which in turn sends projections to the respiratory neuronal network and key autonomic nuclei in the brainstem, such as the rostral ventrolateral medulla (RVLM) [22]. In experimental CHF, CB chemoreceptors become tonically active resulting in hyper-activation of RVLM presympathetic neurons and subsequent increases in sympathetic outflow [9, 23].

Importantly, CB chemoreflex activation in CHF is associated with the severity of the disease [12]. Recent studies using selective ablation of the CB chemoreceptors indicate that the CB chemoreflex plays a pivotal role in the cardiorespiratory alterations in experimental CHF [9, 24]. To date, several experimental models of CHF have been used to characterize the molecular and physiological pathways associated with tonic activation of the CB chemoreflex in CHF and its influence on disease progression.

3. Experimental Heart Failure Models

There are numerous experimental models of CHF that recapitulate many of the pathophysiological abnormalities that occur in human CHF (Table 1). While murine models are the most widely used, rabbits, sheep, and dogs have also been used to study CHF. In the paragraphs to follow we review what is known about the role of CB chemoreflex function in autonomic and respiratory alterations. Also, we discuss the potential mechanisms related to the development of heightened CB chemosensory function in CHF.

3.1. Myocardial Infarction Model. In the myocardial infarction-induced CHF model (MI-CHF), heart failure is generated through the surgical induction of ischemia in cardiac tissue. Two experimental approaches have been used. The first approach is characterized by electrocauterization of the epicardial surface to induce small focal infarctions [25]. The second and more frequently used experimental approach requires ligation of the descending coronary artery [26]. It has been shown that MI-CHF rats display an increase CB chemoreflex and CB chemoreceptor activity within 6–8 weeks of infarction [9, 27]. In addition, MI-CHF rats develop autonomic imbalance characterized by changes in heart rate variability, increased renal sympathetic nerve activity, and increases in circulating norepinephrine levels (Table 2) [28–30]. Moreover, an increased incidence of respiratory disorders is also observed in MI-CHF rats (Table 3) [31]. Importantly, Del Rio et al. (2013) [13] showed for the first time that selective bilateral CB denervation in MI-CHF rats decreased the activity of presympathetic neurons of the RVLM, reversed autonomic imbalance, and markedly reduced mortality risk. Taken together, these findings indicate that CB chemoreflex plays an important role in the pathophysiology of the MI-CHF model.

3.2. Rapid Ventricular Pacing Model. The rapid-pacing CHF (RP-CHF) model is characterized by a tachycardia-induced cardiomyopathy. This CHF model produces elevated ventricular filling pressures and reduced systolic and diastolic ventricular function. Additionally, this model is associated with intense neurohumoral activation and disordered breathing patterns (Shinbane et al. 1997) [32]. Sun et al. (1999) [23] showed that 3 weeks of rapid pacing was necessary to induce CHF in rabbits. Li et al. (2005) [33] showed that RP-CHF rabbits displayed enhanced CB chemoreflex function evidenced by increases in both sympathetic nerve activity [33] and ventilatory responses to acute hypoxic stimulation [34]. Additionally, cardiac autonomic imbalance was also shown in this model by means of reductions in the total power of heart rate variability (Table 2) [35]. Recently,

Table 2: Hemodynamic, autonomic balance, and baroreflex function in CHF models.

	Hemodynamic		Autonomic balance			Baroreflex		References
	BP	HR	U-NE	HRV	Blockers	Oxford	BRS	
MI-CHF	—	—	↑	↓	Symp. ↑ Parasymp. ↓	↓	↓	[13, 55, 61]
RP-CHF	↓	↑	↑	↓	Symp. ↑ Parasymp. ↓	—	↓	[33–35, 61, 62]
AB-CHF	↑	↑	↑	ND	—	ND	—	[39]
G-CHF	ND	—	ND	↓	ND	ND	ND	[41]
ACS-CHF	↓	—	↑	ND	ND	↓	ND	[39, 42]

BP: blood pressure; HR: heart rate; HRV: heart rate variability; U-NE: urinary norepinephrine; Blockers: Propranolol/Atropine test; Oxford: baroreflex test address by phenylephrine and sodium nitroprusside i.v. infusion; BRS: spontaneous baroreflex sensitivity; ND: not described; ↑: increased; ↓: decreased; and —: without difference compared to control healthy condition. MI-CHF: myocardial infarct chronic heart failure; RP-CHF: rapid pacing chronic heart failure; AB-CHF: aortic banding chronic heart failure; G-CHF: genetic chronic heart failure; ACS-CHF: aortocaval shunt chronic heart failure.

Table 3: Periodic breathing, breathing irregularity, and apnea/hypopnea score in experimental CHF.

	Periodic breathing	Breathing irregularities	Apnea/hypopnea index	References
MI-CHF	ND	↑	↑	[26]
RP-CHF	↑	↑	↑	[35]
AB-CHF	ND	ND	ND	
G-CHF	ND	↑	↑	[41]
ACS-CHF	ND	ND	ND	

ND: not described; ↑: increased; ↓: decreased; and —: without difference compared to control healthy condition. MI-CHF: myocardial infarct chronic heart failure; RP-CHF: rapid pacing chronic heart failure; AB-CHF: aortic banding chronic heart failure; G-CHF: genetic chronic heart failure; ACS-CHF: aortocaval shunt chronic heart failure.

Marcus et al. (2014) [24] provided compelling evidence that the CB chemoreceptors play a pivotal role in the progression of RP-CHF. In this model, CB denervation performed after the development of CHF significantly reduced renal sympathetic nerve activity and incidence of disordered breathing patterns, restored cardiac autonomic balance, and reduced exaggerated respiratory-sympathetic coupling (Table 3) [10, 24].

3.3. Ascending Aortic Constriction Model. Banding of the ascending aorta is an experimental technique to produce a pressure-overload form of CHF (AB-CHF). This surgical approach requires reducing aortic diameter by tying a suture around the ascending aorta [36]. Banded animals develop hypertension and left ventricular hypertrophy. After 18 weeks, the banded animals have clear signs of CHF [37]. The CB chemoreflex has not been studied in AB-CHF animals; however it has been shown that hypoxic stimulation induced an increase in the left ventricular end diastolic pressure [38]. This result suggests that CB activation may play a role in the regulation of cardiac function in AB-CHF. In addition, results showing that AB-CHF rats displayed an increased renal sympathetic nerve activity in response to hypercapnic stimulation suggest a plausible contribution of central and/or CB chemoreflex pathways in the regulation of sympathetic outflow [39]. Further studies are needed to determine if the CB chemoreflex pathway plays any role in the progression of AB-CHF.

3.4. Dilated Cardiomyopathy Genetic Model. Genetic models of CHF are less common; however one genetic CHF model (G-CHF) expresses a dominant-negative form of the basic leucine zipper CREB transcription factor $CREB_{A133}$ ($Ser\text{-}Ala^{133}$) [40]. Mutant mice showed clear signs of CHF with the presence of cardiac hypertrophy and neurohumoral activation. Importantly, G-CHF mice showed an increased CB chemoreceptor activity and chemoreflex response to hypoxia [41]. Additionally, breathing regularity was markedly impaired compared to the ventilatory rhythm observed in normal mice (Table 3). Also, G-CHF mice displayed ventricular arrhythmias that were normalized by denervation of the CB chemoreceptors [41]. This result strongly suggests that the CB chemoreflex contributes to the development of cardiac arrhythmias.

3.5. Aorto-Caval Shunt Model. Volume overload is commonly used to induce CHF with preserved ejection fraction [42]. The most used animal model is the aorto-caval shunt CHF model (ACS-CHF). Here an arteriovenous shunt is surgically created between the inferior vena cava and the abdominal aorta to induce a significant cardiac volume overload [43]. This experimental approach leads to diastolic CHF and is characterized by neurohumoral activation and sympathetic hyperactivity (Table 2) [44]. The contribution of the CB chemoreflex in the development of cardiorespiratory impairment in ACS-CHF has not previously been studied. Kristen et al. (2002) [39] showed that hypercapnic stimulation

triggered a modest sympathetic response in rats with ACS-CHF. This result suggests that central and/or CB chemoreceptors may regulate autonomic balance in ACS-CHF. To date, breathing instability has not been evaluated in this model (Table 3). Future studies should focus on the understanding of the contribution of the CB and central chemoreceptors in the progression of autonomic imbalance in ACS-CHF.

4. Mechanisms of Altered Carotid Body Function in CHF

While the mechanisms underpinning CB potentiation in CHF are not fully understood it has been widely accepted that angiotensin peptides and oxidative stress both play a major role in the enhanced CB chemoreflex drive observed in CHF (for review see [45–48]). Circulating angiotensin II (AngII) levels are significantly higher during the progression of CHF. In addition, the presence of a local angiotensin production system in the CB has been described [47] and could contribute as well. In support of this notion, AngII levels are higher in the CBs from CHF rabbits compared to controls [33]. It has been proposed that AngII could alter CB function in CHF by altering redox balance, as increased circulating or local AngII could increase production of superoxide ($O_2^{\bullet-}$) radical via activation of the $AT1_R$ [33]. Indeed, it has been shown that $AT1_R$ blockers effectively reduced CB afferent activity in CHF [33]. The mechanisms that subsided the effects of AngII on CB function have been related to NADPH oxidase-dependent $O_2^{\bullet-}$ production since application of phenylarsine oxide (an NADPH oxidase inhibitor) significantly reduced CB chemosensory afferent activity [49]. Furthermore, the molecular mechanism that relates AngII with changes in CB chemoreceptor cell excitability has also been described [50]. In CHF, increases in AngII-dependent oxidative stress inhibit voltage gated K^+ channels and depolarize CB glomus cells [50]. In addition to increases in prooxidant factors, during CHF the CBs also undergo a marked reduction in the expression of antioxidant enzymes. Indeed, CuZn- and Mn-SOD enzymes, two important cellular scavenger of $O_2^{\bullet-}$ [51], have been shown to be downregulated in the CB from CHF rabbits [52]. Accordingly, *in vivo* CB transfection with CuZn- and Mn-SOD transgenes restores normal CB chemoreceptor cells excitability by normalizing resting membrane potential to values comparable to the ones obtained in control CBs [53]. Taken together, these findings show that AngII and oxidative stress contribute to altered CB function in CHF.

In addition to AngII, endothelin 1 (ET-1), another potent vasoactive peptide, has been shown to be constitutively expressed within the CB tissue along with its type A (ET-A_R) and B (ET-A_R) receptor [54–56]. Furthermore, ET-1 mediated signaling through the ET-A_R has been shown to enhance the CB afferent activity [54]. Moreover, in intermittent hypoxia mimicking obstructive sleep apnea (OSA) model, ET-1 and ET-A_R have been shown to mediate CB chemosensory potentiation [54, 55]. Interestingly, OSA and CHF are both characterized by the presence of an enhanced CB afferent activity and autonomic imbalance [27, 57]. Despite this evidence, the contribution of ET-1 and endothelin receptors in CHF has not been studied. However, ET-1 levels have been found to be increased in the plasma of CHF patients [58]. Therefore, it is plausible that increased ET-1 levels in experimental CHF could also play a role in enhancing CB chemosensory afferent activity. Further studies are needed to uncover the role of ET-1 on CB chemosensory function in CHF.

Recently, a CB type II cell-dependent modulation of glomus cell function has also been described [59, 60]. This novel mechanism seems to be related to the activation of the type II cell and the further paracrine secretion of the putative neurotransmitter ATP to the vicinity of glomus cells and sensory nerve endings [60]. Interestingly, type II cells as well as glomus cells display $AT1_R$ expression [59]. Then, it is plausible that local and/or systemic increases in AngII levels during the progression of CHF could activate type II cells causing ATP release and chemosensory excitation. Future studies should focus on the role of CB type II cells in the augmented CB chemosensory afferent activity during CHF.

5. Conclusions and Perspective

CHF is characterized by sympathetic hyperactivity independent of the etiology of the cardiac failure. In addition, it has been shown that a significant proportion of CHF patients displays elevated CB chemoreflex drive [12]. Several CHF experimental models also display heightened CB chemoreflex drive, and this is positively correlated with the severity of the disease. Recent exciting studies indicate that ablation of the CB chemoreceptors not only improves autonomic function and reduces disordered breathing patterns in experimental CHF but also improves survival. More importantly, Niewiński et al. (2013) [53] has recently shown the relevance of the CBs in human CHF. In a pilot study with one CHF patient (NYHA class II) they show that CB denervation is an effective therapeutic strategy to reduce the progression of the disease. Two and six months after CB denervation the patient showed clear signs of an improvement in autonomic control (total heart rate variability and baroreflex gain), sleep breathing disorders (apnea/hypopnea score), exercise tolerance, and an important improvement in his quality of life [51]. Together, preclinical and clinical studies unveil the relevance of the CB chemoreflex in the progression of systolic CHF. These findings raise the question of whether the CB chemoreflex should be tested in all forms of CHF (i.e., systolic versus diastolic). Unfortunately, CB chemoreflex function has not been investigated in experimental models of diastolic CHF. Taking into account the impressive results of previous studies showing the benefits of CB denervation in experimental and human systolic CHF, future studies addressing the role of the CB in the progression of autonomic imbalance and disordered breathing patterns in nonsystolic CHF are important for the development of future strategies intended to improve quality of life and survival in these patient populations.

Conflict of Interests

The authors declare that they have no conflict of interests.

Acknowledgments

Rodrigo Del Rio is supported by Fondo de Desarrollo Cientifico y Tecnologico (Fondecyt #1140275) and Harold D. Schultz is supported by a Program Project Grant from the Heart, Lung and Blood Institute of NIH (PO1-HL62222).

References

[1] Heart Failure Society of America, "Executive Summary: HFSA 2010 Comprehensive Heart Failure Practice Guideline," *Journal of Cardiac Failure*, vol. 16, no. 6, pp. 475–539, 2010.

[2] W. J. Remme and K. Swedberg, "Guidelines for the diagnosis and treatment of chronic heart failure. The Task Force for the Diagnosis and Treatment of Chronic Heart Failure of the European Society of Cardiology," *European Heart Journal*, vol. 22, no. 17, pp. 1527–1560, 2001.

[3] D. M. Lloyd-Jones, M. G. Larson, E. P. Leip et al., "Lifetime risk for developing congestive heart failure: the Framingham Heart study," *Circulation*, vol. 106, no. 24, pp. 3068–3072, 2002.

[4] P. J. Hanly and N. S. Zuberi-Khokhar, "Increased mortality associated with Cheyne-Stokes respiration in patients with congestive heart failure," *American Journal of Respiratory and Critical Care Medicine*, vol. 153, no. 1, pp. 272–276, 1996.

[5] J. N. Cohn, R. Ferrari, and N. Sharpe, "Cardiac remodeling-concepts and clinical implications: a consensus paper from an international forum on cardiac remodeling," *Journal of the American College of Cardiology*, vol. 35, no. 3, pp. 569–582, 2000.

[6] M. A. Pfeffer and E. Braunwald, "Ventricular remodeling after myocardial infarction. Experimental observations and clinical implications," *Circulation*, vol. 81, no. 4, pp. 1161–1172, 1990.

[7] G. S. Francis, "The relationship of the sympathetic nervous system and the renin-angiotensin system in congestive heart failure," *American Heart Journal*, vol. 118, no. 3, pp. 642–648, 1989.

[8] J. Holtz, "Pathophysiology of heart failure and the renin-angiotensin-system," *Basic Research in Cardiology*, vol. 88, 1, pp. 183–201, 1993.

[9] R. Del Rio, "The carotid body and its relevance in pathophysiology," *Experimental Physiology*, vol. 100, no. 2, pp. 121–123, 2015.

[10] N. J. Marcus, R. Del Rio, and H. D. Schultz, "Central role of carotid body chemoreceptors in disordered breathing and cardiorenal dysfunction in chronic heart failure," *Frontiers in Physiology*, vol. 5, article 438, 2014.

[11] P. Ponikowski, T. P. Chua, S. D. Anker et al., "Peripheral chemoreceptor hypersensitivity: an ominous sign in patients with chronic heart failure," *Circulation*, vol. 104, no. 5, pp. 544–549, 2001.

[12] A. Giannoni, M. Emdin, F. Bramanti et al., "Combined increased chemosensitivity to hypoxia and hypercapnia as a prognosticator in heart failure," *Journal of the American College of Cardiology*, vol. 53, no. 21, pp. 1975–1980, 2009.

[13] R. Del Rio, N. J. Marcus, and H. D. Schultz, "Carotid chemoreceptor ablation improves survival in heart failure: rescuing autonomic control of cardiorespiratory function," *Journal of the American College of Cardiology*, vol. 62, no. 25, pp. 2422–2430, 2013.

[14] H. D. Schultz and S.-Y. Sun, "Chemoreflex function in heart failure," *Heart Failure Reviews*, vol. 5, no. 1, pp. 45–56, 2000.

[15] R. Iturriaga, D. C. Andrade, and R. Del Rio, "Enhanced carotid body chemosensory activity and the cardiovascular alterations induced by intermittent hypoxia," *Frontiers in Physiology*, vol. 5, article 468, 2014.

[16] Y. Ding, Y.-L. Li, and H. D. Schultz, "Role of blood flow in carotid body chemoreflex function in heart failure," *The Journal of Physiology*, vol. 589, part 1, pp. 245–258, 2011.

[17] C. Gonzalez, L. Almaraz, A. Obeso, and R. Rigual, "Carotid body chemoreceptors: from natural stimuli to sensory discharges," *Physiological Reviews*, vol. 74, no. 4, pp. 829–898, 1994.

[18] R. Iturriaga and J. Alcayaga, "Neurotransmission in the carotid body: transmitters and modulators between glomus cells and petrosal ganglion nerve terminals," *Brain Research Reviews*, vol. 47, no. 1–3, pp. 46–53, 2004.

[19] V. J. Dzau, W. S. Colucci, N. K. Hollenberg, and G. H. Williams, "Relation of the renin-angiotensin-aldosterone system to clinical state in congestive heart failure," *Circulation*, vol. 63, no. 3, pp. 645–651, 1981.

[20] E. E. Benarroch, "Neuropeptides in the sympathetic system: presence, plasticity, modulation, and implications," *Annals of Neurology*, vol. 36, no. 1, pp. 6–13, 1994.

[21] A. C. P. Barretto, A. C. Santos, R. Munhoz et al., "Increased muscle sympathetic nerve activity predicts mortality in heart failure patients," *International Journal of Cardiology*, vol. 135, no. 3, pp. 302–307, 2009.

[22] S. B. G. Abbott, S. D. DePuy, T. Nguyen, M. B. Coates, R. L. Stornetta, and P. G. Guyenet, "Selective optogenetic activation of rostral ventrolateral medullary catecholaminergic neurons produces cardiorespiratory stimulation in conscious mice," *The Journal of Neuroscience*, vol. 33, no. 7, pp. 3164–3177, 2013.

[23] S.-Y. Sun, W. Wang, I. H. Zucker, and H. D. Schultz, "Enhanced activity of carotid body chemoreceptors in rabbits with heart failure: role of nitric oxide," *Journal of Applied Physiology*, vol. 86, no. 4, pp. 1273–1282, 1999.

[24] N. J. Marcus, R. Del Rio, E. P. Schultz, X.-H. Xia, and H. D. Schultz, "Carotid body denervation improves autonomic and cardiac function and attenuates disordered breathing in congestive heart failure," *The Journal of Physiology*, vol. 592, part 2, pp. 391–408, 2014.

[25] N. Adler, L. L. Camin, and P. Shulkin, "Rat model for acute myocardial infarction: application to technetium-labeled glucoheptonate, tetracycline, and polyphosphate," *Journal of Nuclear Medicine*, vol. 17, no. 3, pp. 203–207, 1976.

[26] M. A. Pfeffer, J. M. Pfeffer, M. C. Fishbein et al., "Myocardial infarct size and ventricular function in rats," *Circulation Research*, vol. 44, no. 4, pp. 503–512, 1979.

[27] R. Del Rio, N. J. Marcus, and H. D. Schultz, "Inhibition of hydrogen sulfide restores normal breathing stability and improves autonomic control during experimental heart failure," *Journal of Applied Physiology*, vol. 114, no. 9, pp. 1141–1150, 2013.

[28] T. I. Musch and R. Zelis, "Norepinephrine response to exercise of rats with a chronic myocardial infarction," *Medicine and Science in Sports and Exercise*, vol. 23, no. 5, pp. 569–577, 1991.

[29] C. Krüger, A. Kalenka, A. Haunstetter et al., "Baroreflex sensitivity and heart rate variability in conscious rats with myocardial infarction," *The American Journal of Physiology—Heart and Circulatory Physiology*, vol. 273, no. 5, part 2, pp. H2240–H2247, 1997.

[30] G.-Q. Zhu, L. Gao, Y. Li, K. P. Patel, I. H. Zucker, and W. Wang, "AT_1 receptor mRNA antisense normalizes enhanced cardiac sympathetic afferent reflex in rats with chronic heart failure," *The American Journal of Physiology—Heart and Circulatory Physiology*, vol. 287, no. 4, pp. H1828–H1835, 2004.

[31] K. K. V. Haack, N. J. Marcus, R. Del Rio, I. H. Zucker, and H. D. Schultz, "Simvastatin treatment attenuates increased respiratory variability and apnea/hypopnea index in rats with chronic heart failure," *Hypertension*, vol. 63, no. 5, pp. 1041–1049, 2014.

[32] J. S. Shinbane, M. A. Wood, D. N. Jensen, K. A. Ellenbogen, A. P. Fitzpatrick, and M. M. Scheinman, "Tachycardia-induced cardiomyopathy: a review of animal models and clinical studies," *Journal of the American College of Cardiology*, vol. 29, no. 4, pp. 709–715, 1997.

[33] Y.-L. Li, X.-H. Xia, H. Zheng et al., "Angiotensin II enhances carotid body chemoreflex control of sympathetic outflow in chronic heart failure rabbits," *Cardiovascular Research*, vol. 71, no. 1, pp. 129–138, 2006.

[34] Y.-L. Li, Y. Ding, C. Agnew, and H. D. Schultz, "Exercise training improves peripheral chemoreflex function in heart failure rabbits," *Journal of Applied Physiology*, vol. 105, no. 3, pp. 782–790, 2008.

[35] G. Piccirillo, M. Ogawa, J. Song et al., "Power spectral analysis of heart rate variability and autonomic nervous system activity measured directly in healthy dogs and dogs with tachycardia-induced heart failure," *Heart Rhythm*, vol. 6, no. 4, pp. 546–552, 2009.

[36] R. D. Patten and M. R. Hall-Porter, "Small animal models of heart failure development of novel therapies, past and present," *Circulation: Heart Failure*, vol. 2, no. 2, pp. 138–144, 2009.

[37] S. E. Litwin, S. E. Katz, E. O. Weinberg, B. H. Lorell, G. P. Aurigemma, and P. S. Douglas, "Serial echocardiographic-doppler assessment of left ventricular geometry and function in rats with pressure-overload hypertrophy. Chronic angiotensin-converting enzyme inhibition attenuates the transition to heart failure," *Circulation*, vol. 91, no. 10, pp. 2642–2654, 1995.

[38] L. F. Wexler, B. H. Lorell, S.-I. Momomura, E. O. Weinberg, J. S. Ingwall, and C. S. Apstein, "Enhanced sensitivity to hypoxia-induced diastolic dysfunction in pressure-overload left ventricular hypertrophy in the rat: role of high-energy phosphate depletion," *Circulation Research*, vol. 62, no. 4, pp. 766–775, 1988.

[39] A. V. Kristen, A. Just, M. Haass, and H. Seller, "Central hypercapnic chemoreflex modulation of renal sympathetic nerve activity in experimental heart failure," *Basic Research in Cardiology*, vol. 97, no. 2, pp. 177–186, 2002.

[40] R. C. Fentzke, C. E. Korcarz, R. M. Lang, H. Lin, and J. M. Leiden, "Dilated cardiomyopathy in transgenic mice expressing a dominant-negative CREB transcription factor in the heart," *The Journal of Clinical Investigation*, vol. 101, no. 11, pp. 2415–2426, 1998.

[41] T. Wang, G. D. Lang, L. Moreno-Vinasco et al., "Particulate matter induces cardiac arrhythmias via dysregulation of carotid body sensitivity and cardiac sodium channels," *American Journal of Respiratory Cell and Molecular Biology*, vol. 46, no. 4, pp. 524–531, 2012.

[42] R. Willenbrock, H. Stauss, M. Scheuermann, K. J. Osterziel, T. Unger, and R. Dietz, "Effect of chronic volume overload on baroreflex control of heart rate and sympathetic nerve activity," *The American Journal of Physiology—Heart and Circulatory Physiology*, vol. 273, no. 6, part 2, pp. H2580–H2585, 1997.

[43] Z. Abassi, I. Goltsman, T. Karram, J. Winaver, and A. Hoffman, "Aortocaval fistula in rat: a unique model of volume-overload congestive heart failure and cardiac hypertrophy," *Journal of Biomedicine and Biotechnology*, vol. 2011, Article ID 729497, 13 pages, 2011.

[44] R. Yoshimura, T. Sato, T. Kawada et al., "Increased brain angiotensin receptor in rats with chronic high-output heart failure," *Journal of Cardiac Failure*, vol. 6, no. 1, pp. 66–72, 2000.

[45] H. D. Schultz, N. J. Marcus, and R. Del Rio, "Role of the carotid body in the pathophysiology of heart failure," *Current Hypertension Reports*, vol. 15, no. 4, pp. 356–362, 2013.

[46] H. D. Schultz, N. J. Marcus, and R. Del Rio, "Mechanisms of carotid body chemoreflex dysfunction during heart failure," *Experimental Physiology*, vol. 100, no. 2, pp. 124–129, 2015.

[47] A. M. Allen, "Angiotensin AT1 receptor-mediated excitation of rat carotid body chemoreceptor afferent activity," *The Journal of Physiology*, vol. 510, part 3, pp. 773–781, 1998.

[48] H. Schultz, N. Marcus, and R. Del Rio, "Role of the carotid body chemoreflex in the pathophysiology of heart failure: a perspective from animal studies," in *Arterial Chemoreceptors in Physiology and Pathophysiology*, C. Peers, P. Kumar, C. Wyatt, E. Gauda, C. A. Nurse, and N. Prabhakar, Eds., vol. 860 of *Advances in Experimental Medicine and Biology*, pp. 167–185, Springer, 2015.

[49] Y.-L. Li, L. Gao, I. H. Zucker, and H. D. Schultz, "NADPH oxidase-derived superoxide anion mediates angiotensin II-enhanced carotid body chemoreceptor sensitivity in heart failure rabbits," *Cardiovascular Research*, vol. 75, no. 3, pp. 546–554, 2007.

[50] Y.-L. Li and H. D. Schultz, "Enhanced sensitivity of Kv channels to hypoxia in the rabbit carotid body in heart failure: role of angiotensin II," *The Journal of Physiology*, vol. 575, no. 1, pp. 215–227, 2006.

[51] J. M. McCord and I. Fridovich, "Superoxide dismutase. An enzymic function for erythrocuprein (hemocuprein)," *The Journal of Biological Chemistry*, vol. 244, no. 22, pp. 6049–6055, 1969.

[52] Y. Ding, Y.-L. Li, M. C. Zimmerman, and H. D. Schultz, "Elevated mitochondrial superoxide contributes to enhanced chemoreflex in heart failure rabbits," *The American Journal of Physiology—Regulatory Integrative and Comparative Physiology*, vol. 298, no. 2, pp. R303–R311, 2010.

[53] P. Niewiński, D. Janczak, A. Rucinski et al., "Carotid body removal for treatment of chronic systolic heart failure," *International Journal of Cardiology*, vol. 168, no. 3, pp. 2506–2509, 2013.

[54] R. Del Rio, E. A. Moya, and R. Iturriaga, "Differential expression of pro-inflammatory cytokines, endothelin-1 and nitric oxide synthases in the rat carotid body exposed to intermittent hypoxia," *Brain Research*, vol. 1395, pp. 74–85, 2011.

[55] S. Rey, R. Del Rio, and R. Iturriaga, "Contribution of endothelin-1 to the enhanced carotid body chemosensory responses induced by chronic intermittent hypoxia," *Brain Research*, vol. 1086, no. 1, pp. 152–159, 2006.

[56] S. Rey, J. Corthorn, C. Chacón, and R. Iturriaga, "Expression and immunolocalization of endothelin peptides and its receptors, ETA and ETB, in the carotid body exposed to chronic intermittent hypoxia," *Journal of Histochemistry & Cytochemistry*, vol. 55, no. 2, pp. 167–174, 2007.

[57] R. Del Rio, E. A. Moya, and R. Iturriaga, "Carotid body and cardiorespiratory alterations in intermittent hypoxia: the oxidative link," *European Respiratory Journal*, vol. 36, no. 1, pp. 143–150, 2010.

[58] C. M. Wei, A. Lerman, R. J. Rodeheffer et al., "Endothelin in human congestive heart failure," *Circulation*, vol. 89, no. 4, pp. 1580–1586, 1994.

[59] S. Murali, M. Zhang, and C. A. Nurse, "Paracrine signaling in glial-like type II cells of the rat carotid body," *Advances in Experimental Medicine and Biology*, vol. 860, pp. 41–47, 2015.

[60] M. Zhang, N. A. Piskuric, C. Vollmer, and C. A. Nurse, "P2Y2 receptor activation opens pannexin-1 channels in rat carotid body type II cells: potential role in amplifying the neurotransmitter ATP," *The Journal of Physiology*, vol. 590, no. 17, pp. 4335–4350, 2012.

[61] Y. Takimoto, T. Aoyama, K. Tanaka, R. Keyamura, Y. Yui, and S. Sasayama, "Augmented expression of neuronal nitric oxide synthase in the atria parasympathetically decreases heart rate during acute myocardial infarction in rats," *Circulation*, vol. 105, no. 4, pp. 490–496, 2002.

[62] H. Masaki, T. Imaizumi, Y. Harasawa, and A. Takeshita, "Dynamic arterial baroreflex in rabbits with heart failure induced by rapid pacing," *The American Journal of Physiology—Heart and Circulatory Physiology*, vol. 267, no. 1, part 2, pp. H92–H99, 1994.

Hindawi Publishing Corporation
BioMed Research International
Volume 2015, Article ID 949624, 15 pages
http://dx.doi.org/10.1155/2015/949624

Research Article

Transcriptional Changes Associated with Long-Term Left Ventricle Volume Overload in Rats: Impact on Enzymes Related to Myocardial Energy Metabolism

Elise Roussel,[1] Marie-Claude Drolet,[1] Elisabeth Walsh-Wilkinson,[1] Wahiba Dhahri,[1] Dominic Lachance,[1] Suzanne Gascon,[2] Otman Sarrhini,[2] Jacques A. Rousseau,[2] Roger Lecomte,[2] Jacques Couet,[1] and Marie Arsenault[1]

[1]*Groupe de Recherche sur les Valvulopathies, Centre de Recherche, Institut Universitaire de Cardiologie et de Pneumologie de Québec, Université Laval, Quebec City, QC, Canada G1V 4G5*
[2]*Sherbrooke Molecular Imaging Center, Research Center of Centre Hospitalier Universitaire de Sherbrooke (CRCHUS), Université de Sherbrooke, Sherbrooke, QC, Canada J1H 5N4*

Correspondence should be addressed to Jacques Couet; jacques.couet@med.ulaval.ca
and Marie Arsenault; marie.arsenault@criucpq.ulaval.ca

Received 25 June 2015; Accepted 13 September 2015

Academic Editor: John Baugh

Patients with left ventricle (LV) volume overload (VO) remain in a compensated state for many years although severe dilation is present. The myocardial capacity to fulfill its energetic demand may delay decompensation. We performed a gene expression profile, a model of chronic VO in rat LV with severe aortic valve regurgitation (AR) for 9 months, and focused on the study of genes associated with myocardial energetics. *Methods*. LV gene expression profile was performed in rats after 9 months of AR and compared to sham-operated controls. LV glucose and fatty acid (FA) uptake was also evaluated *in vivo* by positron emission tomography in 8-week AR rats treated or not with fenofibrate, an activator of FA oxidation (FAO). *Results*. Many LV genes associated with mitochondrial function and metabolism were downregulated in AR rats. FA β-oxidation capacity was significantly impaired as early as two weeks after AR. Treatment with fenofibrate, a PPARα agonist, normalized both FA and glucose uptake while reducing LV dilation caused by AR. *Conclusion*. Myocardial energy substrate preference is affected early in the evolution of LV-VO cardiomyopathy. Maintaining a relatively normal FA utilization in the myocardium could translate into less glucose uptake and possibly lesser LV remodeling.

1. Introduction

Aortic regurgitation (AR) is associated with a long asymptomatic period during which the left ventricle (LV) progressively dilates and hypertrophies in response to chronic volume overload. This process is accompanied by a decrease in LV function, occurrence of symptoms, and eventually heart failure [1]. No medical therapy has yet been clearly shown to be effective to slow dilation, hypertrophy, and loss of function or to have any impact on morbidity or mortality [2]. Chronic AR often secondary to rheumatic fever is a condition still frequent in developing countries and in populations having less than adequate access to health care [3, 4].

Gene expression profiles have been established in several animal models of LV eccentric hypertrophy, including by us in a rat model after two weeks of severe AR, a period characterized with intense LV remodeling [5–8]. A similar profile has not been performed at a later stage of the disease. Considering that AR is a chronic condition often evolving over decades in human, the study of animals later in the disease is of great interest. Contrary to the fast evolution of other VO models such as aortocaval fistula (ACF), severe AR in rats is associated with important LV hypertrophy and dilation, moderate loss of systolic function, diastolic dysfunction, and a low rate of congestive heart failure [9–11]. Significant LV fibrosis and increased myocardial collagen

content are present later in the evolution of this disease which is associated with increased mortality [9].

Abnormalities in energy metabolism in the rat AR model are consistent with a pattern of substrate utilization favoring glucose instead of fatty acid oxidation (FAO) [12–14]. These changes have been associated with a general decrease in the activity of enzymes implicated in FAO and PPARα expression, a transcription factor controlling a number of genes implicated in this process [14, 15].

Here, we present LV gene expression profiling late (9 months) during the evolution of this eccentric hypertrophy model caused by severe aortic valve regurgitation in male Wistar rats. We show a general downregulation of genes involved in fatty acid oxidation and bioenergetics. These anomalies occur early in the disease and result in observable changes of *in vivo* myocardial substrate preference as investigated by micropositron emission tomography. We also demonstrate that this can be countered by treating AR rats with a PPARα agonist, fenofibrate.

2. Methods

2.1. Animal Experiments. Six groups of Wistar male rats (350–375 g) purchased from Charles River (Saint-Constant QC, Canada) were studied for either 2, 14, or 270 days. For each end-point time, the animals were divided in two groups: sham-operated animals or AR. Groups were composed of 8 animals with the exception of the 270-day AR group which is composed of 15 animals. The protocol was approved by the Université Laval's Animal Protection Committee and followed the recommendations of the Canadian Council on Laboratory Animal Care. Severe AR was induced by retrograde puncture of the aortic valve leaflets under echocardiographic guidance as previously described [16–18]. Only animals with >65% regurgitation were included in the study. A complete echo exam was performed before AR induction and at the end of the protocol as previously described [13, 14]. Left ventricular and arterial pressures and dP/dt (positive and negative) were measured invasively using a dedicated catheter under 1.5% isoflurane anesthesia (5 animals/gr.) [10, 11, 16]. The hearts were harvested as previously described [13].

2.2. Microarray Analysis. Total LV RNA was extracted from stored LV tissues (Sham and AR-sed ($n = 5$/group)) as previously described [8]. The biotin-labeled cRNA preparations were hybridized to BeadChip RatRef-12 microarrays (Illumina; San Diego, CA) according to supplier's protocol (11286340 rev. A), using 750 ng per array. After hybridization and washes, arrays were incubated in streptavidin-Cy3 solution and washed, and fluorescence data were collected on a BeadArray reader (Illumina). Treatment of data was performed with the FlexArray software package (version 1.6.3, http://genomequebec.mcgill.ca/FlexArray). Raw fluorescence data were processed and normalized with the lumi Bioconductor package (http://bioconductor.org/) version 1.1.0., and differential expression was determined according to the random variance model of Wright and Simon (SAM analysis) [19]. Complete data (complying with MIAME guidelines) are available at the GEO database (NCBI) under the Accession number GSE17050. Genes were considered regulated when their fold change value was greater than 1.5 or less than 0.67. The change p value had to be below 0.01 for regulated genes. The comparative analysis of expression data using the gene ontology (GO) vocabulary was performed using the EASE software [20].

2.3. Analysis of mRNA Accumulation by Quantitative RT-PCR. The analysis of LV mRNA levels by quantitative RT-PCR has been described in detail elsewhere [8]. QuantiTect and IDT (Coralville, Iowa) Primer Assays (preoptimized specific primer pairs (see Tables 1 and Supplementary Table S1 in Supplementary Material available online at http://dx.doi.org/10.1155/2015/949624)) and QuantiFast SYBR Green PCR kits (Qiagen) were used. We also used one pair of nonpreoptimized primers for ECHS1 (5′-GCTTTCAGGGTGTCTTGATTTG-3′ and 5′-GAGCTATGCACTGCAGATAGT-3′; 95 bp transcript). Cyclophilin A (PPIA) was used as the control "housekeeping" gene.

2.4. Enzyme Activity Determination. Left ventricle samples were kept at −80°C until assayed for maximal (V_{max}) enzyme activities as described elsewhere [12–15].

2.5. Mitochondrial DNA Quantification. LV tissue DNA was isolated using standard procedure and ten nanograms of each sample were analyzed in triplicate using the QuantiFast SYBR Green PCR kit. QuantiTect primers (QT00371308) for the rat Edn1 intronless gene were used for the relative quantification of nuclear DNA, whereas the mitochondrial DNA was quantified with a rat Cox1 (GenBank AY172581) specific primer pair: forward, 5′-AGAAGCTGGAGCTGGAACAG-3′; reverse, 5′-AGATAGAAGACACCCCGGCT-3.

The relative cell mitochondrial DNA copy number was calculated in a similar way as for gene expression analysis.

2.6. Staining for Capillaries Density Measurement. Sections of 8 μm thickness were cut from the frozen left ventricle and were stained with isolectin B4 from *Bandeiraea simplicifolia* coupled with horseradish peroxidase (Sigma, Mississauga, ON, Canada), and capillary density was analyzed in the subendocardial region of the LV myocardium (inner third) as described elsewhere [21].

2.7. Small Animal μPET Protocol. Adult male Wistar rats were divided into 3 groups as follows: (1) Sham-operated control animals (Sham; $n = 5$); (2) AR controls (AR; $n = 5$); (3) AR rats treated with fenofibrate (100 mg/kg/day PO in unsweetened fruit gelatin daily; SF; $n = 5$). Fenofibrate was started one week before surgery and continued for 9 weeks until sacrifice [15]. Imaging experiments and data analysis were performed essentially as described before [13, 14, 22–26] on a LabPET avalanche photodiode-based small animal PET scanner (Gamma Medica, Northridge, CA) at the Sherbrooke Molecular Imaging Centre. [^{18}F]-fluorodeoxyglucose ([^{18}F]-FDG) or [^{18}F]-fluorothioheptadecanoic acid ([^{18}F]-FTHA) (30–40 MBq, in 0.3 mL plus 0.1 mL flush of 0.9% NaCl) was

Table 1: Primer assays used in Q-PCR analysis of gene expression.

mRNA	Symbol	Cat. number	Amplicon (bp)
Acetyl CoA acyltransferase 2	Acaa2	Rn.PT.58.5300756	111
Acyl CoA dehydrogenase, very long chain	Acadvl	Rn.PT.58.13279450	147
Acetyl CoA acetyltransferase 1	Acat1	Rn.PT.58.18447027	102
Carnitine O-acetyltransferase	Crat	Rn.PT.58.36282119	97
Carnitine palmitoyltransferase 1b, muscle	CPT1b	QT01084069	98
Carnitine palmitoyltransferase 2	CPT2	QT00186473	150
Cyclophilin a	Ppia	QT00177394	106
2,4-dienoyl CoA reductase 1	Decr1	Rn.PT.58.44352482	120
Enoyl-CoA hydratase 1	Ech1	Rn.PT.58.33832465	99
Enoyl-CoA delta isomerase 1	Eci1	Rn.PT.58.37662439	119
Hydroxyacyl-CoA dehydrogenase	Hadh	Rn.PT.58.17867024	135
Hydroxyacyl-CoA dehydrogenase alpha	Hadha	Rn.PT.58.46222281	138
Hydroxyacyl-CoA dehydrogenase beta	Hadhb	Rn.PT.58.7613498	130
Methylmalonyl CoA epimerase	Mcee	Rn.PT.58.10789169	101
Peroxisome proliferator activated receptor alpha	PPAR alpha	QT00176575	66
Peroxisome proliferator activated receptor gamma, coactivator 1 alpha	PGC1alpha	QT00189196	108
Retinoid X receptor alpha	Rxra	Rn.PT.58.33966638	103
Retinoid X receptor beta	Rxrb	Rn.PT.58.7033263	89
Retinoid X receptor gamma	Rxrg	Rn.PT.58.6519292	103
Solute carrier family 22, member 5	Slc22a5	Rn.PT.58.6675481	131
Solute carrier family 25, member 20	Slc25a20	Rn.PT.58.6247859	116

injected via the caudal vein over 30 s. A 45 min dynamic PET data acquisition followed by a 15 min static acquisition was done to determine glucose utilization [myocardial metabolic rate of glucose (MMRG)] using multicompartmental analysis as previously described [25, 27]. The static scan served to draw regions-of-interest (ROIs) on each segment of the LV wall. Blood samples were taken before and after the scans to determine an average blood glucose level. In another experiment, a 45 min dynamic acquisition with [^{18}F]-FTHA was used to determine myocardial nonesterified fatty acid (NEFA) uptake (K_m). Myocardial NEFA fractional uptake (K_i) was determined by a Patlak graphical analysis of the [^{18}F]-FTHA data.

2.8. Statistical Analysis. Results are presented as mean ± SEM unless specified otherwise. Intergroup comparisons were done using Student's t-test or Mann-Whitney t-test for μPET protocol. One-way was also used for the analysis of data when required with Dunnett's posttest. Statistical significance was set at a $p < 0.05$. Data and statistical analysis were performed using Graph Pad Prism version 6.04 for Windows, Graph Pad Software (San Diego, CA).

3. Results

After 9 months, eight of fifteen (8/15) AR animals were still alive whereas all sham-operated animals were alive. No differences in body weight were observed between the sham and AR groups. Overall growth was similar between groups (similar tibial lengths, results not shown). Indexed wet heart tissue weights were significantly increased in the AR group compared to controls (Table 2).

3.1. Hemodynamics. Systolic arterial pressure was similar between 9-month AR and sham-operated rats (Table 2). As expected, diastolic arterial pressure was significantly lower in AR animals resulting in a significantly increased pulse pressure and lowered mean arterial pressure.

Invasive measurements showed a decrease in both negative (an index of diastolic function) and positive (systolic function) dP/dt in AR after 9 months (35% and 24%, resp.). Left ventricular end-diastolic pressure was significantly increased in AR rats.

3.2. Echocardiographic Data. LV end-diastolic and end-systolic diameters were significantly increased in AR rats (Table 3). Stroke volume was also increased. The same was true for diastolic LV wall thickness.

3.3. Microarray Study. Changes in the profile of LV gene expression in AR rats after 9 months of severe volume overload were evaluated using microarray analysis. Fold change level threshold between AR LV samples and sham controls was arbitrarily fixed to 1.5 times with a p value below 0.01 in order to consider a gene as regulated. Three hundred and ninety-four transcripts met these criteria (230 were upregulated and 164 were downregulated). As listed in Tables 4 and 5, gene ontology analysis showed that the most significantly upregulated gene categories were associated with extracellular space and matrix and the most downregulated

Table 2: Heart remodeling and hemodynamics at 9 months.

Parameters	Sham ($n = 8$)	AR ($n = 8$)	p value
Ind heart, mg/mm	21.3 ± 2.7	40.1 ± 1.6	<0.0001
SAP, mm Hg	120 ± 4.0	120 ± 3.3	0.84
DAP, mm Hg	90 ± 4.6	64 ± 2.0	<0.0001
PP, mm Hg	30 ± 2.1	56 ± 2.4	<0.0001
MAP, mm Hg	99 ± 4.3	83 ± 2.5	0.007
dP/dt_{min}, mm Hg/sec	−5994 ± 327	−3871 ± 143	<0.0001
dP/dt_{max}, mm Hg/sec	7483 ± 328	5657 ± 277	<0.0001
LVEDP, mm Hg	9.6 ± 1.6	14.4 ± 1.4	0.044

Measurements obtained under inhaled 1.5% isoflurane anesthesia in surviving animals. Ind heart: indexation was made using tibial length; SAP: systolic arterial pressure; DAP: diastolic arterial pressure; PP: pulse pressure (SAP-DAP); MAP: mean arterial pressure; dP/dt_{min}: minimal derivative of pressure/time; dP/dt_{max}: maximal derivative of pressure/time; LVEDP: left ventricular end-diastolic pressure. Values are mean ± SEM of the indicated number of animals with the exception of dP/dt and LVEDP values ($n = 5$).

Table 3: Echocardiographic data at 9 months.

	Sham ($n = 8$)	AR ($n = 8$)	p value
EDD, mm	9.2 ± 0.08	12.2 ± 0.24	<0.0001
ESD, mm	4.5 ± 0.07	7.6 ± 0.09	<0.0001
SW, mm	1.6 ± 0.03	1.8 ± 0.02	<0.0001
PW, mm	1.5 ± 0.42	1.8 ± 0.02	<0.0001
RWT	0.34 ± 0.004	0.29 ± 0.006	<0.0001
FS, %	51 ± 0.3	39 ± 1.3	<0.0001
SV, μL	232 ± 4.8	372 ± 22.2	<0.0001

Measurements obtained under inhaled 1.5% isoflurane anesthesia after 9 months. EDD: end-diastolic diameter, ESD: end-systolic diameter, SW: septal wall, PW: posterior wall, RWT: relative wall thickness, FS: fractional shortening, and SV: stroke volume. Values are expressed as mean ± SEM of the indicated number of animals.

were those associated with the mitochondria and metabolism (Tables S2 and S3). This general downregulation of genes associated with mitochondrial function was present for most of the enzymes implicated in the utilization of fatty acids as an energy substrate (Figures 1(a) and 1(b)). The microarray results were corroborated with quantitative RT-PCR determinations (Figures 1(b) and S1). Peroxisome proliferator activated receptor alpha (PPARα) is the principal regulator of the expression of fatty acid β-oxidation FAO enzymes and transporters [28]. After 9 months of AR, gene expression of PPARα, and its coactivator, PGC1α was strongly downregulated (Figure 1(c)). PPARα binds to sequence-specific target elements as a heterodimer with the retinoid X receptor (RXR). In our microarray, we identified the RXR gamma isoform as the most expressed in the rat myocardium and the most downregulated in AR (not shown). We confirmed this using quantitative RT-PCR (Figure 1(c)). The other isoforms of RXR (alpha and beta) were also downregulated but less strongly.

3.4. Myocardial Capillaries Density. Long-term LV volume overload is associated with increased perivascular fibrosis as demonstrated before [9]. An additional factor that can influence oxygen and metabolic fuel availability and delivery to cardiomyocytes is capillaries density. Myocardial capillaries density was measured and the results can be found in Figure 1(d). Capillaries density was significantly lower in rats with aortic regurgitation after 9 months compared to the sham animals.

3.5. Mitochondrial DNA Content. Considering the important number of downregulated genes related to the mitochondria after 9 months of AR, we evaluated the amount of mitochondria in the LV of AR rats. To do so, the relative content of mitochondrial (mt) DNA was measured and compared to nucleus (n) DNA. The LV ratio of mtDNA to nDNA remained constant (sham: 3305 ± 130.5 units versus AR; 3276 ± 113.8) suggesting a stable proportion of mitochondria.

3.6. Fatty Acid Beta Oxidation (FAO) in Acute AR Rats. We then studied the expression of the same set of genes tested in the 9-month AR animals in the LV of rats with acute AR (2 and 14 days). As illustrated in Figure 2(a), heart hypertrophy had not already developed two days after AR whereas, after two weeks, indexed heart weight had increased by 22%. Eccentric LV remodeling as illustrated by the decrease of the relative wall thickness (as evaluated by echo) was also present. We measured the activity of a central enzyme in FAO, hydroxyacyl-Coenzyme A dehydrogenase (HADH), and the hexokinase (HK), the first step of glycolysis in myocardial tissue of AR rats 2 and 14 days after the surgery. As illustrated in Figure 2(b), a shift in the activity of these enzymes is apparent two weeks after AR, a period of very rapid and active development of LV hypertrophy and remodeling [17]. We did not observe this after 48 hours of AR although a trend for favoring increased FAO was present as demonstrated by an increased HADH/HK ratio. As for the expression of the FAO genes studied at 9 months (Figure 2(c)), the general downregulation begins to appear after two weeks of severe AR. Interestingly, several FAO genes (ACADVL, HADHA, and HAHDB) were upregulated 2 days after AR. LV gene expression for PPARα and its activator PGC1α was downregulated at 14 days. On the other hand, at two days, PPARα expression was significantly increased. The expression of RXR gamma followed a similar trend as illustrated in Figure 2(d).

3.7. Treatment with a PPARα Agonist Can Reverse the Shift in Myocardial Substrate Preference Induced by LVH. We showed recently that fenofibrate (a PPARα agonist) can help reduce LV dilation in the AR rat model [15]. We studied *in vivo* the impact of fenofibrate on free fatty acid and glucose uptake by μPET quantification as shown in Figure 3. This approach also allowed us to evaluate LV volumes and to measure the ejection fraction (EF). As illustrated in Figure 3(a), AR increased significantly both the end-diastolic (EDV) and end-systolic (ESV) LV volumes which resulted in a decreased EF compared to control sham-operated animals. Fenofibrate treatment reduced both EDV and ESV in AR animals and helped normalize the EF. A three-dimensional reconstruction of the LVs of a sham-operated and of an AR rat is illustrated in Figure 3(b).

Table 4: Upregulated genes in the category "extracellular" from the GO cellular component in 9-month LVs from severe volume overload compared to age-matched sham-operated animals.

Target ID	Definition	Fold change	p value
NPPA	Natriuretic peptide precursor type A	6,775	0.00018
TGFB2	Transforming growth factor, beta 2	4,311	0.00005
CTGF	Connective tissue growth factor	4,059	0.00012
CHI3L1	Chitinase 3-like 1	3,775	0.00117
HAMP	Hepcidin antimicrobial peptide	3,397	0.00080
MGP	Matrix Gla protein	3,256	0.00011
LTBP2	Latent transforming growth factor beta binding protein 2	3,067	0.00073
TIMP1	Tissue inhibitor of metallopeptidase 1	2,954	0.00215
CTSS	Cathepsin S	2,912	0.00003
LOXL1	Lysyl oxidase-like 1	2,869	0.00047
PRSS23	Protease, serine, 23	2,788	0.00002
FSTL1	Follistatin-like 1	2,673	0.00033
GPX3	Glutathione peroxidase 3	2,672	0.00011
C1QB	Complement component 1, q subcomponent, beta polypeptide	2,613	0.00007
PTGIS	Prostaglandin I2 (prostacyclin) synthase	2,574	0.00005
SERPING1	Serine (or cysteine) peptidase inhibitor, clade G, member 1	2,520	0.00037
LGALS3	Lectin, galactose binding, soluble 3	2,419	0.00042
PMP22	Peripheral myelin protein 22	2,235	0.00025
IGFBP6	Insulin-like growth factor binding protein 6	2,231	0.00023
FN1	Fibronectin 1	2,230	0.00361
COL1A2	Procollagen, type I, alpha 2	2,212	0.00024
TGFA	Transforming growth factor alpha	2,177	0.00112
C1QA	Complement component 1, q subcomponent, alpha polypeptide	2,142	0.00013
ECM1	Extracellular matrix protein 1	2,098	0.00023
FBN1	Fibrillin 1	2,093	0.00056
MFAP4	Microfibrillar-associated protein 4	2,076	0.00009
FXYD6	FXYD domain-containing ion transport regulator 6	2,074	0.00115
PLOD2	Procollagen lysine, 2-oxoglutarate 5-dioxygenase 2	2,068	0.00021
WISP2	WNT1 inducible signaling pathway protein 2	2,060	0.00136
CTSK	Cathepsin K	2,051	0.00018
C1S	Complement component 1, s subcomponent	2,028	0.00210
APOE	Apolipoprotein E	2,027	0.00059
MXRA8	Matrix-remodelling associated 8	1,964	0.00027
NPPB	Natriuretic peptide precursor type B	1,924	0.00016
LUM	Lumican	1,902	0.00021
PCDH21	MT-protocadherin	1,861	0.00102
CD14	CD14 antigen	1,845	0.00003
TF	Transferrin	1,844	0.00089
C2	Complement component 2	1,807	0.00119
PPT1	Palmitoyl-protein thioesterase 1	1,753	0.00007
GDF15	Growth differentiation factor 15	1,705	0.00016
CX3CL1	Chemokine (C-X3-C motif) ligand 1	1,679	0.00108
AOC3	Amine oxidase, copper containing 3	1,666	0.00093
CCL7	Chemokine (C-C motif) ligand 7	1,665	0.00284
NBL1	Neuroblastoma, suppression of tumorigenicity 1	1,661	0.00048
GRN	Granulin	1,634	0.00010
SERPINF1	Serine (or cysteine) peptidase inhibitor, clade F, member 1	1,634	0.00038
CTSB	Cathepsin B	1,610	0.00005

Table 4: Continued.

Target ID	Definition	Fold change	p value
FXYD5	FXYD domain-containing ion transport regulator 5	1,604	0.00167
TRH	Thyrotropin releasing hormone	1,588	0.00306
PRELP	Proline arginine-rich end leucine-rich repeat protein	1,580	0.00127
STC1	Stanniocalcin 1	1,550	0.00049
COL5A1	Procollagen, type V, alpha 1	1,536	0.00065
CD48	CD48 antigen	1,533	0.00047
PON3	Paraoxonase 3	1,522	0.00508
ITGB1	Integrin beta 1	1,519	0.00002
RARRES2	Retinoic acid receptor responder	1,509	0.00004

FC: fold change versus sham controls.

The overall myocardial uptake of fatty acids in AR rats was similar to sham-operated animals. Fenofibrate treatment increased the myocardial avidity for [^{18}F]-FTHA to supranormal levels (Figure 3(c)). On the other hand, glucose uptake by the LV of AR was significantly increased and this was reversed by fenofibrate. When the analysis was made on different LV regions (Figure 3(d)), fatty acid uptake was slightly decreased in the lateral wall (opposite to the septum) whereas glucose uptake was increased in both the lateral and the anterior walls. Fenofibrate treatment increased fatty acid uptake homogeneously in each LV wall. This was accompanied by a normalization of glucose uptake. Interestingly, at 8 weeks, fenofibrate upregulated the expression of a subset of the FAO genes studied (HADHB, ECI, ECH1, DECR1, ACAA2, and CPT2) in sham animals but not in AR rats (Figure S2).

4. Discussion

The factors influencing the development of eccentric LV hypertrophy from chronic VO and the evolution of the disease are poorly understood. In order to improve our knowledge of this condition, the need for animal models is important. As for many patients with significant AR, an important proportion of the AR rats can live more than a third of their normal lifespan with important heart dilation and without overt signs of HF. The study of chronic heart adaptations to hemodynamic overload in rodent models has received little attention in the past mainly for practical reasons (rapid evolution of some models toward HF, housing costs of larger protocol, etc.). Here, we present a gene profiling study of the left ventricles from an aging model of eccentric LVH after 9 months of severe AR.

We observed that many upregulated genes in the left ventricles of AR rats were linked to the extracellular matrix remodeling whereas those downregulated were often associated with myocardial metabolism. We had observed in a previous evaluation of the gene profile of left ventricles from rats after only 14 days of AR [8] that many genes associated with extracellular matrix remodeling were also upregulated very early in the disease process. This made sense considering that 14 days after AR corresponds to an early rapid LV remodeling phase in response to severe and acute LV volume overload [17, 29]. We had previously reported that the myocardial LV collagen tissue content in AR animals increased but only after 9 months [9]. An upregulation of genes related to the extracellular matrix is still present after 9 months suggesting a disruption in the balance between collagen synthesis and its degradation during the evolution of the disease. This probably takes place in the preceding months and leads to increase interstitial and perivascular fibrosis [9].

Eccentric LV hypertrophy is not normally associated with an accumulation of myocardial fibrosis at least during the early stages of VO. Myocardial collagen loss has even been observed [30, 31]. In the rat AR model, we did not observe such loss of collagen or downregulation of ECM genes in the early stages of the disease [29]. This can possibly be explained by an early pressure overload component often associated with AR at least before LV dilation has taken place. After 9 months, the presence of interstitial fibrosis is most likely linked to the loss and replacement of apoptotic myocytes by fibrotic tissue. This is accompanied with decreased myocardial relaxation as demonstrated by the decrease of $dP/dt_{\min}$. This could increase the occurrence of arrhythmias which we believe is the main cause of mortality in the AR rat model [9, 10, 13].

We have summarized in Figure 4 most of the observations made in this study related to myocardial FAO in the AR rat mode. Soon after AR induction, FAO seems to be increased before LV dilation has taken place. Then, FAO becomes downregulated as eccentric LVH develops. During the compensated phase of the disease, glucose uptake is clearly above normal levels and seems to be the main way for the heart muscle to fuel its augmented energy needs. We had previously shown that, during this compensated phase at 8 weeks, myocardial oxidative metabolism was still unchanged compared to sham animals [26]. At 8 weeks, FA uptake is still normal or little decreased [26]. Then, late in the disease at 9 months, FAO is clearly downregulated both at the level of FA intake and HADH activity [14].

The present microarray analysis showed that an important number of downregulated genes was associated with the mitochondrial compartment confirming alterations in myocardial energetics in 9-month AR rats [14]. We had not clearly observed this in the microarray analysis we previously conducted from 14-day AR LVs [8]. Our results on acute AR rats confirm that FAO gene expression only begins to

Table 5: Downregulated genes in the category "mitochondrion" from the GO cellular component in 9-month LVs from severe volume overload compared to age-matched sham-operated animals.

Target ID	Definition	Fold change	*p* value
CYP11A1	Cytochrome P450, family 11, subfamily a, polypeptide 1	0,482	0.00057
ECH1	Enoyl-Coenzyme A hydratase 1, peroxisomal	0,497	0.00039
HADHA	Hydroxyacyl-Coenzyme A dehydrogenase/3-ketoacyl-Coenzyme A thiolase/enoyl-Coenzyme A hydratase (trifunctional protein), alpha subunit	0,517	0.00030
DECR1	2,4-Dienoyl CoA reductase 1, mitochondrial	0,519	0.00343
ACAA2	Acetyl-Coenzyme A acyltransferase 2 (mitochondrial 3-oxoacyl-Coenzyme A thiolase)	0,523	0.00536
LDHD	Lactate dehydrogenase D	0,540	0.00088
DCI	Dodecenoyl-coenzyme A delta isomerase	0,541	0.00037
ACAT1	Acetyl-coenzyme A acetyltransferase 1	0,541	0.00023
PKM2	Pyruvate kinase, muscle	0,547	0.00020
MLYCD	Malonyl-CoA decarboxylase	0,554	0.00111
BCAT2	Branched chain aminotransferase 2, mitochondrial	0,557	0.00184
GSTK1	Glutathione S-transferase kappa 1	0,572	0.00035
FAHD1	Fumarylacetoacetate hydrolase domain containing 1	0,581	0.00008
DHRS4	Dehydrogenase/reductase (SDR family) member 4	0,585	0.00035
HSD17B8	Hydroxysteroid (17-beta) dehydrogenase 8	0,585	0.00018
ACSL1	Acyl-CoA synthetase long-chain family member 1	0,589	0.00023
BCKDHA	Branched chain ketoacid dehydrogenase E1, alpha polypeptide	0,593	0.00109
ACADVL	Acyl-Coenzyme A dehydrogenase, very long chain	0,597	0.00089
SLC25A20	Solute carrier family 25 (mitochondrial carnitine/acylcarnitine translocase), member 20	0,598	0.00021
ACO2	Aconitase 2, mitochondrial	0,601	0.00173
LOC56764	DNAJ-like protein	0,607	0.00045
PECR	Peroxisomal trans-2-enoyl-CoA reductase	0,610	0.00033
ECHS1	Enoyl-Coenzyme A hydratase, short chain, 1, mitochondrial	0,616	0.00065
IVD	Isovaleryl coenzyme A dehydrogenase	0,618	0.00098
PDK2	Pyruvate dehydrogenase kinase, isoenzyme 2	0,622	0.00071
MGST1	Microsomal glutathione S-transferase 1	0,623	0.00001
CRAT	Carnitine acetyltransferase	0,630	0.00125
ACADS	Acetyl-Coenzyme A dehydrogenase, short chain	0,635	0.00507
SUCLG1	Succinate-CoA ligase, GDP-forming, alpha subunit	0,637	0.00048
NDUFS7	NADH dehydrogenase (ubiquinone) Fe-S protein 7	0,638	0.00280
NDUFA10	NADH dehydrogenase (ubiquinone) 1 alpha subcomplex 10	0,654	0.00101
IDH3G	Isocitrate dehydrogenase 3 (NAD), gamma	0,655	0.00041
ATAD3A	ATPase family, AAA domain containing 3A	0,658	0.00060
RGD735029	SEL1 domain containing protein	0,659	0.00097
RGD1303003	Homolog of zebrafish ES1	0,661	0.00011
RGD1303272	Similar to RIKEN cDNA 2010311D03	0,662	0.00218
HADHB	Hydroxyacyl-Coenzyme A dehydrogenase/3-ketoacyl-Coenzyme A thiolase/enoyl-Coenzyme A hydratase (trifunctional protein), beta subunit	0,662	0.00078
CS	Citrate synthase	0,663	0.00559
GRPEL1	GrpE-like 1, mitochondrial	0,666	0.00101
PDP2	Pyruvate dehydrogenase phosphatase isoenzyme 2	0,668	0.00489
HSD17B10	Hydroxysteroid (17-beta) dehydrogenase 10	0,670	0.00185

FC: fold change versus sham controls.

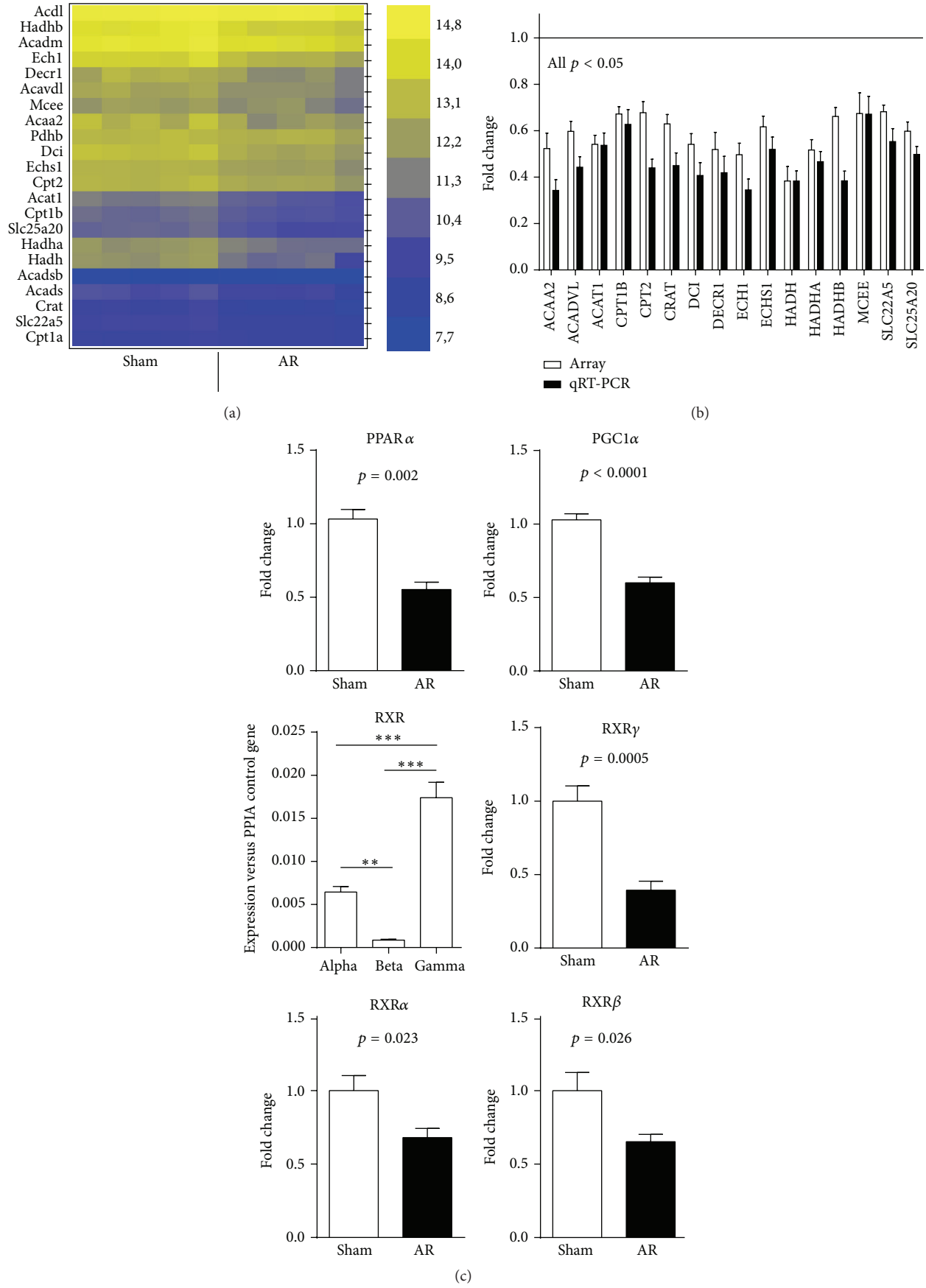

Figure 1: Continued.

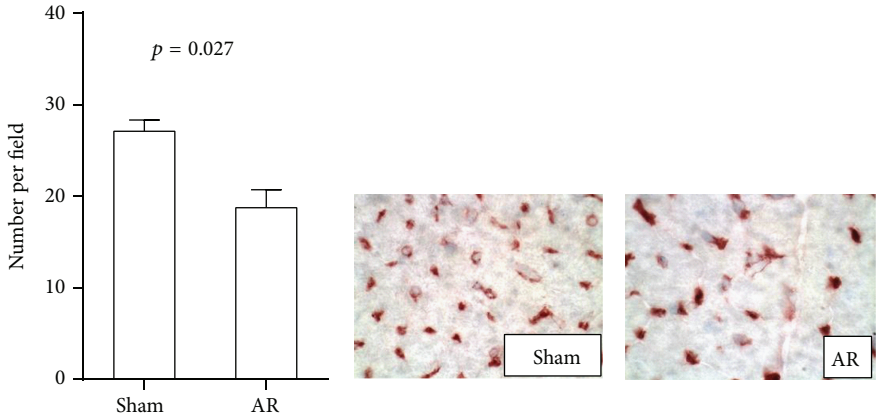

(d)

Figure 1: (a) Heat map of expression of 22 genes associated with FAO in LV of 9-month rats. Levels of expression are illustrated from the highest (bright yellow) to the lowest (dark blue). Five animals were studied per group and their expression levels are illustrated individually. (b) Comparison between fold change results obtained from the microarray and by quantitative RT-PCR for a subset of 16 genes illustrated in (a). Results are reported in fold change compared to sham controls as the mean ± SEM ($n = 5$ per group for array and $n = 6$ for qRT-PCR). Levels in sham animals were fixed to 1. (c) PPARα, PGC1α, and RXRs LV mRNA levels in 9-month AR rats are strongly downregulated. Exact p values are indicated when two groups were compared. $^{**}p < 0.01$ and $^{***}p < 0.001$ between groups. (d) Evaluation of capillaries density in LV myocardium, expressed as the number of capillaries per field (a). Results are reported as mean ± SEM ($n = 8$/gr). Representative LV sections from sham-operated or AR rats showing isolectin B4-stained capillaries (brown-red) are illustrated.

be downregulated two weeks after induction. It is intriguing that FAO activity seemed to be related to the state of LV dilation in acute AR rats. LV dilation can bring a state of ischemia if the increase in myocytes size is not accompanied with an activation of angiogenesis and the formation of new blood vessels. It is not the case in the AR myocardium as evidenced by our observation of a decreased capillary network. Glucose constitutes a less oxygen-consuming choice when LVH develops. Prior to this, at two days, increased FAO probably remains a more efficient option to fuel the heart with enough ATP. We had shown in the past that, during the first two days after AR induction, both LV inotropy and contractility were higher than normal to compensate for the sudden increase of blood to pump [17].

Heart FA uptake seemed to be maintained later in the disease as evidenced by the μPET study. We only noticed a slight decrease in FA uptake after 8 weeks in the LV lateral wall. At this compensated phase of the disease, FAO enzyme activity is also only slightly reduced [12, 15]. In fact, we observed clearer differences here in the enzymatic activities related to FAO and glycolysis 2 weeks after AR induction than at 8 weeks in previous studies [12, 15, 26]. It is possible that, at two weeks, the intense LV remodeling necessitates an increased amount of energy whereas later, at 8 weeks, the LV has probably entered in a more stable and compensated phase of the disease.

A balance between FA uptake and utilization has to be stricken to avoid the accumulation of unwanted lipids in the cardiac muscle cell causing lipotoxicity. This has been observed in another model of eccentric LVH (mitral regurgitation in dogs) [32]. We reported in a previous study that the myocardial triglycerides content in 8-week AR rats was unchanged [12] and we did not observe positive staining for lipids using the oil red O method on LV section of 6-month AR rats (unpublished observation).

PPARα and RXRγ gene expression mirrored the different observations we made on the state of myocardial FAO in AR rats at different times. PPARs dimerize with RXRs to bind to their sequence-specific target sequences. Our microarray and qRT-PCR data showed that RXRγ was the most highly expressed in the heart and that it was strongly downregulated in AR in parallel to PPARα and PGC1α expression. Interestingly, PPARα and RXRγ gene expression was upregulated early after AR induction again suggesting that FAO is first stimulated before glycolysis becomes more central in the energy production of the dilating heart.

The evaluation of energy substrates uptake *in vivo* in 8-week AR rats with or without treatment with fenofibrate showed that glucose uptake is clearly elevated before FA uptake decreased. This is an interesting observation indicating that, during the early phases of eccentric LVH, the heart relies on glucose to sustain its additional energy needs before FAO starts to decrease. Interestingly, FAO gene downregulation is also clearly present at 8 weeks whereas fatty acid uptake and oxidation are still relatively normal (Figure S2). This could be explained by a possible decrease in the protein turnover of the enzymes implicated in FAO. This hypothesis remains to be confirmed, however.

Fenofibrate treatment decreased LV dilation in our model. We had previously observed that LV weight was not reduced by fenofibrate treatment, but we observed that its remodeling tended to be more concentric with less chamber dilation and increased wall thickness [15]. Our present μPET analysis did not contradict these previous observations and confirmed that fenofibrate can indeed limit LV dilation. If the fenofibrate effects on FA uptake can be associated with

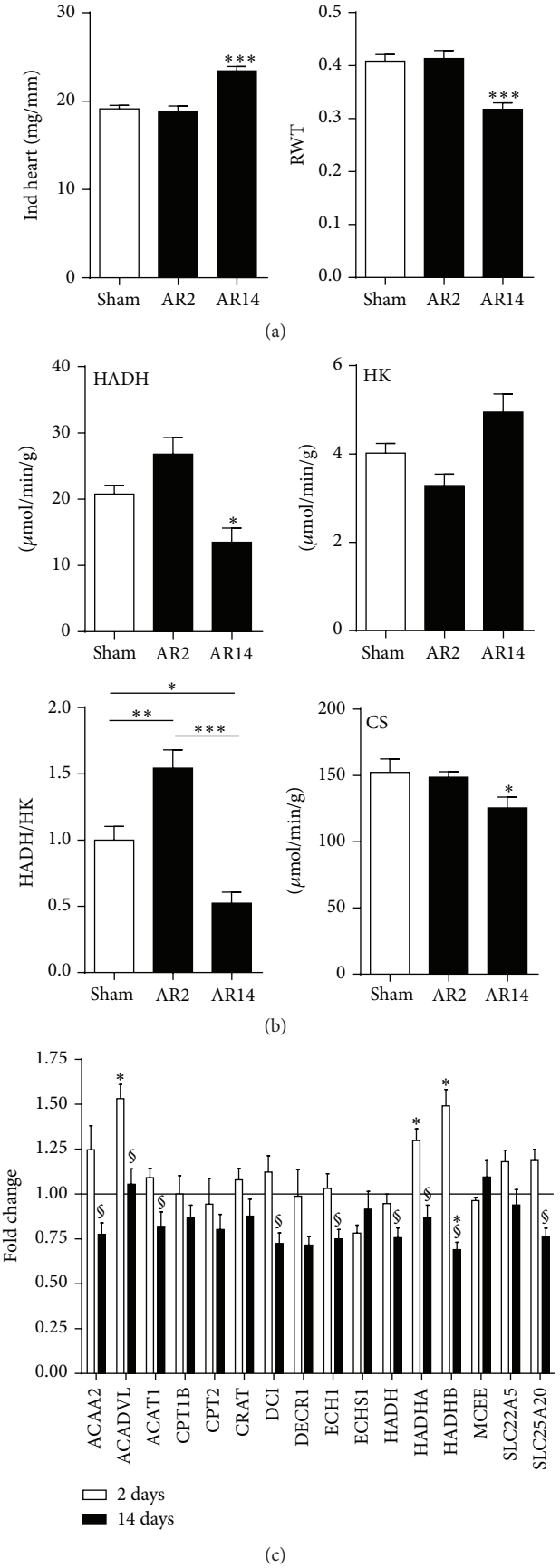

Figure 2: Continued.

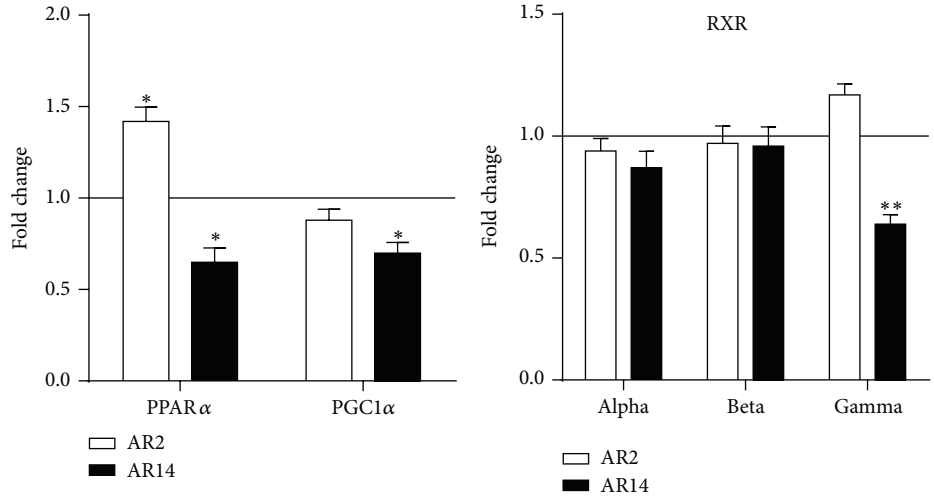

(d)

Figure 2: (a) Evolution of LV remodeling in experimental volume overload from severe aortic valve regurgitation in Wistar rats after 2 (AR2) and 14 days (AR14). Indexed heart weights were corrected for tibial length whereas relative wall thickness (RWT) was evaluated by echocardiography before sacrifice. Results are reported as the mean ± SEM (n = 6–8 per group). $^{***}p < 0.001$ between sham and AR groups. (b) LV myocardial activity levels of enzymes implicated in fatty acid β-oxidation, glucose metabolism, and mitochondrial energy production in 9-month AR rats relative to controls. HADH (hydroxyacyl-Coenzyme A dehydrogenase), HK (hexokinase), and citrate synthase (CS) enzymatic activities were measured in LV homogenates from at least 6 animals in each group as described in Section 2. Results are reported in μmoles/min/mg of tissue or as the ratio of HADH/HK activities arbitrarily fixed at 1 for sham group. $^{*}p < 0.05$, $^{**}p < 0.01$, and $^{***}p < 0.001$ between groups. (c) LV expression of the 16 genes studied in Figure 1(b) in AR rats at 2 and 14 days. Levels in sham animals were fixed to 1 (Line). $^{*}p < 0.05$ versus sham animals and $^{\S}p < 0.05$ between 2-day AR rats and 14-day animals. (d) PPARα, PGC1α, and RXRs LV mRNA levels in 2- and 14-day AR rats. $^{*}p < 0.05$ and $^{**}p < 0.01$ compared to sham controls (Line at 1).

its PPARα agonist activity, it is less clear if its effects on LV remodeling are completely mediated via PPARα although some evidences in the literature point to this direction [33, 34]. We observed previously that fenofibrate restored PPARα gene expression in AR rats [15]. PPARα null mice develop more hypertrophy, production of more reactive oxygen species as well as an exaggerated production of extracellular matrix components [35, 36]. Treatment of PPARα null mice with fenofibrate exacerbates LVH development in a pressure overload situation suggesting that the benefits observed here are mostly via PPARα activation [37]. Fenofibrate can slow the development of LVH and protect the heart, namely, via its anti-inflammatory, antioxidant, and antifibrotic properties. Fenofibrate can also reduce the formation of endothelin-1, a prohypertrophic molecule [38–40]. We had showed previously that fenofibrate was able to reverse the decrease in HADH activity observed in the LV of 8-week AR rats [15]. Interestingly, 8-week AR rats treated with fenofibrate showed no upregulation of all the FAO genes studied whereas sham animals displayed an increase for several of them (Figure S2). It is possible that the response of FAO genes to fenofibrate becomes altered during the progression of the disease, however. One aspect we did not investigate here is the effects of fenofibrate towards the inflammatory component of hypertrophy. Many inflammation-related genes have been found to be upregulated late in the disease in rats with ACF [41]. Our microarray results also showed a number of genes associated with the inflammation (not shown). Fenofibrate has been shown to have beneficial impact by reducing myocardial inflammation in hypertrophy models which could limit its development [42, 43].

5. Study Limitations

The results of this study have to be viewed in the light of some limitations. Rodent heart metabolism may differ in some aspects from humans. This study relied mainly on the evaluation of gene expression levels and more thorough analysis at the level of protein content, activity, and localization are needed. The role of various signaling pathways in controlling the energy substrate preference shift involved in the development of eccentric LVH and metabolic alterations will need to be explored more in detail.

6. Conclusions

Our results clearly show that the myocardium with chronic VO sustains a significant metabolic stress and develops important energetics adaptations. These findings may improve our view of the dilated and hypertrophied hearts of patients with severe VO from valve disease. Clinicians currently follow those patients without any intervention for a good number of years, simply waiting for the LV to become too dilated, for the occurrence of symptoms or until systolic function begins to fall. Based on our findings, we suggest that those hearts develop severe metabolic abnormalities even when systolic function seems preserved and that intervention then can limit dilation and metabolic abnormalities. Focusing

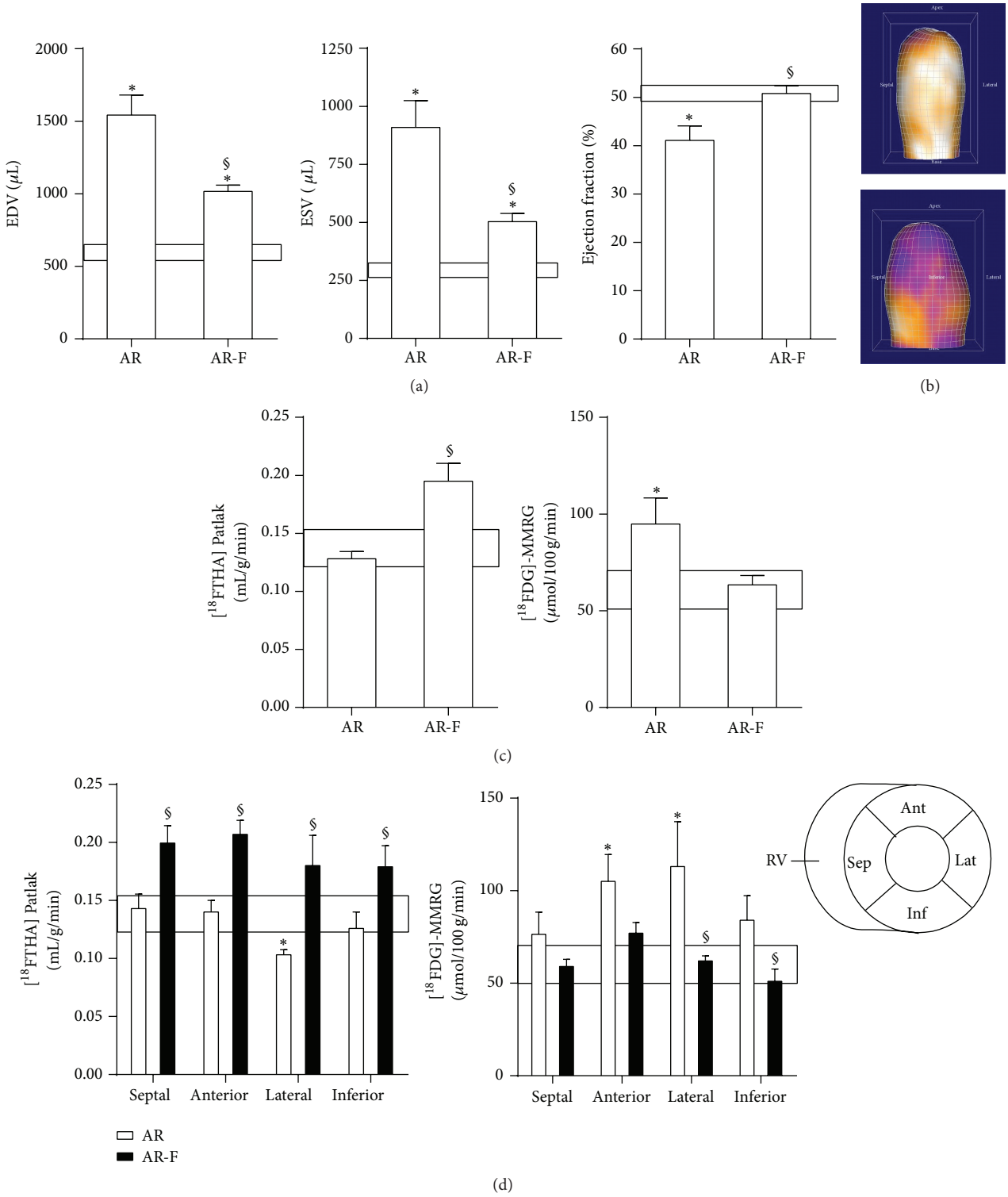

Figure 3: Impact of an 8-week fenofibrate treatment on LV remodeling, function, and energetics as evaluated by μPET. (a) Left ventricular volumes and ejection fraction as evaluated by [^{18}F]-FTHA μPET. End-diastolic (EDV) and end-systolic (ESV) volumes were measured as described in Section 2. The ejection fraction is the ratio of SV (EDV-ESV) on EDV. Results are reported as the mean of data obtained from four animals/group ± SEM.: $^{*}p < 0.05$ between sham and AR groups. $^{\S}p < 0.05$ and untreated AR group. The box represents the mean ± SEM of sham animals. (b) A three-dimensional reconstruction of the LV of a sham (top) and an AR rat (bottom) 6 months after surgery. (d) The same analysis was then reproduced for each segment of the LV wall as schematized in the bottom right of this panel. $^{*}p < 0.05$ between sham and AR groups. Sept: septal wall, Ant: anterior wall, Lat: lateral wall, and Inf: inferior wall. $^{*}p < 0.05$ between sham and AR groups. $^{\S}p < 0.05$ and untreated AR group.

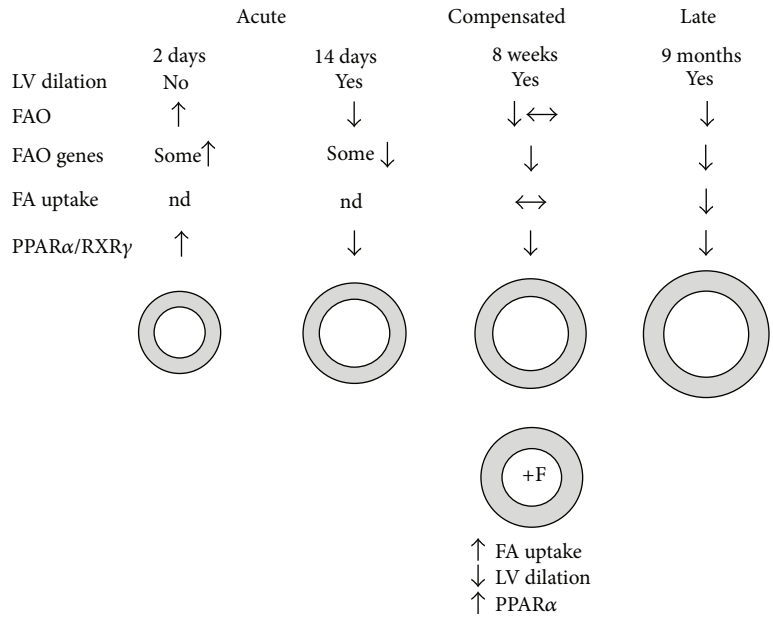

Figure 4: Summary of the observations related to myocardial FAO in the AR rat model made in this study. Soon after AR induction, FAO seems to be increased even before LV dilation has taken place. Then, FAO becomes downregulated as eccentric LVH develops. During the compensated phase of the disease, FAO is relatively stable although FAO genes are downregulated. Later in the disease, LV dilation is even more important. This is accompanied with a general decrease in fatty acids utilization by the heart. See Section 4 for additional information. F: fenofibrate. Nd: not determined.

on myocardial metabolism by various interventions such as targeted drugs, specific diets, or exercise may help this metabolically stressed myocardium to improve its energy production and maybe prolong the preheart failure state significantly. Some of our previous studies support this view [9, 15, 26], but additional work will be needed to substantiate it.

Conflict of Interests

The authors declare that there is no conflict of interests regarding the publication of this paper.

Acknowledgments

The authors want to thank Serge Champetier, Eve Maheux, Andrée-Anne Bouchard-Thomassin, Alexandra Auclair, and Adnane Zendaoui for their contribution to the realization of this study. This work was supported by operating Grants to Drs. Couet and Arsenault from the Canadian Institutes of Health Research (MOP-61818 and MOP-106479), the Heart and Stroke Foundation of Canada, and the Quebec Heart Institute Corporation.

References

[1] R. O. Bonow, "Chronic mitral regurgitation and aortic regurgitation: have indications for surgery changed?" *Journal of the American College of Cardiology*, vol. 61, no. 7, pp. 693–701, 2013.

[2] R. A. Nishimura, C. M. Otto, R. O. Bonow et al., "2014 AHA/ACC guideline for the management of patients with valvular heart disease: a report of the American College of Cardiology/American Heart Association Task Force on Practice Guidelines," *Journal of the American College of Cardiology*, vol. 63, no. 22, pp. e57–e185, 2014.

[3] J. R. Carapetis, A. C. Steer, E. K. Mulholland, and M. Weber, "The global burden of group A streptococcal diseases," *The Lancet Infectious Diseases*, vol. 5, no. 11, pp. 685–694, 2005.

[4] J. R. Carapetis, M. McDonald, and N. J. Wilson, "Acute rheumatic fever," *The Lancet*, vol. 366, no. 9480, pp. 155–168, 2005.

[5] J. Barnes, B. Pat, Y.-W. Chen et al., "Whole-genome profiling highlights the molecular complexity underlying eccentric cardiac hypertrophy," *Therapeutic Advances in Cardiovascular Disease*, vol. 8, no. 3, pp. 97–118, 2014.

[6] J. Zheng, Y. Chen, B. Pat et al., "Microarray identifies extensive downregulation of noncollagen extracellular matrix and profibrotic growth factor genes in chronic isolated mitral regurgitation in the dog," *Circulation*, vol. 119, no. 15, pp. 2086–2095, 2009.

[7] H. Miyazaki, N. Oka, A. Koga, H. Ohmura, T. Ueda, and T. Imaizumi, "Comparison of gene expression profiling in pressure and volume overload-induced myocardial hypertrophies in rats," *Hypertension Research*, vol. 29, no. 12, pp. 1029–1045, 2006.

[8] S. Champetier, A. Bojmehrani, J. Beaudoin et al., "Gene profiling of left ventricle eccentric hypertrophy in aortic regurgitation in rats: rationale for targeting the β-adrenergic and renin-angiotensin systems," *American Journal of Physiology—Heart and Circulatory Physiology*, vol. 296, no. 3, pp. H669–H677, 2009.

[9] D. Lachance, É. Plante, A.-A. Bouchard-Thomassin et al., "Moderate exercise training improves survival and ventricular remodeling in an animal model of left ventricular volume

overload," *Circulation: Heart Failure*, vol. 2, no. 5, pp. 437–445, 2009.

[10] E. Plante, D. Lachance, S. Champetier et al., "Benefits of long-term β-blockade in experimental chronic aortic regurgitation," *American Journal of Physiology—Heart and Circulatory Physiology*, vol. 294, no. 4, pp. H1888–H1895, 2008.

[11] D. Lachance, S. Champetier, E. Plante et al., "Effects of exercise in volume overload: insights from a model of aortic regurgitation," *Medicine and Science in Sports and Exercise*, vol. 41, no. 6, pp. 1230–1238, 2009.

[12] A.-A. Bouchard-Thomassin, D. Lachance, M.-C. Drolet, J. Couet, and M. Arsenault, "A high-fructose diet worsens eccentric left ventricular hypertrophy in experimental volume overload," *American Journal of Physiology—Heart and Circulatory Physiology*, vol. 300, no. 1, pp. H125–H134, 2011.

[13] M. Arsenault, A. Zendaoui, É. Roussel et al., "Angiotensin II-converting enzyme inhibition improves survival, ventricular remodeling, and myocardial energetics in experimental aortic regurgitation," *Circulation: Heart Failure*, vol. 6, no. 5, pp. 1021–1028, 2013.

[14] D. Lachance, W. Dhahri, M. Drolet et al., "Endurance training or beta-blockade can partially block the energy metabolism remodeling taking place in experimental chronic left ventricle volume overload," *BMC Cardiovascular Disorders*, vol. 14, article 190, 2014.

[15] W. Dhahri, J. Couet, É. Roussel, M.-C. Drolet, and M. Arsenault, "Fenofibrate reduces cardiac remodeling and improves cardiac function in a rat model of severe left ventricle volume overload," *Life Sciences*, vol. 92, no. 1, pp. 26–34, 2013.

[16] W. Dhahri, M.-C. Drolet, E. Roussel, J. Couet, and M. Arsenault, "Chronic high-fat diet-induced obesity decreased survival and increased hypertrophy of rats with experimental eccentric hypertrophy from chronic aortic regurgitation," *BMC Cardiovascular Disorders*, vol. 14, no. 1, article 123, 2014.

[17] E. Plante, J. Couet, M. Gaudreau, M.-P. Dumas, M.-C. Drolet, and M. Arsenault, "Left ventricular response to sustained volume overload from chronic aortic valve regurgitation in rats," *Journal of Cardiac Failure*, vol. 9, no. 2, pp. 128–140, 2003.

[18] M. Arsenault, E. Plante, M.-C. Drolet, and J. Couet, "Experimental aortic regurgitation in rats under echocardiographic guidance," *Journal of Heart Valve Disease*, vol. 11, no. 1, pp. 128–134, 2002.

[19] G. W. Wright and R. M. Simon, "A random variance model for detection of differential gene expression in small microarray experiments," *Bioinformatics*, vol. 19, no. 18, pp. 2448–2455, 2003.

[20] D. A. Hosack, G. Dennis Jr., B. T. Sherman, H. C. Lane, and R. A. Lempicki, "Identifying biological themes within lists of genes with EASE," *Genome Biology*, vol. 4, no. 10, article R70, 2003.

[21] A. Zendaoui, D. Lachance, É. Roussel, J. Couet, and M. Arsenault, "Usefulness of carvedilol in the treatment of chronic aortic valve regurgitation," *Circulation: Heart Failure*, vol. 4, no. 2, pp. 207–213, 2011.

[22] S. L. Ménard, E. Croteau, O. Sarrhini et al., "Abnormal *in vivo* myocardial energy substrate uptake in diet-induced type 2 diabetic cardiomyopathy in rats," *American Journal of Physiology—Endocrinology & Metabolism*, vol. 298, no. 5, pp. E1049–E1057, 2010.

[23] S. L. Ménard, X. Ci, F. Frisch et al., "Mechanism of reduced myocardial glucose utilization during acute hypertriglyceridemia in rats," *Molecular Imaging and Biology*, vol. 11, no. 1, pp. 6–14, 2009.

[24] E. Croteau, S. Gascon, M. Bentourkia et al., "[^{11}C]Acetate rest–stress protocol to assess myocardial perfusion and oxygen consumption reserve in a model of congestive heart failure in rats," *Nuclear Medicine and Biology*, vol. 39, no. 2, pp. 287–294, 2012.

[25] E. Croteau, F. Bénard, J. Cadorette et al., "Quantitative gated PET for the assessment of left ventricular function in small animals," *Journal of Nuclear Medicine*, vol. 44, no. 10, pp. 1655–1661, 2003.

[26] W. Dhahri, É. Roussel, M. C. Drolet et al., "Metformin reduces left ventricular eccentric re-modeling in experimental volume overload in the rat," *Journal of Clinical & Experimental Cardiology*, vol. 3, article 217, 2012.

[27] E. Croteau, F. Bénard, M. Bentourkia, J. Rousseau, M. Paquette, and R. Lecomte, "Quantitative myocardial perfusion and coronary reserve in rats with 13N-ammonia and small animal PET: impact of anesthesia and pharmacologic stress agents," *Journal of Nuclear Medicine*, vol. 45, no. 11, pp. 1924–1930, 2004.

[28] J.-C. Fruchart, B. Staels, and P. Duriez, "PPARS, metabolic disease and atherosclerosis," *Pharmacological Research*, vol. 44, no. 5, pp. 345–352, 2001.

[29] D. Lachance, É. Plante, É. Roussel, M.-C. Drolet, J. Couet, and M. Arsenault, "Early left ventricular remodeling in acute severe aortic regurgitation: insights from an animal model," *Journal of Heart Valve Disease*, vol. 17, no. 3, pp. 300–308, 2008.

[30] J. Barnes and L. J. Dell'Italia, "The multiple mechanistic faces of a pure volume overload: implications for therapy," *The American Journal of the Medical Sciences*, vol. 348, no. 4, pp. 337–346, 2014.

[31] T. D. Ryan, E. C. Rothstein, I. Aban et al., "Left ventricular eccentric remodeling and matrix loss are mediated by bradykinin and precede cardiomyocyte elongation in rats with volume overload," *Journal of the American College of Cardiology*, vol. 49, no. 7, pp. 811–821, 2007.

[32] S. Nemoto, P. Razeghi, M. Ishiyama, G. De Freitas, H. Taegtmeyer, and B. A. Carabello, "PPAR-gamma agonist rosiglitazone ameliorates ventricular dysfunction in experimental chronic mitral regurgitation," *The American Journal of Physiology—Heart and Circulatory Physiology*, vol. 288, no. 1, pp. H77–H82, 2005.

[33] H. N. Althurwi, O. H. Elshenawy, and A. O. S. El-Kadi, "Fenofibrate modulates cytochrome P450 and arachidonic acid metabolism in the heart and protects against isoproterenol-induced cardiac hypertrophy," *Journal of Cardiovascular Pharmacology*, vol. 63, no. 2, pp. 167–177, 2014.

[34] J. Zou, K. Le, S. Xu et al., "Fenofibrate ameliorates cardiac hypertrophy by activation of peroxisome proliferator-activated receptor-alpha partly via preventing p65-NFkappaB binding to NFATc4," *Molecular and Cellular Endocrinology*, vol. 370, no. 1-2, pp. 103–112, 2013.

[35] P. J. H. Smeets, H. M. de Vogel-van Den Bosch, P. H. M. Willemsen et al., "Transcriptomic analysis of PPARα-dependent alterations during cardiac hypertrophy," *Physiological Genomics*, vol. 36, no. 1, pp. 15–23, 2008.

[36] P. J. H. Smeets, B. E. J. Teunissen, P. H. M. Willemsen et al., "Cardiac hypertrophy is enhanced in PPARα-/- mice in response to chronic pressure overload," *Cardiovascular Research*, vol. 78, no. 1, pp. 79–89, 2008.

[37] T.-A. S. Duhaney, L. Cui, M. K. Rude et al., "Peroxisome proliferator-activated receptor α-independent actions of fenofibrate exacerbates left ventricular dilation and fibrosis in chronic pressure overload," *Hypertension*, vol. 49, no. 5, pp. 1084–1094, 2007.

[38] P. Balakumar, A. Rohilla, and N. Mahadevan, "Pleiotropic actions of fenofibrate on the heart," *Pharmacological Research*, vol. 63, no. 1, pp. 8–12, 2011.

[39] D. S. de Silva, R. M. Wilson, C. Hutchinson et al., "Fenofibrate inhibits aldosterone-induced apoptosis in adult rat ventricular myocytes via stress-activated kinase-dependent mechanisms," *American Journal of Physiology—Heart and Circulatory Physiology*, vol. 296, no. 6, pp. H1983–H1993, 2009.

[40] N. K. LeBrasseur, T.-A. S. Duhaney, D. S. De Silva et al., "Effects of fenofibrate on cardiac remodeling in aldosterone-induced hypertension," *Hypertension*, vol. 50, no. 3, pp. 489–496, 2007.

[41] Y.-W. Chen, B. Pat, J. D. Gladden et al., "Dynamic molecular and histopathological changes in the extracellular matrix and inflammation in the transition to heart failure in isolated volume overload," *The American Journal of Physiology—Heart and Circulatory Physiology*, vol. 300, no. 6, pp. H2251–H2260, 2011.

[42] Q. N. Diep, K. Benkirane, F. Amiri, J. S. Cohn, D. Endemann, and E. L. Schiffrin, "PPARα activator fenofibrate inhibits myocardial inflammation and fibrosis in angiotensin II-infused rats," *Journal of Molecular and Cellular Cardiology*, vol. 36, no. 2, pp. 295–304, 2004.

[43] Z. Jia, R. Xue, G. Liu et al., "HMGB1 is involved in the protective effect of the PPAR alpha agonist fenofibrate against cardiac hypertrophy," *PPAR Research*, vol. 2014, Article ID 541394, 9 pages, 2014.

Hindawi Publishing Corporation
BioMed Research International
Volume 2015, Article ID 409350, 10 pages
http://dx.doi.org/10.1155/2015/409350

Research Article

Angiotensinase C mRNA and Protein Downregulations Are Involved in Ethanol-Deteriorated Left Ventricular Systolic Dysfunction in Spontaneously Hypertensive Rats

Jinyao Liu, Ayako Hakucho, and Tatsuya Fujimiya

Department of Legal Medicine, Yamaguchi University Graduate School of Medicine, Ube, Yamaguchi 755-8505, Japan

Correspondence should be addressed to Jinyao Liu; czhliu@yamaguchi-u.ac.jp

Received 25 June 2015; Revised 10 August 2015; Accepted 11 August 2015

Academic Editor: Bodh I. Jugdutt

The influences of angiotensinase C on ethanol-induced left ventricular (LV) systolic function were assessed in spontaneously hypertensive rats (SHRs). SHRs were fed by a liquid diet with or without ethanol for 49 days. The normotensive Wistar Kyoto rats (WKY) were fed by the liquid diet without ethanol and used as control. We evaluated LV systolic function, angiotensinase C mRNA and protein expressions, activation of the renin-angiotensin system (RAS), and the gene expressions of LV collagen (Col) III a1 and matrix metalloproteinases- (MMP-) 9. Compared to the WKY, LV systolic dysfunction (expressed by decreased fractional shortening and ejection fraction) was observed in the SHRs before ethanol treatment and further deteriorated by ethanol treatment. In the ethanol-treated SHRs, the following were observed: downregulations of angiotensinase C mRNA and protein, increased RAS activity with low collagen production as evidenced by angiotensin II and angiotensin type 1 receptor (AT_1R) protein upregulation, $AT_{1a}R$ mRNA downregulation, and an MMP-9 mRNA expression upregulation trend with the downregulation of Col III a1 mRNA expression in LV. We conclude that chronic ethanol regimen is sufficient to promote the enhanced RAS activity-induced decrease in the production of cardiac collagen via downregulated angiotensinase C, leading to the further deterioration of LV systolic dysfunction in SHRs.

1. Introduction

Chronic heavy alcohol consumption is a common cause of heart failure and it leads to approximately one-fifth of all sudden cardiac deaths [1]. The underlying mechanisms through which alcohol produces this condition remain poorly understood [2].

Hypertensive heart disease, the leading cause of death from hypertension, causes left ventricular hypertrophy (LVH) through neural and humoral factors [3, 4]. As does compensatory cardiomyocyte hypertrophy, myocardial fibrosis makes a considerable contribution to LVH and leads to the development of LV diastolic and systolic dysfunction and ultimately to heart failure [5]. The activation of renin-angiotensin system (RAS) is a significant risk factor for the development of arterial hypertension, LVH, and heart failure [6–8]. Components of the RAS have been detected at both the cardiac mRNA and protein levels [9], and angiotensin II, the final mediator of the RAS, has been implicated in the production of matrix metalloproteinases (MMPs) and the breakdown of collagen [10]. In the spontaneously hypertensive rat (SHR), a widely studied animal model of human essential hypertension, MMPs damage cells directly by inducing the cleavage of the extracellular domain of several key receptors, resulting in the diverse cell dysfunctions characteristic of SHR [11]. Enhanced RAS activity thus acts on several different components of extracellular matrix formation and deposition to influence the matrix turnover that is responsible for the production of collagen and finally leads to cardiac dysfunction. However, the role of RAS in the development of alcohol-induced LV systolic function in essential hypertensive heart requires further investigation.

Angiotensinase C, also known as prolylcarboxypeptidase (PRCP) and reported to have antihypertensive and

antiproliferative roles via inactivation of the RAS, is responsible for RAS activity by the degradation of angiotensin II, the final mediator of the RAS [12]. The functions of angiotensinase C include the hydrolysis of angiotensin II to angiotensin 1–7 [13], which play a vital role in cardiac hypertrophy and remodeling [14–16].

SHR is hypertensive rat and that itself contributes to the cardiac remodeling and hypertrophy with the reduced cardiac angiotensinase C gene and protein expressions [17]. However, it is not known if the gene defect itself leads to specific heart defects in alcoholics. The present study thus provides, for the first time, direct evidence that enhanced RAS activity may be involved in the chronic ethanol consumption-induced development of LV systolic dysfunction via an angiotensinase C-dependent pathway in the essential hypertensive heart.

2. Methods

2.1. Animal and the Chronic Ethanol Treatment. Seven-week-old male normotensive Wistar Kyoto rats (WKY) ($n = 6$) and 7-week-old male SHRs ($n = 13$) were purchased from Japan SLC (Hamamatsu, Shizuoka, Japan). The rats were housed in a temperature-controlled room on a 12 hr light/dark cycle at the Institute of Laboratory Animals of Yamaguchi University. All rats were fed a nutritionally adequate liquid diet originally formulated by Lieber and DeCarli, purchased from Oriental Yeast Co., (Tokyo). The rats were divided into control liquid diet-fed WKY (WKY, $n = 6$), control liquid diet-fed SHR (SHR, $n = 6$), and ethanol liquid diet-fed SHR (SHR + Et, $n = 7$) groups. The protocol used for chronic ethanol exposure was as described [18]. Briefly, at the beginning of the study, all rats were given the control liquid diet and standard rat pellet chow for 4 days. For the next 4 days, the rats were fed either the control liquid diet or the ethanol liquid diet at a concentration of 3 g/dL. The control liquid diet-fed rats (WKY and SHR groups) received the further control liquid diet for 45 days, whereas the ethanol group (SHR + Et) received a diet containing 4 g/dL ethanol for the next 3 days, followed by 5 g/dL for 42 days, resulting in an overall exposure to ethanol of 49 days.

All animal experiments were performed according to the protocol approved by the Ethics Committee on Animal Experiments of the Yamaguchi University School of Medicine and were controlled by the committee's guidelines for animal experiments (#13-012).

2.2. Measurements of Arterial Blood Pressure (BP) and LV Functional Performance. Before and at the end of the experiments, the arterial blood pressure (BP) was measured in conscious rats by a tail-cuff monitoring system (BP-98A, Softron Co., Tokyo), and the LV systolic functional performance was evaluated by echocardiography (echocardiograph model SSD-1000 with a 10 MHz sector scan probe, Hitachi Aloka Medical, Tokyo) in anesthetized rats as described [18]. To avoid the influence of acute ethanol consumption, BP measurements and echocardiographic studies were performed between 2:00 and 4:00 p.m. in the ethanol group as described [19].

Systolic, diastolic, and mean BP values were recorded; however, only the mean blood pressure (MBP) data were used for the statistical analysis.

The internal LV end-diastolic diameter (LVDd) and the LV end-systolic diameter (LVDs) were measured according to the recommendations of the American Society of Echocardiography [20]. LV fractional shortening (LVFS) was calculated using the following formula: LVFS = (LVDd − LVDs)/LVDd × 100%. The LV end-diastolic and end-systolic volumes were calculated using the Teichholz formula, and the LV ejection fractions (LVEFs) were obtained.

2.3. Preparation of Tissue Samples. After the BP measurements and echocardiographic study, the rats were weighed and anesthetized with 1%-2% isoflurane in oxygen as described [18]. The heart was removed intact and the LV was then dissected and weighed. The LV weight was calculated by dividing the LV by the body weight of each animal. Each LV was excised and was cut perpendicular to the apex-to-base axis into three pieces. Two of these pieces were immediately frozen in liquid nitrogen and stored at −80°C for later mRNA and protein analyses.

2.4. Real-Time Reverse Transcriptase Polymerase Chain Reaction (RT-PCR). The total RNA was extracted from the LV tissue using the RNeasy Fibrous Tissue Mini Kit (Qiagen, Tokyo). ReverTra Ace qPCR RT Master Mix with gDNA Remover was used to remove gDNA and to synthesize cDNA according to the manufacturer's instruction. Real-time reverse transcriptase polymerase chain reaction (RT-PCR) was performed for the quantitative assessment of mRNA expression using an Applied Biosystems StepOne system (Applied Biosystems, Foster City, CA, USA). The gene expression assays for angiotensinase C (ID: Rn01511011_m1), angiotensin type 1a receptor ($AT_{1a}R$, ID: Rn01435427_m1), angiotensin type 2 receptor (AT_2R, ID: Mm01341373_m1), MAS-related G protein-coupled receptor D (MrgD, ID: Rn01785783_s1), matrix metalloproteinases-9 (MMP-9, ID: RnRn01423075_g1), collagen III a1 (Col III a1, ID: Rn01437681_m1), and GAPDH (ID: Rn99999916_s1) were purchased from Applied Biosystems. The relative expression genes were normalized to the amount of the GAPDH mRNA in an identical cDNA sample, using the comparative quantitative method recommended by the manufacturer; the relative expression is expressed as the fold change from the values of WKY.

2.5. Western Blot Assay. LV tissues harvested at the end of the study were homogenized using the Protein Extract Transmembrane Protein Extraction Kit (Novagen, Merck, Darmstadt, Germany) to extract the myocardial cytoplasm and transmembrane fraction proteins, respectively, according to the manufacturer's recommendations. Cytoplasm fraction proteins were used to evaluate the cardiac renin, angiotensin II, and angiotensinase C protein expressions. Transmembrane fraction proteins were used to evaluate the angiotensin type 1 receptor (AT_1R), angiotensin type 2 receptor (AT_2R), and G protein-coupled receptor-1 Mas subfamily (MAS1L)

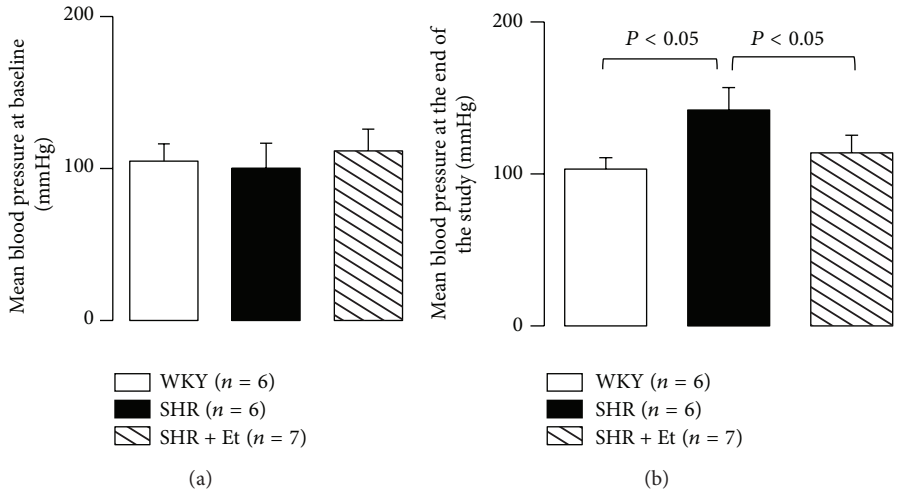

Figure 1: Mean blood pressure (MBP) at baseline and the end of the experiment. (a) MBP at baseline. (b) MBP at the end of the experiment. All values are means ± SDs.

protein expressions. The protein concentration was measured by the Bradford method.

Proteins of the LV were separated by sodium dodecyl sulfate polyacrylamide gel electrophoresis (SDS-PAGE, 10% (w/v) gel for cytoplasm fraction proteins and 4–20% (w/v) gel for transmembrane fraction proteins) and transferred to a polyvinyl difluoride membrane. Each blot was incubated with anti-GAPDH (1 : 200, rabbit polyclonal; Santa Cruz Biotechnology, Santa Cruz, CA), anti-renin (1 : 500, rabbit polyclonal; Abcam, Cambridge, MA), anti-angiotensin II (1 : 200, rabbit polyclonal; Bioss, Woburn, MA), anti-AT_1R (1 : 100, rabbit polyclonal; Santa Cruz Biotechnology), anti-AT_2R (1 : 100, rabbit polyclonal; Santa Cruz Biotechnology), anti-MAS1L (1 : 200, rabbit monoclonal; Abcam, Cambridge, MA), and anti-angiotensinase C (1 : 200, rabbit polyclonal; Santa Cruz Biotechnology) and then incubated with the appropriate secondary horseradish peroxidase-conjugated anti-rabbit IgG antibodies. Finally, the Western blotting bands were analyzed using Quantity One software (Bio-Rad Laboratories, Hercules, CA). The reaction products of LV renin, angiotensin II, AT_1R, AT_2R, MAS1L, and angiotensinase C were normalized to GAPDH and are expressed as the fold change from the values of WKY.

2.6. Statistical Analysis. Data were collected from repeated experiments and are presented as mean ± SD. Extreme values were excluded by the Smirnov-Grubbs test. For the statistical analysis, a one-way analysis of variance (ANOVA) was used with an overall F-test analysis. When an F-value was determined to be significant by the ANOVA, the Bonferroni/Dunn post hoc test was performed for multiple comparisons. The statistical analyses were performed using Statcel2 for Windows software (OMS Publishing, Saitama, Japan). Values of $P < 0.05$ were considered significant.

3. Results

3.1. Animal Characteristics. The SHR + Et group consumed 140 ± 10 g ethanol per animal during the 49-day feeding period.

No significant differences were found among the groups in MBP at baseline (7-week-old, Figure 1(a)). At the end of the feeding period (15-week-old), the SHR group showed increased MBP values with age compared to the WKY group, but the SHR + Et group showed decreased MBP values after 49-day ethanol treatment compared to the SHR group (Figure 1(b)).

Compared to the WKY group, the heart rate showed an upward trend in the SHR rats at baseline. There was a nonsignificant change in heart rate among the groups at the end of the experiments (Figures 2(a) and 2(b)).

There was a nonsignificant change in LV weight among the groups, although there were the upward trends in both of SHR and SHR + Et groups (Figure 3).

3.2. Ethanol Treatment Contributed to LV Systolic Dysfunction in the SHRs. Representative echocardiograms and data are shown in Figure 4. Before ethanol treatment, the 7-week-old SHR (both the SHR and SHR + Et groups) showed enlarged LVDs with decreased LVFS and LVEF compared to the WKY group (Figures 4(a) and 4(b)). The LV chamber sizes (both LVDd and LVDs) were enlarged with the decreased LVFS and LVEF at the end of the experiments in the 15-week-old SHR, especially in the SHR that had undergone the 49-day ethanol treatment (Figures 4(a) and 4(c)).

3.3. Ethanol Was Responsible for the Lower Collagen Production in the LV Myocardium. To determine whether the cardiac collagen production was related to the LV systolic dysfunction in the SHRs, especially those treated with ethanol,

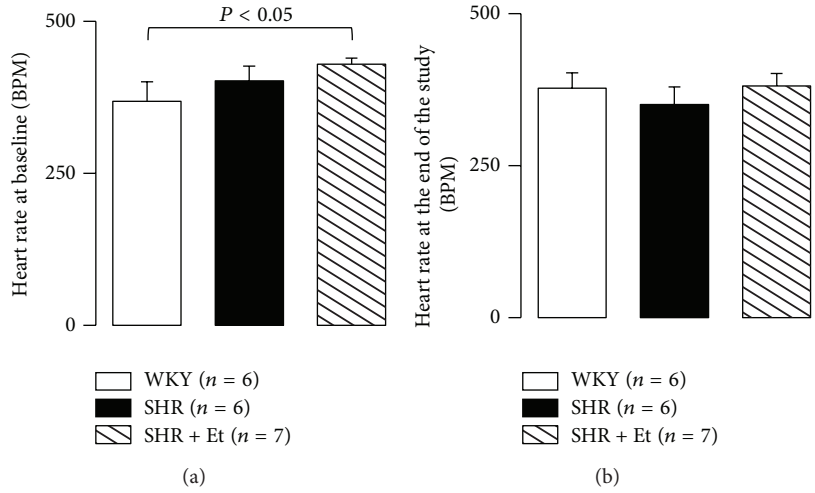

Figure 2: Heart rate at baseline and the end of the experiment. (a) Heart rate at baseline. (b) Heart rate at the end of the experiment. All values are means ± SDs.

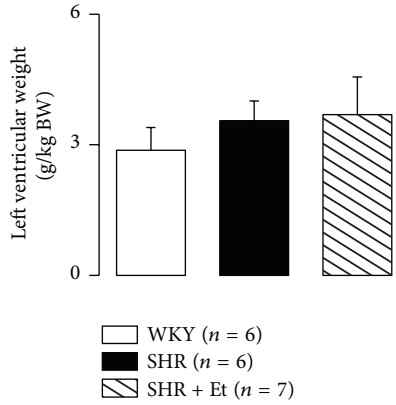

Figure 3: LV weight at the end of the study. All values are means ± SDs.

we evaluated the collagen production in LV myocardium by assessing the Col III a1 and MMP-9 mRNA expressions. There was a nonsignificant change in MMP-9 mRNA expression among the groups, although there were the upward trends in both of the SHR and SHR + Et groups (Figure 5(a)). A significant downregulation of Col III a1 (Figure 5(b)) mRNA expressions was observed in the LV myocardium of the ethanol-treated SHRs compared to the age-matched WKY rats.

3.4. Chronic Ethanol Consumption Enhanced the Activation of the RAS. Previous experiments have shown that activation of the RAS is an important growth factor, causing cell proliferation, cell differentiation, and apoptosis [21] and that angiotensin II, the final mediator of the RAS, stimulates the production of MMPs [22]. In the present study, we measured the LV protein expressions of renin, angiotensin II, and AT_1R and $AT_{1a}R$ mRNA expressions to evaluate the LV myocardial RAS activation. We observed an upregulating trend of renin, the significant upregulated angiotensin II, and AT_1R protein expressions in the SHR with 49-day ethanol treatment (Figures 6(a)–6(f)). The significant downregulation of $AT_{1a}R$ mRNA (Figure 6(g)) expressions was shown in both of the SHR and SHR + Et groups. AT_1R serves as a control point for regulating the ultimate effects of the RAS on its target tissue [23]. Our present findings indicate that ethanol was responsible for the enhanced RAS activity, which downregulated its own receptor ($AT_{1a}R$) gene expression due to the negative feedback control, as reported [23]. We also evaluate the changes of LV gene and protein expressions in AT_2R and receptor Mas. However, there was a nonsignificant change in mRNA expressions of AT_2R and MrgD and protein expressions of AT_2R and MAS1L among the groups (data not shown).

3.5. Downregulations of LV Angiotensinase C mRNA and Protein in SHRs. Angiotensinase C gene mutations with loss of function induced the inadequate degradation of angiotensin II followed by blood pressure elevation with the elevated RAS activation [24]. Angiotensinase C mRNA and protein expressions were used to evaluate the LV myocardial angiotensinase C function in the present study. The angiotensinase C mRNA (Figure 7(a)) and protein (Figures 7(b) and 7(c)) expressions were significantly downregulated in the LV myocardium of the SHRs (both of SHR and SHR + Et groups) compared to the age-matched WKY rats.

4. Discussion

We observed that in spontaneously hypertensive rats (SHRs), 49-day 5 g/dL ethanol consumption downregulated the expressions of angiotensinase C mRNA and protein and enhanced the activation of the RAS, as evidenced by the upregulated angiotensin II and AT_1R protein expressions, and the downregulated $AT_{1a}R$ mRNA expression, followed by LV dilation and dysfunction. This was associated with

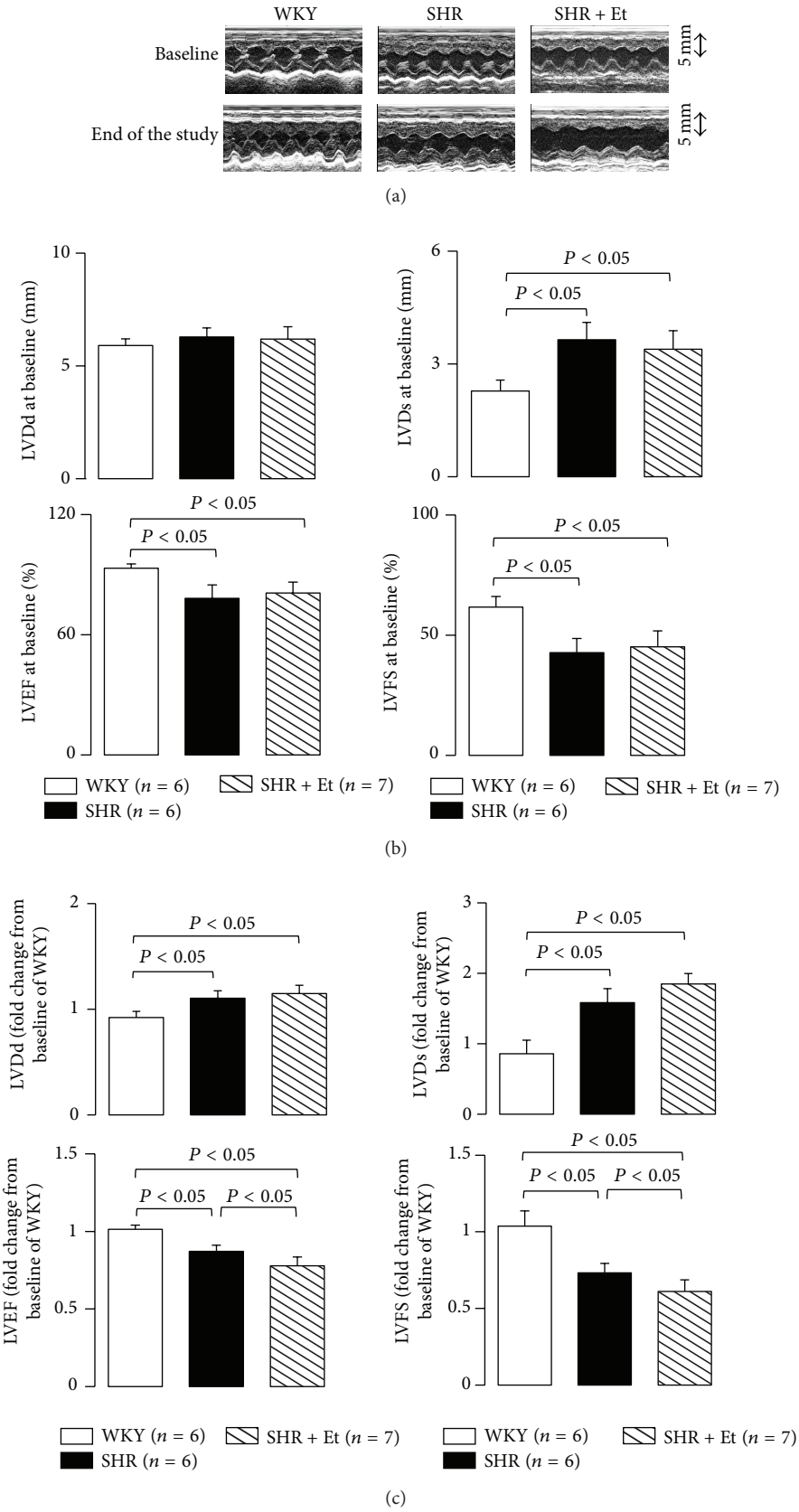

Figure 4: Chronic ethanol consumption damaged the LV systolic function in the SHRs. (a) Representative echocardiograms. (b) Before ethanol treatment, the SHRs showed enlarged LVDs with decreased LVFS and LVEF. (c) The LV chamber sizes were enlarged with the decreased LVFS and LVEF at the end of the experiments, especially in the SHR with 49-day ethanol treatment. All values are means ± SDs.

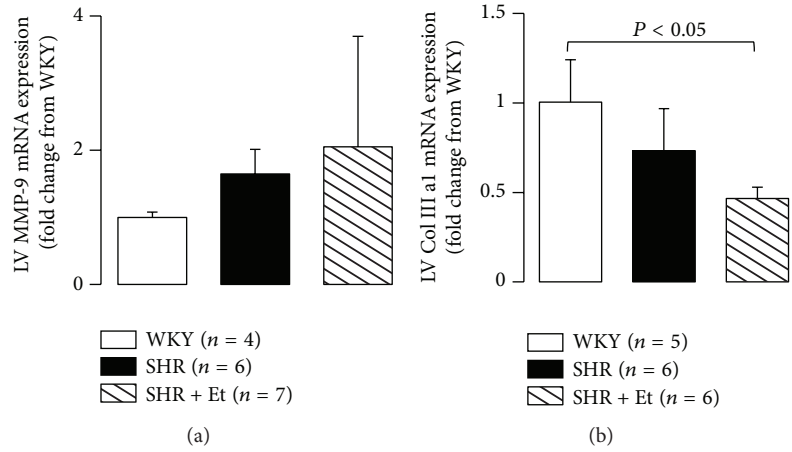

Figure 5: Collagen production in LV myocardium. (a) There was a nonsignificant change in MMP-9 mRNA expression among the groups, although there were the upward trends in both of SHR and SHR + Et groups. (b) Downregulated Col III a1 was observed in the ethanol-treated SHRs. All values are means ± SDs.

a low collagen production by the LV myocardium, expressed as a significant downregulation of Col III a1 mRNA expression. Thus, the results of the present study demonstrate the key role of angiotensinase C acting through an activated RAS-induced low collagen production in the development of LV dilation and systolic dysfunction in essential hypertensive heart with chronic ethanol consumption.

The main effect of alcohol ingestion is a loss of cardiac contractility that induces the development of dilated cardiomyopathy and leads to heart failure [2]. However, the experimental evaluation of cardiac contractile performance as alcoholism progresses has been difficult in the past due to the lack of experimental heart failure animal models that closely resemble the human condition [2]. Acute alcohol consumption is reported to have a direct cardiac depressant effect [25]. However, chronic alcohol intake has been variably reported to impair LV function [26, 27].

Myocyte orientation and myocardial fiber angles are organized and moved from the endocardium to the epicardium. It is the structural network of matrix proteins such as type I and type III collagen that provides structural integrity to adjoining myocytes and contribute to overall LV pump function through the coordination of myocyte shortening [28]. The loss of collagen fibrils and struts, which are regulated in part by the activity of MMP [29], leads to LV dilation and progressive contractile dysfunction [30]. The present study showed that chronic ethanol consumption promoted the deterioration of the impairment of LV systolic function in SHRs, and the LV systolic dysfunction was associated with a downward trend of LV collagen production, expressed as the upregulating trend of MMP-9 expression and a significant downregulation of Col III 3a1 mRNA expression.

Increased circulating levels of angiotensin II and elevated plasma renin activity occur with the development of severe heart failure in patients [31]. Chronic alcohol-induced LV dysfunction and cardiac failure have been prevented in humans by the administration of an angiotensin receptor blocker during the ingestion of alcohol, which indicates that the chronic administration of a specific AT_1R antagonist can provide a protective effect on the LV and myocyte contractile performance during ethanol consumption by humans [31]. The effects of the enhanced RAS activity and the elevated angiotensin II on regulating the physiological processes of the cardiovascular system depend on the cellular expression and activation of AT_1Rs. AT_1Rs are seven-membrane superfamily of G protein-coupled receptors. The human AT_1R gene has been mapped to chromosome. In rats, two isoforms have been pointed out: $AT_{1a}R$ on chromosome 17 and the $AT_{1b}R$ on chromosome 2; however, in vivo experiments showed that the $AT_{1a}R$ may be more important than $AT_{1b}R$ as reviewed by Mehta and Griendling [16]. Receptor Mas, a receptor for angiotensin (1–7), is an important player of the RAS. Mas-related genes are a large family of G protein-coupled receptors, which localized in chromosome 1 in the rat and chromosome 11 in humans. Angiotensin (1–7) has proved to be a weak agonist of the MAS-related G protein-coupled receptor D [32]. In the present study, chronic ethanol induced the upregulation of cardiac angiotensin II protein accompanied with the upregulated cardiac AT_1R protein expression. However, we could not find the differences among the groups in neither cardiac AT_2R and MrgD genes nor AT_2R and MAS1L proteins expressions (data not shown). Contrary to heart failure due to other causes, changes in the RAS occur early in the course of chronic alcohol consumption. Consistent with past reports [33], the chronic ethanol ingestion in the present study was accompanied by a similar profile of RAS activation. An accumulation of extracellular matrix and its reduced turnover is responsible for the development of hypertrophy and heart failure [16]. Activation of the RAS is implicated in the synthesis of the extracellular matrix protein collagen via both AT_1Rs and AT_2Rs [34].

The production of MMPs and the breakdown of collagen are also modulated by RAS activation [10, 22]. Thus, activation of the RAS acts on several different components of extracellular matrix formation and deposition to influence

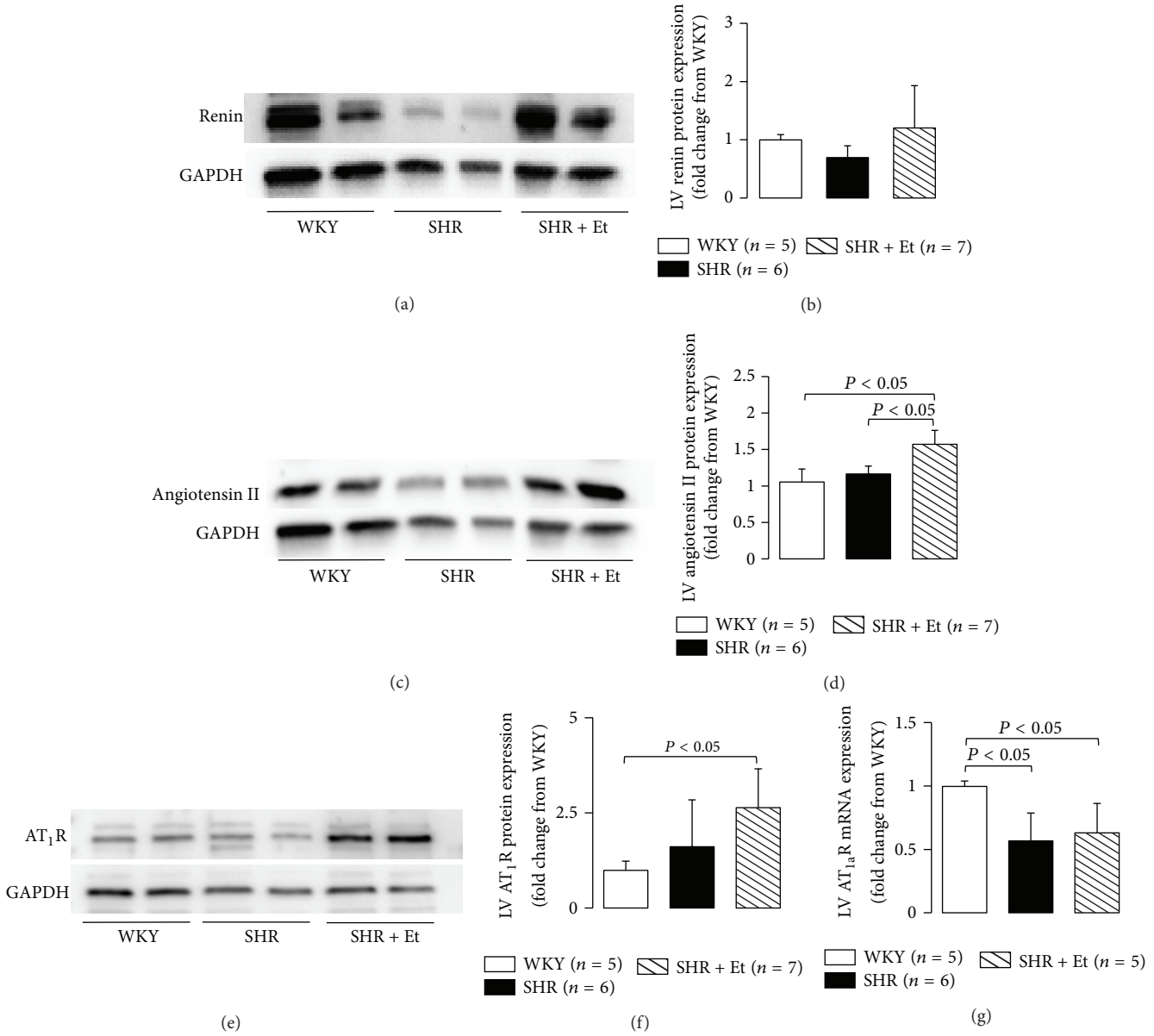

Figure 6: Ethanol consumption and the activation of RAS in the SHRs. (a) Representative Western blot of renin protein expression. (b) There was a nonsignificant change in renin protein expression among the groups, although there was an upward trend in the ethanol-treated SHRs. (c) Representative Western blot of angiotensin II protein expression. (d) Significant upregulated angiotensin II protein expression was observed in the ethanol-treated SHRs. (e) Representative Western blot of AT_1R protein expression. (f) A significant upregulated AT_1R protein expression was observed in the ethanol-treated SHRs. (g) Significant downregulated $AT_{1a}R$ mRNA expressions were observed in both of SHR and SHR + Et groups. All values are means ± SDs.

matrix turnover. MMPs are zinc-dependent endopeptidases that cleave extracellular matrix proteins and affect the outcome of various physiological and pathological processes including myocardial infarction, atherosclerosis, and cardiac dysfunction. In addition to structural extracellular matrix components, MMP substrates include a multitude of ligand and receptor substrates such as cytokines, chemokines, growth factors, and adhesion molecules that alter cellular migration, adhesion, and activation [35, 36]. In SHRs, elevated MMPs cause direct damage to cells by cleavage of the extracellular domain of several key receptors, which results in the diverse cell dysfunctions characteristic of the SHR as discussed by Berry et al. in 2013 [37]. Our present data suggest that the regulation of the collagenase III a1/MMP-9 system via activation of the LV myocardial RAS is altered in the hypertrophied LV of SHRs, especially in SHRs with chronic ethanol treatment-induced systolic dysfunction.

Gene manipulation studies in animals showed that hypertension is associated with diminished angiotensinase C gene expression [38]. Angiotensinase C gene mutations with loss of

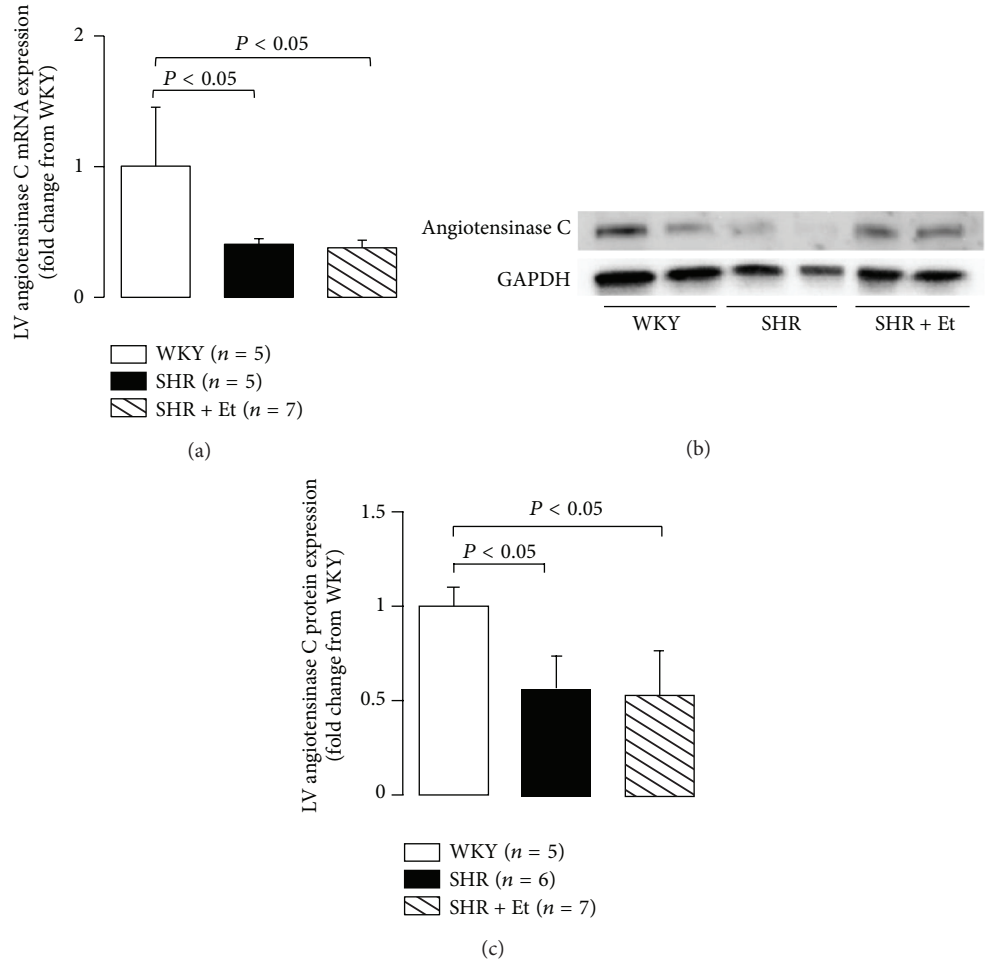

Figure 7: Downregulations of angiotensinase C gene and protein in LV myocardium. (a) Downregulation of angiotensinase C mRNA expressions in the SHRs. (b) Representative Western blot. (c) Downregulated angiotensinase C protein expressions in the LV myocardium of the SHRs. All values are means ± SDs.

function induced the inadequate degradation of angiotensin II, the final mediator of the RAS, followed by blood pressure elevation [24]. The present findings revealed downregulated angiotensinase C mRNA and protein expressions in the LV tissue of SHRs, a widely studied animal model of human essential hypertension, especially in SHRs with chronic ethanol consumption.

5. Conclusions

The conscious instrumented SHR model represents a clinically relevant, chronic ethanol consumption model for studies of ethanol-induced LV systolic function impairment. With the use of this model, the present study revealed that chronic ethanol ingestion produced progressive LV systolic functional impairment, a downward trend in the production of collagen in LV myocardium, and upregulated RAS activation, which was paralleled by downregulated expressions of angiotensinase C mRNA and protein. This indicates a key role for angiotensinase C acting through the enhanced activation of an RAS-induced low production of LV collagen during the development of LV dilation and systolic dysfunction after chronic ethanol consumption.

Conflict of Interests

The authors declare that there is no conflict of interest regarding the publication of this paper.

Authors' Contribution

Jinyao Liu designed the research; Jinyao Liu and Ayako Hakucho performed the research; Jinyao Liu, Ayako Hakucho, and Tatsuya Fujimiya analyzed and interpreted the data; Jinyao Liu wrote the paper.

Acknowledgments

The authors thank Hiroko Kodama, Yuki Kubo, and Xu Liu (Yamaguchi University) for their kind assistance in the animal preparation and blood pressure measurements.

The work presented in this study was partly supported by the Japan Society for the Promotion of Science Grants-in-Aid for Scientific Research (to Jinyao Liu, Grant no. 25460869).

References

[1] E. Hookana, M. J. Junttila, V.-P. Puurunen et al., "Causes of nonischemic sudden cardiac death in the current era," *Heart Rhythm*, vol. 8, no. 10, pp. 1570–1575, 2011.

[2] D. L. Lucas, R. A. Brown, M. Wassef, and T. D. Giles, "Alcohol and the cardiovascular system: research challenges and opportunities," *Journal of the American College of Cardiology*, vol. 45, no. 12, pp. 1916–1924, 2005.

[3] M. Zhao, S. Zheng, J. Yang et al., "Suppression of TGF-β1/Smad signaling pathway by sesamin contributes to the attenuation of myocardial fibrosis in spontaneously hypertensive rats," *PLoS ONE*, vol. 10, no. 3, Article ID e0121312, 2015.

[4] E. S. Muxfeldt, F. de Souza, V. S. Margallo, and G. F. Salles, "Cardiovascular and renal complications in patients with resistant hypertension," *Current Hypertension Reports*, vol. 16, p. 471, 2014.

[5] B. C. Berk, K. Fujiwara, and S. Lehoux, "ECM remodeling in hypertensive heart disease," *Journal of Clinical Investigation*, vol. 117, no. 3, pp. 568–575, 2007.

[6] L. Barlucchi, A. Leri, D. E. Dostal et al., "Canine ventricular myocytes possess a renin-angiotensin system that is upregulated with heart failure," *Circulation Research*, vol. 88, no. 3, pp. 298–304, 2001.

[7] Z. Abassi, I. Goltsman, T. Karram, J. Winaver, and A. Hoffman, "Aortocaval fistula in rat: a unique model of volume-overload congestive heart failure and cardiac hypertrophy," *Journal of Biomedicine and Biotechnology*, vol. 2011, Article ID 729497, 13 pages, 2011.

[8] F. C. Luft, "Present status of genetic mechanisms in hypertension," *Medical Clinics of North America*, vol. 88, no. 1, pp. 1–18, 2004.

[9] M. Paul, A. P. Mehr, and R. Kreutz, "Physiology of local renin–angiotensin systems," *Physiological Reviews*, vol. 86, no. 3, pp. 747–803, 2006.

[10] P. Libby and R. T. Lee, "Matrix matters," *Circulation*, vol. 102, no. 16, pp. 1874–1876, 2000.

[11] N. Duansak and G. W. Schmid-Schönbein, "The oxygen free radicals control MMP-9 and transcription factors expression in the spontaneously hypertensive rat," *Microvascular Research*, vol. 90, pp. 154–161, 2013.

[12] N. Grobe, N. M. Weir, O. Leiva et al., "Identification of prolyl carboxypeptidase as an alternative enzyme for processing of renal angiotensin II using mass spectrometry," *The American Journal of Physiology—Cell Physiology*, vol. 304, no. 10, pp. C945–C953, 2013.

[13] C. E. Odya, D. V. Marinkovic, K. J. Hammon, T. A. Stewart, and E. G. Erdös, "Purification and properties of prolylcarboxypeptidase (angiotensinase C) from human kidney," *The Journal of Biological Chemistry*, vol. 253, no. 17, pp. 5927–5931, 1978.

[14] M. Iwata, R. T. Cowling, D. Gurantz et al., "Angiotensin-(1-7) binds to specific receptors on cardiac fibroblasts to initiate antifibrotic and antitrophic effects," *The American Journal of Physiology—Heart and Circulatory Physiology*, vol. 289, no. 6, pp. H2356–H2363, 2005.

[15] E. A. Tallant, C. M. Ferrario, and P. E. Gallagher, "Angiotensin-(1–7) inhibits growth of cardiac myocytes through activation of the mas receptor," *The American Journal of Physiology—Heart and Circulatory Physiology*, vol. 289, no. 4, pp. H1560–H1566, 2005.

[16] P. K. Mehta and K. K. Griendling, "Angiotensin II cell signaling: physiological and pathological effects in the cardiovascular system," *The American Journal of Physiology—Cell Physiology*, vol. 292, no. 1, pp. C82–C97, 2007.

[17] R. A. Marangoni, R. A. Santos, and C. Piccolo, "Deficient prolylcarboxypeptidase gene and protein expression in left ventricles of spontaneously hypertensive rats (SHR)," *Peptides*, vol. 61, pp. 69–74, 2014.

[18] J. Liu, M. Yano, A. Shimamoto, T. Noma, M. Matsuzaki, and T. Fujimiya, "Chronic effects of ethanol on pharmacokinetics and left ventricular systolic function in rats," *Alcoholism: Clinical and Experimental Research*, vol. 31, no. 3, pp. 493–499, 2007.

[19] J. Liu, S. Shirafuji, and T. Fujimiya, "Rats in acute withdrawal from ethanol exhibit left ventricular systolic dysfunction and cardiac sympathovagal balance shift," *Alcohol*, vol. 43, no. 3, pp. 207–216, 2009.

[20] M. D. Cheitlin, W. F. Armstron, G. P. Aurigemma et al., "ACC/AHA/ASE 2003 Guideline update for the clinical application of echocardiography: summary article. A report of the American College of Cardiology/American Heart Association Task Force on Practice Guidelines (ACC/AHA/ASE Committee to update the 1997 Guidelines for the clinical application of echocardiography)," *Journal of the American Society of Echocardiography*, vol. 16, pp. 1091–1110, 2003.

[21] V. J. Dzau, "Theodore Cooper Lecture: tissue angiotensin and pathobiology of vascular disease: a unifying hypothesis," *Hypertension*, vol. 37, no. 4, pp. 1047–1052, 2001.

[22] V. J. Dzau, G. H. Gibbons, and R. E. Pratt, "Molecular mechanisms of vascular renin-angiotensin system in myointimal hyperplasia," *Hypertension*, vol. 18, no. 4, pp. II100–II105, 1991.

[23] B. Lassegue, R. W. Alexander, G. Nickenig, M. Clark, T. J. Murphy, and K. K. Griendling, "Angiotensin II down-regulates the vascular smooth muscle AT1 receptor by transcriptional and post-transcriptional mechanisms: evidence for homologous and heterologous regulation," *Molecular Pharmacology*, vol. 48, no. 4, pp. 601–609, 1995.

[24] B. Watson Jr., N. J. Nowak, A. D. Myracle, T. B. Shows, and D. G. Warnock, "The human angiotensinase C gene (HUMPCP) maps to 11q14 within 700 kb of D11S901: a candidate gene for essential hypertension," *Genomics*, vol. 44, no. 3, pp. 365–367, 1997.

[25] C.-P. Cheng, Z. Shihabi, and W. C. Little, "Acute effects of mildly intoxicating levels of alcohol on left ventricular function in conscious dogs," *Journal of Clinical Investigation*, vol. 85, no. 6, pp. 1858–1865, 1990.

[26] G. R. Noren, N. A. Staley, S. Einzig, F. L. Mikell, and R. W. Asinger, "Alcohol-induced congestive cardiomyopathy: an animal model," *Cardiovascular Research*, vol. 17, no. 2, pp. 81–87, 1983.

[27] G. Thomas, B. Haider, H. A. Oldewurtel, M. M. Lyons, C. K. Yeh, and T. J. Regan, "Progression of myocardial abnormalities in experimental alcoholism," *American Journal of Cardiology*, vol. 46, no. 2, pp. 233–241, 1980.

[28] D. D. Streeter Jr., H. M. Spotnitz, D. P. Patel, J. Ross Jr., and E. H. Sonnenblick, "Fiber orientation in the canine left ventricle during diastole and systole," *Circulation Research*, vol. 24, no. 3, pp. 339–347, 1969.

[29] S. Heymans, F. Lupu, S. Terclavers et al., "Loss or inhibition of uPA or MMP-9 attenuates LV remodeling and dysfunction

after acute pressure overload in mice," *The American Journal of Pathology*, vol. 166, no. 1, pp. 15–25, 2005.

[30] J. S. Janicki and G. L. Brower, "The role of myocardial fibrillar collagen in ventricular remodeling and function," *Journal of Cardiac Failure*, vol. 8, no. 6, pp. S319–S325, 2002.

[31] C.-P. Cheng, H.-J. Cheng, C. Cunningham et al., "Angiotensin II type 1 receptor blockade prevents alcoholic cardiomyopathy," *Circulation*, vol. 114, no. 3, pp. 226–236, 2006.

[32] G. M. Etelvino, A. A. B. Peluso, and R. A. S. Santos, "New components of the renin-angiotensin system: alamandine and the Mas-related G protein-coupled receptor D," *Current Hypertension Reports*, vol. 16, no. 6, article 433, 2014.

[33] M. R. Piano, "Alcoholic cardiomyopathy: incidence, clinical characteristics, and pathophysiology," *Chest*, vol. 121, no. 5, pp. 1638–1650, 2002.

[34] M. Mifune, H. Sasamura, R. Shimizu-Hirota, H. Miyazaki, and T. Saruta, "Angiotensin II type 2 receptors stimulate collagen synthesis in cultured vascular smooth muscle cells," *Hypertension*, vol. 36, no. 5, pp. 845–850, 2000.

[35] M. L. Lindsey, "MMP induction and inhibition in myocardial infarction," *Heart Failure Reviews*, vol. 9, no. 1, pp. 7–19, 2004.

[36] M. L. Lindsey and R. Zamilpa, "Temporal and spatial expression of matrix metalloproteinases and tissue inhibitors of metalloproteinases following myocardial infarction," *Cardiovascular Therapeutics*, vol. 30, no. 1, pp. 31–41, 2012.

[37] E. Berry, A. M. Bosonea, X. Wang, and C. Fernandez-Patron, "Insights into the activity, differential expression, mutual regulation, and functions of matrix metalloproteinases and a disintegrin and metalloproteinases in hypertension and cardiac disease," *Journal of Vascular Research*, vol. 50, no. 1, pp. 52–68, 2013.

[38] A. H. Schmaier, "The plasma kallikrein-kinin system counterbalances the renin-angiotensin system," *The Journal of Clinical Investigation*, vol. 109, no. 8, pp. 1007–1009, 2002.

Hindawi Publishing Corporation
BioMed Research International
Volume 2015, Article ID 539805, 11 pages
http://dx.doi.org/10.1155/2015/539805

Research Article

Neonatal Death and Heart Failure in Mouse with Transgenic HSP60 Expression

Tsung-Hsien Chen,[1] Shan-Wen Liu,[1,2] Mei-Ru Chen,[1] Kuan-Hung Cho,[1] Tzu-Yin Chen,[1] Pao-Hsien Chu,[3] Yu-Ying Kao,[4] Ching-Han Hsu,[2] and Kurt Ming-Chao Lin[1]

[1]*Institute of Biomedical Engineering and Nanomedicine, National Health Research Institutes, Zhunan, Miaoli County, Taiwan*
[2]*Department of Biomedical Engineering and Environmental Sciences, National Tsing Hua University, Hsinchu, Taiwan*
[3]*Division of Cardiology, Department of Internal Medicine, Chang Gung Memorial Hospital, College of Medicine, Chang Gung University, Taipei, Taiwan*
[4]*Department of Biotechnology, Chia Nan University of Pharmacy and Science, Tainan, Taiwan*

Correspondence should be addressed to Kurt Ming-Chao Lin; klin@nhri.org.tw

Received 27 June 2015; Accepted 26 August 2015

Academic Editor: Bodh I. Jugdutt

Mitochondrial heat shock proteins, such as HSP60, are chaperones responsible for the folding, transport, and quality control of mitochondrial matrix proteins and are essential for maintaining life. Both prosurvival and proapoptotic roles have been proposed for HSP60, and HSP60 is reportedly involved in the initiation of autoimmune, metabolic, and cardiovascular diseases. The role of HSP60 in pathogenesis of these diseases remains unclear, partly because of the lack of mouse models expressing HSP60. In this study we generated HSP60 conditional transgenic mice suitable for investigating *in vivo* outcomes by expressing HSP60 at the targeted organ in disease models. Ubiquitous HSP60 induction in the embryonic stage caused neonatal death in mice at postnatal day 1. A high incidence of atrial septal defects was observed in HSP60-expressing mice, with increased apoptosis and myocyte degeneration that possibly contributed to massive hemorrhage and sponge-like cardiac muscles. Our results showed that neonatal heart failure through HSP60 induction likely involves developmental defects and excessive apoptosis. The conditional HSP60 mouse model is useful for studying crucial biological questions concerning HSP60.

1. Introduction

Heat shock proteins (HSPs) are molecular chaperones responsible for critical functions, such as protein folding, transport, and signaling. Under stress, HSPs preserve proteins in their native forms and refold denatured proteins [1]. Mitochondrial chaperonins, such as HSP60, together with HSP10, refold all proteins imported into the mitochondrial matrix and facilitate the restoration of unfolded or misfolded matrix proteins under normal and stressed environments; hence, they are vital for maintaining mitochondrial functions, including ATP synthesis [2–4]. Although the fundamental biology of HSP60 particularly on mechanisms of substrate folding has been explored extensively, HSP60-related studies are gaining increasing attention because new findings about the roles of mitochondrial, cytosolic, and extracellular HSP60 in a wide array of diseases have emerged [5]. Most HSPs are prosurvival, although both prosurvival and prodeath roles of HSP60 have been reported. The protective role of HSP60 in various cell types, including cardiac myocytes, has been reported [6–13]. Preservation of mitochondrial capacity by HSP60 with reduced cytochrome C release during stress challenges and subsequent apoptosis reduction were among the common findings of the protection by HSP60. Upregulated HSP60 expression in several studies suggested the prosurvival and antiapoptotic roles of HSP60 in cancers [14], such as cervical [15], prostate [16], and colorectal cancers [17] and Hodgkin lymphoma [18]. The proapoptotic role of HSP60 was documented in muscles [19] and in various cancer cell lines [20, 21]; for example, malignancy of esophageal squamous cell carcinoma [22] and ovarian [23] and bladder cancers [24] was found inversely correlated with

HSP60 expression. The findings of HSP60 accumulation in cytoplasm in various apoptosis models and HSP60 binding to procaspase-3 supported the proapoptotic properties of HSP60 [21, 25]. Besides the discrepancy among reports of *in vitro* studies, the roles of HSP60 in physiology and pathology cannot be fully elucidated without using transgenic (Tg) mouse models expressing HSP60 *in vivo*.

The role of extracellular HSP60 in viral infection, innate or adaptive immunity, and atherosclerosis has been widely documented [26–28]. Hepatitis B virus replication induced HSP60 production, and HSP60 has a critical role in regulatory T cells functions, particularly in IL-10 secretion [28]. Innate immune cell surface receptors, namely, TLR2, TLR4, and CD14, are known receptors for extracellular HSP60, resulting in the release of mediators such as TNF-α, IL-1β, IL-6, and NO, which in turn enhance inflammation in type 1 diabetes mellitus (DM), atherosclerosis, arthritis, and transplant rejection.

HSP60 expression in the heart is reduced in ageing and metabolic diseases [29]. Caloric restriction that is shown increases lifespan restored aging-related decline of HSP60 expression in the heart and improved cardiovascular functions [29]. The reduction in HSP60 level contributing to low insulin sensitivity and to dysfunctions in metabolic syndrome and type 2 DM was proposed [30]. Because of the importance of HSP60 in many diseases, Tg mouse models with inducible and tissue-specific HSP60 expression can provide useful insights and expand the current understanding of these diseases.

Previously nonobese diabetic (NOD) HIIEα-HSP60 Tg mice, in which HSP60 is driven by the MHC class II-Eα (HIIEα) promoter, achieved HSP60 expression specifically in the thymus and bone marrow and suppressed susceptibility to autoimmunity induced DM [31]. Tg mice expressing truncated HSP60 instead of the entire HSP60 were also reported, and the resultant cytosolic HSP60 Tg mice were resistant to hepatic stress with increased cell survival [32]. However, Tg mice with HSP60 expression in other tissues have not been reported. Attempts to generate a conventional HSP60 mouse model did not succeed because Tg founders as chimeras failed to survive (personal communications). In this report, we present a viable and healthy inducible HSP60 Tg mouse (G-Lox-HSP60) in FVB strain driven by a ubiquitous CMV early enhancer/chicken β-actin promoter (CAGGS). This model overcame the early lethality of the conventional Tg approach. After crossing the G-Lox-HSP60 mouse with the Cre mouse, we observed neonatal death in mice with HSP60 expression from the embryo stage.

2. Materials and Methods

2.1. Generation of G-Lox-Hsp60 and EGFP-Cre Transgenic Mice. A G-Lox-Hsp60 mouse, FVB/N-Tg(ACTB-EGFP/HSPD1)14Klin, was generated by using the Tg vector (Figure 1(a)) and constructed by inserting the following fragments: CAGGS promoter, 2 LoxP sites at the start and the end separated by an EGFP coding sequence and an SV40 polyA sequence (pEGFP-C2, Clontech, Mountain View, CA), and a human HSP60 cDNA (NM_002156, 102–1920 bp) inserted into the pDsRed-N1 vector (Clontech), in which the CMV enhancer was removed. An *Apa*LI-*Afl*II fragment was used for microinjection into the FVB blastocysts. EGFP-Cre mouse, FVB/N-Tg(ACTB-EGFP.CRE)21Klin, was constructed by inserting CAGGS and Cre (AF334827, 1767–2789 bp) into the pEGFP-C2 vector, in which the CMV enhancer was removed [33]. For unknown reasons, the green fluorescence of the EGFP-Cre mouse was extremely weak. G-Lox-DsRed mice have been described previously [34]. All animal experiments were conducted in accordance with the accepted standards of animal care and were approved by the Institutional Animal Care and Use Committee of the National Health Research Institutes, Taiwan. The following PCR primers pairs were used for genotyping for the results in Figure 1(b)(A): (I) 5′-AATGCTCACCGTAAGCCTTT-3′, 5′-CCATCTGAAAGTTTTGCAAG-3′, T_m = 65.5°C, 407 bp; (II) 5′-CTGCTAACCATGTTCATGCC-3′, 5′-ACCGTCAGTACGTGAGATATCTT-3′, T_m = 58°C, 1443 bp; and (III) 5′-CTGCTAACCATGTTCATGCC-3′, 5′-CCATCTGAAAGTTTTGCAAG-3′, T_m = 60°C, 1442 bp.

2.2. Analysis of mRNA, Semiquantitative RT-PCR, and Protein Expression. Total RNA was isolated from heart homogenates with a TRIzol reagent (Invitrogen, Carlsbad, CA). Genomic DNA contamination in the RNA samples was removed through DNase I digestion, and cDNA of the first strand was synthesized using ReverTra Ace reverse transcriptase (Toyobo, Japan) and oligo(dT) as the primer. The following PCR primers were used for amplifying the target genes for the results in Figure 1(b)(B): Human HSP60: the same as listed in (I); human and mouse HSP60: 5′-GTCAGAAATGTG-AATTCCAG-3′, 5′-TTGACTGCCACAACCTGAAGAC-3′, T_m = 55°C, 200 bp; and GAPDH: 5′-GTGGCAAAGTGG-AGATTGCC-3′, 5′-GATGATGACCCGTTTGGCTCC-3′, T_m = 58°C, 290 bp. Ten micrograms of total proteins isolated from tissue homogenates was subjected to 10% SDS-PAGE, followed by Western blotting using anti-HSP60 (ab5479, Abcam) and anti-GFP (ab290) antibodies. Ten micrograms of total proteins isolated from MDA-MB231 cells was used for comparison.

2.3. Fluorescence Detection and Histological Analysis. Hearts of neonatal mice and E17 mouse embryos were washed with PBS and fixed by 10% neutral formalin. Stereo microscope (Olympus SZX10) with fluorescence module was used for observing green fluorescence of neonatal mouse hearts. For investigating septum defects, unfixed neonatal hearts were immersed in OCT matrix (Tissue-Tek, USA) and frozen quickly in liquid nitrogen. The samples were cryosectioned 10 μm thick followed by hematoxylin and eosin (H&E) staining to reveal the four-chamber view of hearts. In parallel, formalin-fixed hearts were embedded in paraffin and cut into serial 5 μm sections and stained with H&E to evaluate morphology.

2.4. Immunohistochemical and Immunofluorescence Assay. Paraffin-embedded tissue sections were dewaxed, rehydrated, and treated by 3% hydrogen peroxide in methanol for 30 min.

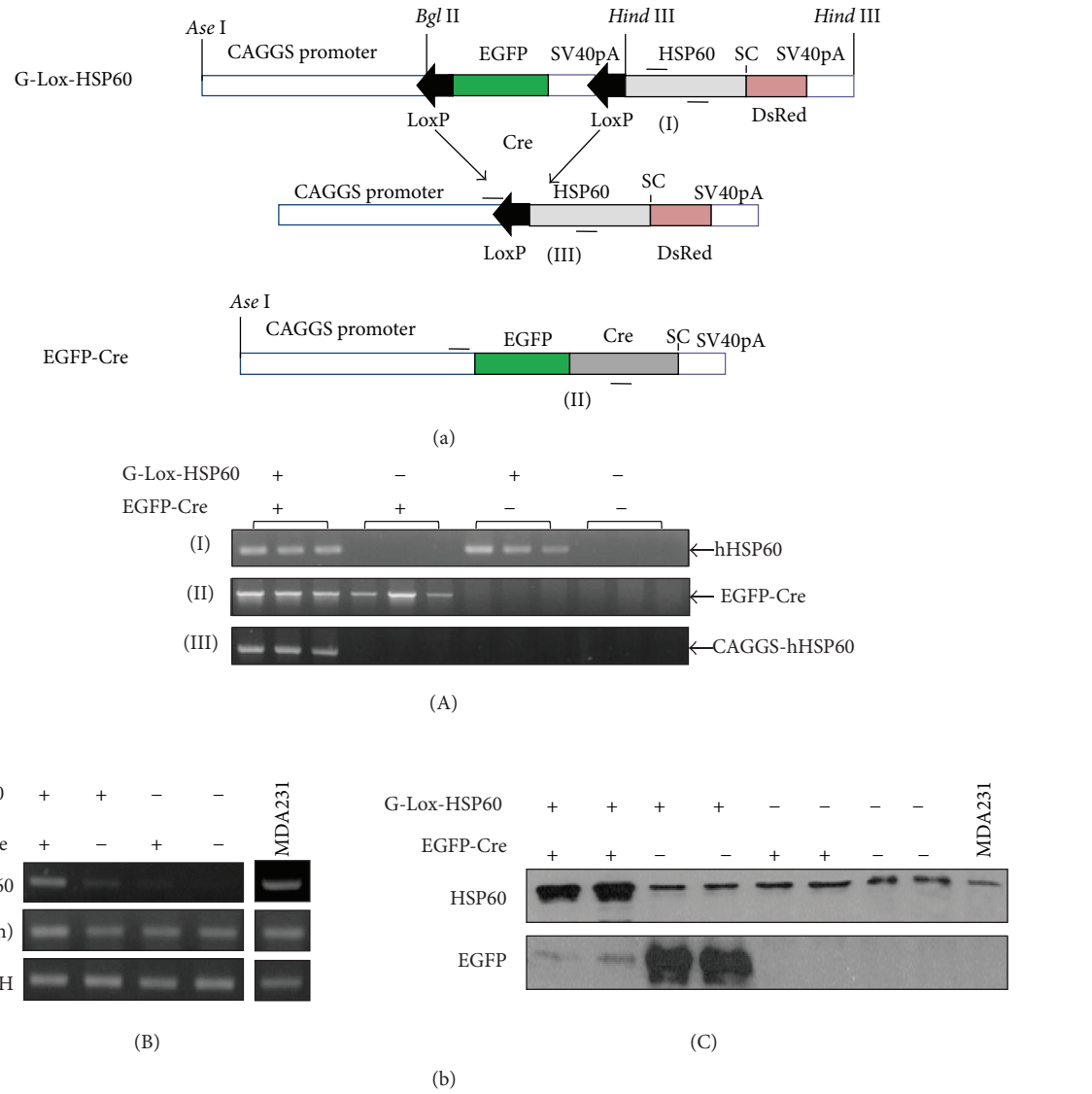

Figure 1: Generation of conditional human HSP60 transgenic mice. (a) G-Lox-HSP60 and EGFP-Cre Tg vectors. The CAGGS promoter was used to drive both Tg vectors. Placed between two LoxP sites, the GFP cDNA with 3 stop codons (SC) and the SV40 polyA sequence was used to inhibit the expression of the downstream transgene. After the second LoxP site, a full-length human HSP60 cDNA with endogenous SC and a portion of the last exon was inserted in front of ATG of the DsRedT1 cDNA sequence. After the LoxP sites were rejoined using the Cre DNA recombinase, the HSP60/DsRedT1 transcript was expressed; however, only HSP60 translated into proteins. (b) (A) Analysis of four possible littermate genotypes using PCR on tail DNA. (I) PCR amplification using the primer pair complementary to human HSP60 but not to mouse HSP60, (II) amplification of EGFP-Cre, and (III) the reaction to identify double transgenic (H^+/C^+) mice by amplifying the abridged sequence from CAGGS promoter to human HSP60. (B) RT-PCR results of human HSP60 mRNA expression in the neonatal mouse heart. HSP60 (m, h) indicates the PCR reaction to amplify HSP60 mRNA of both mouse and human origions. GAPDH amplification served as the internal control. MDA-MB231 human breast tumor cells mRNA were used as the positive control for human HSP60. (C) Western blotting for HSP60 and EGFP proteins in neonatal hearts. Anti-HSP60 antibodies recognize both mouse and human HSP60.

Tissue sections were then incubated in blocking solution (5% normal goat serum and 0.3% Triton-X 100 in PBS) followed by incubating with HSP60 (SC-1052, Santa Cruz, CA) overnight at 4°C. The sections were rinsed and incubated with biotinylated donkey anti-goat immunoglobulin G (IgG) and then reacted to Vector Elite ABC in which the color was developed with diaminobenzidine. Images were taken by using the Olympus DP72 CCD attached to an Olympus BX51 microscope with DP controller. For the immunofluorescence staining, antibodies of cleaved caspase-3 (Cell Signaling 9961), CD4 (MAB554), and CD8α (MAB116) were used for incubating samples overnight in blocking solution at 4°C. Alexa Fluor 488 conjugated goat anti-rabbit IgG (H+L) or goat anti-mouse IgG (H+L) secondary antibodies (Invitrogen) were used instead. The mounting media containing DAPI (Invitrogen) were used for counterstaining cell nucleus.

2.5. TUNEL Assay. Terminal deoxynucleotidyl transferase-mediated dUTP nick-end labeling (TUNEL) assay was performed for detecting nuclear DNA fragmentation in paraffin-embedded tissue sections as a measure of apoptosis. Fluorescein-12-dUTP was used as the substrate in TUNEL reaction (DeadEnd Fluorometric TUNEL System, Promega); the slides were counterstained by DAPI, and the images were taken by the Olympus microscope system.

2.6. T2-Weighted Thoracic Region MR Images. Magnetic resonance imaging (MRI) was performed and images were acquired using 9.4 Tesla MRI system (Bruker, Ettlingen, Germany) with a maximum gradient strength of 140 G cm^{-1}. A quadrature volume coil (internal diameter = 10 mm) was used for RF transmission and reception. We used a rapid acquisition with relaxation enhancement sequence to obtain the T2-weighted images. The repetition and echo times were set at 2500 and 3.4 milliseconds, respectively. The field of view was $10 \times 10\ mm^2$ and the matrix size was 100×100. The images were sliced without gaps, and the slice thickness was 0.2 mm. The voxel size for acquisition was $0.1 \times 0.1 \times 0.2\ mm^3$. Finally, the images were interpolated to 400×400 using cubic interpolation.

2.7. Electron Micrograph. Neonatal heart tissues were collected and fixed in 4% cold glutaraldehyde, postfixed using 1% osmium oxide, and progressively dehydrated using alcohol. After resin embedding and polymerization, 1 μm thick sections were cut for initial observation. Ultrathin (60–80 nm thick) sections were cut from the Epon-embedded blocks, stained with uranyl acetate and lead citrate, and examined using transmission electron microscopy (TEM, Hitachi H-7500, Tokyo, Japan) at 75 kV.

3. Results and Discussion

3.1. Generation of HSP60 Conditional Transgenic Mice. Unlike Tg mice expressing HSP10 [35], HSP20 [36], HSP27 [37], or HSP70 [38], founders for establishing the ubiquitous HSP60 Tg mouse were not viable. In this study, we generated a conditional Tg mouse model using Cre-LoxP tools to allow inducible and tissue-specific HSP60 expression. G-Lox-HSP60 mouse was generated by using the Tg vector illustrated in Figure 1(a). CAGGS was used to drive the expression of transgenes, enhanced green fluorescent protein (EGFP), or human HSP60 full-length cDNA. Multiple stop codons and the SV40 polyA sequences between the 2 LoxP sites of the Tg vector prevent the expression of downstream human HSP60 sequence. The G-Lox-HSP60 mice were normal in development, weight, and reproduction, with EGFP expression in most organs. During Cre-mediated recombination, 2 LoxP sites of the G-Lox-HSP60 vector are joined, and the HSP60 expression is directly enhanced by CAGGS. In the present study, we generated an FVB ubiquitous Cre Tg mouse expressing the EGFP-Cre fusion protein [33]. We used the tail DNA-PCR method for studying the genotypes of the littermates in the crossing studies of G-Lox-HSP60 and EGFP-Cre mice; the results are described in Figure 1(b). Deletion of the LoxP-flanked cassette was detected by the presence of the shorter PCR fragment in the double Tg mice. Littermates with all 4 possible genotypes were acquired in accordance with the Mendelian frequency, indicating no prenatal loss of the double Tg mice (H^+/C^+), which were positive for both G-Lox-HSP60 and EGFP-Cre alleles (Table 1). Strong induction of human HSP60 expression in the cardiac tissues of the double Tg mice was confirmed through RT-PCR, Western blotting (Figure 1(b)), and IHC staining (Figure 2).

Table 1: Summary of crossings between G-Lox-HSP60 (H) and EGFP-Cre (C) mice.

Genotype	H^+/C^+	H^+/C^-	H^-/C^+	H^-/C^-	Total
Newborn number	72	76	69	86	303
Neonatal death number	72	5	2	2	81
Ratio	72/72	5/76	2/69	2/86	81/303

H^+/C^+, double Tg mouse; H^+/C^-, H^-/C^+, single Tg mouse carrying either allele, H^-/C^-, wild-type mouse.

3.2. HSP60 Expression Led to Neonatal Deaths. In more than 20 crossing experiments using G-Lox-HSP60 and EGFP-Cre mice, all double Tg HSP60 mice litters died within a few hours after birth. A few survived the first day but none survived more than a few days (72/72, Table 1). Neonatal deaths were rare in single Tg mice—H^+/C^- (5/76) and H^-/C^+ (2/69)—which carried only G-Lox-HSP60 or EGFP-Cre, and in the wild-type mice (H^-/C^-, 2/86). At birth, neonatal HSP60 mice were slightly smaller in size than average, with signs of mild cyanosis and internal bleeding at the abdominal segments before death (Figure 3). Severe cardiovascular or pulmonary abnormality was suspected to contribute to the neonatal deaths in the HSP60 mice. H^+/C^- mice exhibited strong whole-body green fluorescence, whereas the HSP60 mice displayed green fluorescent spots, indicating remaining EGFP that was produced before recombination. H^-/C^+ and H^-/C^- mice did not exhibit fluorescence. Thoracic chamber dissection of HSP60 mice revealed a smaller heart, and the color of the ventricles was more reddish, containing more blood than the hearts of other genotypes (Figure 3).

Postmortem analysis of the HSP60 mice was performed through MRI and histology. MRI revealed that the HSP60 P1 mouse heart was smaller than that of H^+/C^- mouse (Figure S1 in Supplementary Material available online at http://dx.doi.org/10.1155/2015/539805). The HSP60 mouse heart chambers and lungs were filled with liquids that were absent in those of H^+/C^- mouse. The interventricular septum and chamber walls of the HSP60 mice were thinner than normal (Figure S1). Histological examination revealed massive hemorrhage at the heart and lungs of double Tg mouse. The cardiac muscle appeared degenerated or incompletely differentiated, with sponge-like cardiac tissues fenestrated with blood or blood vessels, and signs of myocardium necrosis were observed (Figure 4). The lungs of the HSP60 mice appeared to have developed normally except for the presence of hemorrhage that potentially resulted in only partial inflation of the lungs. Other organs, such as the brain, kidneys, and liver, of the HSP60 mice appeared grossly

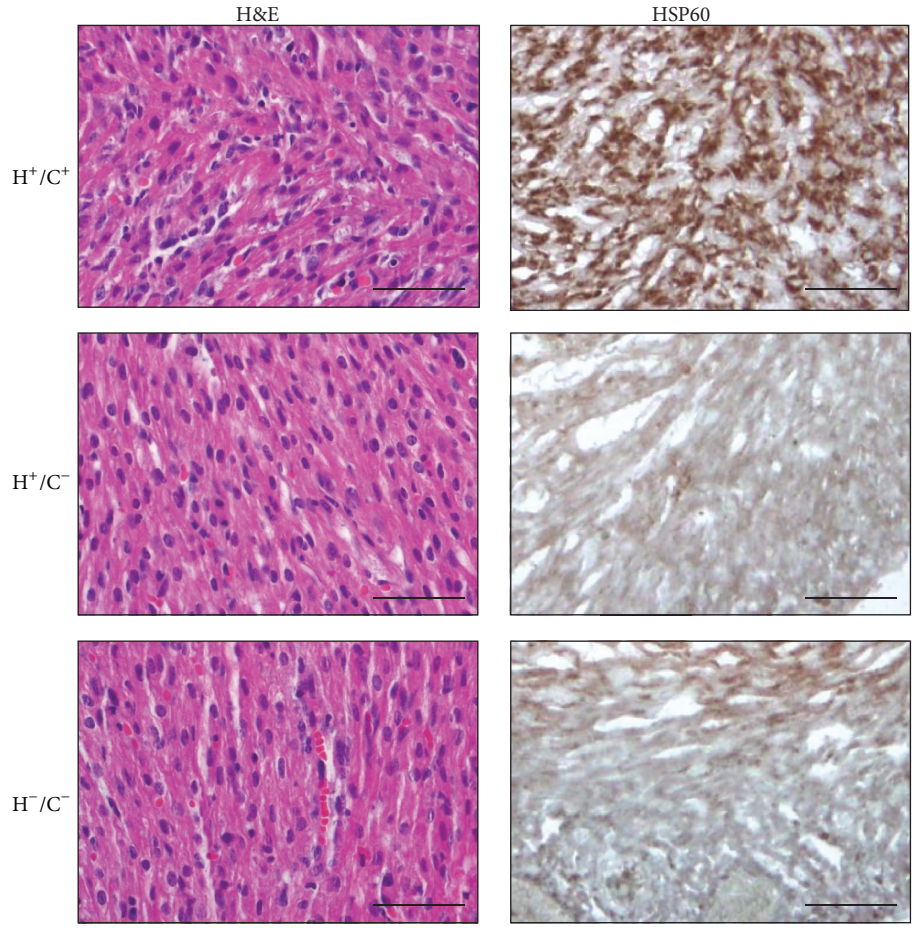

Figure 2: HSP60 detection in neonatal H^+/C^+ mice heart. H&E and immunohistochemical staining of HSP60 induction in H^+/C^+ heart sections, but not in H^+/C^- or H^-/C^- heart sections. Scale bar = 50 μm.

normal (data not shown). Spotty hemorrhage was observed in the skeletal muscles of the neck, spine, and between the ribs; however, the hemorrhage in these organs was not as severe as that in the heart and lungs. Because cardiovascular and respiratory stresses were observed and because the hearts were smaller than normal, we speculate that congenital defects may contribute to the neonatal deaths of the HSP60 mice. Of the 10 HSP60 mice studied for septal defects, 4 had atrial septal defect (ASD) and one had ventricular septal defect (VSD), as illustrated in Figure 5. Septum defects were not observed in the control mice.

Because the atrial septum is closed when the lungs are inflated during birthing and because ASD manifests as a serious problem only after birth, we examined whether the HSP60 mice had developmental defects during the embryonic stage in the E17 embryos. No apparent abnormalities were visible externally in the HSP60 mouse E17 embryos. However, the embryo sections revealed excessive hemorrhage, vascularization, and tissue necrosis in the heart, similar to those in the postnatal heart. Lungs of E17 of HSP60 mouse appeared grossly normal (Figure S2). Thus, histological evidence suggested that congenital heart disease caused by cardiomyopathy or incomplete heart development in HSP60 mouse embryos results in ASD or VSD, which aggravates respiratory stress and congestive heart failure at postnatal day 1.

We searched for ultrastructural abnormality as features of cardiac myopathy in neonatal HSP60 mouse using electron micrographs. G-Lox-HSP60 mouse contained organized arrays of myofibril filaments with intact mitochondrion appearing in high contrast with dense laminae cristae throughout the mitochondrial cross-sectional areas (Figure 6). In contrast, the myofibrils of HSP60 mouse heart exhibited pronounced fragmentation and disorganization, shown as ragged Z lines, with shorter sarcomere length on average compared with G-Lox-HSP60 myofibrils. Mitochondrion between myofibrils was mostly broken, losing both outline and inner cristae, indicating a disintegrated mitochondrial structure. Thus, TEM results confirmed severe cardiac myopathy in HSP60 mouse.

3.3. Increasing Apoptosis in HSP60 Mouse Heart. HSP60 was previously linked to apoptosis induction; thus, we studied apoptotic cardiac myocytes in the HSP60 mouse by using the TUNEL assay. Many cells in the HSP60 mouse heart sections were positively labeled by fluorescein-dUTP at

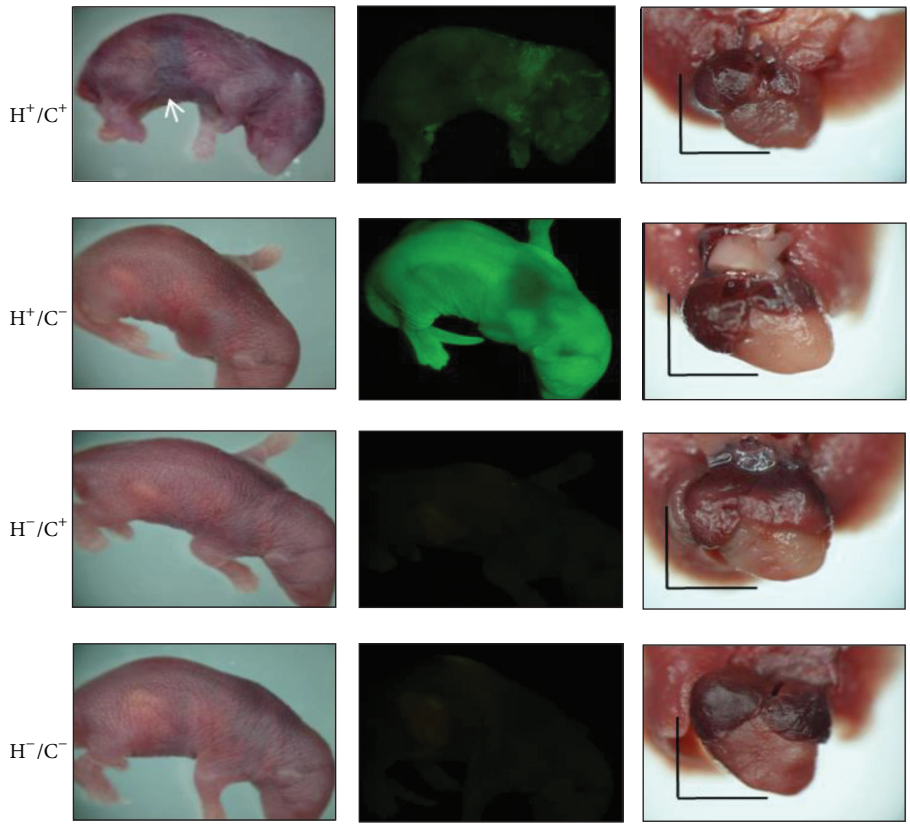

FIGURE 3: Neonatal Tg mice. Left, neonatal Tg mice. The white arrow indicates cyanosis and abdominal bleeding in H^+/C^+ neonates; middle, fluorescent images of the same mice; right, the lungs and heart of neonatal mice. H^+/C^+ hearts appear more dark reddish and smaller than hearts of other genotypes. Scale bar = 3 mm.

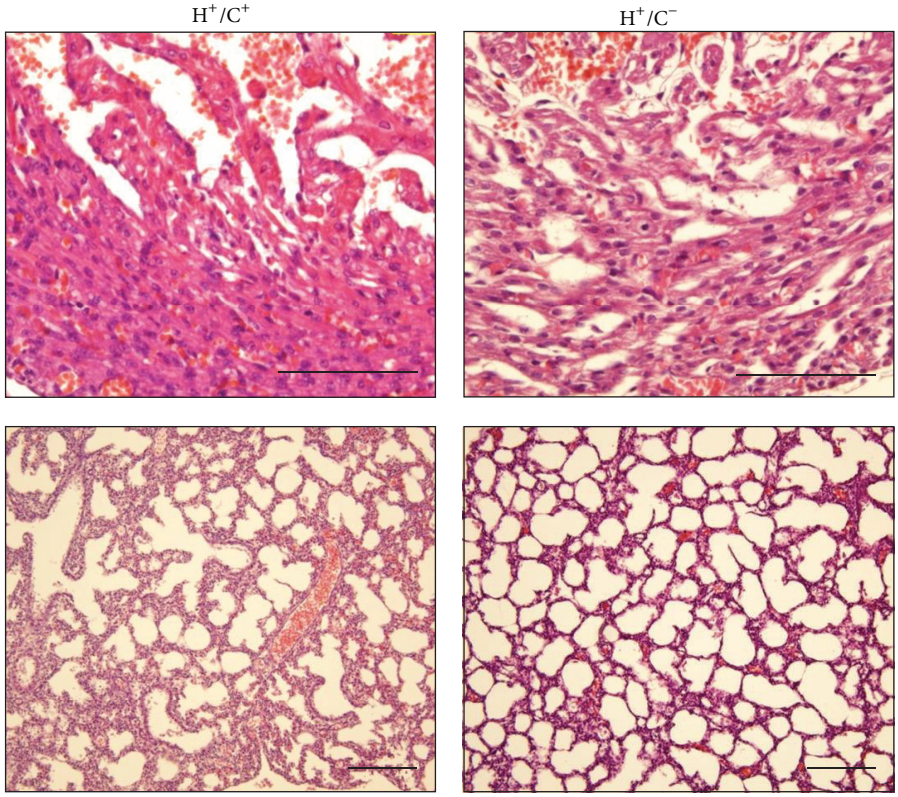

FIGURE 4: Histology of the neonatal heart and lung. Top, H&E staining of the neonatal heart of H^+/C^+ mouse compared with that of H^+/C^- mouse, showing hemorrhage, necrosis, and degenerated cardiac muscles in H^+/C^+ mouse heart. Bottom, the lung of H^+/C^+ mouse shows signs of hemorrhage, liquid congestion, and tissue necrosis. The alveolar lung structures appeared to have developed normally but poorly inflated. Scale bar = 100 μm.

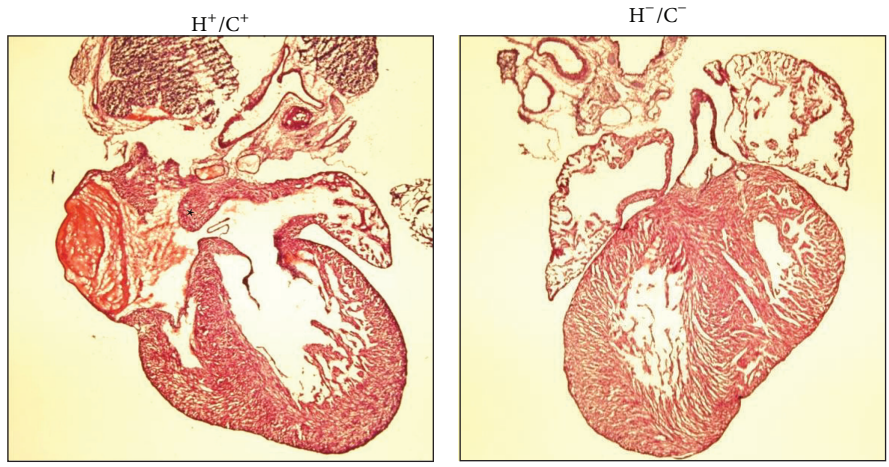

Figure 5: Atrial septal defect in H^+/C^+ neonatal mice. H&E images of the neonatal heart from H^+/C^+ and H^-/C^- mice. Asterisk indicates the atrial septal defect.

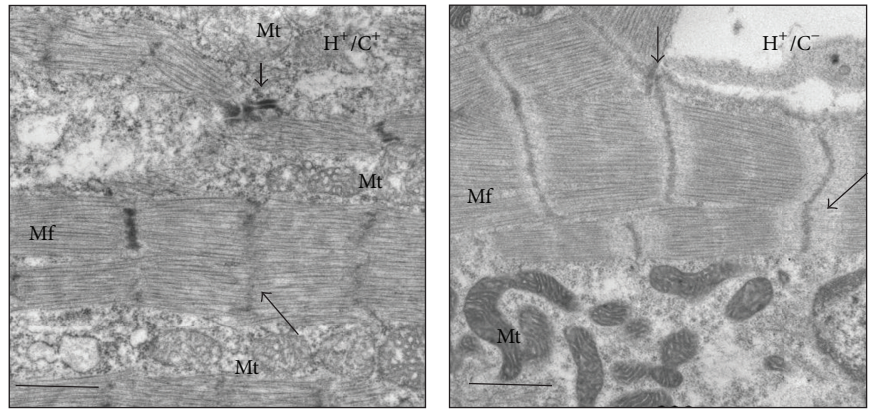

Figure 6: Transmission electron microscopy showing ultrastructure of myofibril defect in H^+/C^+ neonatal heart. Transmission electron microscopy results of H^+/C^+ (left) and H^+/C^- (right) mice left ventricular tissue. Mf, myofibrils; Mt, mitochondria; long arrow, Z disk. Original magnification 10,000x; scale bar = 1 μm.

the cell nucleus through TUNEL assay, whereas very few TUNEL positively cells were in H^+/C^- mouse heart sections (Figure 7(a)). In parallel, a few cells in the HSP60 mouse heart section were positively stained by anti-activated caspase-3 antibody, significantly more than that of H^+/C^- mouse heart (Figure 7(b)). The data clearly demonstrated that HSP60 overexpression results in caspase-3 activation and apoptosis of myocardial cells in HSP60 mice. Because the HSP60 mouse heart became a sponge-like muscular tissue infiltrated by small capillaries and HSP60 involvement in rejection and autoimmune diseases was suggested previously, we studied the presence of activated inflammatory cells in HSP60 mice. The pathology neither showed infiltrated mononuclear cells (Figure 4) nor detected CD4 or CD8 positive cells in HSP60 mouse heart (Figure S3); thus inflammatory response or T cell activation is absent in the HSP60 mouse heart.

Accumulation of HSP60 in the cytoplasm during apoptosis induction and the binding of HSP60 to procaspase-3 and modulating caspase activity has been demonstrated in many cancer cell lines [21, 25, 39]. Similar to most proteins of the mitochondrial matrix, HSP60, which is synthesized in the cytoplasm with N-terminal targeting peptides, is transported to the mitochondrial matrix, where the targeting sequence is cleaved. Both unprocessed (cytosolic) and matured (mitochondrial) HSP60 strongly increased in the cardiac tissue of HSP60 mouse (Figure 1(b)). Consequently, accumulation of cytosolic HSP60, capable of inducing apoptosis, cannot be overlooked and our data provided *in vivo* evidence of apoptosis and caspase-3 activation in the HSP60 mouse heart (Figure 7). Apoptosis is a highly regulated process during embryonic and postnatal heart development and critical for heart development. Increasing apoptosis in HSP60 mouse heart and its causal relation to cardiac myopathy must be interpreted with caution because (1) apoptosis frequently occurs in embryonic and neonatal tissues than in adult cardiac tissues; (2) increasing apoptosis is often observed in cardiac tissues of myopathy and congestive heart failure; thus apoptosis can be secondarily induced in myopathy and heart failure, and (3) it can directly result from cytosolic HSP60 accumulation or HSP60 binding to caspases. Thus,

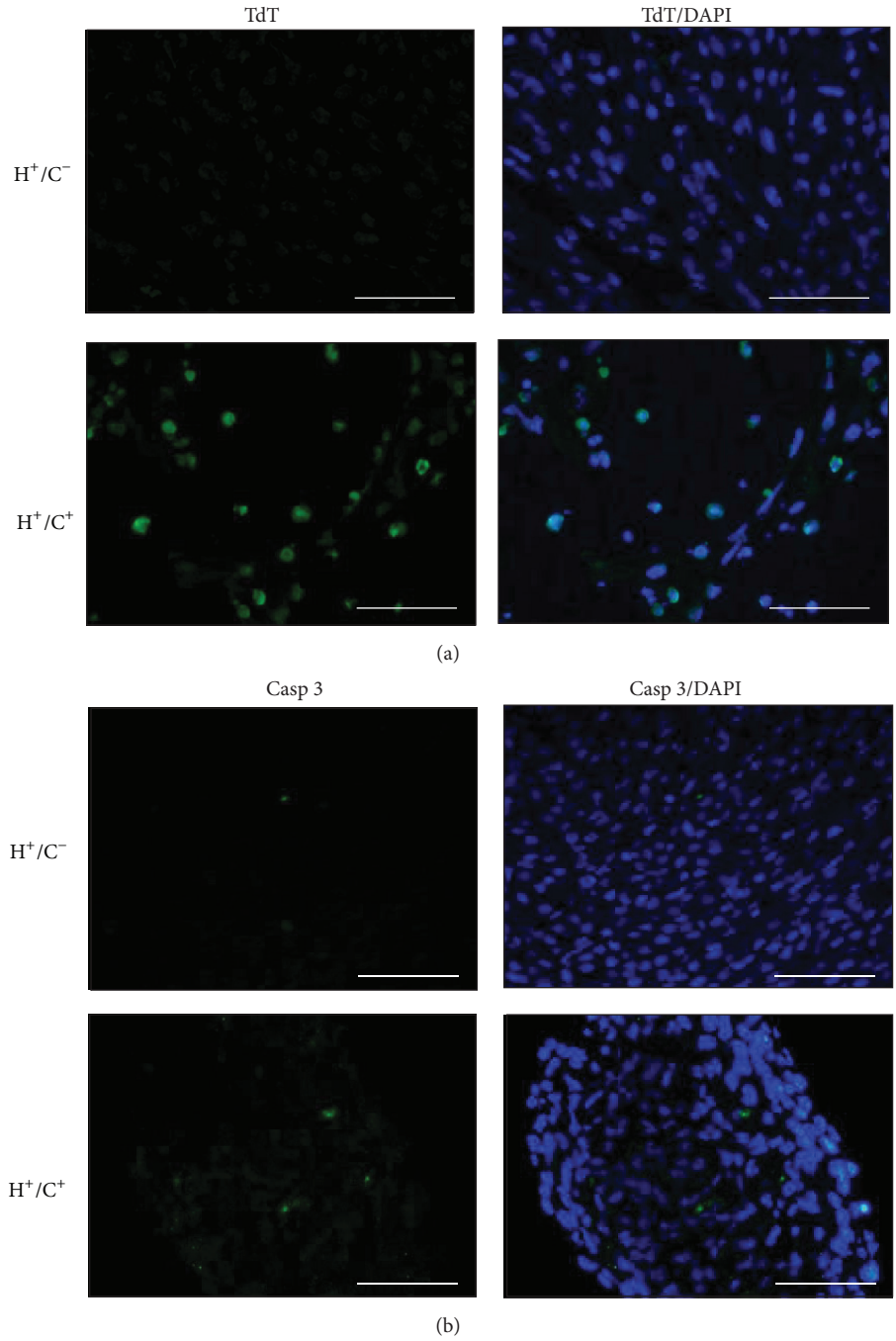

Figure 7: TUNEL staining and activated caspase-3 detection in neonatal heart sections. (a) Detection of nuclear DNA fragmentation with TUNEL reaction in the left ventricle sections of neonatal H^+/C^+ and H^+/C^- mice. Fluorescein-12-dUTP (TdT) and DAPI were used for TUNEL and nuclear staining. (b) Immunofluorescence detection of activated (cleaved) caspase-3 induction in H^+/C^+ and in H^+/C^- heart sections. Scale bar = 50 μm.

additional studies are required in this regard. Our current model, which uses the ubiquitous Cre mouse, increased HSP60 and potentially induced cell apoptosis of multiple tissues; thus it is unable to clarify phenotypes contributed by the HSP60 induction in a specific organ, for example, vascular ECs, smooth muscle cells, or cardiac myocytes. This limitation can be overcome by combinatory uses of G-Lox-HSP60 with vascular- or cardiac-specific Cre mice. We have explored HSP60 expression in cardiac tissues of the adult mice by using inducible cardiac cell-restricted Cre mouse (unpublished results).

In addition to the roles of mitochondrial and cytosolic chaperonins and caspase induction, additional functions of HSP60 have been reported. Cytosolic HSP60 regulates the

phosphorylation of IKKα/β and promotes NF-κB prosurvival pathway. Transgenic expression of the cytosolic HSP60 prevented stress-induced hepatic cell deaths *in vivo* [32]. Overexpressing HSP60 in the human stem cells increased HSP60 nuclear localization, which suppressed ROS and p38/JNK signaling and regulated genes relating to stem cell proliferation, differentiation, and stemness [40]. Whether the aforementioned mechanisms are also involved in mediating neonatal deaths remains unclear, and future clarification is awaited.

In this study, congenital ASD was observed in a large number of HSP60 mice. Although ASD exacerbated the existing myopathy of HSP60 mice and was partially responsible for neonatal death, ASD *per se* was unlikely directly caused by HSP60 induction. We speculate that ASD in neonatal HSP60 mice may be the consequence of incomplete embryonic development, existing myopathy, and increasing apoptosis. Similar phenomenon has been demonstrated in the eNOS knockout mouse model, in which high incidence of ASD or VSD was precipitated through increased apoptosis during embryonic and postnatal stages [41]. Our main findings indicate that severe hemorrhage and myocyte death occurred in mice with HSP60 expression, and increased apoptosis in a macerated and spongy-like heart failed to meet the cardiovascular demands after birth and was the primary cause of HSP60-induced heart failure and neonatal death.

4. Conclusions

HSP60 not only is the essential mitochondrial chaperone protein but also plays critical roles outside the mitochondrion. Although numerous studies indicated the wide involvement of HSP60 in broad biological processes and many diseases, reports of transgenic mouse models of increasing or knockdown HSP60 expression are rare. Thus, the consequences of altering HSP60 levels *in vivo* in these disease settings remain unknown. We used a floxed vector to establish conditional HSP60 transgenic mice, which allows studies on inducible and organ-targeted HSP60 expression in adult mice and is potentially useful in pursuing essential questions related to HSP60 *in vivo*. In this study, we show that ubiquitous HSP60 expression from the embryonic stage results in increased apoptosis, myopathy, high incidence of ASD, and neonatal deaths.

Abbreviation

ATP: Adenosine triphosphate
TNF-α: Tumor necrosis factor-α
IL-1β: Interleukin 1β
IL-6: Interleukin 6
NO: Nitric oxide
NOD: Nonobese diabetic
ASD: Atrial septum defect
VSD: Ventricular septum defect
ROS: Reactive oxygen species
eNOS: Endothelial nitric oxide synthase
CAGGS: CMV enhancer/chicken β-actin
H&E: Hematoxylin and eosin.

Conflict of Interests

The authors declare that there is no conflict of interests regarding the publication of this paper.

Authors' Contribution

Tsung-Hsien Chen and Shan-Wen Liu contribute equally to this paper.

Acknowledgments

The authors gratefully acknowledge the technical assistance provided by Tzu-Chin Wu and Mei-Yu Fan in NHRI-IBEN and Functional and Micro-Magnetic Resonance Imaging Center supported by NRPGM (NSC97-3112-B-001-013). This research was supported by grants from NHRI (BN-104-PP-02, BN-104-PP-24) and from Ministry of Science and Technology (103-2320-B-400-018).

References

[1] I. J. Benjamin and D. R. McMillan, "Stress (heat shock) proteins: molecular chaperones in cardiovascular biology and disease," *Circulation Research*, vol. 83, no. 2, pp. 117–132, 1998.

[2] F. U. Hartl, "Molecular chaperones in cellular protein folding," *Nature*, vol. 381, no. 6583, pp. 571–580, 1996.

[3] J. C. Ranford and B. Henderson, "Chaperonins in disease: mechanisms, models, and treatments," *Molecular Pathology*, vol. 55, no. 4, pp. 209–213, 2002.

[4] C. C. Deocaris, S. C. Kaul, and R. Wadhwa, "On the brotherhood of the mitochondrial chaperones mortalin and heat shock protein 60," *Cell Stress and Chaperones*, vol. 11, no. 2, pp. 116–128, 2006.

[5] F. Cappello, A. M. Gammazza, A. P. Piccionello et al., "Hsp60 chaperonopathies and chaperonotherapy: targets and agents," *Expert Opinion on Therapeutic Targets*, vol. 18, no. 2, pp. 185–208, 2014.

[6] S. Lau, N. Patnaik, M. R. Sayen, and R. Mestril, "Simultaneous overexpression of two stress proteins in rat cardiomyocytes and myogenic cells confers protection against ischemia-induced injury," *Circulation*, vol. 96, no. 7, pp. 2287–2294, 1997.

[7] K. M. Lin, B. Lin, I. Y. Lian, R. Mestril, I. E. Scheffler, and W. H. Dillmann, "Combined and individual mitochondrial HSP60 and HSP10 expression in cardiac myocytes protects mitochondrial function and prevents apoptotic cell deaths induced by simulated ischemia-reoxygenation," *Circulation*, vol. 103, no. 13, pp. 1787–1792, 2001.

[8] J. J. Malago, J. F. J. G. Koninkx, and J. E. van Dijk, "The heat shock response and cytoprotection of the intestinal epithelium," *Cell Stress and Chaperones*, vol. 7, no. 2, pp. 191–199, 2002.

[9] Y.-X. Shan, T.-L. Yang, R. Mestril, and P. H. Wang, "Hsp10 and Hsp60 suppress ubiquitination of insulin-like growth factor-1 receptor and augment insulin-like growth factor-1 receptor signaling in cardiac muscle: implications on decreased myocardial protection in diabetic cardiomyopathy," *The Journal of Biological Chemistry*, vol. 278, no. 46, pp. 45492–45498, 2003.

[10] H.-S. Chen, Y.-X. Shan, T.-L. Yang et al., "Insulin deficiency downregulated heat shock protein 60 and IGF-1 receptor signaling in diabetic myocardium," *Diabetes*, vol. 54, no. 1, pp. 175–181, 2005.

[11] V. Calabrese, A. Ravagna, C. Colombrita et al., "Acetylcarnitine induces heme oxygenase in rat astrocytes and protects against oxidative stress: Involvement of the transcription factor Nrf2," *Journal of Neuroscience Research*, vol. 79, no. 4, pp. 509–521, 2005.

[12] V. Veereshwarayya, P. Kumar, K. M. Rosen, R. Mestril, and H. W. Querfurth, "Differential effects of mitochondrial heat shock protein 60 and related molecular chaperones to prevent intracellular β-amyloid-induced inhibition of complex IV and limit apoptosis," *The Journal of Biological Chemistry*, vol. 281, no. 40, pp. 29468–29478, 2006.

[13] C. Xu, Y. Lu, Z. Pan et al., "The muscle-specific microRNAs miR-1 and miR-133 produce opposing effects on apoptosis by targeting HSP60, HSP70 and caspase-9 in cardiomyocytes," *Journal of Cell Science*, vol. 120, part 17, pp. 3045–3052, 2007.

[14] J. C. Ghosh, T. Dohi, H. K. Byoung, and D. C. Altieri, "Hsp60 regulation of tumor cell apoptosis," *The Journal of Biological Chemistry*, vol. 283, no. 8, pp. 5188–5194, 2008.

[15] P. E. Castle, R. Ashfaq, F. Ansari, and C. Y. Muller, "Immunohistochemical evaluation of heat shock proteins in normal and preinvasive lesions of the cervix," *Cancer Letters*, vol. 229, no. 2, pp. 245–252, 2005.

[16] P. A. Cornford, A. R. Dodson, K. F. Parsons et al., "Heat shock protein expression independently predicts clinical outcome in prostate cancer," *Cancer Research*, vol. 60, no. 24, pp. 7099–7105, 2000.

[17] F. Cappello, S. David, F. Rappa et al., "The expression of Hsp60 and Hsp10 in large bowel carcinomas with lymph node metastases," *BMC Cancer*, vol. 5, article 39, 2005.

[18] P.-L. Hsu and S.-M. Hsu, "Abundance of heat shock proteins (hsp89, hsp60, and hsp27) in malignant cells of Hodgkin's disease," *Cancer Research*, vol. 58, no. 23, pp. 5507–5513, 1998.

[19] S. Gupta and A. A. Knowlton, "HSP60, Bax, apoptosis and the heart," *Journal of Cellular and Molecular Medicine*, vol. 9, no. 1, pp. 51–58, 2005.

[20] S. Xanthoudakis, R. Sophie, D. Rasper et al., "Hsp60 accelerates the maturation of pro-caspase-3 by upstream activator proteases during apoptosis," *The EMBO Journal*, vol. 18, no. 8, pp. 2049–2056, 1999.

[21] A. Samali, J. Cai, B. Zhivotovsky, D. P. Jones, and S. Orrenius, "Presence of a pre-apoptotic complex of pro-caspase-3, Hsp60 and Hsp10 in the mitochondrial fraction of Jurkat cells," *The EMBO Journal*, vol. 18, no. 8, pp. 2040–2048, 1999.

[22] A. Faried, M. Sohda, M. Nakajima, T. Miyazaki, H. Kato, and H. Kuwano, "Expression of heat-shock protein Hsp60 correlated with the apoptotic index and patient prognosis in human oesophageal squamous cell carcinoma," *European Journal of Cancer*, vol. 40, no. 18, pp. 2804–2811, 2004.

[23] J. Schneider, E. Jiménez, K. Marenbach, H. Romero, D. Marx, and H. Meden, "Immunohistochemical detection of HSP60-expression in human ovarian cancer. Correlation with survival in a series of 247 patients," *Anticancer Research*, vol. 19, no. 3, pp. 2141–2146, 1999.

[24] T. Lebret, R. W. G. Watson, V. Molinié et al., "Heat shock proteins HSP27, HSP60, HSP70, and HSP90: expression in bladder carcinoma," *Cancer*, vol. 98, no. 5, pp. 970–977, 2003.

[25] A. Samali and S. Orrenius, "Heat shock proteins: regulators of stress response and apoptosis," *Cell Stress and Chaperones*, vol. 3, no. 4, pp. 228–236, 1998.

[26] W. Van Eden, G. Wick, S. Albani, and I. Cohen, "Stress, heat shock proteins, and autoimmunity: how immune responses to heat shock proteins are to be used for the control of chronic inflammatory diseases," *Annals of the New York Academy of Sciences*, vol. 1113, pp. 217–237, 2007.

[27] C. Habich and V. Burkart, "Heat shock protein 60: regulatory role on innate immune cells," *Cellular and Molecular Life Sciences*, vol. 64, no. 6, pp. 742–751, 2007.

[28] Y. Kondo, Y. Ueno, K. Kobayashi et al., "Hepatitis B virus replication could enhance regulatory T cell activity by producing soluble heat shock protein 60 from hepatocytes," *The Journal of Infectious Diseases*, vol. 202, no. 2, pp. 202–213, 2010.

[29] C. Colotti, G. Cavallini, R. L. Vitale et al., "Effects of aging and anti-aging caloric restrictions on carbonyl and heat shock protein levels and expression," *Biogerontology*, vol. 6, no. 6, pp. 397–406, 2005.

[30] P. L. Hooper, "Insulin signaling, GSK-3, heat shock proteins and the natural history of type 2 diabetes mellitus: a hypothesis," *Metabolic Syndrome and Related Disorders*, vol. 5, no. 3, pp. 220–230, 2007.

[31] O. S. Birk, D. C. Douek, D. Elias et al., "A role of Hsp60 in autoimmune diabetes: analysis in a transgenic model," *Proceedings of the National Academy of Sciences of the United States of America*, vol. 93, no. 3, pp. 1032–1037, 1996.

[32] J. N. Chun, B. Choi, K. W. Lee et al., "Cytosolic Hsp60 is involved in the NF-kappaB-dependent survival of cancer cells via IKK regulatio," *PLoS ONE*, vol. 5, no. 3, Article ID e9422, 2010.

[33] M.-R. Chen, S.-W. Liu, T.-C. Wu et al., "RU486-inducible recombination in the salivary glands of lactoferrin promoter-driven green fluorescent Cre transgenic mice," *Genesis*, vol. 48, no. 10, pp. 585–595, 2010.

[34] H.-Y. Lin, C.-H. Kao, K. M.-C. Lin, V. Kaartinen, and L.-T. Yang, "Notch signaling regulates late-stage epidermal differentiation and maintains postnatal hair cycle homeostasis," *PLoS ONE*, vol. 6, no. 1, Article ID e15842, 2011.

[35] A. C. Kayani, G. L. Close, W. H. Dillmann, R. Mestril, M. J. Jackson, and A. McArdle, "Overexpression of HSP10 in skeletal muscle of transgenic mice prevents the age-related fall in maximum tetanic force generation and muscle Cross-Sectional Area," *The American Journal of Physiology—Regulatory Integrative and Comparative Physiology*, vol. 299, no. 1, pp. R268–R276, 2010.

[36] G.-C. Fan, X. Ren, J. Qian et al., "Novel cardioprotective role of a small heat-shock protein, Hsp20, against ischemia/reperfusion injury," *Circulation*, vol. 111, no. 14, pp. 1792–1799, 2005.

[37] J. M. Hollander, J. L. Martin, D. D. Belke et al., "Overexpression of wild-type heat shock protein 27 and a nonphosphorylatable heat shock protein 27 mutant protects against ischemia/reperfusion injury in a transgenic mouse model," *Circulation*, vol. 110, no. 23, pp. 3544–3552, 2004.

[38] J.-C. L. Plumier, A. M. Krueger, R. W. Currie, D. Kontoyiannis, G. Kollias, and G. N. Pagoulatos, "Transgenic mice expressing the human inducible Hsp70 have hippocampal neurons resistant to ischemic injury," *Cell Stress and Chaperones*, vol. 2, no. 3, pp. 162–167, 1997.

[39] D. Chandra, G. Choy, and D. G. Tang, "Cytosolic accumulation of HSP60 during apoptosis with or without apparent mitochondrial release: Evidence that its pro-apoptotic or pro-survival functions involve differential interactions with caspase-3," *The Journal of Biological Chemistry*, vol. 282, no. 43, pp. 31289–31301, 2007.

[40] J. H. Jang, J. S. Jung, J. I. Choi, and S. K. Kang, "Nuclear Ago2/HSP60 contributes to broad spectrum of hATSCs function via Oct4 regulation," *Antioxidants and Redox Signaling*, vol. 16, no. 5, pp. 383–399, 2012.

[41] Q. Feng, W. Song, X. Lu et al., "Development of heart failure and congenital septal defects in mice lacking endothelial nitric oxide synthase," *Circulation*, vol. 106, no. 7, pp. 873–879, 2002.

Hindawi Publishing Corporation
BioMed Research International
Volume 2015, Article ID 163564, 6 pages
http://dx.doi.org/10.1155/2015/163564

Research Article

Pressure Overload by Transverse Aortic Constriction Induces Maladaptive Hypertrophy in a Titin-Truncated Mouse Model

Qifeng Zhou,[1] Scott Kesteven,[2] Jianxin Wu,[2] Parwez Aidery,[1] Meinrad Gawaz,[1] Michael Gramlich,[1,2] Michael P. Feneley,[2,3,4] and Richard P. Harvey[2,3,5]

[1] *Department of Cardiology and Cardiovascular Diseases, Eberhard Karls University, 72076 Tübingen, Germany*
[2] *Victor Chang Cardiac Research Institute, Darlinghurst, NSW 2010, Australia*
[3] *St. Vincent's Clinical School, University of New South Wales, Kensington, NSW 2010, Australia*
[4] *Cardiology Department, St. Vincent's Hospital, Darlinghurst, NSW 2010, Australia*
[5] *School of Biological and Biomolecular Sciences, University of New South Wales, Kensington, NSW 2010, Australia*

Correspondence should be addressed to Michael Gramlich; michael.gramlich@med.uni-tuebingen.de

Received 27 June 2015; Accepted 16 August 2015

Academic Editor: Bodh I. Jugdutt

Mutations in the giant sarcomeric protein titin (TTN) are a major cause for inherited forms of dilated cardiomyopathy (DCM). We have previously developed a mouse model that imitates a TTN truncation mutation we found in a large pedigree with DCM. While heterozygous *Ttn* knock-in mice do not display signs of heart failure under sedentary conditions, they recapitulate the human phenotype when exposed to the pharmacological stressor angiotensin II or isoproterenol. In this study we investigated the effects of pressure overload by transverse aortic constriction (TAC) in heterozygous (Het) *Ttn* knock-in mice. Two weeks after TAC, Het mice developed marked impairment of left ventricular ejection fraction ($p < 0.05$), while wild-type (WT) TAC mice did not. Het mice also trended toward increased ventricular end diastolic pressure and volume compared to WT littermates. We found an increase in histologically diffuse cardiac fibrosis in Het compared to WT in TAC mice. This study shows that a pattern of DCM can be induced by TAC-mediated pressure overload in a TTN-truncated mouse model. This model enlarges our arsenal of cardiac disease models, adding a valuable tool to understand cardiac pathophysiological remodeling processes and to develop therapeutic approaches to combat heart failure.

1. Introduction

Dilated cardiomyopathy (DCM), a heart disease that is characterized by left ventricular dilatation, reduction in left ventricular function, and occurrence of cardiac arrhythmias, is a major cause for congestive heart failure [1]. About 20–48% of DCM cases are inherited with mutations in a variety of genes encoding sarcomeric, cytoskeletal, and nuclear membrane proteins, as well as proteins involved in Ca^{2+} metabolism [2].

The sarcomeric protein titin (TTN) is the biggest known single-copy protein in humans, mainly expressed in muscle tissue [3]. A single TTN molecule spans half the sarcomere and links the Z-disc with the M-line. As a pivotal building block of the sarcomere, it provides passive forces and mainly contributes to the elasticity of a muscle [4]. TTN also plays a major role in scaffolding and coordinating structural and signal proteins for mechanotransduction [5].

TTN mutations were linked to DCM more than a decade ago [6]. Recently, TTN truncating mutations emerged as the leading genetic cause of DCM in human patients, accounting for about 25% of cases of familial DCM and 18% for idiopathic DCM [7]. TTN truncating mutations are not randomly distributed in this big protein but are predominantly presented at the A-band region [8].

We have previously generated a mouse model that imitates a human truncation mutation we found in a large DCM pedigree. The 2 bp insertion is located in exon 326 of titin, resulting in a premature stop codon with stop of translation in A-band TTN [6].

While the homozygous TTN knock-in mice die *in utero* on about day 9.0 of gestation due to severe defects in sarcomeric assembly, the Het animals do not develop a cardiac phenotype under sedentary conditions. However, when exposed to pharmacological stress (e.g., angiotensin II or isoproterenol), they show all features of DCM and therefore recapitulate the human disease [9].

Efforts to dissect pathways that are involved in DCM development and progression in this mouse model have failed so far, since the pharmacological agents (e.g., angiotensin) enormously disturbed expression levels of TTN binding partners, making it impossible to trace subtle differences induced by the TTN mutation [9]. To omit this, we attempted the use of aortic constriction as a mechanical stressor to induce DCM in our mouse model.

2. Materials and Methods

2.1. TTN Knock-In Mice. The TTN knock-in mouse line, harbouring a 2 bp insertion mutation in A-band TTN, was described previously [9]. Briefly, the mutation was introduced into mouse embryonic stem cells by homologous recombination with a plasmid carrying the mutation with flanking genomic DNA sequences, followed by antibiotic selection of ES cell clones, blastocyst injections, and embryo transfer. Pups were tested for chimerism and the mice were evaluated for transmission of the mutation to their offspring. Het mice were back-crossed to a C57Bl/6 background for at least 9 generations. All animal investigations were approved by the Institutional Animal Care and Use Committee, as well as the local Animal Review Board.

2.2. Transverse Aortic Constriction on Mouse. Mice at the age of 3-4 months were anesthetized with ketamine (100 mg/kg) and xylazine (10 mg/kg) and transferred to a heated platform. Anesthetized mice were intubated, followed by midline cervical incision to expose the aorta. Aortic constriction was achieved by placing a 7.0 nylon suture ligature against a 27-gauge needle on transverse aorta. The needle was removed promptly to create an aortic constriction of 0.4 mm in diameter and the chest was sealed. In Sham operated mice, the procedure was the same besides the constriction of aorta. The mice were maintained on a heating pad for recovery.

2.3. Echocardiography. Echocardiography was performed as described previously [9]. Briefly, anesthesia was induced with 4-5% isoflurane in an anesthetic chamber; mice were then restrained supine on a heated platform. Anesthesia was maintained with 0.5–1.5% isoflurane; body temperature was kept at 37°C. An ultrasound system (Vevo 770, VisualSonics, Toronto, ON, Canada) was used for the echocardiographic analysis with a 30-MHz probe. Images were acquired and stored as a digital cine loop for offline calculations. Standard imaging planes, M-mode, Doppler, and functional calculations were obtained according to the American Society of Echocardiography guidelines. M-mode derived from parasternal short-axis view of the left ventricle recorded at 1 kHz (EKV) was used to determine wall thickness, end systolic and end diastolic diameters, ventricular dimensions and volumes, and ejection fraction.

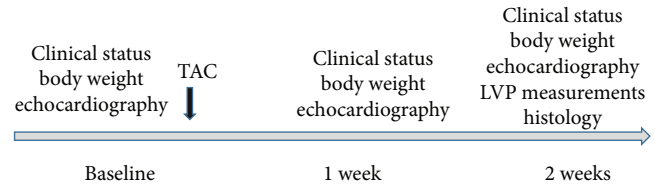

Figure 1: Schematic of the study design.

2.4. Left Ventricular Hemodynamics. On day 14 after TAC surgery, hemodynamic measurements were obtained. Mice were anesthetized with isoflurane and transferred to a heated platform where a nose cone delivered isofurane (0.5–2.0%). A micromanometer-tipped catheter (Millar Inc., Texas, US) was introduced into the left ventricle through the right carotid artery. The transducer was connected to an external recorder and aortic pressure and ventricular pressure were recorded at 1 kHz (BIOPAC Inc., CA, US). Immediately after removal of the catheter mice were sacrificed and heart tissue was obtained for histological analysis.

2.5. Masson's Trichrome Staining. Heart tissue was fixed with 4% PFA, dehydrated in serial graded ethanol (70%, 80%, and 90%, each for 1 hour and twice in 100% ethanol for 1 hour), and embedded into paraffin blocks. The tissue blocks were sectioned with a Leica Microtome and transferred to glass slides. To remove paraffin, the slides went through serial graded ethanol (100%, 90%, 80%, and 70%, each for 5 minutes) and rehydrated in H_2O for 5 minutes. Sections (8 μm) were stained with Masson's trichrome to detect fibrosis. Quantification of fibrosis was performed using an image analysis system (ImageJ).

2.6. Statistics. Within-group statistical comparisons for each genotype were made with ANOVA for repeated measures. Between-group comparisons were made with two-way ANOVA. Dunnett's multiple comparison test was used to isolate the source of difference. Data are reported as mean ± SEM. Values of $p < 0.05$ were considered significant.

3. Results

3.1. TAC-Mediated Pressure Overload Induced Maladaptive Left Ventricular Hypertrophy and Impaired Systolic Function in Heterozygous Ttn Knock-In Mice. We performed TAC banding in heterozygous *Ttn* knock-in mice and wild-type littermate controls. As an additional control, an equally sized Sham group (heterozygous and wild-type) was used.

The study was designed as shown in Figure 1. Prior to surgery, clinical status and body weight were assessed in all mice. In addition, heart function and morphology were determined by echocardiography. On the same day, thoracic aortic constriction (TAC) surgery was performed by an experienced operator. Follow-up clinical assessment and echocardiography were obtained on day 7 and day 14 after

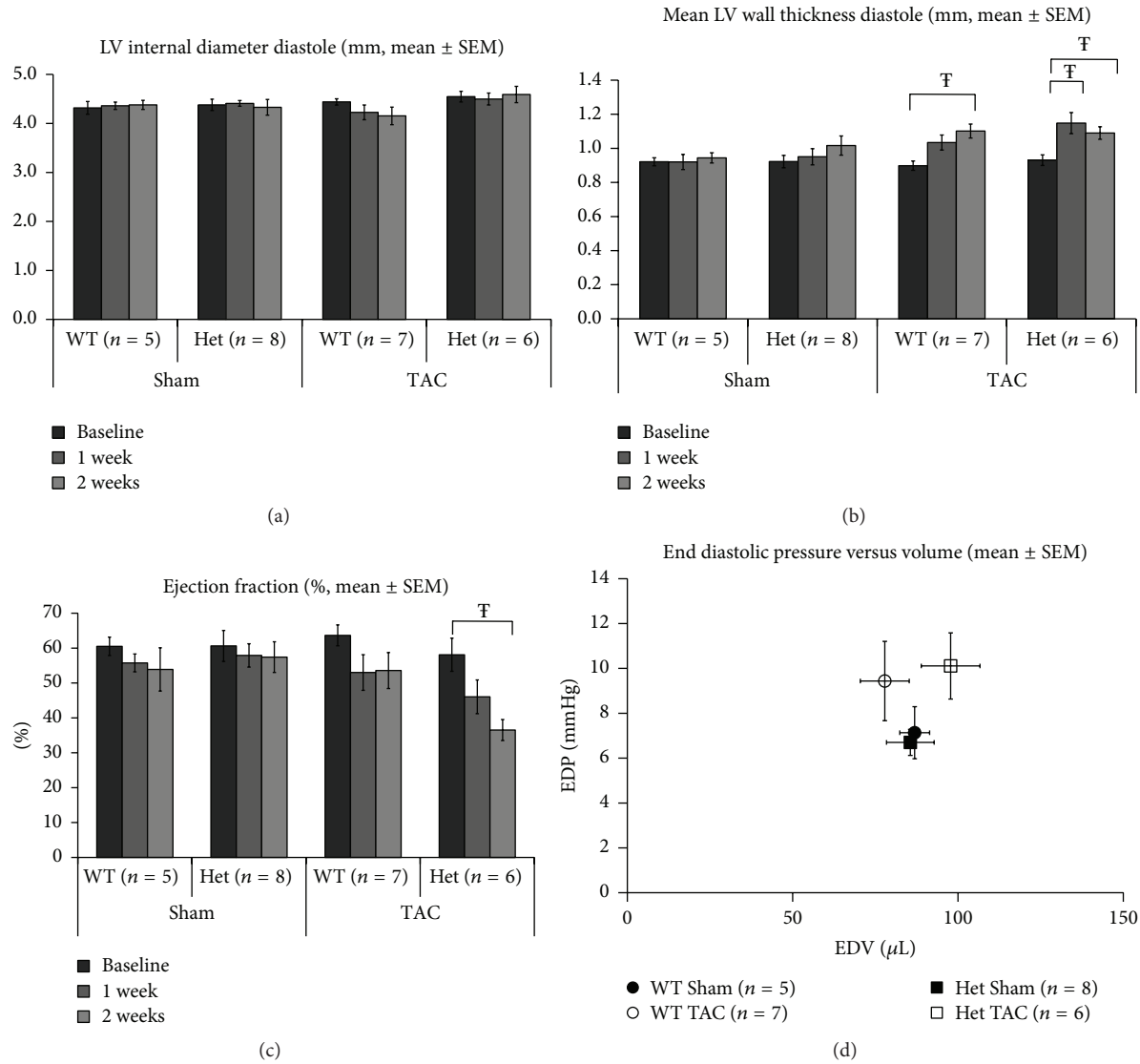

Figure 2: Echocardiographic and LV pressure assessments of WT and Het mice at baseline, week 1, and week 2 following TAC. (a) There is no evidence of LV dilatation in either genotype in either the presence or absence of TAC. (b) The onset of ventricular hypertrophy appears to be more rapid in the Het group demonstrating significant increases by week 1 unlike WT mice which only manifest significant thickening by week 2. (c) The reduction in EF% induced by TAC in the Het group is significant by week 2, unlike the WT TAC mice which tended to demonstrate a fall in this measure of contractile function but did not reach significance at either time point after TAC surgery. (d) Differences in EDP between groups do not reach significance although the trend is towards increase in both TAC groups. Interestingly the EDV trend although also not significant for the Het TAC group moves to the right of the Sham Het group, a change reflective of ventricular dilatation, whereas the EDV of the WT TAC mice changes little and even moves to the left more aligned to a physiological adaptation ($^{Ŧ}p < 0.05$). Sample sizes are also shown.

TAC. On day 14 after TAC, left ventricular and aortic pressure loops were recorded, the mice were sacrificed, and the heart was processed for histology studies.

As reported previously [9], there were no differences in left ventricular diameters, left ventricular end diastolic dimension (LVEDD) and left ventricular end systolic dimension (LVESD), ventricular wall thicknesses (interventricular septum in diastole, IVSd), and cardiac contractility (ejection fraction, EF) between Het *Ttn* knock-in mice and their WT littermates at baseline (Figure 2). One week after TAC signs of cardiac hypertrophy were apparent with significant increases in LV mean wall thickness in diastole (LVMWd) only in the TTN group (LVMWd; Het; baseline 0.93 ± 0.03 mm versus wk1 1.15 ± 0.06 mm; $p < 0.05$). At the same time point no significant changes in left ventricular end diastolic diameters or EDV were noted in Het mice (LVEDd; WT: Sham 4.36 ± 0.07 mm versus TAC 4.39 ± 0.21 mm, Het Sham 4.41 ± 0.06 mm versus TAC 4.50 ± 0.12 mm). TAC induced increased wall thickness in both WT and Het mice but this increase from baseline was statistically significant at both week 1 and week 2 in Het mice whereas it was significant only at week 2 in WT mice (LVMWd: WT; baseline 0.92 ± 0.03 mm

versus wk2 1.10 ± 0.04 mm, Het; baseline 0.93 ± 0.03 mm versus wk2 1.09 ± 0.04 mm; $p < 0.05$). Strikingly, contractile cardiac function (EF%) demonstrated a continuing fall in the Het TAC group from 58 ± 5% at baseline to 46 ± 5% at week 1 and to 37 ± 3% at week 2 ($p < 0.05$), whereas in WT animals falls in EF% did not reach significance from baseline to the first or second week (WT; baseline 64 ± 3%, wk1 53 ± 5%, wk2 54 ± 5, Figure 2).

The Sham operated mice did not show signs of cardiac remodeling in both the WT and Het group animals, and there was no impairment of cardiac function until the experiment was terminated. A complete list with all echocardiographic data is available in Supplementary Figure 1 (see Supplementary Material available online at http://dx.doi.org/10.1155/2015/163564).

3.2. Alterations of Hemodynamic Parameters Mediated by TAC. Two weeks after TAC banding, cardiac catheterization was performed and left ventricular pressure as well as aortic pressure was recorded (Figure 2).

Two weeks after TAC, systolic aortic pressure (AoPs) increased in the TAC groups compared to their corresponding Sham operated controls, respectively (WT TAC, 180 ± 6.9 mmHg versus WT Sham, 128 ± 11 mmHg; Het TAC, 164 ± 5 mmHg versus Het Sham, 116 ± 3 mmHg, $p < 0.01$), demonstrating successfully performed aortic constriction. There was no significant difference in AoPs between the WT TAC group and the Het TAC group. We also found no significant differences in diastolic aortic pressure (AoPd) between Het and WT animals. Two weeks after TAC, left ventricular systolic pressure (LVSP) was increased in the TAC groups compared to their Sham operated controls (WT TAC, 181 ± 7 mmHg versus WT Sham, 130 ± 7 mmHg; Het TAC, 168 ± 4 mmHg versus Het Sham, 115 ± 4 mmHg, $p < 0.01$). Interestingly, TAC banding induced a trend to higher left ventricular end diastolic pressure (LVEDP) in the Het TAC group compared to Het Sham group and WT TAC compared to WT Sham groups (Het TAC, 10.1 ± 1.5 mmHg versus Het Sham, 6.7 ± 0.6 mmHg, or WT TAC, 9.4 ± 1.8 mmHg versus WT Sham, 7.1 ± 1.2). Heart rate during LV measurements was as follows: WT Sham 457 ± 14 bpm; Het Sham 441 ± 37 bpm; WT TAC 437 ± 61 bpm; Het TAC 498 ± 90 bpm (n.s. between groups).

3.3. Cardiac Fibrosis in TTN A-Band Truncating Mutation Knock-In Mice. Cardiac extracellular matrix (ECM) remodeling is a process adapted by the heart to deal with physiological and pathophysiological hemodynamic changes. Excess ECM protein production and deposition in the myocardium (cardiac fibrosis) is a hallmark of maladaptive remodeling in a failing heart. We analyzed cardiac fibrosis in 7 hearts per genotype by Masson's trichrome staining in heart muscle tissue obtained 2 weeks after TAC. While WT mice showed only distinct fibrotic areas, heterozygous animals developed massive cardiac fibrosis (5.2 ± 1.5% versus 14.1 ± 4%, $p < 0.01$) (Figure 3). There was no cardiac fibrosis detectable in Sham operated mice.

4. Discussion

In this study, we showed that pressure overload by thoracic aortic constriction induces maladaptive hypertrophy with impaired left ventricular function in a mouse model with a TTN truncation mutation we found in a family with dilated cardiomyopathy.

TTN truncating variants have been described as the major disease gene for dilated cardiomyopathy, accounting for approximately 25% of all cases [7]. However, TTN truncations can also be found in the healthy population, which gives some uncertainty to the pathogenic value of such variants. Recently, Roberts et al. [8] used genetic, transcriptome, and protein information to differentiate between polymorphisms and true disease causing mutations. This landmark study gave strong evidence that truncation mutations located in A-band TTN are most commonly disease causing, whereas I-band variants can generally be well compensated by the organism. Our mouse model harbors a truncation variant in A-band TTN, making it a good mouse model for a wide spectrum of human DCM. In addition, our data strongly support the evidence of a pathogenetic role for A-band variants.

As described previously, heterozygous *Ttn* knock-in mice do not develop a cardiac phenotype under resting conditions [9]. Interestingly, disease penetrance in the family with the corresponding mutation [6], as well as in most other described DCM families, is incomplete, indicating that a "second hit" (environmental or a second genetic modifier) is required for disease development and progression. The need of a cardiac stressor in our mouse model (here: pressure overload by TAC) supports the "second hit" hypothesis in titin-based DCM.

TTN is a major contributor of cardiac stiffness. We have previously performed active and passive tension measurements in skinned ventricular papillary muscle fibers as well as echocardiographic evaluation of diastolic function in our Het *Ttn* mouse model [9]. We did not find any changes in viscoelastic properties in these animals. This is most likely because the predominant mechanism of disease in our model is haploinsufficiency, with degradation of the mutant protein and compensatory upregulation of the wild-type protein. Under the hypertrophic stimulus of pressure overload, this compensatory mechanism seems to fail, resulting in a lack of sarcomeric TTN. Presumably, the shortage of the sarcomeric "ruler" TTN results in cardiac disarray with fibrosis and impaired systolic function.

Cardiac extracellular matrix (ECM) remodeling is an adaptive process to deal with physiological and pathophysiological hemodynamic changes [10]. Excess ECM protein production and deposition in the myocardium (cardiac fibrosis) is a hallmark of maladaptive remodeling [11, 12]. A-band TTN truncation mutations produce a shorter TTN protein with impaired M-band signaling. TTN M-band, one of the "hot spots" for mechanotransduction in the sarcomere, contributes to pathological cardiac remodeling [13, 14]. For example, DRAL/FHL2 binds to TTN at the M-line [15] and shuttles between the cytoplasm and the nucleus to regulate gene transcription. MURF1, an E3 ubiquitinase, binds to M-band titin and regulates gene expression and protein turnover

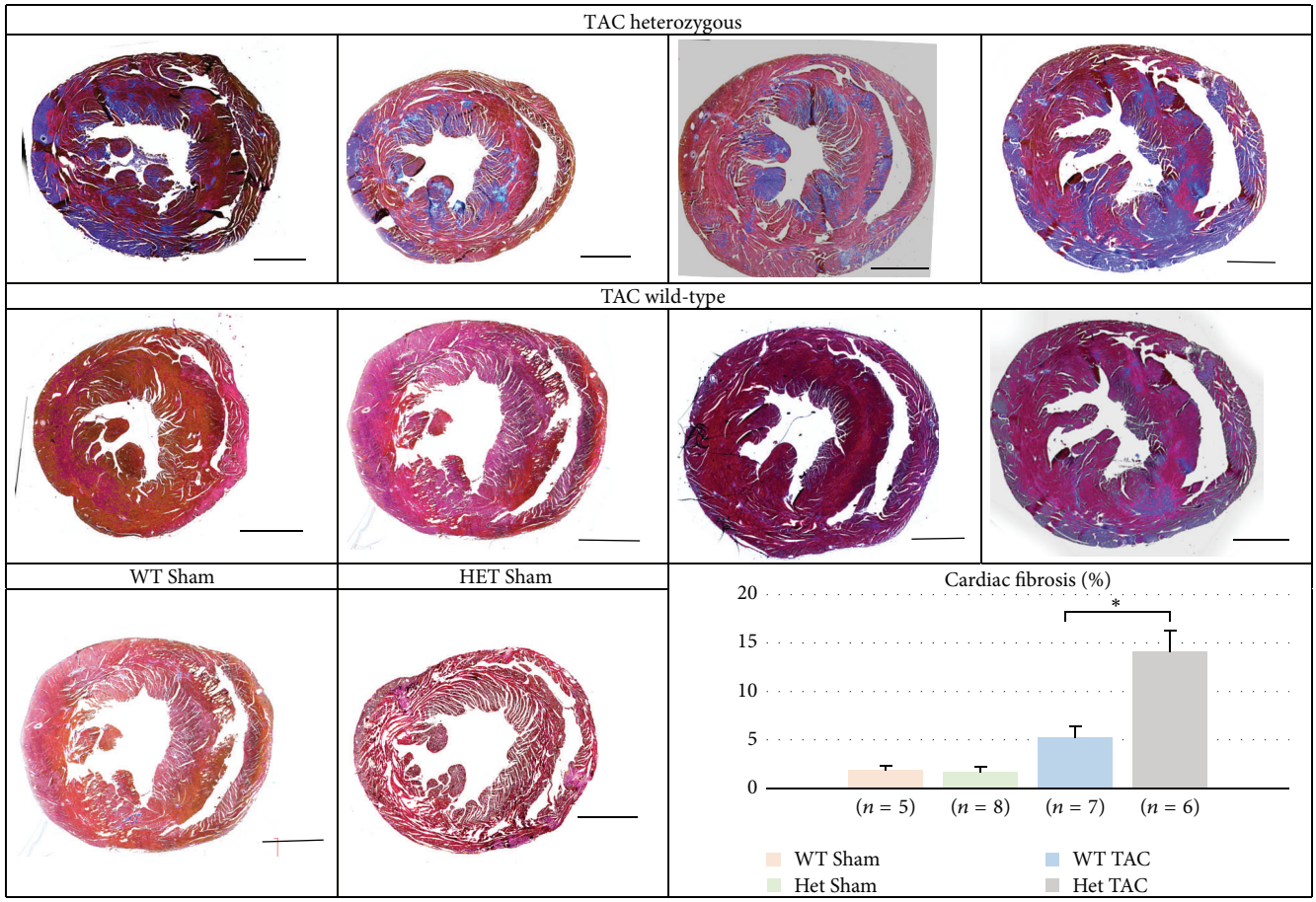

FIGURE 3: Myocardial histology of 4 representative heart sections from wild-type and Het animals 2 weeks after TAC, stained with Masson's trichrome. One representative Sham heart per genotype is also shown. Note the increased level of fibrosis in Het hearts ($^{*}p < 0.01$) compared to their WT littermates. Bar = 1 mm.

[16]. TTN kinase (TK) domain associates with nbr1 and p62, which are receptors for the selective degradation of ubiquitinated proteins by the autophagosome [17]. Together, these findings suggest that TTN A-band truncating mutations could possibly result in defected M-band mechanosensing and transduction, which in turn impairs cardiac protein turnover and remodeling. Hyperactivation of cardiac fibrosis could be one of the consequences of impaired mechanotransduction pathways in the TTN A-band truncating mutant mice, which would contribute to systolic dysfunction in those mice under pressure overload.

In previous studies [9, 18], we used pharmacological stress (angiotensin II, isoproterenol) to induce DCM in our mouse model. Since TTN is known to play a role in biomechanical sensing and signalling [19–21], we performed extensive expression studies with known TTN ligands involved in those functions [9], but we could not find any significant changes in our heterozygous mice. However, expression levels of these binding partners were enormously influenced by the pharmacological agent (angiotensin) itself. Therefore, subtle differences between wild-type and Het mice were supposedly below the detection level. In this study, we used a mechanical stressor and could therefore exclude pharmacological confounders. This should enable us to dissect pathways involved in TTN-based DCM and to develop novel therapeutic strategies to combat heart failure.

5. Conclusions

In this study, we showed that TAC-mediated pressure overload leads to hemodynamic impairment and rapid cardiac remodeling in heterozygous TTN A-band truncated mice, resulting in a DCM-like phenotype. Since TTN A-band truncating variants are a major cause for human DCM, the mouse model is a useful tool for the elucidation of disease mechanisms and for the development of novel therapeutic interventions.

Conflict of Interests

The authors declare that there is no conflict of interests regarding the publication of this paper.

Authors' Contribution

Qifeng Zhou and Scott Kesteven contributed equally to this work. Michael Gramlich, Michael P. Feneley, and Richard P. Harvey contributed equally to this work.

Acknowledgments

This work was supported by grants from Deutsche Forschungsgemeinschaft (DFG) (GR 3411/2-1), Bundesministerium für Bildung und Forschung (BMBF) (01ZX1407B), and the National Health and Medical Research Council of Australia (NHMRC) (573732; 1074386). Richard P. Harvey held an NHMRC Australia Fellowship (573705).

References

[1] M. Nichols, N. Townsend, P. Scarborough, and M. Rayner, "Cardiovascular disease in Europe 2014: epidemiological update," *European Heart Journal*, vol. 35, no. 42, pp. 2950–2959, 2014.

[2] H. Morita, J. Seidman, and C. E. Seidman, "Genetic causes of human heart failure," *The Journal of Clinical Investigation*, vol. 115, no. 3, pp. 518–526, 2005.

[3] H. L. Granzier and S. Labeit, "The giant protein titin. A major player in myocardial mechanics, signaling, and disease," *Circulation Research*, vol. 94, no. 3, pp. 284–295, 2004.

[4] S. Labeit and B. Kolmerer, "Titins: giant proteins in charge of muscle ultrastructure and elasticity," *Science*, vol. 270, no. 5234, pp. 293–296, 1995.

[5] W. A. Linke, "Sense and stretchability: the role of titin and titin-associated proteins in myocardial stress-sensing and mechanical dysfunction," *Cardiovascular Research*, vol. 77, no. 4, pp. 637–648, 2008.

[6] B. Gerull, M. Gramlich, J. Atherton et al., "Mutations of TTN, encoding the giant muscle filament titin, cause familial dilated cardiomyopathy," *Nature Genetics*, vol. 30, no. 2, pp. 201–204, 2002.

[7] D. S. Herman, L. Lam, M. R. G. Taylor et al., "Truncations of titin causing dilated cardiomyopathy," *The New England Journal of Medicine*, vol. 366, no. 7, pp. 619–628, 2012.

[8] A. M. Roberts, J. S. Ware, D. S. Herman et al., "Integrated allelic, transcriptional, and phenomic dissection of the cardiac effects of titin truncations in health and disease," *Science Translational Medicine*, vol. 7, no. 270, 2015.

[9] M. Gramlich, B. Michely, C. Krohne et al., "Stress-induced dilated cardiomyopathy in a knock-in mouse model mimicking human titin-based disease," *Journal of Molecular and Cellular Cardiology*, vol. 47, no. 3, pp. 352–358, 2009.

[10] J. N. Cohn, R. Ferrari, and N. Sharpe, "Cardiac remodeling—concepts and clinical implications: a consensus paper from an international forum on cardiac remodeling," *Journal of the American College of Cardiology*, vol. 35, no. 3, pp. 569–582, 2000.

[11] I. Kehat and J. D. Molkentin, "Molecular pathways underlying cardiac remodeling during pathophysiological stimulation," *Circulation*, vol. 122, no. 25, pp. 2727–2735, 2010.

[12] M. Yoshimura, H. Yasue, K. Okumura et al., "Different secretion patterns of atrial natriuretic peptide and brain natriuretic peptide in patients with congestive heart failure," *Circulation*, vol. 87, no. 2, pp. 464–469, 1993.

[13] M. Gotthardt, R. E. Hammer, N. Hübner et al., "Conditional expression of mutant M-line titins results in cardiomyopathy with altered sarcomere structure," *Journal of Biological Chemistry*, vol. 278, no. 8, pp. 6059–6065, 2003.

[14] M. Hoshijima, "Mechanical stress-strain sensors embedded in cardiac cytoskeleton: Z disk, titin, and associated structures," *The American Journal of Physiology—Heart and Circulatory Physiology*, vol. 290, no. 4, pp. H1313–H1325, 2006.

[15] S. Lange, D. Auerbach, P. McLoughlin et al., "Subcellular targeting of metabolic enzymes to titin in heart muscle may be mediated by DRAL/FHL-2," *Journal of Cell Science*, vol. 115, no. 24, pp. 4925–4936, 2002.

[16] S. H. Witt, H. Granzier, C. C. Witt, and S. Labeit, "MURF-1 and MURF-2 target a specific subset of myofibrillar proteins redundantly: towards understanding MURF-dependent muscle ubiquitination," *Journal of Molecular Biology*, vol. 350, no. 4, pp. 713–722, 2005.

[17] T. Lamark, V. Kirkin, I. Dikic, and T. Johansen, "NBR1 and p62 as cargo receptors for selective autophagy of ubiquitinated targets," *Cell Cycle*, vol. 8, no. 13, pp. 1986–1990, 2009.

[18] M. Gramlich, L. S. Pane, Q. F. Zhou et al., "Antisense-mediated exon skipping: a therapeutic strategy for titin-based dilated cardiomyopathy," *EMBO Molecular Medicine*, vol. 7, pp. 562–576, 2015.

[19] H. Granzier and S. Labeit, "Structure-function relations of the giant elastic protein titin in striated and smooth muscle cells," *Muscle and Nerve*, vol. 36, no. 6, pp. 740–755, 2007.

[20] M. K. Miller, H. Granzier, E. Ehler, and C. C. Gregorio, "The sensitive giant: the role of titin-based stretch sensing complexes in the heart," *Trends in Cell Biology*, vol. 14, no. 3, pp. 119–126, 2004.

[21] S. Lange, F. Xiang, A. Yakovenko et al., "The kinase domain of titin controls muscle gene expression and protein turnover," *Science*, vol. 308, no. 5728, pp. 1599–1603, 2005.

Hindawi Publishing Corporation
BioMed Research International
Volume 2015, Article ID 753210, 10 pages
http://dx.doi.org/10.1155/2015/753210

Research Article

Novel Model of Pulmonary Artery Banding Leading to Right Heart Failure in Rats

Masataka Hirata, Daiki Ousaka, Sadahiko Arai, Michihiro Okuyama, Suguru Tarui, Junko Kobayashi, Shingo Kasahara, and Shunji Sano

Departments of Cardiovascular Surgery, Okayama University Graduate School of Medicine, Dentistry, and Pharmaceutical Sciences, Okayama University Hospital, 2-5-1 Shikata-cho, Kita-ku, Okayama 700-8558, Japan

Correspondence should be addressed to Masataka Hirata; hiraper0916@hotmail.co.jp

Received 23 May 2015; Revised 20 August 2015; Accepted 24 August 2015

Academic Editor: Bodh I. Jugdutt

Background. Congenital heart diseases often involve chronic pressure overload of the right ventricle (RV) which is a major cause of RV dysfunction. Pulmonary artery (PA) banding has been used to produce animal models of RV dysfunction. We have devised a new and easier method of constricting the PA and compared it directly with the partial ligation method. *Methods*. Eight-week-old male Sprague-Dawley rats (240–260 g) were divided into three groups: sham operation, partial pulmonary artery ligation (PAL) procedure, and pulmonary artery half-closed clip (PAC) procedure. RV function and remodeling were determined by echocardiography and histomorphometry. *Results*. Surgical mortality was significantly lower in the PAC group while echocardiography revealed significantly more signs of RV dysfunction. At the 8th week after surgery RV fibrosis rate was significantly higher in the PAC group. *Conclusions*. This procedure of pulmonary artery banding in rats is easier and more efficient than partial ligation.

1. Introduction

The exact prevalence of pediatric heart failure is largely unknown but it is increasing. Recent advances in diagnostic methods, new surgical techniques, and improved perioperative management have contributed to an increased survival for patients with complex congenital heart disease who today often survive into adulthood [1].

Even after successful repair, however, right ventricle (RV) pressure overload remains in some patients and eventually impairs RV function and influences long-term mortality and morbidity [2–4].

Although compensated hypertrophy develops initially, ultimately RV failure will occur. The mechanisms underlying the progression from compensated to decompensated RV hypertrophy have not been well defined [5].

Clinically, the relationship between progressive fibrosis and RV function must be addressed [6, 7]. But studies of the mechanisms underlying the transition from a compensated state of hypertrophy to a decompensated state are difficult in patients, because invasive data cannot be easily obtained. For this purpose, animal models may be beneficial. Small experimental animals, such as rats, are widely used in cardiovascular research since they can provide a range of disease models, including cardiac hypertrophy and failure. A major advantage of these disease models is that cardiac material can be easily sampled to study the pathology of the disease in question.

The partial pulmonary artery ligation procedure has been widely used to produce right heart failure caused by pressure overload, but this procedure might have important drawbacks including a high surgical mortality caused by bleeding, sudden cardiac arrest, or pulmonary thrombus.

Pressure overload may also be induced using half-closed paper clips easily applied with a stopper. We could adjust the closing size by moving the stopper. The objective of this study was to establish rats model of RV failure using the pulmonary artery half-closed clip procedure comparing with partial ligation procedure.

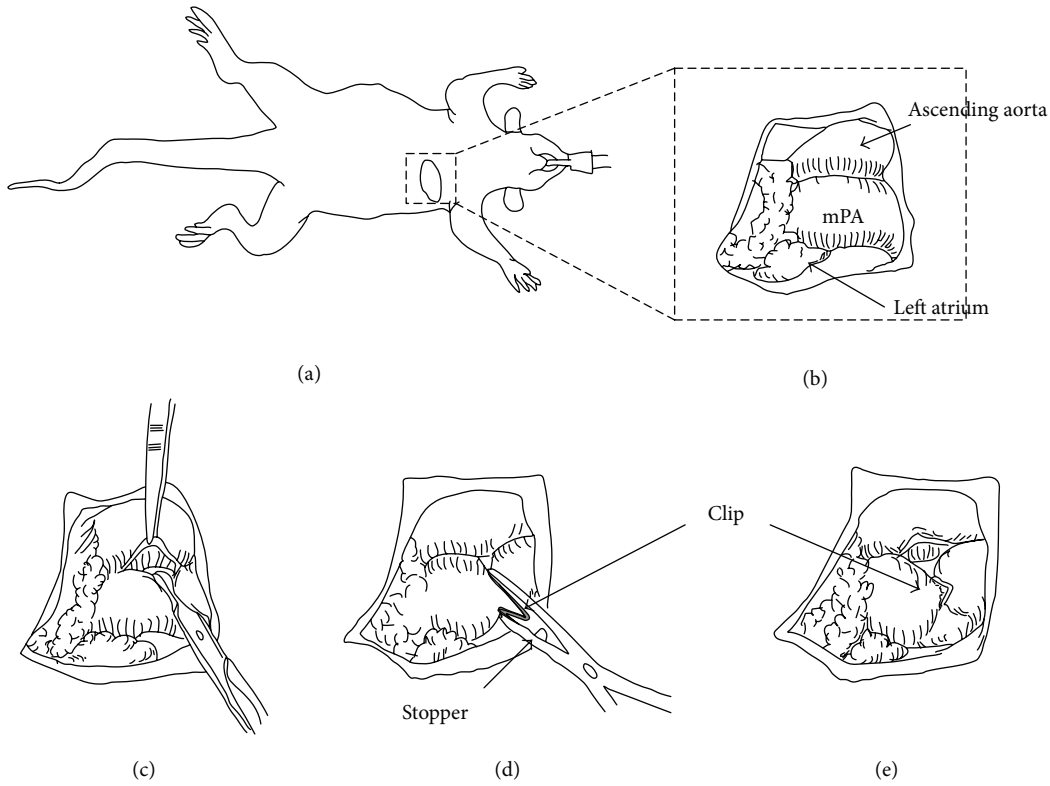

Figure 1: The PAC method. (a) Left thoracotomy was performed in the right semilateral decubitus position. (b) mPA was exposed through the left thoracotomy. ((c), (d)) Placement of a half-closed clip around mPA.

2. Materials and Methods

2.1. Animal Care. All experimental procedures and protocols used in this investigation were reviewed and approved by the institutional animal care and use committee and were in accordance with the National Institutes of Health "guide for the care and use of laboratory animals" (National Institutes of Health publication number 85-23, revised 1996).

2.2. Animal Model. A rat model of the pulmonary artery banding (PAB) was established to create chronic RV pressure overload. Eight-week-old male Sprague-Dawley rats (240–260 g) were anesthetized with intraperitoneal pentobarbital (50 mg/kg body weight) and xylazine (5 mg/kg) and ventilated with 100% O_2 by using a volume controlled respirator (2 mL, 60 cycles/min). A left thoracotomy was performed at the fourth intercostal space, and the main pulmonary artery (mPA) was carefully exposed (Figure 1).

2.2.1. Partial Pulmonary Artery Ligation Model (PAL) (n = 28). A 7-0 prolene suture was tied tightly around an 18-gauge needle alongside the mPA. After subsequent rapid removal of the needle, a fixed constricted opening was created in the lumen equal to the diameter of the needle [5, 8, 9].

2.2.2. Half-Closed Clip Model (PAC) (n = 28). A small clip (LT100 ETHICON) was half-closed around the mPA using a clip applier (LX107 ETHICON) with a stopper (Figure 1). The blood flow through the mPA was restricted to equal the inner segment of the half-closed clip. We selected type (B) clip because this inner size was almost equal to outer size of a 18 G needle (Figure 2).

Thereafter, the thorax was closed in layers, and the ventilator setting was changed (90 cycles/min) for half an hour to reduce the respiratory load.

2.2.3. Sham Operation (n = 12). A left thoracotomy was performed at the fourth intercostal space, and the mPA was carefully exposed. The thorax was closed in layers, and the ventilator setting was changed (90 cycles min^{-1}) for half an hour to reduce the respiratory load.

2.3. Echocardiographic Measurements. Echocardiograms were recorded on the preoperative day and on the 4th week and 8th week after the procedure. The rats were anaesthetized for echos (pentobarbital 50 mg kg^{-1} body weight) but were breathing spontaneously and were positioned on their left side.

Measuring echocardiograms, the dose of anesthetics was reduced to 50% only on the day when a rat had developed clinical signs, loss of activity, body edema, and pleural effusion, of RV failure. Transthoracic 2-dimensional, M-mode (according to the standards of the American Society of Echocardiography) and Doppler imaging were performed with a 6.5 MHz transducer (Xario TOSHIBA, JAPAN).

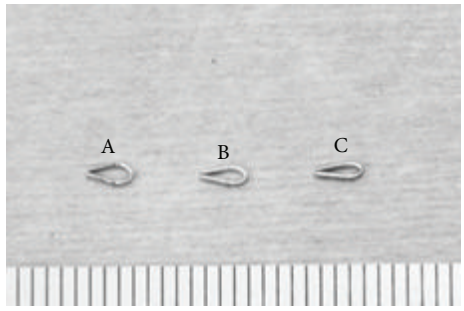

(a)

	Outer area (mm^2)
18 G needle	1.13
	Inner area (mm^2)
Half-closed clip (A)	1.46
Half-closed clip (B)	1.10
Half-closed clip (C)	0.87

(b)

Figure 2: (a) Half-closed clips (A), (B), and (C) with different placed stopper. (b) Size of inner area of clips (A), (B), and (C), respectively, comparing with 18 G needle outer size. In this paper, we used (B) type for the PAC method.

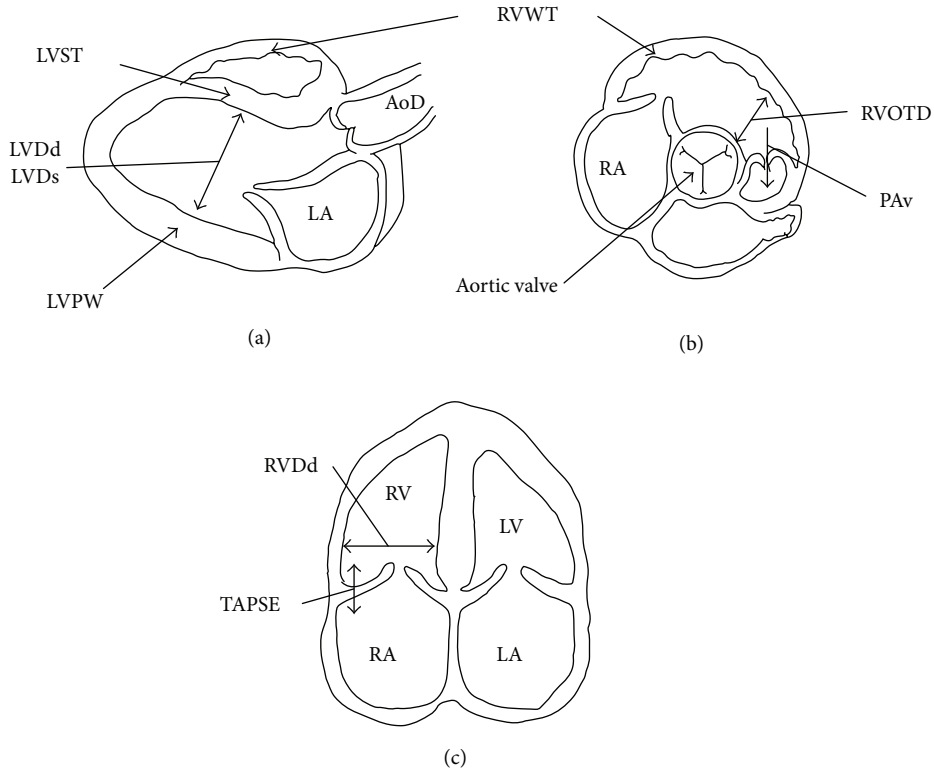

Figure 3: Schemata of echocardiograms measurements. (a) The parasternal long-axis view. (b) Parasternal short-axis view. (c) The apical four-chamber view.

Figure 3 showed schemata of the measurements of echocardiograms, respectively.

The RV morphology was assessed as RV free wall thickness (RVWT) and RV end-diastolic diameter (RVDd) and RV outflow tract dimension (RVOTD). RVWT was measured by M-mode either in the 2-dimensional parasternal short-axis view below the tricuspid valve or in the parasternal long-axis view, depending on the quality of RV free wall visualization. RVDd was measured as the maximal distance from the RV free wall to the septum from the apical four-chamber view.

RVOTD and aortic dimension (AoD) were measured at the aortic valve level in the short-axis view. The ratio of RVOTD to AoD (RVOTD/AoD) was calculated as representative of RV dilatation. The position of the transducer was aligned to visualize the RV apex.

The maximal RV cavity size preceding the frame with the onset of systolic closure of tricuspid valve leaflets was used to measure RVDd. To assess RV function, the tricuspid annular plane systolic excursion (TAPSE) of the lateral portion of the tricuspid annular plane was measured by the base-to-apex shortening during systole. This was recorded in the M-mode format under two-dimensional echocardiographic guidance from the apical four-chamber view.

Furthermore, PA velocity (PAv) was recorded at the aortic valve level in the short-axis view. This was used as an echocardiographic indicator of RV pressure overload [10, 11].

The left ventricle (LV) M-mode echocardiograms were recorded to evaluate LV function, as previously described. LV end-diastolic dimension (LVDd), LV end-systolic dimension (LVDs), interventricular septal wall thickness (IVST), and LV posterior wall thickness (LVPW) were measured at the papillary muscles level, and LV fractional shortening (LVFS) was calculated as follows:

$$\text{LVFS} = \left[\frac{(\text{LVDd} - \text{LVDs})}{\text{LVDd}}\right] \times 100\,(\%)\,. \quad (1)$$

2.4. Histopathological Analysis. In the PAL group, the remaining 4 rats were killed 4 weeks after surgery and all the remaining rats ($n = 8$) were killed 8 weeks after surgery. In the PAC group, 4 rats were killed 4 weeks after surgery and all the remaining rats ($n = 6$) were killed 8 weeks after surgery. In the sham group, 6 rats were killed 4 or 8 weeks after surgery. The hearts were quickly removed, and the ventricles were dissected free of atrial tissue and large blood vessels. The right ventricle was carefully separated from the left ventricle and interventricular septum (IVS). The fresh ventricular tissues were immediately blotted dry and weighted separately to determine the degree of RV hypertrophy based on 2 parameters: RV wall weight/body weight (RV/BW) and RV wall weight/LV and IVS wall weight (RV/LV + IVS).

Tissue specimens for pathological analysis were obtained from whole hearts in cross sections, cut into 5 mm thick sections, and stained with hematoxylin and eosin for morphologic analysis, including measurement of the short-axis dimension of the RV myocardial cell and Masson's trichrome staining to determine the amount of interstitial and myocardial fibrosis. Digital images of cross sections were taken by a CCD camera (OLYMPUS DP-72) with a light microscope (OLYMPUS SZX12). The number of pixels of the blue-stained collagen area was calculated with Adobe Photoshop CS5 soft and then divided by the total number of pixels in the RV wall per slide, analyzed, and averaged.

2.5. Statistical Analysis. All data were expressed as mean ± SEM and range. Student's unpaired t-test or analysis of variance for parametric values was used to compare group means. Probability of 0.05 or less was considered to be statistically significant.

3. Results

3.1. Procedure. Surgical procedure time was defined as the interval from starting to incise the skin to skin closure. The surgical procedure time was 27.6 ± 1.4 min for PAL and 17.3 ± 2.1 min for PAC ($p < 0.01$). For the PAL procedure, 5 major hemorrhages occurred during trimming the mPA compared to only one major hemorrhage for the PAC procedure.

To evaluate the two procedures for RV pressure overload damage, we recorded the postsurgery recovery time. This was defined as the interval from time of extubation until the animal was fully conscious and walking freely. The recovery time was 30.4 ± 5.3 min for the sham procedure and 33.5 ± 5.2 min for PAC which was significantly shorter than the PAL procedure which was 64.9 ± 7.3 min.

3.2. Surgical Risk. Sixty-eight rats underwent PAL ($n = 28$) or PAC ($n = 28$) or sham ($n = 12$) in the surgical risk study. During the perisurgical period, which was the time from the beginning of surgery to 6 hours after surgery, 1 rat in the PAC group out of 28 died due to bleeding (3.6%).

In contrast, 7 of 28 perisurgical deaths were seen in the PAL group (25%). Of those 7 rats, 1 died from an intubation accident, 2 died from bleeding, 2 died from pneumothorax, and 2 died from sudden cardiac arrest. All of the animals in the sham group survived regardless of the surgical procedure. After the perisurgical period, there were 3 and 12 deaths in the PAL and PAC groups, respectively. The most common reasons for post-PAB death in both groups were pleural and/or pericardial effusion (pleural effusion: 66.7% in PAL and 83.3% in PAC, pericardial effusion: 33.3% in PAL and 41.7% in PAC) occurring between weeks 4 and 8 after surgery. Some of the rats died of unknown causes although we assumed these were due to either cardiac arrhythmia or heart failure as autopsy of these rats showed no blood in the thoracic cavity.

3.3. Echocardiographic Study. Table 1 shows the trend for LVDd and AoD to decrease but LV contractility (LVFS) showed no significant difference. Both PAL and PAC groups showed a significantly increased pulsed Doppler Peak PAv, RVOTD, RVDd, and RVWT. In the PAC group, PAv and RVOTD tended to increase more significantly than in the PAL group. The dilatation of the RV associated with the RVDd/LVDd ratio and the RVOTD/AoD ratio. In the PAC group, the RVDd/LVDd ratio was increased and became significantly greater than in the sham and PAL group. The RVOTD/AoD ratio was about 1.0 throughout the observation in the sham group. In contrast, the ratio increased progressively in the PAL and PAC groups, especially in the PAC group.

The signs of RV failure associated with TAPSE were more severe in the PAC group than in the PAL group. The signs of moderate or severe tricuspid regurgitation (TR) or pleural effusion or IVC dilation were detected in the PAC group 5 weeks after the PAC procedure, but we could seldom detect these signs in the PAL group throughout the observation period (PAC versus PAL: moderate or more TR 21/27 (77.8%) versus 3/21 (14.3%), pleural effusion 18/27 (66.7%) versus 2/21 (10.0%), and IVC dilation 20/27 (74.1%) versus 0/21 (0%)).

Furthermore, the standard deviation in the PAC group was greater than the PAL group. In other words, the data of the PAL group varied more widely than that of the PAC group. More stable data might be obtained with the PAC procedure.

3.4. Morphometric and Histological Analysis

3.4.1. RV Hypertrophy. A weight analysis showed the heart weight/BW, RV/BW, and RV/(LV + IVS) weight ratios in the PAC and PAL groups to be similar and significantly higher

Table 1: Ultrasound findings in the sham rats, at 4th or 8th week after the PAB procedure.

	Preoperative day			4th week			8th week		
	Sham	PAL	PAC	Sham	PAL	PAC	Sham	PAL	PAC
n	12	28	28	12	16	22	6	8	6
LVDd (mm)	4.66 ± 0.43	4.75 ± 0.43	4.67 ± 0.39	5.36 ± 0.36	5.10 ± 0.42	5.07 ± 0.51	5.78 ± 0.19	5.40 ± 0.29	5.42 ± 0.38
LVDs (mm)	2.10 ± 0.5	2.15 ± 0.47	2.06 ± 0.47	2.51 ± 0.38	2.88 ± 0.58	2.55 ± 0.31	2.90 ± 0.52	2.38 ± 0.38	2.68 ± 0.45
IVST (mm)	1.06 ± 0.27	1.11 ± 0.29	1.14 ± 0.31	1.57 ± 0.10	1.56 ± 0.16	1.65 ± 0.27	1.93 ± 0.21	1.90 ± 0.10	2.13 ± 0.22
PWT (mm)	1.01 ± 0.24	1.05 ± 0.27	1.04 ± 0.27	1.71 ± 0.29	1.51 ± 0.08	1.62 ± 0.20	2.23 ± 0.22	2.04 ± 0.09	1.97 ± 0.14
FS (%)	55.17 ± 8.74	55.02 ± 8.17	56.15 ± 8.68	53.27 ± 4.42	42.81 ± 15.09	49.78 ± 4.02	49.62 ± 10.14	56.07 ± 5.10	50.64 ± 5.51
RVDd (mm)	2.46 ± 0.31	2.49 ± 0.29	2.49 ± 0.26	2.43 ± 0.28	**5.48 ± 1.47***	**6.26 ± 1.28***	2.80 ± 0.58	**5.26 ± 0.96***	**6.95 ± 0.63***
RVWT (mm)	0.63 ± 0.19	0.65 ± 0.18	0.70 ± 0.17	0.54 ± 0.08	**1.25 ± 0.11***	**1.41 ± 0.28***	0.98 ± 0.1	**1.72 ± 0.15***	**1.80 ± 0.43***
TAPSE (mm)	2.71 ± 0.22	2.69 ± 0.21	2.69 ± 0.23	2.53 ± 0.14	2.40 ± 0.11	**1.67 ± 0.20**$^{\star\$}$	2.58 ± 0.1	2.32 ± 0.20	**1.42 ± 0.25**$^{\star\$}$
HR (bpm)	438 ± 43	441 ± 39	455 ± 24	447 ± 21	436 ± 26	422 ± 31	451 ± 22	419 ± 20	411 ± 30
Peak PAV (m/s)	0.76 ± 0.11	0.73 ± 0.12	0.71 ± 0.12	0.97 ± 0.14	**2.93 ± 0.54***	**3.91 ± 0.38**$^{\star\$}$	1.05 ± 0.13	**3.28 ± 0.37***	**4.03 ± 0.27**$^{\star\$}$
RVOTD (mm)	1.99 ± 0.20	2.00 ± 0.24	1.97 ± 0.25	2.64 ± 0.17	**2.98 ± 0.37**$^{\#}$	**3.22 ± 0.50***	2.20 ± 0.16	**2.78 ± 0.37**$^{\#}$	**3.62 ± 0.16**$^{\star\$}$
AoD (mm)	2.23 ± 0.25	2.25 ± 0.23	2.30 ± 0.21	2.80 ± 0.18	2.65 ± 0.11	**2.55 ± 0.22**$^{\#}$	2.78 ± 0.05	2.44 ± 0.35	2.65 ± 0.10
RVDd/LVDd	0.53 ± 0.08	0.53 ± 0.07	0.53 ± 0.05	0.46 ± 0.07	**1.08 ± 0.28***	**1.25 ± 0.32***	0.48 ± 0.09	**0.971 ± 0.15***	**1.28 ± 0.08**$^{\star\$}$
RVOTD/AoD	0.90 ± 0.16	0.90 ± 0.16	0.86 ± 0.15	0.95 ± 0.07	**1.12 ± 0.14**$^{\#}$	**1.27 ± 0.20***	0.79 ± 0.07	**1.157 ± 0.21**$^{\#}$	**1.37 ± 0.10***†
RVPW/LVPW	0.65 ± 0.23	0.65 ± 0.21	0.69 ± 0.20	0.32 ± 0.05	**0.83 ± 0.08***	**0.87 ± 0.15***	0.44 ± 0.06	**0.844 ± 0.07***	**0.92 ± 0.24***

n, number of rats. #: $p < 0.05$ versus sham, ⋆: $p < 0.01$ versus sham, †: $p < 0.05$ versus PAL, and $: $p < 0.01$ versus PAL.

Table 2: Weight analysis at the 4th and 8th week after the PAB procedure.

(a) Weight analysis at the 4th week after the procedure

	BW (g)	HW/BW ratio (mg/g)	RV/BW ratio (mg/g)	RV/(LV + IVS) ratio
Sham	435 ± 39	3.57 ± 0.16	0.56 ± 0.07	0.21 ± 0.02
PAL	403 ± 21	**4.65 ± 0.17***	**1.40 ± 0.13***	**0.50 ± 0.04***
PAC	398 ± 33	**4.88 ± 0.17***	**1.39 ± 0.03***	**0.49 ± 0.04***

(b) Weight analysis at the 8th week after the procedure

	BW (g)	HW/BW ratio (mg/g)	RV/BW ratio (mg/g)	RV/(LV + IVS) ratio
Sham	508 ± 41	3.30 ± 0.23	0.48 ± 0.04	0.21 ± 0.01
PAL	505 ± 47	**4.34 ± 0.30***	**1.27 ± 0.12***	**0.54 ± 0.02***
PAC	450 ± 50	**4.81 ± 0.32***	**1.40 ± 0.07***	**0.58 ± 0.03***

There was no significant difference between the PAL and PAC groups.
BW: body weight at the sacrifice time, HW: heart weight, and ⋆: $p < 0.05$ versus sham.

than in the sham group (Table 2). Whole heart findings revealed a thickened RV wall, with an enlarged cavity, and the IVS shifted toward the left side in the PAC and PAL groups (Figure 5). Myocardial cell size in the PAC and PAL groups was similar and significantly higher than in the sham group (4th week: sham versus PAL versus PAC: 13.7±1.64 μm versus 21.3 ± 3.47 μm versus 22.8 ± 2.38 μm, 8th week: sham versus PAL versus PAC: 14.3 ± 1.40 μm versus 34.7 ± 7.22 μm versus 35.1 ± 8.19 μm) (Table 1, Figure 4).

3.4.2. Fibrosis. Masson's trichrome staining showed fibrosis in the RV free walls of the sham, PAL, and PAC groups (Figure 6). At the 4th week, the percentage of fibrosis in the PAL and PAC groups was similar and significantly higher than in the sham group (sham versus PAL versus PAC: 0.49 ± 0.06% versus 3.12 ± 1.09% versus 4.68 ± 1.63%) (Figure 6(b)). But at 8 weeks, the percentage fibrosis in the PAC group was significantly higher than in the sham and PAL groups (sham versus PAL versus PAC: 1.51 ± 0.86% versus 9.73 ± 6.05% versus 29.2 ± 6.13%) (Figure 6(b)).

4. Discussion

Definition of heart failure was challenging because there were neither objective cutoff values of cardiac or ventricular dysfunction nor changes in pressure, dimension, or volume that could be reliably used to identify patients with heart failure. According to The European Society of Cardiology task force for the diagnosis and treatment of heart failure, both symptoms at rest or during exertion and objective evidence of cardiac dysfunction at rest should be present to diagnose heart failure [12].

In animal models, however, heart failure symptoms like fatigue or breathlessness are difficult to detect and quantify. Then evaluation of the models depends on objective findings such as reduced cardiac output, increased filling pressure, and progressive fibrosis [6, 7, 13]. In addition, the valuable signs of progressive heart failure are pericardial or pleural effusion [14]. In this paper, we demonstrated right heart failure by the objective findings of cardiac dysfunction.

Most attention is given to LV function, whereas RV function and disease have seldom been focused on. It is an established fact that there is a relationship between LV and RV function. Impairment of the RV might influence LV function [15, 16]. RV function is one independent predictor

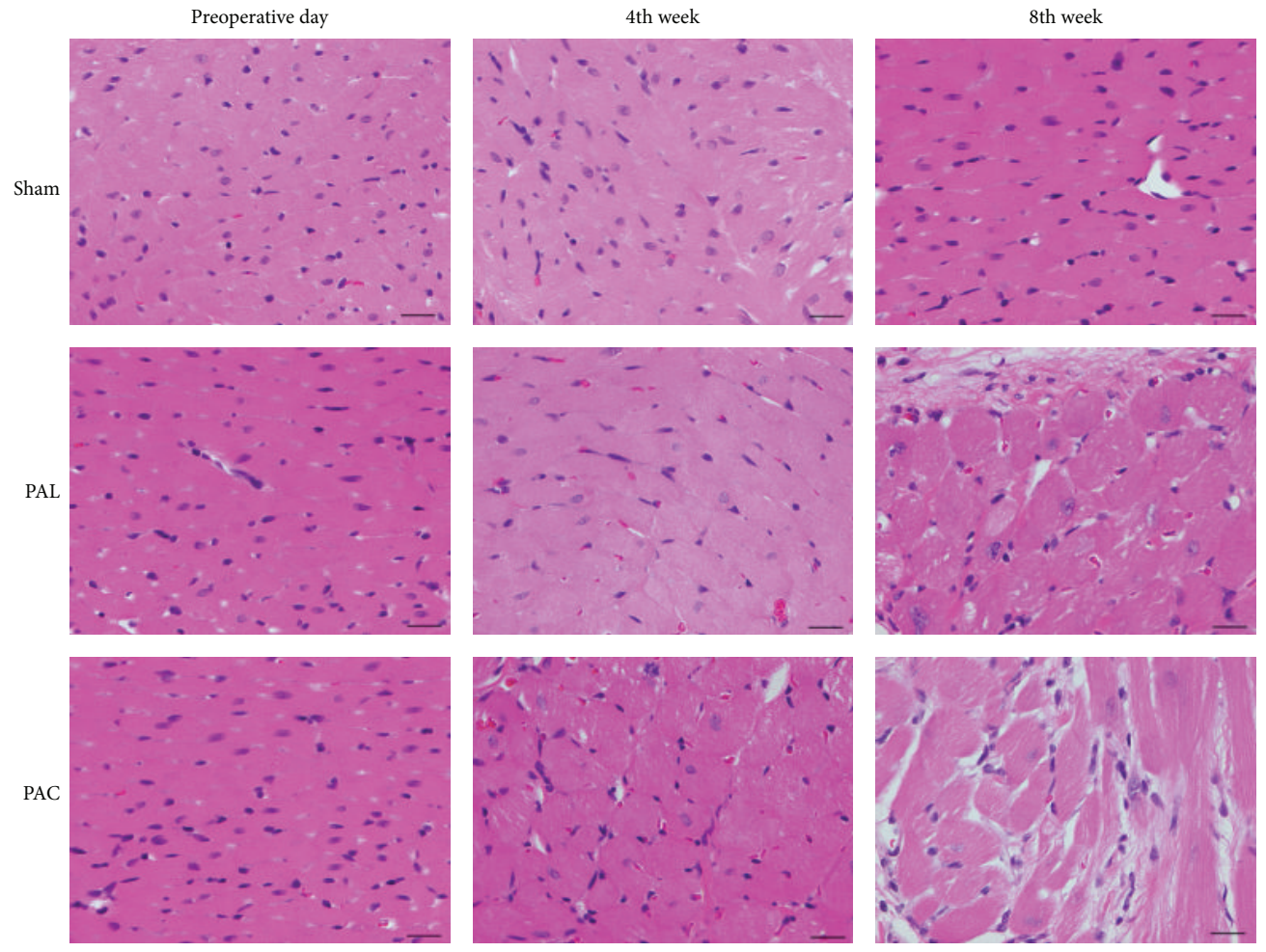

(a)

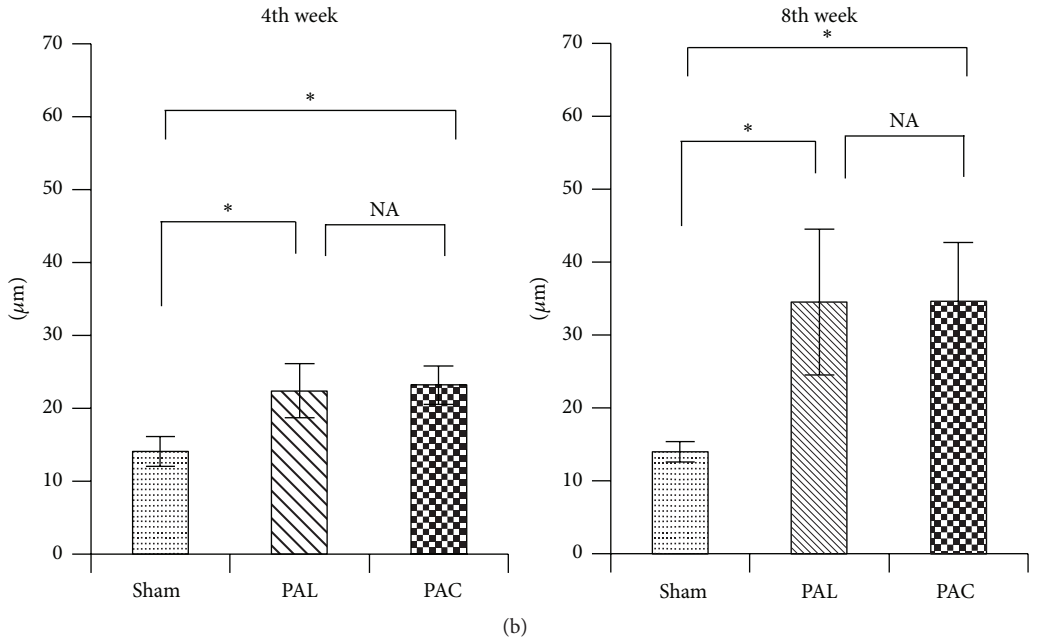

(b)

FIGURE 4: Photomicrographs of hematoxylin and eosin-stained sections showed significantly hypertrophied ventricular myocytes in the PAL and PAC groups. Scale bar: 20 μm. $^{*}p < 0.01$.

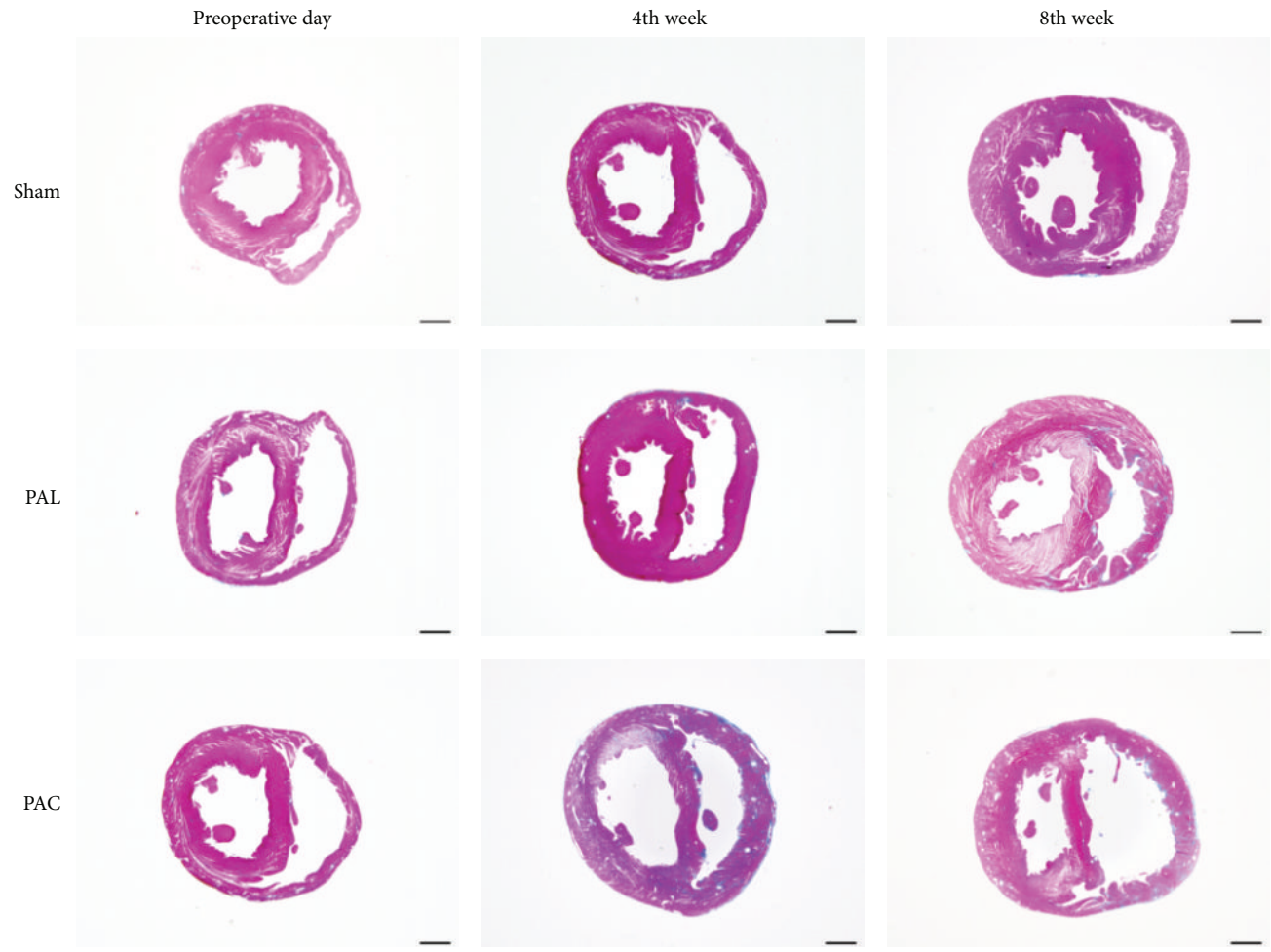

Figure 5: Macroscopic photographs of Masson's trichrome-stained cross sections showed RV wall thickening, cavity enlarging, and the interventricular septum shifting toward the left side in the PAL and PAC groups. Scale bar: 2 mm.

of mortality and the development of heart failure in patients with LV dysfunction [17]. Five to ten percent of patients with advanced chronic obstructive pulmonary disease may suffer from severe pulmonary hypertension and present with a progressively downhill clinical course because of RV dysfunction [18]. Not only in the view point of congenital heart disease, well-established animal models of RV function may be necessary for further investigation of RV function and pathology. Some animal models of RV dysfunction exist (monocrotaline treatment, partial ligation method) [5, 8–10, 19]. Monocrotaline treatment has been used to induce pulmonary hypertension resulting in RV hypertrophy and eventually heart failure [20, 21]. Monocrotaline treatment might have disadvantages in the form of disease manifestations not usually associated with human heart failure and changes in hormones such as endothelin [21, 22]. PAB does not have such side effects and is a promising procedure for inducing symptomatic RV dysfunction. PAL procedure has been used in several hypertrophy experiments; however, slippage of the band and the obvious difficulties ensuring the same degree of constriction among the banded animals when using a surgical nylon (usually prolene) led us to believe that banding with tantalum clips would be a more reliable procedure to create PAB model. In another PAB study using surgical nylon thread, PAL procedure, about 25% of the banded rats showed no hypertrophy [23], suggesting that this was a less reliable way. Also in this study, in the PAL group, the data had greater variance than in the PAC group. In addition, the objective findings of RV dysfunction were present less in the PAL group.

To the best of our knowledge this is the first reported evaluation of a newly devised means of stressing the right ventricle—the half-closed clip procedure—and its comparison with the pulmonary artery banding procedure. Using this new technique we could produce a right heart failure model in significantly less time and with much faster recovery and fewer surgical deaths than the PAL procedure. Most importantly, this novel procedure more fully developed subsequent myocardial damage and postsurgery cardiac dysfunction than did the PAL procedure. Furthermore, if we adjust the position of the stopper, we can produce different PAB models using this procedure.

A recent study in rats who underwent banding of the mPA by the existing partial ligation procedure showed that pressure overload alone was insufficient to explain right heart failure; the rats showed no effect on cardiac output or fibrosis

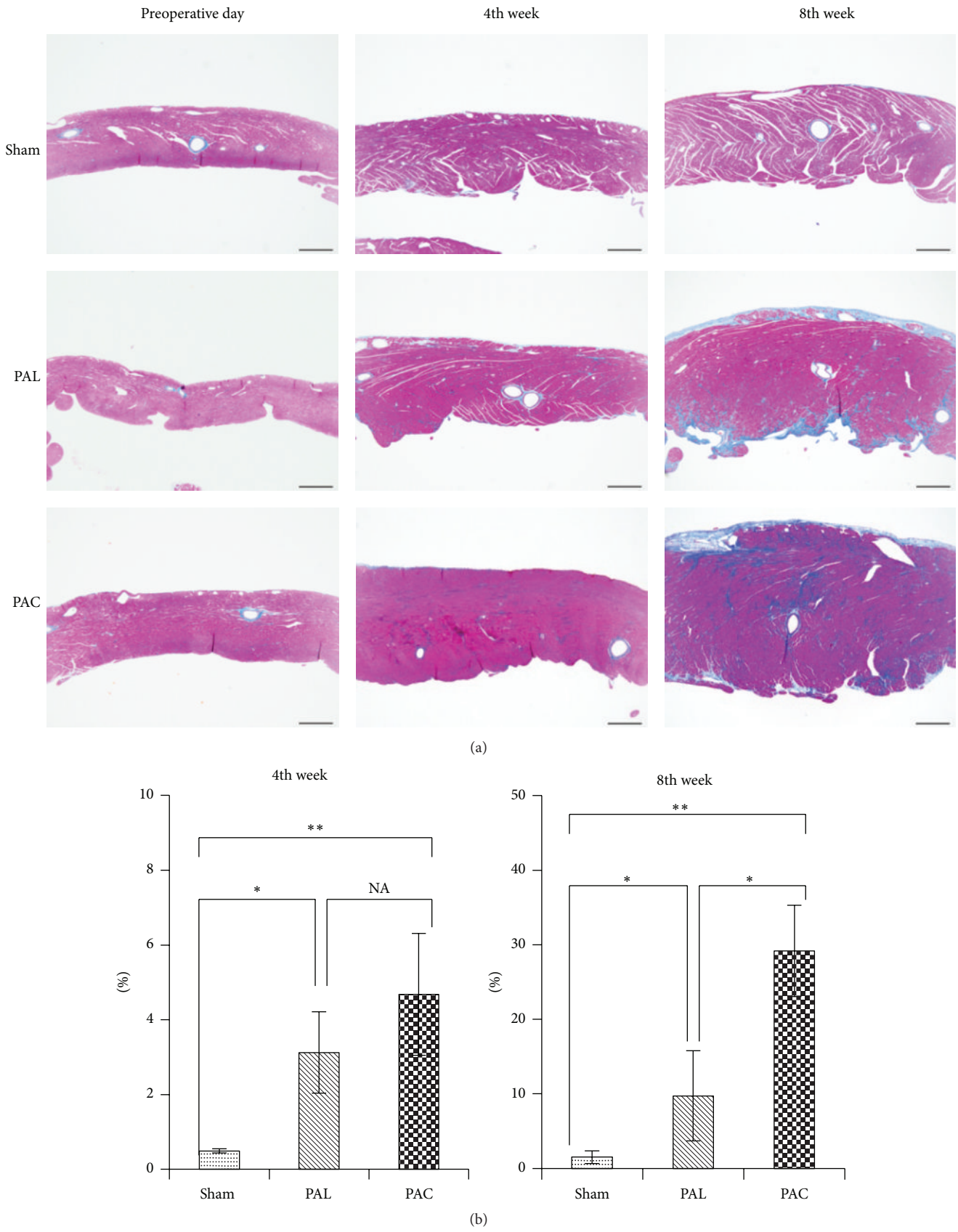

FIGURE 6: (a) Representative photomicrographs of Masson's trichrome-stained RV free wall (scale bar: 500 μm). (b) Evaluation of fibrosis area for RV free wall. $^{*}p < 0.05$, $^{**}p < 0.01$.

[24]. Using the PAC procedure, however, we could produce RV dysfunction models that represent not only RV cavity dilation and RV hypertrophy but also moderate or greater tricuspid regurgitation or pleural and/or pericardial effusion.

Hardziyenka and colleagues reported LV atrophy in pulmonary hypertension [25]. However, we could not detect significant left-sided effects, but we could find a trend towards LV atrophy (Table 1 LVPWT, PAC versus sham, $p = 0.051$).

5. Conclusion

This study demonstrated that the application of a tantalum half-closed clip around the pulmonary artery induced right ventricle dysfunction in a reproducible manner. This model should prove valuable in the investigation and treatment of right heart failure caused by pressure overload.

Conflict of Interests

The authors declare that there is no conflict of interests regarding the publication of this paper.

References

[1] M. S. Patel and B. E. Kogon, "Care of the adult congenital heart disease patient in the United States: a summary of the current system," *Pediatric Cardiology*, vol. 31, no. 4, pp. 511–514, 2010.

[2] A. P. Bolger, A. J. S. Coats, and M. A. Gatzoulis, "Congenital heart disease: the original heart failure syndrome," *European Heart Journal*, vol. 24, no. 10, pp. 970–976, 2003.

[3] J. G. Murphy, B. J. Gersh, D. D. Mair et al., "Long-term outcome in patients undergoing surgical repair of tetralogy of Fallot," *The New England Journal of Medicine*, vol. 329, no. 9, pp. 593–599, 1993.

[4] M. A. Gatzoulis, S. Balaji, S. A. Webber et al., "Risk factors for arrhythmia and sudden cardiac death late after repair of tetralogy of Fallot: a multicentre study," *The Lancet*, vol. 356, no. 9234, pp. 975–981, 2000.

[5] M. J. Faber, M. Dalinghaus, I. M. Lankhuizen et al., "Right and left ventricular function after chronic pulmonary artery banding in rats assessed with biventricular pressure-volume loops," *American Journal of Physiology—Heart and Circulatory Physiology*, vol. 291, no. 4, pp. H1580–H1586, 2006.

[6] S. V. Babu-Narayan, P. J. Kilner, W. Li et al., "Ventricular fibrosis suggested by cardiovascular magnetic resonance in adults with repaired tetralogy of Fallot and its relationship to adverse markers of clinical outcome," *Circulation*, vol. 113, no. 3, pp. 405–413, 2006.

[7] U. K. Chowdhury, S. Sathia, R. Ray, R. Singh, K. K. Pradeep, and P. Venugopal, "Histopathology of the right ventricular outflow tract and its relationship to clinical outcomes and arrhythmias in patients with tetralogy of Fallot," *The Journal of Thoracic and Cardiovascular Surgery*, vol. 132, no. 2, pp. 270.e4–277.e4, 2006.

[8] T. Hoashi, G. Matsumiya, S. Miyagawa et al., "Skeletal myoblast sheet transplantation improves the diastolic function of a pressure-overloaded right heart," *Journal of Thoracic and Cardiovascular Surgery*, vol. 138, no. 2, pp. 460–467, 2009.

[9] M. U. Braun, P. Szalai, R. H. Strasser, and M. M. Borst, "Right ventricular hypertrophy and apoptosis after pulmonary artery banding: regulation of PKC isozymes," *Cardiovascular Research*, vol. 59, no. 3, pp. 658–667, 2003.

[10] J. E. Jones, L. Mendes, M. A. Rudd, G. Russo, J. Loscalzo, and Y.-Y. Zhang, "Serial noninvasive assessment of progressive pulmonary hypertension in a rat model," *American Journal of Physiology—Heart and Circulatory Physiology*, vol. 283, no. 1, pp. H364–H371, 2002.

[11] R. Martin-Duran, M. Larman, A. Trugeda et al., "Comparison of Doppler-determined elevated pulmonary arterial pressure with pressure measured at cardiac catheterization," *The American Journal of Cardiology*, vol. 57, no. 10, pp. 859–863, 1986.

[12] K. Swedberg, J. Cleland, H. Dargie et al., "Guidelines for the diagnosis and treatment of chronic heart failure: executive summary (update 2005)," *European Heart Journal*, vol. 26, no. 11, pp. 1115–1140, 2005.

[13] J. R. R. Heyen, E. R. Blasi, K. Nikula et al., "Structural, functional, and molecular characterization of the SHHF model of heart failure," *American Journal of Physiology—Heart and Circulatory Physiology*, vol. 283, no. 5, pp. H1775–H1784, 2002.

[14] H. Shigematsu, Y. Hirooka, K. Eshima, M. Shihara, T. Tagawa, and A. Takeshita, "Endogenous angiotensin II in the NTS contributes to sympathetic activation in rats with aortocaval shunt," *American Journal of Physiology—Regulatory Integrative and Comparative Physiology*, vol. 280, no. 6, pp. R1665–R1673, 2001.

[15] C. M. Yu, J. E. Sanderson, S. Chan, L. Yeung, Y. T. Hung, and K. S. Woo, "Right ventricular diastolic dysfunction in heart failure," *Circulation*, vol. 93, no. 8, pp. 1509–1514, 1996.

[16] M. F. Hill and P. K. Singal, "Right and left myocardial antioxidant responses during heart failure subsequent to myocardial infarction," *Circulation*, vol. 96, no. 7, pp. 2414–2420, 1997.

[17] L. A. M. Zornoff, H. Skali, M. A. Pfeffer et al., "Right ventricular dysfunction and risk of heart failure and mortality after myocardial infarction," *Journal of the American College of Cardiology*, vol. 39, no. 9, pp. 1450–1455, 2002.

[18] R. Naeije, "Pulmonary hypertension and right heart failure in chronic obstructive pulmonary disease," *Proceedings of the American Thoracic Society*, vol. 2, pp. 20–22, 2005.

[19] Y. Kato, M. Iwase, H. Kanazawa et al., "Progressive development of pulmonary hypertension leading to right ventricular hypertrophy assessed by echocardiography in rats," *Experimental Animals*, vol. 52, no. 4, pp. 285–294, 2003.

[20] L. Chen, X. T. Gan, J. V. Haist et al., "Attenuation of compensatory right ventricular hypertrophy and heart failure following monocrotaline-induced pulmonary vascular injury by the Na+ −H+ exchange inhibitor cariporide," *Journal of Pharmacology and Experimental Therapeutics*, vol. 298, no. 2, pp. 469–476, 2001.

[21] S. A. Doggrell and L. Brown, "Rat models of hypertension, cardiac hypertrophy and failure," *Cardiovascular Research*, vol. 39, no. 1, pp. 89–105, 1998.

[22] T. Miyauchi, R. Yorikane, S. Sakai et al., "Contribution of endogenous endothelin-1 to the progression of cardiopulmonary alterations in rats with monocrotaline-induced pulmonary hypertension," *Circulation Research*, vol. 73, no. 5, pp. 887–897, 1993.

[23] R. H. LekanneDeprez, M. J. B. van den Hoff, P. A. J. de Boer et al., "Changing patterns of gene expression in the pulmonary trunk-banded rat heart," *Journal of Molecular and Cellular Cardiology*, vol. 30, no. 9, pp. 1877–1888, 1998.

[24] H. J. Bogaard, R. Natarajan, S. C. Henderson et al., "Chronic pulmonary artery pressure elevation is insufficient to explain right heart failure," *Circulation*, vol. 120, no. 20, pp. 1951–1960, 2009.

[25] M. Hardziyenka, M. E. Campian, H. J. Reesink et al., "Right ventricular failure following chronic pressure overload is associated with reduction in left ventricular mass: evidence for atrophic remodeling," *Journal of the American College of Cardiology*, vol. 57, no. 8, pp. 921–928, 2011.

Hindawi Publishing Corporation
BioMed Research International
Volume 2015, Article ID 893051, 9 pages
http://dx.doi.org/10.1155/2015/893051

Research Article

Comparative Analysis of Methods to Induce Myocardial Infarction in a Closed-Chest Rabbit Model

Marc-Antoine Isorni,[1,2] Amaury Casanova,[3] Julie Piquet,[3] Valérie Bellamy,[3] Charly Pignon,[4] Etienne Puymirat,[1,2,3] and Philippe Menasche[2,3,5]

[1] *Department of Cardiology, Hôpital Européen Georges Pompidou, Assistance Publique des Hôpitaux de Paris, France*
[2] *Université Paris Descartes, Paris, France*
[3] *INSERM U970, Paris Cardiovascular Research Center PARCC, Paris, France*
[4] *National Veterinary School of Alfort, Maisons-Alfort, France*
[5] *Department of Cardiovascular Surgery, Hôpital Européen Georges Pompidou, Assistance Publique des Hôpitaux de Paris, France*

Correspondence should be addressed to Marc-Antoine Isorni; marco.isorni@gmail.com

Received 25 March 2015; Accepted 25 May 2015

Academic Editor: Bastian Schmack

Objective. To develop a rabbit model of closed-chest catheter-induced myocardial infarction. *Background.* Limitations of rodent and large animal models justify the search for clinically relevant alternatives. *Methods.* Microcatheterization of the heart was performed in 47 anesthetized 3-4 kg New Zealand rabbits to test five techniques of myocardial ischemia: free coils ($n = 4$), interlocking coils ($n = 4$), thrombogenic gelatin sponge ($n = 4$), balloon occlusion ($n = 4$), and alcohol injection ($n = 8$). In order to limit ventricular fibrillation, an antiarrhythmic protocol was implemented, with beta-blockers/amiodarone before and xylocaine infusion during the procedure. Clinical, angiographic, and echographic data were gathered. End points included demonstration of vessel occlusion (TIMI flow grades 0 and 1 on the angiogram), impairment of left ventricular function at 2 weeks after procedure (by echocardiography), and pathologically confirmed myocardial infarction. *Results.* The best arterial access was determined to be through the right carotid artery. The internal mammary guiding catheter 4-Fr was selected as the optimal device for selective intracoronary injection. Free coils deployed prematurely and tended to prolapse into the aorta. Interlocking coils did not deploy completely and failed to provide reliable results. Gelatin sponge was difficult to handle, adhered to the catheter, and could not be clearly visualized by fluoroscopy. Balloon occlusion yielded inconsistent results. Alcohol injection was the most efficient and reproducible method for inducing myocardial infarction (4 out of 6 animals), the extent of which could be fine-tuned by using a coaxial balloon catheter as a microcatheter (0.52 mm) to achieve a superselective injection of 0.2 mL of alcohol. This approach resulted in a 20% decrease in LVEF and infarcted myocardium was confirmed histologically. *Conclusions.* By following a stepwise approach, a minimally invasive, effective, and reproducible rabbit model of catheter-induced myocardial infarction has been developed which addresses the limitations of rodent experiments while avoiding the logistical and cost issues associated with large animal models.

1. Introduction

Heart failure (HF) is a major health and economic burden in developing countries and its prevalence is increasing [1, 2]. It is a complex, heterogeneous disorder that can result from primary cardiomyopathy or, more commonly, from myocardial infarction (MI), hypertension, or disorders of the valve [3, 4]. Because many HF cases are secondary to ischemic heart disease, animal models that closely mimic the characteristics and development of human MI are essential for better understanding the pathophysiology of heart failure and for developing medical or surgical therapies. Many of these models entail a surgical ligation of the coronary artery (with or without reperfusion), which is a reasonably reproducible technique, with the caveat that it results in a HF pattern different from what is seen in humans [5–7]. Percutaneous intracoronary embolization of various materials more closely duplicates acute coronary syndromes caused

by embolization of atherosclerosis debris or thrombosis in the coronary microcirculation. Furthermore, the minimally invasive nature of the procedure reduces surgical complications and maintains the integrity of anatomical structures, particularly the pericardium which is involved in the regulation of myocardial inflammation and remodeling [6, 8–13]. However, the embolization technique also has limitations. First, it may be challenging to precisely control the location and duration of the coronary artery occlusion. Second, so far, it has been primarily applied to large animals (specifically pig and sheep). In an attempt to find an acceptable trade-off between rodent models, whose cardiac physiology is far from that of humans [14], and large animal models, which raise logistical and economic issues, the present study was designed to develop a straightforward and reproducible model of percutaneously induced MI in rabbits.

2. Materials and Methods

2.1. Animals. This study was approved by the University of Paris René Descartes Ethics Committee and by the *ad hoc* board of the French Ministry of Research and Education. Animals were cared for in accordance with the Guide for the Care and Use of Laboratory Animals [15].

2.2. Experimental Design. Adult male White New Zealand rabbits weighing 3.8–4.4 kg were used in this study. During the procedure, animals were anaesthetised using 5 mg/kg ketamine-HCl and 20 mg/kg propofol via the ear vein and anticoagulated with heparin (300 IU/kg). An antiarrhythmic protocol was implemented, which included beta-blockers/amiodarone and lidocaine (1 mg/kg load followed by a 20 μg/kg/min infusion) to reduce ischemic ventricular arrhythmias. Electrocardiogram and peripheral oxygen saturation were continuously recorded. Procedure success was assessed by the demonstration of a widening of the QRS complex or of ST segment elevation in the electrocardiogram and by TIMI 0 or 1 angiographic blood flow grades. After induction of MI, animals were kept under clinical observation. Animals with postprocedural heart failure received furosemide at 0.3 mg/kg/d for 3 days. After 3 weeks, animals were sedated as described above, examined clinically and echographically, and sacrificed. End points included impairment of left ventricular (LV) function at 3 weeks after procedure (by echocardiography using the Simpson method) and histologically confirmed myocardial infarction.

2.3. Experimental Procedures. Three series of experiments were sequentially performed.

(1) Assessment of vascular access and coronary catheterization procedures: after having selected the right carotid artery as the vascular access entry site, 3 rabbits were used to test two devices (cathlons and fine needles); 2 animals were used for vessel catheterization and to select the optimal introducer sheath size. Four additional rabbits were then used for selecting the type and size of the guiding catheter for coronary catheterization and to determine the dilution of the contrast medium.

(2) Assessment of the coronary occlusion site: to determine the coronary artery branch most suitable for occlusion to induce a functionally relevant MI, 14 rabbits underwent release of free and droppable coils. They were divided into three groups according to the target territory: the left descending artery area (n = 6), the circumflex artery territory (n = 5), or the right coronary artery territory (n = 3). After three weeks, sedated animals were evaluated clinically and echographically, according to the protocol described above, before being sacrificed and studied histologically.

(3) Comparison of MI-inducing techniques: five different techniques of coronary occlusion were finally investigated: free coils (n = 4), interlocking coils (n = 4), balloon occlusion (n = 4), release of a thrombogenic sponge (n = 4), and injection of alcohol (n = 8).

For coils, a guiding catheter was positioned under fluoroscopic guidance at the coronary ostium and a 0.014-in. floppy wire was advanced into the coronary vessel. The wire was advanced into the dominant coronary artery branch, as determined by angiography (Figure 3). Over the wire, a microcatheter (FineCross MG, Terumo Corporation, Tokyo, Japan) was tracked into the coronary artery. Free coils were loaded into the microcatheter and dropped to the desired site. For interlocking coils, the procedure was modified in that the microcatheter was tracked, the floppy wire was removed, and the interlocking coil was loaded into the inner lumen of the microcatheter. It was then advanced to the optimal site and deployed. If interlocking coils failed to deploy, they could be removed. For balloon occlusion, an angioplasty balloon was tracked over the wire, placed into the target vessel, and inflated to occlude it. The desired period of occlusion was 300 seconds. In the thrombogenic sponge-injected group, a collagen sponge (Gelfoam, Pfizer, New York, NY, USA) was cut according to the size of the target vessel, impregnated with a contrast solution and dropped through the microcatheter. For alcohol injection, the microcatheter had to be positioned so as to occlude the coronary artery. When a lack of retrograde flow was confirmed by angiography, the alcohol was injected into the microcatheter. Because of insufficient selectivity, we used a coaxial total chronic coronary occlusion balloon catheter as a microcatheter to achieve a superselective injection of 0.2 mL of alcohol (Mini-Trek, Abbott, Chicago, IL, USA). This device offers a better crossing profile and a better push. After removal of the 0.014-in. floppy wire, contrast medium was injected into the inner lumen of the balloon to verify vascular occlusion. Alcohol was then injected into the target artery to induce necrosis of the adjacent tissue and hence induce an infarction.

2.4. Histological Examination. Hearts in which a myocardial infarct was macroscopically observed at autopsy underwent a histological analysis (Figures 1 and 2). Hearts were excised, cut in the coronal plane into three sections from apex to

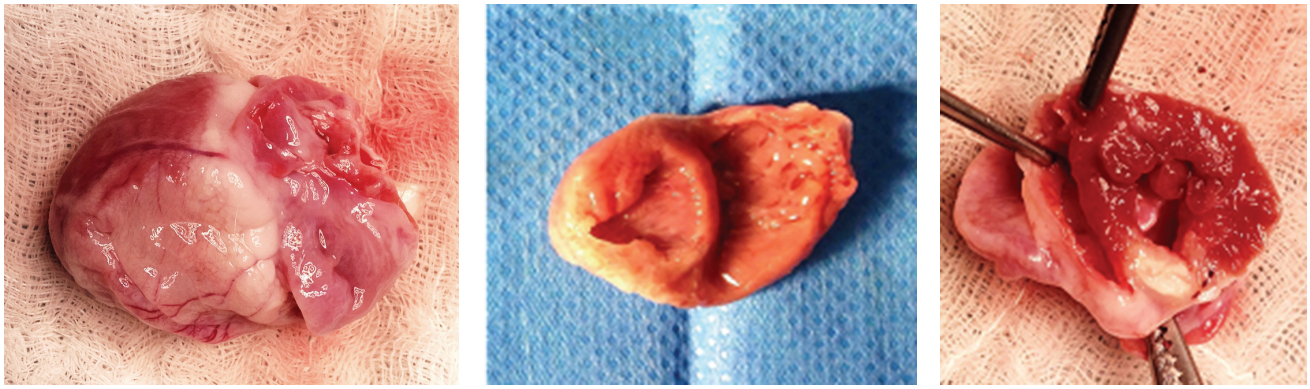

(a) (b) (c)

Figure 1: Macroscopic views. Macroscopic views of a heart that underwent embolization of the middle segment of the right coronary artery; rear side view shows myocardial scarring of the right ventricle and the inferior wall of the left ventricle (a). The area of fibrosis is the inferior wall of the left ventricle and right ventricle (b). Heart that underwent embolization of the middle segment of the circumflex artery; apical section shows lateral wall transmural myocardial infarction (c).

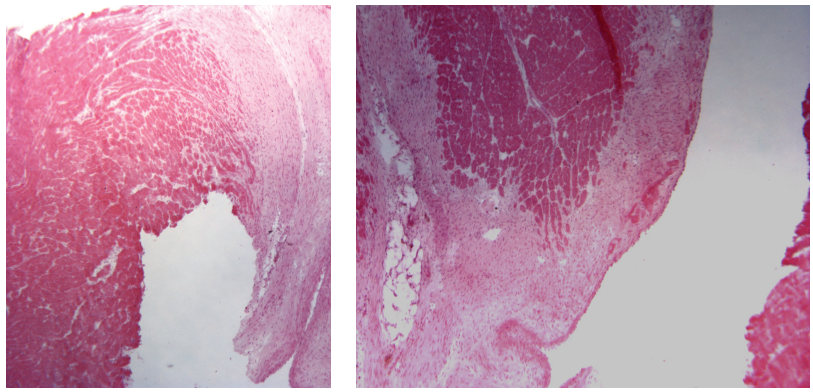

(a) (b)

Figure 2: Histological analysis of left ventricle lateral wall transmural infarction. Histological views of left ventricle lateral wall infarction focused on left ventricle anterior wall after mid segment circumflex artery alcohol injection (a) and of the interventricular septum focused on the basal segment after proximal segment right coronary artery alcohol injection (b) showing muscle and fibrosis. Heart was excised, cut, then embedded in OCT, flash frozen in liquid nitrogen, and stored at −80°C. Ten-micrometer cryosections were stained to confirm the presence of ischemic tissue.

base, embedded in OCT, flash-frozen in liquid nitrogen, and stored at −80°C. Ten-micrometer cryosections were stained with hematoxylin-eosin to confirm the presence of ischemic tissue.

2.5. Echocardiography. *In vivo* heart function was evaluated by echocardiography three weeks after ischemic injury. Transthoracic echocardiography was performed on sedated animals by an experienced cardiologist using an echocardiography machine equipped with an appropriate probe for imaging rabbit hearts (Vivid E9 ultrasound platform, GE Health Care, Pittsburgh, PA, USA). Two-dimensional mages were taken using both long axis and short axis views. Measurements were taken to evaluate the following parameters: dimensions of the LV, left atrium, wall thickness, valve function, and LV ejection fraction (calculated using Simpson's method).

2.6. Statistical Analysis. Data are given in percentages and means ± standard deviations. Comparisons between groups were made using the nonparametric ANOVA test for continuous variables. A $p < 0.05$ value was considered statistically significant. Statistical analysis was performed with JMP 9.1 software (SAS, Cary, NC, USA).

3. Results

3.1. Assessment of Vascular Access and Coronary Catheterization Procedures. The safest micropuncture vascular access was achieved using needles and 0.018-in. wires. A 4-Fr micropuncture sheath was effective. It was advanced over the wire and exchanged for a 0.035-in. guidewire to support the placement of a 4-Fr internal mammary guide catheter (Cordis Corporation, Miami, FL, USA), with custom alteration for use in a rabbit. The guiding catheter was advanced

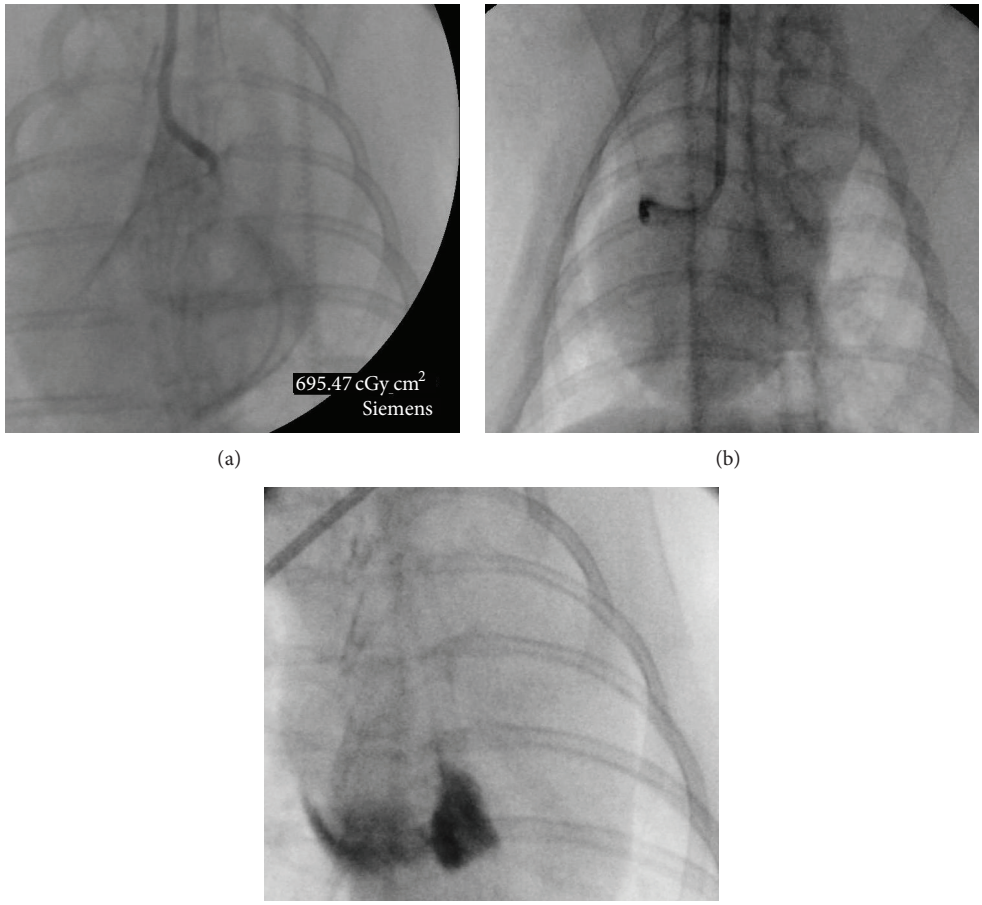

Figure 3: Angiography of the coronary artery after mid segment alcohol injection. Selective angiography of the left main coronary artery, of the left anterior descending along the anterior interventricular sulcus reaching the apex of the heart, of a diagonal coronary artery, and of the circumflex coronary artery along the atrioventricular groove (a). Embolization of the right coronary artery ostium with free coil (b). Angiography of the right coronary artery after mid segment alcohol injection (c). The contrast product injected after alcohol injection stagnates in the necrotic area thus achieving an aspect of myography.

retrogradely to the ascending aorta using fluoroscopy, and an angiography of the coronary artery was then performed to check for its adequate location. Dilution of the contrast medium was kept at 50% of the total volume to reduce the risk of ventricular arrhythmias.

3.2. Assessment of the Coronary Occlusion Site. Middle or proximal segment occlusion of the left anterior descending coronary artery led to severe heart failure with massive hemorrhagic infarction of the LV, while distal segment occlusion caused severe conduction disturbances requiring isoprenaline infusion. The occlusion of the branches (diagonal and septal branches) needed a custom device and led to only small nontransmural infarcted areas, without a relevant decrease in LVEF. Occlusion of obtuse marginal branches yielded a very limited, nontransmural LV infarction without functional consequences, as assessed by echocardiography. Only occlusion either of the mid segment of the right coronary artery or of the mid segment of the circumflex coronary artery was finally found to be the most reliable procedure for inducing an extensive infarction of the supplied LV area. Such infarcts led to an akinesia/hypokinesia of the right ventricle and of the inferior wall of the left ventricle (right coronary occlusion or circumflex coronary occlusion, resp.) with, in both cases, a 25% decrease in LVEF and only nonsustained ventricular arrhythmias. These data (summarized in Table 1) led to the conclusion that, according to the coronary artery distribution, the dominant vessel would be the best target for embolization.

3.3. Comparison of MI-Inducing Techniques

3.3.1. Free Coil Embolization. Four rabbits underwent free coil embolization. Two coils deployed at the left main artery ostium and protruded into the aorta. One coil deployed at the circumflex artery proximal segment and one deployed at the right coronary artery ostium. All of these rabbits died from intraoperative refractory ventricular fibrillation. Histological examination revealed large left and right ventricle hemorrhagic necrosis, depending on the occlusion site (Tables 2 and 3).

Table 1: Distribution and follow-up depending on embolization site.

Embolization site (n =)	Intraoperative events	3-week survival (n =)	Echographic assessment	Histologic assessment
LAD				
Proximal segment (1)	VF	0	—	Transmural infarct
Mid segment (2)	VF	0	—	Transmural infarct
Distal segment (2)	ACD	0	—	Transmural infarct
S. branch vessel (1)	—	1	No LV dysfunction	Nontransmural infarct
CA				
Proximal segment (1)	NSVT, CHF	0	—	Transmural infarct
Mid segment (2)	NSVT	2	LV dysfunction	Transmural infarct
Distal segment (0)	—	—	—	—
S. branch vessel (2)	—	2	No LV dysfunction	Nontransmural infarct
RCA				
Proximal segment (1)	CHF	0	—	Transmural infarct
Mid segment (2)	NSVT	2	LV and RV dysfunction	Transmural infarct
Distal segment (0)	—	—	—	—

LAD: left anterior descending; CA: circumflex artery; RCA: right coronary artery; LV: left ventricle; RV: right ventricle; VF: ventricular fibrillation; ACD: atrioventricular conduction disorder; NSVT: nonsustained ventricular tachycardia; CHF: congestive heart failure; S. branch vessel: secondary branch vessel.

Table 2: Distribution and follow-up depending on embolization device.

Embolization device (n =)	Intraoperative events	3-week survival (n =)	Echographic assessment	Histologic assessment
Free coil				
CA (3)	VF	0	—	Transmural infarct
RCA (1)	VF	0	—	Transmural infarct
Interlocking coil				
CA (2)	VF	1	LVEF decrease <15%	Nontransmural infarct
RCA (2)	VF	1	No dysfunction	No infarct
Gelatin sponge				
CA (3)	—	3	No dysfunction	Nontransmural infarct
RCA (1)	—	1	No dysfunction	No infarct
Balloon occlusion				
CA (2)	NSVT	2	No dysfunction	No infarct
RCA (2)	NSVT	2	No dysfunction	No infarct
Alcoholization				
CA (5)	VF	4	15% decrease in LVEF	Transmural infarct
RCA (3)	CHF	2	RV dysfunction 15% decrease in LVEF	Transmural infarct

CA: circumflex artery; RCA: right coronary artery; LV: left ventricle; RV: right ventricle; VF: ventricular fibrillation; NSVT: nonsustained ventricular tachycardia; CHF: congestive heart failure.

3.3.2. Interlocking Coil Embolization. Four rabbits underwent interlocking coil embolization in the mid segment of the target coronary artery. Two animals died from intraoperative refractory ventricular fibrillation during coil deployment in the circumflex and right coronary arteries, possibly due to the unwanted occlusion of the more proximal arterial segment due to excessively long coils. Two animals survived the procedure and until the end of the study. In both of these cases, the coils were too short, causing their migration towards the distality of the target vessel (the circumflex artery in one case and the right coronary artery in the other). Expectedly, this resulted in limited nontransmural or even undetectable infarct areas without changes in LVEF (Tables 2 and 3).

3.3.3. Gelatin Sponge Embolization. Gelatin sponges were used in four procedures (three right coronary artery mid segment embolization and one circumflex mid segment embolization). No intraoperative or postoperative arrhythmias occurred and all animals survived until the end of the study. The likely reason was that only histologically limited nontransmural LV lateral wall infarcts were detectable after circumflex embolization while no myocardial damage could be identified in the case of right coronary artery embolization.

Table 3: Ultrasound assessment of alcoholization group.

	Before embolisation	After embolisation	F	Prob. > F
DIVS (mm)	3.8 ± 0.2	4.0 ± 0.2	2,354	0,155
DLVID (mm)	17.4 ± 0.4	20.1 ± 1.1	29,236	<0,001
DLVPW (mm)	5.5 ± 0.2	5.5 ± 0.3	0,052	0,823
SIV (mm)	4.1 ± 0.2	4.1 ± 0.2	0,220	0,648
SLVID (mm)	12.1 ± 0.5	16.5 ± 0.9	104,824	<0,001
SLVPW (mm)	5.7 ± 0.2	5.7 ± 0.2	0,018	0,894
LVEF (Teichholz (%))	58.0 ± 2.9	43.5 ± 1.6	113,648	<0,001
FS (%)	30.5 ± 1.8	18.0 ± 0.9	240,384	<0,001
LVESV (mL)	2.9 ± 0.2	3.4 ± 0.1	19,736	0,001
LVEDV (mL)	1.2 ± 0.2	1.8 ± 0.2	37,097	<0,001
LVEF (biplane Simpson (%))	58.3 ± 2.6	47.0 ± 2.4	60,8421	<0,001
SV (mL)	1.7 ± 0.2	1.6 ± 0.2	1,680	0,223

DIVS: diastolic interventricular septum; DLVID: diastolic left ventricle inner diameter; DLVPW: diastolic left ventricle posterior wall; SIVS: systolic interventricular septum; SLVID: systolic left ventricle inner diameter; SLVPW: systolic left ventricle posterior wall; LVEF: left ventricle ejection fraction; FS: fractional shortening; LVESV: left ventricle end systolic volume; LVEDV: left ventricle end diastolic volume; SV: stroke volume.

No LVEF decrease could be echographically detected in any of these cases (Figure 4; Tables 2 and 3).

3.3.4. Balloon Occlusion. Four animals underwent balloon occlusion, of the right coronary mid segment (two cases) and of the circumflex mid segment (two remaining cases). All animals survived despite the occurrence of nonsustained ventricular tachycardia which resolved after balloon deflation. Both echocardiographic and histological examinations failed to reveal any cardiac abnormality (Tables 2 and 3).

3.3.5. Alcohol Injection. Eight animals underwent alcohol injection in the mid segment of the right coronary artery and of the circumflex artery in five and three cases, respectively. All angiograms performed after alcohol injection showed coronary artery TIMI flow 0 or I and a pattern of myography in the infarcted area. One animal with circumflex artery alcoholization died from refractory ventricular fibrillation. Another rabbit which had undergone alcohol injection in the right coronary artery died two days after surgery from drug-refractory heart failure. However, the 6 remaining rabbits survived until the end of the study. Four of them were then found to have a macroscopically massive infarction of the right ventricle and of the LV inferior wall, which was confirmed by histological analysis. Two other rabbits had massive infarction of the left ventricle lateral wall. In all of these survivors, LVEF was significantly reduced from its baseline value (19,4 ± 2,4%; Tables 2 and 3).

4. Discussion

It is generally accepted that proof-of-concept studies designed to test the efficacy of new drug-, cell-, or other biologics-based therapies for HF can be reliably performed in rat and mouse [16, 17]. However, the drawbacks of these rodent models are also well recognized. They primarily include major differences in heart physiology compared with humans and a limited lifespan which precludes long-term follow-up assessments. These hurdles can be overcome by the use of large animal models, primarily pig and sheep, which offer distinct advantages: a more clinically relevant cardiac physiology, a size allowing testing catheter-based delivery devices, and the possibility of realistically studying dose-effect relationships [14, 18, 19]. However, these models are more logistically complex and costly as they require dedicated facilities and highly trained personnel. In this setting, the rabbit appears as an attractive trade-off. The physiology of this species is not so far from that of humans with regard to heart rate and patterns of contractility-related calcium handling and myosin heavy chain isoforms, while vessels size is compatible with the testing of catheter-based interventions [20, 21]. Indeed, several studies have used a rabbit model of MI induced by permanent or transient coronary artery ligation, but, in most cases the procedure has been performed through a direct surgical approach of the target artery [22]. Closed-chest procedures have been less commonly reported despite distinct advantages such as a limited invasiveness and the possibility of keeping the pericardium untouched and free from adhesions. The latter avoids the confounding effect of pericardial incision on postinfarction remodeling. This model also allows, when indicated, a subsequent direct intramyocardial delivery of the product under investigation [5, 23]. The recognition of these advantages prompted the present study which entailed the first angiography-based characterization of the coronary artery anatomical patterns in rabbits and the development of a reproducible percutaneous catheter-based technique of myocardial necrosis induction.

Our review of the angiograms that we performed in our initial series of 14 rabbits did not yield results which matched those previously published [24, 25]. Basically, the coronary artery anatomy of the rabbit seems to be organized as in humans with a constant left main coronary artery and left or right coronary artery dominance depending on whether the posterior descending artery originates from the circumflex coronary artery or the right coronary artery, respectively.

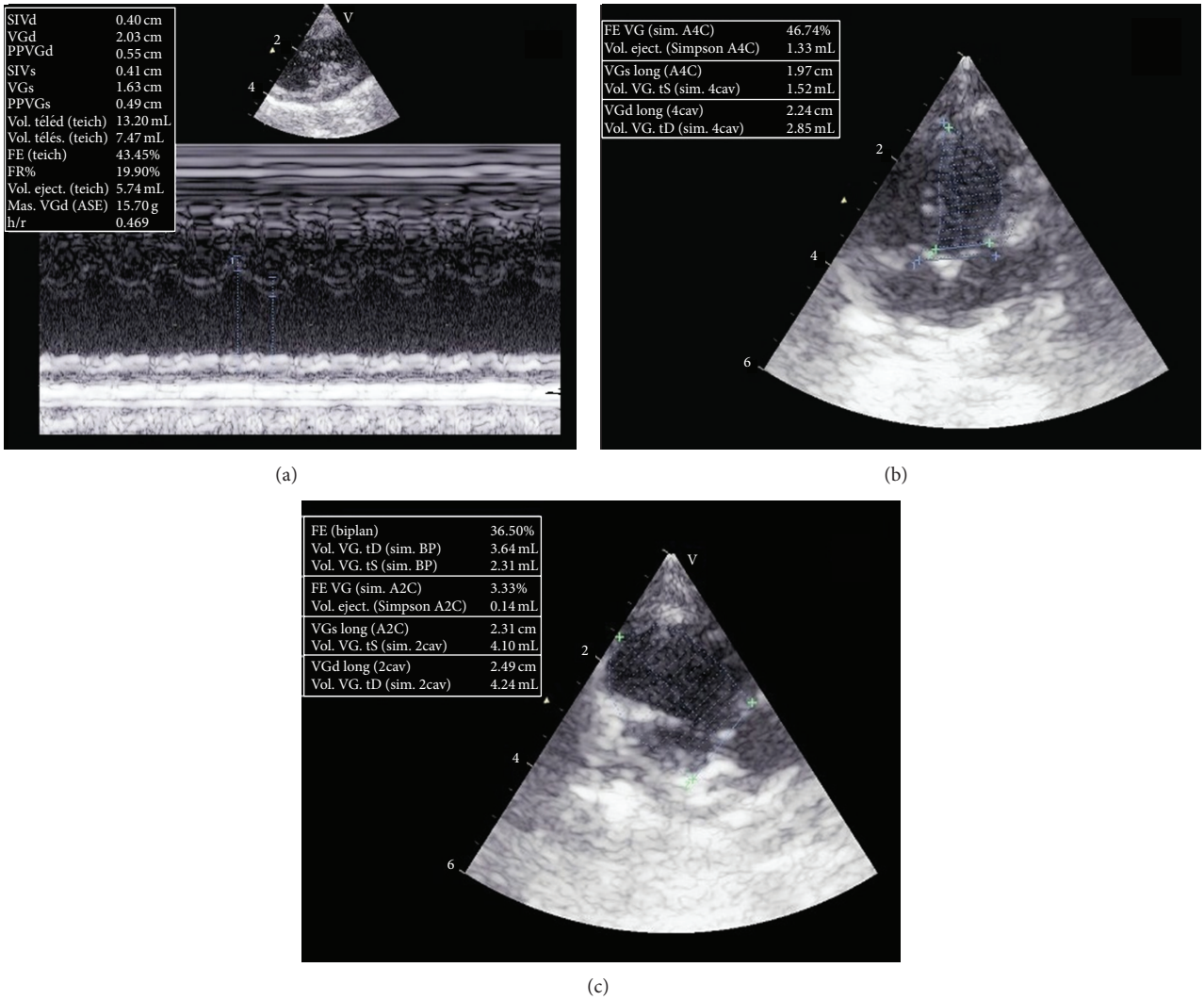

Figure 4: Echographic assessment of left ventricular ejection fraction. Left ventricular measurements are made with the M-mode. Both ventricular diameters (systolic and diastolic) are measured from the leading edge to leading edge of each interface, and LVEF by Teichholz is then calculated (a). Ventricular volumes are calculated in the two orthogonal apical views: four-chamber (b) and (c) *biplane Simpson*. Left ventricular endocardium is traced in end-diastole and end-systole in both views.

The left main artery divides into the left anterior descending (LAD) and the circumflex arteries. The LAD travels in the anterior interventricular groove and continues up to the apex of the heart. It supplies the anterior part of the septum with septal branches and the anterior wall of the left ventricle with diagonal branches. The circumflex and right coronary arteries supply the lateral wall of the left and right ventricle, respectively.

Given this configuration, embolization of secondary branches of epicardial vessels such as marginal, septal, and diagonal branches only resulted in functionally inconsequent infarctions at the cost of complicated procedures while, contrariwise, embolization of the LAD was associated with much too extensive myocardial damage. We thus elected to focus on the dominant vessel; however the high sensitivity of the rabbit to ischemia required carefully controlling the level of its occlusion to ensure a substantial impairment of LV function, but with an acceptable mortality rate. Targeting a decrease in LVEF of 20% from baseline targeting was found to be a reasonable objective which could then be reproducibly achieved by locating the occlusion site at the mid segment of either the right coronary or the circumflex coronary artery.

These screening experiments then set the stage for the comparison of different infarction-inducing techniques which, to our knowledge, have not yet been reported. So far, the few studies which have used a closed-chest approach for inducing MI in rabbits have relied on the use of coils [5, 23]. We thus started our experiments with this type of material but, in our hands, neither free nor interlocking coils could generate reproducible results. It was difficult to load free coils into the delivery catheter and to control the exact site, timing, and extent of their deployment in the target artery and it was equally challenging to release interlocking coils in such a way as to occlude to coronary resulting

in a substantial impairment of LV function that was still compatible with survival of the rabbit. The high cost of coils is another limiting factor. Both the release of gelatin sponge and the balloon inflation then looked initially attractive because of their purported simplicity. Indeed, gelatin sponge was plastic enough to yield an excellent conformability within the catheter but featured several disadvantages such as difficult handling, adherence to the catheter inner lumen, and poor visualization under fluoroscopy. Balloon-induced vessel occlusions, in turn, were arrhythmogenic unless inflations were kept short, in which case large infarcts could not be generated. Inspired by alcohol septal ablation performed in patients with hypertrophic obstructive cardiomyopathy, we finally tested alcohol injection. In contrast to the other techniques, alcohol injection allowed assessment of the TIMI flow grade just after the injection without removing the device. Because of the lack of selective injections, the first attempts performed with the microcatheter resulted in massive infarction. Optimized injections were then made possible using a coaxial total chronic occlusion balloon catheter as the microcatheter to achieve a superselective injection of 0.2 mL of alcohol. Considering both the amount of pathologically damaged myocardium, the resulting loss of echocardiographically measured pump function, and the survival of animals, this technique proved to offer the best risk to benefit ratio.

We acknowledge several limitations of the present study. Coils which were tested were those commercially available and we cannot exclude that customizing these devices would not have resulted in better outcomes. Second, functional assessments only consisted of gross measurements of EF and a more detailed analysis of the patterns of regional contraction and relaxation is clearly required to better characterize the hemodynamic effects of any coronary artery occlusion technique. Finally, the damage induced by alcohol injection may not accurately model that seen in patients with ischemic heart disease, although alcohol injection was found to depress LV function to a sufficient extent as to give room for detecting treatment effects for testing interventions. Despite these caveats, the present data can provide a useful benchmark for improving catheter-based techniques of coronary artery occlusion in rabbits and facilitate a broader use of this model for testing drugs or interventions designed to mitigate the consequences of ischemically induced LV dysfunction.

5. Conclusion

By following a stepwise approach, a minimally invasive, effective, and reproducible rabbit model of catheter-induced myocardial infarction has been developed which addresses the limitations of rodent experiments while avoiding the logistical and cost issues associated with large animal models.

Conflict of Interests

The authors declare that there is no conflict of interests regarding the publication of this paper.

References

[1] V. L. Roger, "Epidemiology of heart failure," *Circulation Research*, vol. 113, no. 6, pp. 646–659, 2013.

[2] A. S. Go, D. Mozaffarian, V. L. Roger et al., "Executive summary: heart disease and stroke statistics—2013 update: a report from the American Heart Association," *Circulation*, vol. 127, no. 1, pp. 143–152, 2013.

[3] R. S.-Y. Foo, K. Mani, and R. N. Kitsis, "Death begets failure in the heart," *The Journal of Clinical Investigation*, vol. 115, no. 3, pp. 565–571, 2005.

[4] M. Chiong, Z. V. Wang, Z. Pedrozo et al., "Cardiomyocyte death: mechanisms and translational implications," *Cell Death & Disease*, vol. 22, no. 2, pp. 222–244, 2011.

[5] R. Edwards, Z. Yousef, R. Rakhit et al., "A model of closed chest regional myocardial infarction in the rabbit: a clinically relevant in vivo assay system of post-infarction remodelling," *Basic Research in Cardiology*, vol. 97, no. 5, pp. 374–383, 2002.

[6] R. Klocke, W. Tian, M. T. Kuhlmann, and S. Nikol, "Surgical animal models of heart failure related to coronary heart disease," *Cardiovascular Research*, vol. 74, no. 1, pp. 29–38, 2007.

[7] A. M. Abarbanell, J. L. Herrmann, B. R. Weil et al., "Animal models of myocardial and vascular injury," *Journal of Surgical Research*, vol. 162, no. 2, pp. 239–249, 2010.

[8] D. H. Spodick, *The Pericardium: A Comprehensive Textbook*, edited by: D. H. Spodick, CRC Press, New York, NY, USA, 1996.

[9] D. Hasdai, V. Barak, E. Leibovitz et al., "Serum basic fibroblast growth factor levels in patients with ischemic heart disease," *International Journal of Cardiology*, vol. 59, no. 2, pp. 133–138, 1997.

[10] M. Fujita, M. Ikemoto, M. Kishishita et al., "Elevated basic fibroblast growth factor in pericardial fluid of patients with unstable angina," *Circulation*, vol. 94, no. 4, pp. 610–613, 1996.

[11] S. Corda, A. Mebazaa, M.-P. Gandolfini et al., "Trophic effect of human pericardial fluid on adult cardiac myocytes: differential role of fibroblast growth factor-2 and factors related to ventricular hypertrophy," *Circulation Research*, vol. 81, no. 5, pp. 679–687, 1997.

[12] B. Schumacher, P. Peecher, B. U. von Specht, and T. Stegmann, "Induction of neoangiogenesis in ischemic myocardium by human growth factors: first clinical results of a new treatment of coronary heart disease," *Circulation*, vol. 97, no. 7, pp. 645–650, 1998.

[13] C. Landau, A. K. Jacobs, and C. C. Haudenschild, "Intrapericardial basic fibroblast growth factor induces myocardial angiogenesis in a rabbit model of chronic ischemia," *American Heart Journal*, vol. 129, no. 5, pp. 924–931, 1995.

[14] A. Halapas, A. Papalois, A. Stauropoulou et al., "In vivo models for heart failure research," *In Vivo*, vol. 22, no. 6, pp. 767–780, 2008.

[15] National Research Council (US) Institute for Laboratory Animal Research, *Guide for the Care and Use of Laboratory Animals*, National Academies Press (US), Washington, DC, USA, 1996.

[16] R. J. Figueroa, T. G. Koch, and D. H. Betts, *Stem Cells and Animal Therapies*, edited by M. Moo-Young, 2011.

[17] N. Milani-Nejad and P. M. L. Janssen, "Small and large animal models in cardiac contraction research: advantages and disadvantages," *Pharmacology and Therapeutics*, vol. 141, no. 3, pp. 235–249, 2014.

[18] C. A. Muller, L. H. Opie, C. A. Pineda, and M. Peisach, "Bucindolol, a beta blocker, decreased ventricular fibrillation

and maintained mechanical function in a pig model of acute myocardial ischemia," *Cardiovascular Drugs and Therapy*, vol. 6, no. 3, pp. 233–237, 1992.

[19] H. N. Sabbah, P. D. Stein, T. Kono et al., "A canine model of chronic heart failure produced by multiple sequential coronary microembolizations," *The American Journal of Physiology—Heart and Circulatory Physiology*, vol. 260, no. 4, pp. H1379–H1384, 1991.

[20] V. Piacentino III, C. R. Weber, X. Chen et al., "Cellular basis of abnormal calcium transients of failing human ventricular myocytes," *Circulation Research*, vol. 92, no. 6, pp. 651–658, 2003.

[21] T. Suzuki, B. M. Palmer, J. James et al., "Effects of cardiac myosin isoform variation on myofilament function and crossbridge kinetics in transgenic rabbits," *Circulation: Heart Failure*, vol. 2, no. 4, pp. 334–341, 2009.

[22] K. W. Mahaffey, T. E. Raya, G. D. Pennock, E. Morkin, and S. Goldman, "Left ventricular performance and remodeling in rabbits after myocardial infarction: effects of a thyroid hormone analogue," *Circulation*, vol. 91, no. 3, pp. 794–802, 1995.

[23] O. Ziv, L. Schofield, E. Lau et al., "A novel, minimally invasive, segmental myocardial infarction with a clear healed infarct borderzone in rabbits," *American Journal of Physiology—Heart and Circulatory Physiology*, vol. 302, no. 11, pp. H2321–H2330, 2012.

[24] B. Podesser, G. Wollenek, R. Seitelberger et al., "Epicardial branches of the coronary arteries and their distribution in the rabbit heart: the rabbit heart as a model of regional ischemia," *The Anatomical Record*, vol. 247, no. 4, pp. 521–527, 1997.

[25] T. A. Pearson, H. Malmros, J. Dillman, N. Sternby, and R. H. Heptinstall, "Atherosclerosis in the hypercholesterolemic hare. Comparison of coronary artery lesions induced by dietary cholesterol in the hare and the rabbit," *Atherosclerosis*, vol. 63, no. 2-3, pp. 125–135, 1987.